SYNTHESIS OF LIQUID CRYSTALLINE COPOLYESTERS WITH LOW
MELTING TEMPERATURE FOR IN SITU COMPOSITE APPLICATIONS

A THESIS SUBMITTED TO
THE GRADUATE SCHOOL OF NATURAL AND APPLIED SCIENCES
OF
MIDDLE EAST TECHNICAL UNIVERSITY

BY

SELAHATTİN ERDOĞAN

IN PARTIAL FULFILLMENT OF THE REQUIREMENTS
FOR
THE DEGREE OF DOCTOR OF PHILOSOPHY
IN
POLYMER SCIENCE AND TECHNOLOGY

JUNE 2011

Approval of the thesis:

SYNTHESIS OF LIQUID CRYSTALLINE COPOLYESTERS WITH LOW MELTING TEMPERATURE FOR IN SITU COMPOSITE APPLICATIONS

submitted by **SELAHATTİN ERDOĞAN** in partial fulfillment of the requirements for the degree of **Doctor of Philosophy in Polymer Science and Technology Department, Middle East Technical University** by,

Prof. Dr. Canan ÖZGEN
Dean, Graduate School of **Natural and Applied Sciences**   _____

Prof. Dr. Necati ÖZKAN
Head of Department, **Polymer Science and Technology**   _____

Prof. Dr. Erdal BAYRAMLI
Supervisor, **Chemistry Dept., METU**   _____

Examining Committee Members:

Prof. Dr. Ülkü YILMAZER
Chemical Eng. Dept., METU   _____

Prof. Dr Erdal BAYRAMLI
Chemistry Dept., METU   _____

Prof. Dr. Serpil AKSOY
Chemistry Dept., Gazi University   _____

Prof. Dr. Ali USANMAZ
Chemistry Dept., METU   _____

Assist. Prof. Dr. Ali ÇIRPAN
Chemistry Dept., METU   _____

Date: 22.06.2011

I hereby declare that all information in this document has been obtained and presented in accordance with academic rules and ethical conduct. I also declare that, as required by these rules and conduct, I have fully cited and referenced all material and results that are not original to this work.

Name, Last name   :   Selahattin ERDOĞAN

Signature   :

ABSTRACT

SYNTHESIS OF LIQUID CRYSTALLINE COPOLYESTERS WITH LOW MELTING TEMPERATURE FOR IN SITU COMPOSITE APPLICATIONS

ERDOĞAN, Selahattin
Ph.D., Department of Polymer Science and Technology
Supervisor: Prof. Dr. Erdal BAYRAMLI

June 2011, 203 pages

The objective of this study is to synthesize nematic-thermotropic liquid crystalline polymers (LCP) and determine their possible application areas. In this context, thirty different LCP's were synthesized and categorized with respect to their fiber formation capacity, melting temperature and mechanical properties. The basic chemical structure of synthesized LCP's were composed of p-acetoxybenzoic acid (p-ABA), m-acetoxybenzoic acid (m-ABA), hydroquinone diacetate (HQDA), terephthalic acid (TPA) and isophthalic acid (IPA) and alkyl-diacids monomers. In addition to mentioned monomers, polymers and oligomers were included in the backbone such as polyethylene terephthalate (PET) and polyethylene naphthalate (PEN) polymers, and polybutylene naphthalate (PBN), polyhexylene naphthalate (PHN) and poly butylene terephthalate (PBT) oligomers that contain different kinds of alkyl-diols.

We adjusted the LCP content to have low melting point (180°C-280°C) that is processable with thermoplastics. This was achieved by balancing the amount of linear (para) and angular (meta) groups on the aromatic backbones together with the use of linear hydrocarbon linkages in the random copolymerization (esterification) reaction. LCP species were characterized by the following techniques; Polarized Light Microscopy, Nuclear Magnetic Resonance (NMR), Fourier Transform Infrared Analysis (FTIR), Differential Scanning Calorimetry (DSC), Thermogravimetric Analysis (TGA), X-ray Scattering (WAXS, Fiber

diffraction), surface free energy, end group analysis (CEG), intrinsic viscosity (IV) and tensile test. According to these analysis LCPs were classified into five main categories; (I) fully aromatics, (II) aromatics+ PET/PEN, (III) aromatics + oligomers (IV) aromatics + short aliphatic diacids, (V) aromatics + long aliphatic diacids. The foremost results of the analysis can be given as below.

DSC analysis shows that some LCPs are materials that have stable LC mesogens under polarized light microscopy. In TGA analysis LCPs that have film formation capacity passed the thermal stability test up to 390°C. NMR results proved that predicted structures of LCPs from feed charged to the reactor are correct. In FTIR due to the inclusion of new moieties, several peaks were labeled in the finger-print range that belongs to reactants. In X-ray analysis, LCP24 (containing PET) was found to be more crystalline than LCP25 (containing PEN) which is due to the symmetrical configuration. Block segments were more pronounced in wholly aromatic LCP2 than LCP24 that has flexible spacers. Another important finding is that, as the amount of the charge to the reactor increases CEG value increases and molecular weight of the product decreases.

Selected group V species were employed as reinforcing agent and mixed with the thermoplastics; acrylonitrile butadiene styrene (ABS), nylon6 (PA6), polyethylene terephthalate (PET), polypropylene (PP) and appropriate compatibilizers in micro compounder and twin screw extruder. The blends of them were tested in dog-bone and/or fiber form. In general LCPs do not improve the mechanical properties except in composite application with polypropylene. A significant increase in tensile properties is observed by LCP24 and LCP25 usage. Capillary rheometer studies show that the viscosity of ABS decreases with the inclusion PA6 and LCP2 together. In addition to the composite applications, some LCPs are promising with new usage areas. Such as nano fibers with 200nm diameter were obtained from LCP27 by electrospinning method. The high dielectric constant of LCP29 has shown that it may have application areas in capacitors.

Keywords: Condensation polymerization, Thermotropic Liquid Crystalline Polymers, Composites, ABS/PA6, PET and PP Blends

ÖZ

IN SITU KOMPOZİT UYGULAMALARI İÇİN DÜŞÜK SICAKLIKTA ERİYEBİLEN
SIVI KRİSTAL KOPOLİESTERLERİN SENTEZİ

ERDOĞAN, Selahattin
Doktora, Polimer Bilimi ve Teknolojisi Bölümü
Tez Yöneticisi: Prof. Dr. Erdal BAYRAMLI

Haziran 2011, 203 Sayfa

Bu çalışmada farklı tipte nematik-termotropik sıvı kristal polimerler (LCP) sentezlenmesi ve bu sentezlenen LCP'lerin olası uygulama alanlarının belirlenmesi amaçlanmıştır. Bu çerçevede otuz farklı LCP sentezlenip elyaf formasyon kapasitesi, erime sıcaklığı ve mekanik özelliklerine göre sınıflandırıldı. Sentezlenen LCP içeriğinde bulunan yapılar; p-asetoksi benzoik asit (p-ABA), m- asetoksi benzoik asit (m-ABA), hidrokinon diasetat (HQDA), teraftalik acid (TPA), isoftalik asit (IPA), alkil-diasit monomerleridir. Bu monomerlere ek olarak polimerler ve oligomerler yapıya eklenmiştir: örneğin polietilen terafıtalat (PET) ve polietilen naftalat (PEN) polimerleri ve farklı tipte alkil-diol içeren polibutilen naftalat (PBN) polihegzilen naftalat (PHN), polibutilen terefitalat (PBT) oligomerleri olarak sıralanabilir.

Sentezlenen LCP'lerin termoplastiklerle işlenebilir olması için düşük sıcaklıkta (180°C-280°C) eriyebilmeleri sağlandı. Bu özellik kullanılan aromatik moleküllerin doğrusal (para), açılı (meta) oranlarıyla ve esneklik sağlayan hidrokarbon gruplarının (etilen) uzunluklarıyla kondensasyon (esterleşme) reaksiyonu yoluyla sağlandı. Karakterizasyon için yapılan testler: Polarize Işık Mikroskobu, Nükleer Manyetik Resonans (NMR), Fourier Transfer Infrared (FTIR), Diferansiyel Taramalı Kalorimetre (DSC), Termogravimetrik Analiz (TGA), X ışını saçınımı (Geniş açılı ve Elyaf difraksiyonu), serbest yüzey enerjisi, uç grup analizi (CEG), intrinsik viskozite (IV) ve çekme dayanımı olarak sıralanabilir. Analiz sonuçlarına göre beş ana

kategoride gruplama yapıldı; (I) tam aromatikler, (II) tam aromatikler + PET/PEN, (III) tam aromatikler + oligomerler, (IV) tam aromatikler + kısa alifatik zincirli dikarboksilik asitler, (V) tam aromatikler + uzun alifatik zincirli dikarboksilik asitler olarak sıralandı. Analiz sonuçlarındaki öne çıkan özellikler aşağıdaki gibi sıralanabilir.

Sentezlenen LCP'lerden bir çoğu DSC analizinin de gösterdiği gibi stabil malzemelerdir ve polarize ışık mikroskobu altında kararlı mesojen yapılardan oluşmaktadır. TGA analizlerine göre film olma özelliği taşıyan LCP'lerin termal dayanımı 390°C ye kadar çıkmaktadır. Reaksiyona giren yapılardan yola çıkılarak tahmin edilen moleküler yapılar NMR spektraları trafından doğrulanmaktadır. FTIR spektrumunda oluşan karakteristik piklerin reaksiyona giren yapılardan dolayı oluştuğu anlaşılmaktadır ve pikler yapılarla eşleştirilmiştir. X-ray analizine göre PET içeren LCP24, PEN içeren LCP25 e göre simetrik yapısından dolayı daha kristal yapıdadır. Tam aromatik yapıdaki LCP2 esnek yapı içeren LCP24'e göre daha bloklu yapıdadır. CEG analizi sonucuna göre bileşenler aynı oranda olsa bile miktar arttıkça CEG artmaktadır ve moleküler ağırlık azalmaktadır.

Amacımıza uygun olan beşinci gurup LCP'ler akrilonitril butadien stiren (ABS), nylon6 (PA6), polietilen teraftalat (PET), polipropilen (PP) termoplastiklerinde uygun uyumlaştırıcılarla birlikte güçlendirici eleman olarak kullanıldı, çift vidalı extruder ve mikro karıştırıcı yardımıyla karıştırıldı. Karışımlar plaka veya elfay formuna getirildi. Genel olarak PP haricinde belirgin mekanik artış görülmedi. LCP24 ve LCP25 in PP ile kullanılmasında çekme dayanımında artış gözlendi. Kapilar reometre sonucuna göre ABS nin viskozitesi PA6 ve LCP2 nin birlikte kullanılmasıyla belirgin olarak azaldı. Kompozit kullanımın yanında LCP'lerin saf halde kullanılması konusunda kayda değer gelişmeler gözlendi. Örneğin LC27'den elektrospin ile 200nm çapında nano elyaflar elde edildi. LCP29'un yüksek dielektrik özelliği sayesinde kapasitörlerde kullanılabileceği görüldü.

Anahtar Kelimeler: Kondensasyon Polimerizasyonu, Termotropik Sıvı Kristal Polimerler, Kompozitler, ABS/PA6, PET ve PP Karışımları

to my family ...

ACKNOWLEDGEMENTS

TABLE OF CONTENTS

LIST OF TABLES

TABLES

LIST OF FIGURES

FIGURES

xix

ABBREVIATIONS

ABS	Acrylonitrile-butadiene-styrene rubber
ASTM	American Society for Testing and Materials
ATR	Attenuated Total Reflectance
BPA	Bisphenol A
CEG	Carboxyl End Group
DIM	Diiodomethane
DMAc	Dimethylacetamide
DMF	Dimethylformamide
DSC	Differential Scanning Calorimetry
DSC	Differential Scanning Calorimetry
EG	Ethylene Glycol
E-GMA	Ethylene-Glycidyl Methacrylate
E-MA-GMA	Ethylene-Methyl Acrylate-Glycidyl Methacrylate
E-nBA-MAH	Ethylene-Butyl Acrylate-Maleic Anhydride
FA	Formamide
HQDA	Hydroquinone diacetate
IPA	Isophthalic acid
LCP	Liquid Crystalline Polymer
m-ABA	3-Acetoxybenzoic acid
MA	Maleic Anhydride
MA-g-PP	Maleic anhydride grafted polypropylene
MFI	Melt Flow Index
NMP	N-Methyl-2-pyrrolidone
NMR	Nuclear Magnetic Resonance
OH	Hydroxyl end group
PA6	Polyamide 6
p-ABA	4-Acetoxybenzoic acid
PBN	Poly (Butylene 2,6 naphthalate)

PBT	Poly(Butylene terephthalate)
PEN	Poly Ethylene 2,6 naphthalate
PET	Poly(ethylene terephthalate)
PHN	Poly(hexylene 2,6 naphthalate)
PP	Polypropylene
S	Siemens, Ω^{-1}
SMA	Styrene Maleic Anhydride
SEM	Scanning Electron Microscopy
TGA	Thermogravimetric Analysis
TLCP	Thermotropic Liquid Crystalline Polymer
TPA	Terephthalic acid
WAXS	Wide angle X-Ray Diffraction

Nomenclature

A_0	Initial cross sectional area, (mm^2)
Ca	Capillary number
E	Young's Modulus, (MPa)
F	Instantaneous load, (N)
L	Total length of mechanical test specimen, (mm)
L_0	Initial gauge length, (mm)
n	Order of diffraction peak
n	Rabinowitsch correction factor
Q	Volumetric flow rate, (cm^3.s^{-1})
Rc	Inside capillary tube radius, (mm)
T	Thickness of mechanical test specimen, (mm)
T_c	Crystallization Temperature, (°C)
T_{cn}	Crystal to nematic transition temperature, (°C)
T_g	Glass Transition Temperature, (°C)
T_m	Melting Temperature, (°C)
T_{ni}	Nematic to isotropic transition temperature, (°C)
W	Width of tensile test specimen, (mm)

Greek Letters

[η]	Intrinsic Viscosity
ΔL	Change in sample length, (mm)
ε'	Dielectric constant
IV	Intrinsic Viscosity
tanδ	Electrical dissipation factor
Γ	Apparent shear rate, (s^{-1})
ΔP	Pressure drop across capillary tube, (Pa)
ε	Engineering strain
η	Newtonian Viscosity, (Pa.s)
θ	Surface contact angle, (degree)
θ	Monochromatic light scattering angle, (degree)
λ	Wavelength, (nm)
μ	Non - Newtonian Viscosity, (Pa.s)
σ	Conductivity, (S/m)
σ	Nominal Tensile stress, (MPa)
σ_m	Tensile strength, (MPa)
τ	Shear stress at capillary wall, (Pa)
τ	Surface tension, (mN/m)
Ý	True shear rate, (s^{-1})
γ	Shear rate, (s^{-1})
γ_s^{LW}	Nonpolar surface energy, (mN/m)
γ_s^{+}	Cationic surface energy, (mN/m)
γ_s^{-}	Anionic surface energy, (mN/m)
γ_s^{AB}	Acid-base interactive surface energy, (N/m)

CHAPTER I

INTRODUCTION

To produce materials of superior properties is the basic goal of material science and technology. The production of lighter, stiffer and tougher thermoplastic is one of them. Conventional materials, such as asbestos, glass and carbon fiber in thermoplastics have been satisfactory to a degree for industrial, military and home use. Many difficulties occur during processing of these materials, such as viscosity increase, fiber breakage, machinery wearing, high energy consumption. To overcome these difficulties in thermoplastic composites many studies were done to synthesize new materials. Polymers which combine liquid and crystalline properties together (LCPs) have been synthesized from the beginning of last century but relatively new class of synthetic materials called as thermotropic liquid crystalline polymers (TLCP) which have thermoplastic characters were firstly synthesized by Jackson and Kuhfuss (1976) [1]. Since then, many applications of TLCPs have been found.

In conventional organic polymers molecular chains are mainly composed of aliphatic chains and have demonstrated entangled random coils even at ultimate draw down ratio. Contrary to this behavior, LCPs are rigid rod like molecules inherently and do not need post processing for chain alignment. LCPs mainly consist of disc shaped benzyl molecules.

Percent aromaticity & aliphaticity in LCP chain shows itself as strength & processability like a pair of scales in a balance. Researchers' main aim is to balance between these two contrary parts by dwelling on the constituents for valuable

TLCPs then putting them in a matrix. Fiber formation of LCP droplets in thermoplastic matrix depends on viscosity ratio, relaxation time of the coil, droplet size and distribution. Some difficulties occur during processing, shear adjustment in injection molding for exceeding threshold intermolecular force for singular chain separation and orienting.

Besides composite application LCPs have features to be used in pure form such as electrospinning. Micro or nano scale fibers can be obtained via electrospinning of specific thermoplastics and LCPs. Composition, molecular weight and solvent type and concentration determine the phase morphology of resultant product. Depending on morphology, these fibers can be used in many application area, such as nanotechnology, bioengineering, nonwoven fabrics.

The dielectric constants of thermoplastics are largely predictable from composition which determines polar, non-polar nature and find application area in variety of electrical situations such as capacitors. The electrical properties of thermoplastics may also change quite dramatically by the environmental conditions, such as moisture and/or temperature. At this point, LCP as a new material can be employed to solve problems.

Because of economical and application ease, preferred matrices of composites are; acrylonitrile butadiene styrene (ABS), Polyamide (PA6), Polyethylene terephthalate (PET), Polypropylene (PP). They are suitable for composite application but also they have some disadvantages that need to be improved. Due to reactive end groups and polar character of LCP, PET and PA6 blends do not require any additive which is known as compatibilizer. ABS and PP are basically non polar, their adhesion in blends occur via entanglement and needs to be improved by reactive groups such as anhydrides, epoxy, amine, etc.

A wide range of ABS grades can be achieved by acrylonitrile, styrene, butadiene content which contributes to the heat resistance, chemical resistance and surface hardness of the system. Reactive group addition to ABS via compatibilizers can be achieved by styrene-maleic anhydride (SMA), ethyl-butylacrylate-maleic anhydride

(E-nBA-MAH), ethylene-butylacrylate-carbon monoxide-maleic anhydride (EnBACO-MAH).

PA6 has good strength and toughness with fatigue resistance. It is resistant to hydrocarbons, esters, glycols, and alkali solutions. Properties that need improvement are solubility in alcohols and acids, moisture absorption and low dimensional stability.

Superior clarity and barrier capacities of PET make it unique thermoplastics but small amount of moisture makes it more susceptible to thermal degradation. Excessive shear heat should be avoided therefore low screw speed and back pressure are required while processing. Hydroxyl and carboxyl end groups of PET make it suitable for composite application without compatibilizer.

PP has rare properties such as, high impact strength, toughness, low brittleness easy processability, chemical resistance to polar compounds, but it has low thermal resistance and stability. Lack of functional groups is compensated by maleic anhydride functionalized polypropylene (Exxelor PO-1015) as compatibilizer.

In this work, liquid crystalline copolyesters are synthesized and the effects of various constituents to the LCP character are investigated. A structurally systematic approach is carried out to find suitable LCP materials that have low, comparable melting points to common commodity polymers such as PP, PA6, ABS and PET or PEN. The aim was to achieve LCP reinforced thermoplastic composites that can be produced with ease and have superior qualities to glass-fiber reinforced composites. A couple of advantages can be given as lightness, ease of processing and recycling of the LCP composites. As it is known, to recycle glass or carbon fiber reinforced composites are very difficult. The main body of this study is the synthesis of new copolyesters with low T_m, LCP character. For some of the promising LCP copolyesters, applications such as processing aid in fiber formation, reinforcement material in structural composites and use as electrostatic material are tested.

CHAPTER II

BACKGROUND INFORMATION

2.1   Brief History

Polymers which are placed in intermediate state of matter between liquid (isotropic, amorphous) and crystalline (three dimensional order) called as liquid crystalline polymers (LCP). Friedrich Reinitzer (1888) who is considered as the precursor of this field observed that esters of cholesterol have two melting points between which opaque liquids become transparent upon raising the temperature shows colorful and birefringence under polarized light [2]. In addition to generic term of LCP, George Friedel (1922) cleared up the developing terminology and defined nematic, smectic, mesomorphic from Greek vocabulary [3]. Mesos, meaning median interpret the intermediate state between crystal and liquid. Vorlander (1923) pursued main chain LCPs and synthesized co-continuous benzene ring and para-linked esters at different molecular weight but they showed thermoset properties and turns to char without softening. Liquid crystalline domains were recorded in phase (lyotropic solution) of tobacco mosaic viruses by Bawden and Pirie (1937). X-ray diffraction studies (1941) and light scattering measurements (1950) were made on LCP. Flory postulated the factors to induce liquid crystallinity e.g. anisotropy, rigidity, linearity, and planarity [4]. First commercialized LCP, poly aromatic amide (Kevlar) spun from lyotropic sulphuric acid solution at DuPont in 1965. Jackson and Kuhfuss (1976) synthesized moldable aromatic polyesters and defined as thermotropic liquid crystalline polymers (TLCP) which have thermoplastic characters [1]. In the 1960s,

4

the electro optical property of LCP was discovered and first major application on display technology was identified in the following years [3].

Mechanical, thermal and rheological properties of LCPs make it useful in industry. Several application area can be listed as reinforcing agent in composites, electrical connectors, capacitors, disk drives etc. Whilst industrial markets demand various TLCP types, leading LCP manufacturers currently produce only about 10 000 tones/year which represents a small fraction of global annual polymer production [3]. The difference between supply-demand is one of the processing difficulties results, e.g. high and homogenous process temperature needed, weld line distortion may occur during molding. Most manufacturers are offering their own LCP variations in a kind of monopoly such as. Kevlar, Zenite (DuPont), LC (Rodrun), Xydar (Solvay), Vectra (Ticona).

The structural model for perfectly aligned and straight polymer crystals is firstly proposed by Staudinger. Synthesis of high temperature resistant aromatic heterocyclic polymer systems began in the 1950s, and proceeded to the synthesis of ladder-like polymers. However, the actual development of such fibers has been relatively slow until 1970s when DuPont commercially manufacture the new polyaromatic amide fiber under the trade name Kevlar This simple graph summarizes the importance and place of LCPs among the synthetic materials (Figure 2-1).
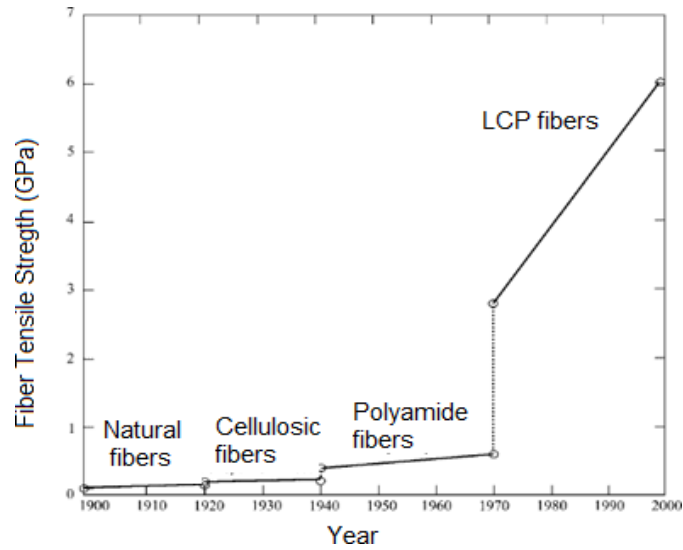
Figure 2-1 History of the development of polymer fibers and place of the LCP

2.2 Application Area

Depending on the type of LCPs they have wide application areas from electronic to composite application. The strongest motivation for exploring high performance materials was provided by the aerospace industry. It generated needs for novel polymer fiber and composites products with better properties and lower weight to be used in structural composites. The field of high performance polymer fiber developed quickly in the 1970s and 1980s. Using unique and superior properties of LCPs in the composites to enhance thermal and engineering resins have been conducted since 1980s [5-12].

The unique feature of LCPs is high orientational order retained in the solid state that has remarkable mechanical properties and thermal stability of fibers from precursor polymer in structural applications where weight savings are critical. The technology for the formation of highly oriented lyotropic LCPs from anisotropic polymers is feasible, however, biaxially oriented films and other shapes of it still under development. Moreover, novel processing might make thermotropic LCPs eligible for crucial structural applications. The feature of LCPs is itself problematic in the current understanding of processing with control of features e.g. anisotropic thermal expansivity and transport anisotropy even carefully designed. The exploit of

6

features of liquid crystallinity will be retarded until there is a detailed understanding of how processing promotes morphology in conjunction with how molecular structure affects the mechanical and the unusual physical properties of these new classes of polymers [13, 14]. The combination of moderately high strength and modulus extension of LCP gives a very high energy to break, or work of rupture when compared with the other fibers that opens wide application areas where high performance candidates are needed (Figure 2-2).
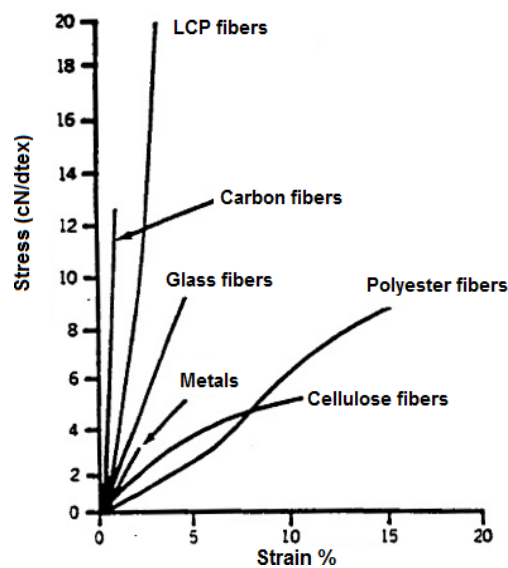
Figure 2-2 Strength of LCP fibers and others as a function of % strain

In textiles, the strength of a fiber is measured based on deci-text (dtex) units (Figure 2-2) that is related with diameter and corresponds to weight in grams of a 10km length of the fibre.

In the first glance, LCP word remind the electronic screens for many people, actually it has wide application area in this sector. Due to enantiomeric structures of smectic LCPs, they have optical properties, piezoelectricity, and pyroelectricity that make it a candidate as a high technology material. As a specific example, smectic C side chain LCPs has ferroelectric behavior and widely used in thermochromic application such as electronic device screen[15].

Another important property of LCP copolyesters is their use as low diffusivity material the medical vacuum test tube and food packing applications.

2.3 Molecular Order and LCP Types

Long range order of 'rod like' or 'plate like' benzene and derivatives in polymer longitudinal axis builds mesophases (Figure 2-3). Depending on mesophase size and order three types of LCPs are defined; nematic, smectic, cholesteric (Figure 2-4). Whilst one dimensional organization creates nematic LCPs, two-dimensional organization creates smectic LCPs and three dimensional organizations creates discotic and cholesteric LCPs. In nematic LCPs bond energy between atoms determines LCP properties. In smectic LCPs in addition to the primary forces, secondary forces have importance, interaction between the chains of a mesophase that are quite larger than those between the layers, and fluidity results from the relative slipping of these layers. In cholesteric LCPs in addition to the forces mentioned above, interactive forces between layers is so high that prevent slippage on each other and are infusible, may soluble depends on conditions and solvents. At this point LCPs are needed to be classified as melt processable or soluble, referred as thermotropic and lyotropic respectively. In thermotropic LCP, the formation of mesophases is temperature-dependent; as for lyotropic liquid crystals, they necessitate the use of a solvent for forming mesophases. In addition to temperature and solvent dependence of LCPs they are also sensitive to other stimuli such as magnetic, electric fields and pressure to generate mesophases.
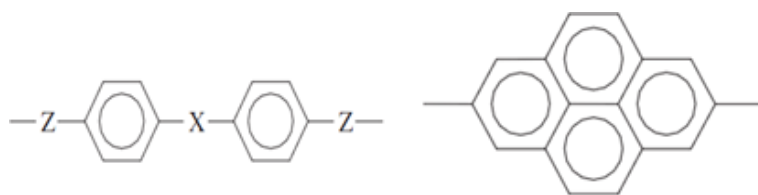
Figure 2-3 Rod like and plate like mesogens
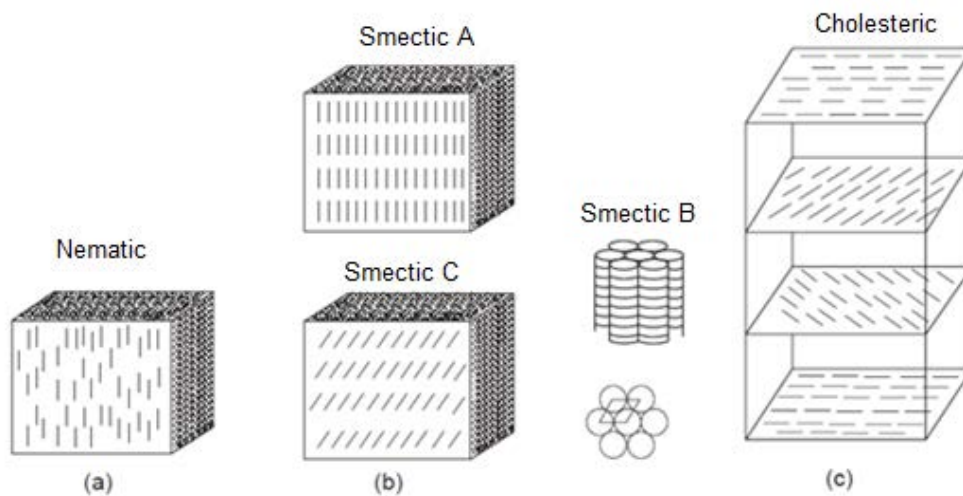
Figure 2-4 Mesogen alignments within LCP types: (a); nematic, (b); smectic ; (c) ;cholesteric [16].

The least ordered form of LCP is nematic mesophases (N) that shows only a one dimensional order (Figure 2-4a). From simple to complex LCP types variables increase that brings sub species (Figure 2-4b), where eight different smectic phases were found. Smectic A(SA) is characterized by a random lateral distribution of mesogens even if their longitudinal axis is perpendicular to the layer plane. When hexagonal order of mesogens within the layer is found it is referred to as smectic B (SB). If layers are tilted at specific angle θ with respect to the axis perpendicular to the layer new there are several packing possibilities and smectic groups are created as SC, SE, SG, SH and so on that are known for their ferro and piezoelectric properties.

Cholesteric phase can be defined as chiral nematic (N*) phase due to the director of twisting about the axis normal to the molecular orientation, (Figure 2-4c). The distance over helical length when molecular director turns 2π is defined as length of helix pitch, P (Figure 2-5). Depend on turning characteristics of this helix, iridescent colors scatters when exposed to polarized light [16].
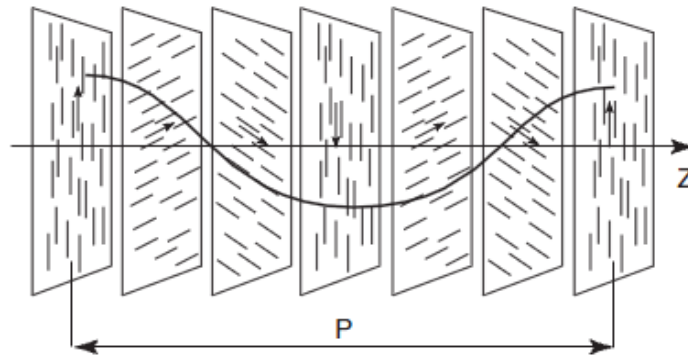
Figure 2-5 Representation of "cholesteric." phase

Classifications of LCPs have been proposed in a wide range and a few of them mentioned above. Another categorization of LCP is depends on type of mesogen attachment to backbone that defined as main-chain and side-chain LCP (Figure 2-6) [15].
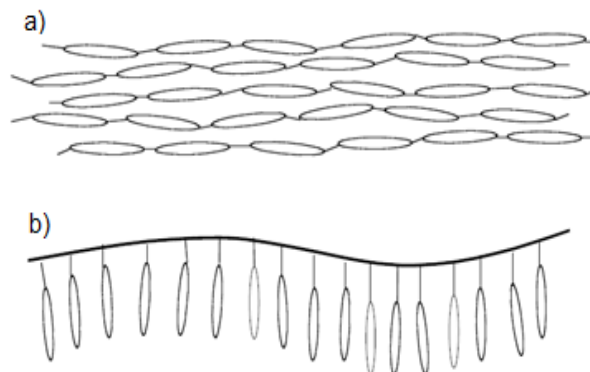
Figure 2-6 Mesogen sequences in a) Main-chain LCP b) side-chain LCP

2.3.1 LCP in 3D Dimension

LCP chains are generally shown as rigid rods in two dimensional flat surfaces. To understand conformation and position of chain in bulk form, a few smectic LCP is studied and schematized. One of them is composed of biphenly and methylene spacer with simple and linearly high symmetrical structures (Figure 2-7) [17].
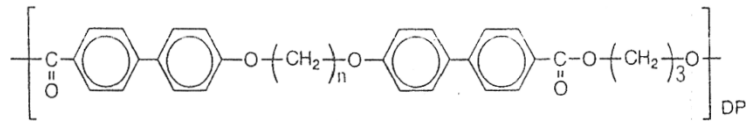
Figure 2-7 A Smectic LCP, composed of biphenly and methylene flexible spacer

In addition to conformational restriction, another effect can be considered, on the smectic structure in the main chain type of polymer in which the two different alkylene spacers are sequenced in a regularly alternate fashion. If the two spacers are incompatible satirically and if there is sufficient lateral attraction between identical spacers of adjacent polymer molecules, segregation into a bilayer may occur. Conformational restriction and interaction forces between neighboring chain brings unique holozoic shapes that has periodicity and shown as c-director (Figure 2-8).
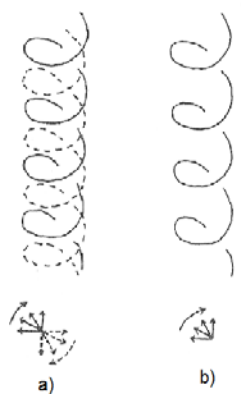
Figure 2-8 Schematic illustration of arrangement of c-directors in a) chiral ScA and b) chiral ScC phases of LCP (Figure 2-7) chains

As a result of coupling with the conformational constraints in the structure (Figure 2-7) four possible types of bilayer structures (Figure 2-9) will arise in the molecular order.

11
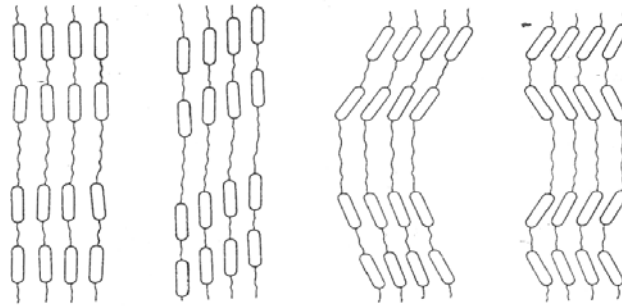
Figure 2-9 Four possible smectic structures with the bilayer modifications that may be formed in the main chain polymers of LCP (Figure 2-7)

Space geometry of LCP mentioned can be generated by using possible smectic structures and X-ray studies (Figure 2-10). However this highly ordered periodicity cannot be reached in the most LCPs that are not suitable for space geometry dissolution by X-ray analysis or any other traditional techniques.
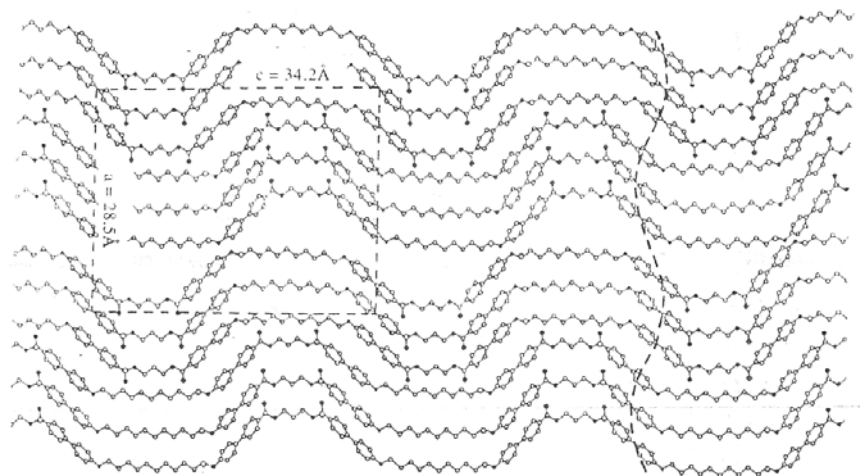
Figure 2-10 A structural model of LCP (Figure 2-7), polymer chains are assumed in all-trans conformation [18]

2.3.2 Temperature and Order Relation

The temperature and structure relation shows variation in LCP types such as some chiral liquid crystals, as the temperature is increased, exhibit the order change in mesophases from smectic-A, to cholesteric than isotropic phases (Figure 2-11) [19]. During transition, at visible temperature range it exhibits Bragg reflection at the

wavelength λ=ηxP where η is the average refractive index of the material and P is pitch of the cholesteric phases. These types of LCPs are called as thermochromic and they are capable of reflect the visible light as in the electronic device screens.
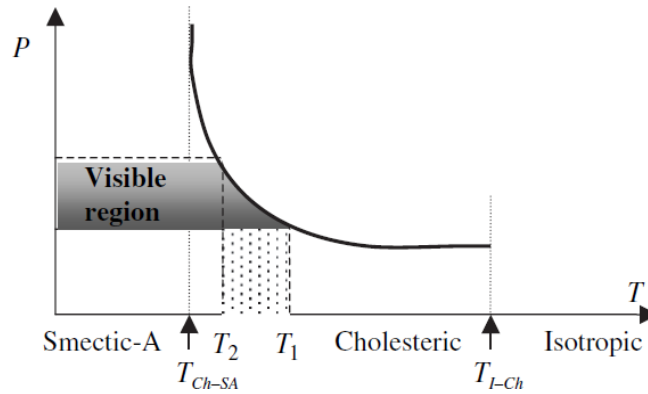
Figure 2-11 Transition of mesophase order in the thermochromic LCP as a function of temperature [19]

However less ordered thermotropic nematic LCPs have simple transition with temperature, from solid to nematic and then isotropic liquid (Figure 2-12). These types of LCPs are capable of reflecting polarized light between clearing temperature and melting temperature so called 'liquid crystalline phase'.
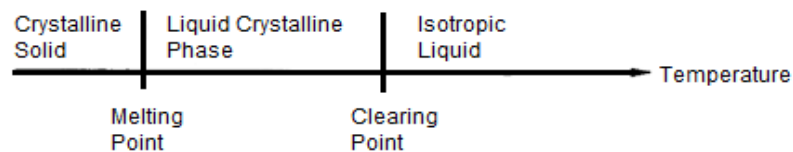
Figure 2-12 Nematic LCP phase transitions as a function of temperature

2.4   Tailoring of Thermotropic LCPs

All LCPs which has commercial value has higher processing temperature (above 300 °C) than the most engineering thermoplastics. The processing of these LCPs with conventional plastics requires new processing equipment and techniques. Accordingly, to produce low melting point of LCPs gain importance for composite applications with conventional processing techniques. There are several ways to

achieve the structural disorder effects in rigid-rod LCPs leading to lower melting temperatures such as i) random copolymerization, ii) Inclusion of kink groups, iii) inclusion of flexible segments, iv) inclusion of pendant groups, where moieties are connected each other with the linkage groups that are listed in Figure 2-13.
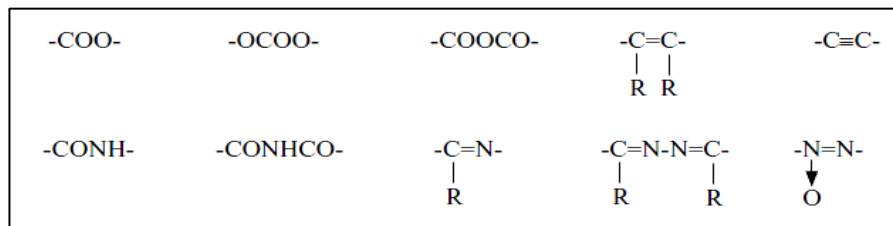
Figure 2-13 General linkage groups in LCPs [20]

i) Random copolymerization of unsymmetrical and symmetrical collinearly bonded structural units along the main chain disturbs periodicity and inhibits crystallization that depress melting point (T_m). Stable LCPs can be synthesized by copolymerization in thin film method [21-25]. If periodicity is disturbed by copolymerization of monomers with different length and side steps (crank shaft) together, it can be exemplified as in the Figure 2-14.
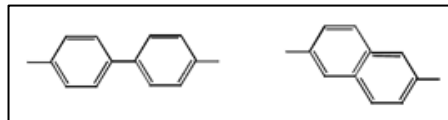
Figure 2-14 Different length monomers with linear and side-step growing capacity

ii) Inclusion of angular moiety so called kink into the polymer backbone effectively reduces the regularity of the LCP, and thus lowers the T_m. The incorporation of kink units has unfavorable influences such as the disruption of the molecules is unfavorable for the thermal stability of the LCPs [20, 26-31]. Some schematized kink groups can be listed as in Figure 2-15.
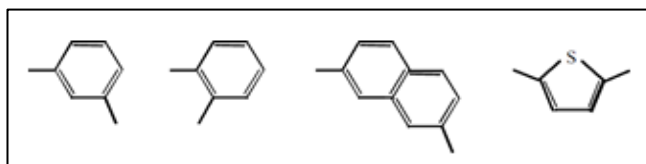
Figure 2-15 Kink groups using in the backbone of the LCPs

Meta linkage can introduce a kink in LCPs such as *m*-acetoxybenzoic acid (mABA) and isophthalic acid (IA) are extensively employed to modify LCPs. However IA content should be lower than 26% to preserve LCP properties [32]. The thin-film polymerization with m-ABA indicate that the LC phase may still be observed even when the m-ABA content is as high as 66 mole% however, preferred content of it should be less than 33 mole% for mechanical properties [25]. Phthalic acid and o-acetoxy benzoic acid are also kink groups but LC phases of them is not suitable for stable mesophases [33].

iii) Modification with Flexible Segments is another strategy to synthesize the melt processible semirigid polymers. This method applied by inserting flexible segments to separate the mesogenic units along the polymer chain. By this way, random distribution of the chain increases together with the mobility of the chain, thus T_m decreases. However thermal stability of the resultant polymer decreases with the mole % of the flexible spacers. This leads to appreciable decrease in melting and isotropization temperatures but also reduces the mechanical strength and the thermal stability of resulting polymers unless spacer length is kept short. The most typical segments used in this area is polymethylene $(CH_2)_n$ with varying length [34, 35]. Flexible spacer linkages using in the LCP backbone are exemplified in Figure 2-16.

$$-(CH_2)n- \qquad -(CH_2O)n- \qquad \overset{\displaystyle -(CH\ CH_2)n-}{\underset{R}{|}} \qquad \overset{\displaystyle -(CH\ CH_2O)n-}{\underset{R}{|}} \qquad -O-$$

$$\overset{R}{\underset{|}{-(SiO)n-}} \qquad \overset{H}{\underset{|}{-(SiO)n-}} \qquad \overset{\displaystyle -N(CH_2)nN-}{\underset{R \qquad R}{|\qquad |}} \qquad -S(CH_2)nS- \qquad -S-$$
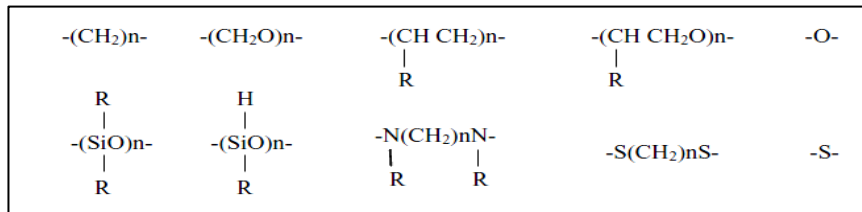
Figure 2-16 Flexible spacers using in the backbone of LCPs

This approach is applied in PET/p-ABA random copolyesters (X7G, Rodrun), which can be regarded as thermotropic copolyesters containing short 1, 2-ethylene spacers between rigid terephthalate and 4-oxybenzoyl moieties.

iv) Inclusion of lateral groups (pendant) effectively increases the interchain distance and reduces the interchain forces so that the efficiency of the chain packing is reduced. The use of unsymmetrically substituted monomers, resulting in a random distribution of head-to-head and head-to-tail structures in polymer chains, further helps in disrupting regularity. However, randomness of the polymer chain decreases the crystallinity so much that formation of LC is generally unfavorable [3, 35]. Effect of pendant group linearly grows with the size, such as bulky fluorine atom deteriorate LC phase [36]. Some pendant groups in LCPs are listed in Figure 2-17.

$$-R \qquad \qquad -\hspace{-4pt}\bigcirc \qquad -Cl \qquad -OR$$
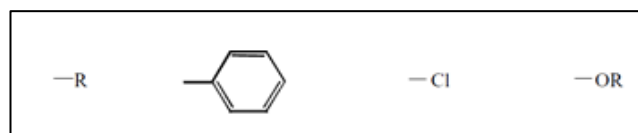
Figure 2-17 Lateral groups used in the LCP synthesis

Synthesis of nematic LCPs with flexible spacers and PET based types together with the use in ternary blend systems studied by the few scientists. The ease of melt processing is proportional with alkyl groups in polymers and should not exceed optimized values in formulation to protect LCP properties [37-50]. In Synthesis of low T_m polymers with linear p-acetoxybenzoic acid, torsional mobile hydroquinone and kinked m-acetoxy benzoic and isophthalic acid (IPA) together disturb the nematic structure so much and that prevent the formation mechanically improved LCPs for composite applications [51-53].

2.5   Commercial LCPs

Some commercial LCPs can be categorized by tailoring (modification) procedure. As mentioned in LCP tailoring section, side group inclusion not preferably used for high performance engineering LCPs. Other modification techniques are exemplified on some trademarks Figure 2-18.
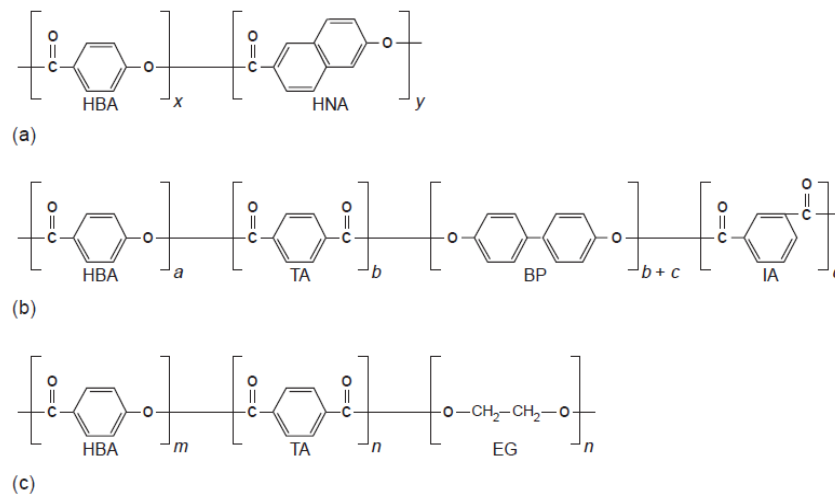
Figure 2-18 Commercial LCP structures and sources

Modification technique, firms, and trade names of corresponding LCP products in Figure 2-18 are listed below.

a) **Modification technique:** Random copolymerization,
    Firms: Hoechst Celanese Corporation
    Trade names: Vectra A and C

b) **Modification technique:** Kink groups with random copolymerization:
    Firms: Dartco, Amoco, Nippon Petrochemical, Sumitomo, Toyo Soda
    Trade names: Xydar SRT 300 and 500, Ekonol, MA, HB

c) **Modification technique:** Flexible segments with random copolymerization
    Firms: Eastman Kodak, Unitika, Mitsubishi, Demits
    Trade names: X7G, X7H, Rodrun, EPE, LCP2000

17

From up to down in thermotropic LCP in Figure 2-18, mechanical performance, and processing temperature decreases together. Vectra trademark is the only fully aromatic polyester LCP that can be melt processed and produced as a result of more than 15 years of dedicated study and work in the Celanese Corporation Laboratories.

Vectra B, for example, has a melting point of 280°C and is processed at approximately 320°C [54]. Commercial LCPs with 80% p-ABA and 20% content PET can reduce viscosity of poly(ethylene naphthalate) and polycarbonate effectively at 300°C, however due to the high temperature, mechanical properties of thermoplastic alone decreases, nevertheless an increase the mechanical properties of the blend is observed [55, 56]. The processing temperatures of these materials are still higher than degradation temperatures of most thermoplastics. New modification techniques with a different concept are needed.

2.6   Synthesis of Nematic LCPs

Polyesters based LCPs are important series of main-chain thermotropic LCPs and synthesized by polycondensation reactions. The transesterification reactions start above temperature 240 °C with phenyl esters of diacids with acetylated aryl diols. To increase the reactivity between acid (-COOH) groups and hyroxly (-OH) groups of monomers, OH side have to be acetylated before conducting the polycondensation reaction [14, 57, 58].

In order to prevent oxidation, the polymerization is conducted under inert atmosphere generally nitrogen or argon gases. The melt becomes turbid when low melt viscosity oligomers appear, due to the fluctuations of the mesogenic domains in the visible range. Vacuum is then applied gradually to the reaction system to further remove the by-products such as acetic acid from the melt to increase molecular weights. A high speed with high torque stirrer is desirable in order to facilitate the diffusion process.

On the other hand, mixer creates shear flow on high molecular weight mesophases and 'shear whitening' is observed that gives information whether the reaction

succeeded in LCP synthesis or not [58]. In the polycondensation reaction of polyesters there are six main reactions occur together. The reactions used in polyesterification were classified by Solomon, and Pradet and Marechal (Figure 2-19) [59-61].

Direct esterification of alcohols with carboxylic acids:

$$ROH + R_1COOH \rightleftharpoons R_1COOR + H_2O$$

$$ROH + (R_1CO)_2O \rightleftharpoons R_1COOR + R_1COOH$$
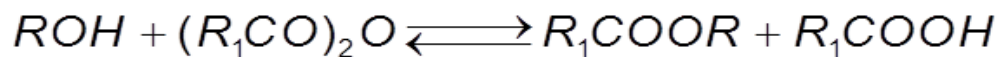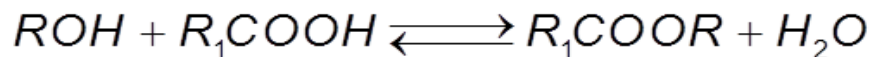
Self-condensation of hydroxyl acids:

$$nHO - R - COOH \rightleftharpoons HO(R - COO)_{n-1}RCOOH + (n-1)H_2O$$
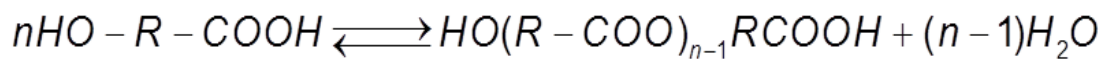
Ester interchange reaction has three sub reactions:

Alcoholysis:

$$ROH + R_1COOR_2 \rightleftharpoons R_1COOR + R_2OH$$

Acidolysis:

$$RCOOH + R_1COOR_2 \rightleftharpoons RCOOR_2 + R_1COOH$$

Ester exchange:

$$R_1COOR_2 + R_3COOR_4 \rightleftharpoons R_1COOR_4 + R_3COOR_2$$
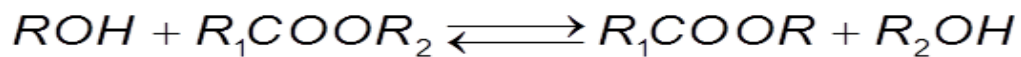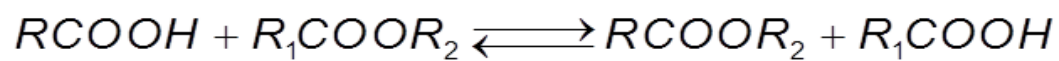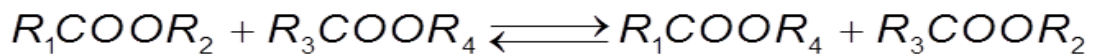
Figure 2-19 Main polycondensation reactions

2.7 Loss of Stoichiometry

There are a few handicaps that cause to lose stoichiometry and should be surmounted to synthesize LCP by ester exchange condensation reaction. Decarboxylation, back-biting reactions, sublimation, insufficient mixing, acidolysis, alcoholysis, are the major factors that deteriorate the stoichiometric ratio [62]. Accordingly, they are mentioned above and following section.

- Sublimation of hyroquinone based monomers occur linearly with vacuum and temperature [63].

- Inefficient mixing causes to delay the removing the acetic acid from reaction mixture that delay the reaction time. This phenomenon may bring more side product under possibly occurring side reaction.

2.7.1 Decarboxylation

Decarboxylation is a kind of decomposition of aliphatic diacids with heat (Figure 2-20). Increase in the length of carbon chain of the acid increases its stability to the action of high temperature [64].
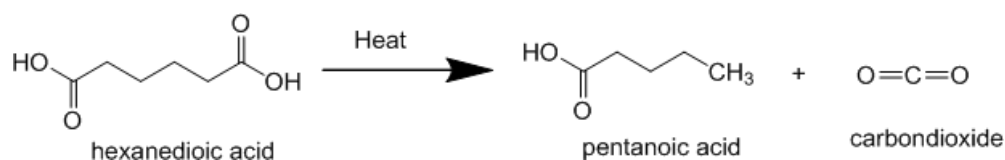
Figure 2-20 Decarboxylation of hexanedioic acid to side product and carbon dioxide

Generally polycondensation reactions of polyesters are takes place between $200^{\circ}C$-$300^{\circ}C$, thus octanedioic and decanedioic acids are appropriate for this purpose (Table 2-1).

Table 2-1 Decarboxylation temperature and melting temperature of aliphatic diacids

Diacids	# of Carbons	Melting Temp. ($^{\circ}C$)	Decarboxylation Temp.($^{\circ}C$)
Propanedioic acid	3	135	140
Butanedioic acid	4	185	160
Hexanedioc acid	6	152	200
Octanedioic acid	8	140	300
Decanedioic acid	10	130	350

As melt condensation copolyester synthesis is favorable above $250^{\circ}C$, diacids less than eight membered carbons need to be put reaction under mild condition to prevent decarboxylation. For this purpose hexanedioic acid and butanedioic acid are replaced by hexanedioyl dichloride and butanedioyl dichloride respectively. Unfortunately copolyester synthesis by chlorinated alkyl is scarce in literature and

different types of solvents and catalyst need to be tried for inclusion of them in LCP backbones [65].

2.7.2 Back-biting Reaction and Cyclic Products

If diols in polyesters have more than two CH_2 group as in the butanediol or hexanediol back-biting reaction above $270^{\circ}C$ is possible and cause to loose stoichiometry as in the Figure 2-21.
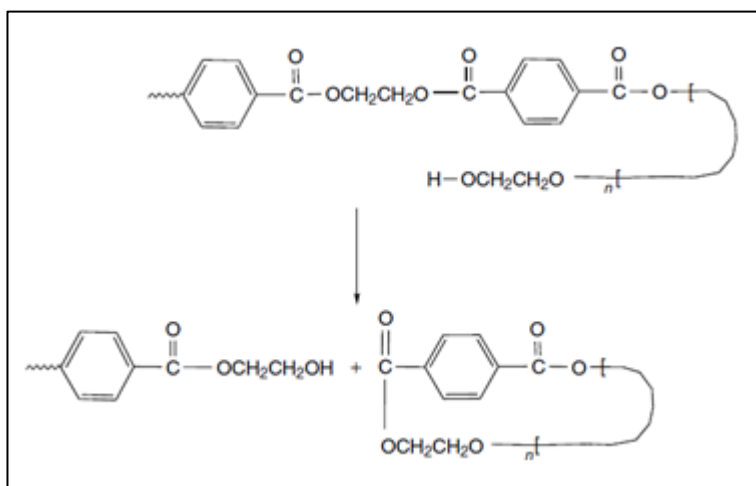
Figure 2-21 Back-biting reaction of diols in polyester

Etherification of ethylene glycol to form dietylene glycol leading to dioxane is an important side reaction in PET synthesis and take place as in the (Figure 2-22) [66].
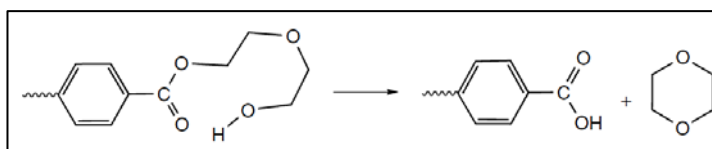
Figure 2-22 Mechanism for the formation of dioxane

Excess butanediol is necessary to compensate for the undesired to tetrahydrofuran (THF) plus water in polybutylene terephthalate (PBT) synthesis (Figure 2-23) [62]. However, because of stoichiometric importance in the reactant in LCP synthesis excess usage is not possible.
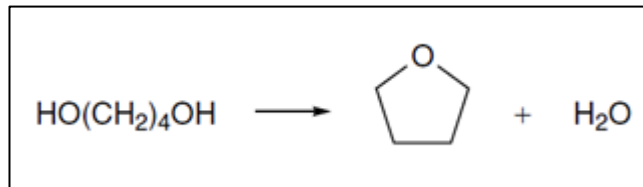
Figure 2-23 Butanediol side reaction gives THF and water[62]

2.8 Polymer Matrix

Polymer blends are mixtures of at least two polymers and generally processed in melt form. The main reason of blending is to get lower-cost material with equal or higher physical and chemical properties than the constituents. Blends of Acrylonitrile-butadiene-styrene (ABS) together with polycarbonate (PC), polyvinyl chloride (PVC), and poly ethylene terephthalate (PET) are currently dominating the markets.

Poly (acrylonitrile-butadiene-styrene) (ABS) terpolymer consists of a two-phase system in which polybutadiene phase disperses as fine particles in continuous styrene acrylonitrile matrix. In ABS, acrylonitrile contributes to the chemical and heat resistance, together with surface hardness of the system. In addition, styrene component improves the processability, rigidity and strength whilst butadiene increases the toughness and impact strength. The overall properties of ABS are determined by the ratio of monomers present in the system that brings several grades of ABS with different impact strengths in the markets. However ABS has some drawbacks that need to be improved such as low thermal stability and low mechanical properties when compared with the engineering plastics.

Polyamide6 is used in a wide range of engineering applications and present combination of good processability together with mechanical properties. However, Nylon 6 suffers from poor toughness and low dimensional stability.

Due to the promising superior combinational properties of ABS/PA6 blends such as good mechanical and impact strength, high modulus, heat resistance, chemical

resistance and abrasion resistances they are in the scope of scientific and technological interests.

2.9   Nematic Reinforcing Agents

In contrary to classical composites, morphology of in situ composite is more complicated and explanation of each section is related with each other. Generally in the composite studies, the properties of matrix, reinforcing agents and composites are represented in a sequence. To comply with this rule, formation of fully extended nematic forms of LCP, which represent reinforcing agent in the matrix, is examined in this section.

Oriented solids like nematic state formation from quasi-isotropic melt is facilitated by stress induced shear forces applied in the process. In melt spinning, high shear rates is applied to melt polymer stream and fully extended nematic chain can be observed. However, in in situ composite varying shear rates with respect to fiber spinning causes differently extended nematic structure formation that depends on the position such as in the core and shell. In the ideal case of in situ composite the shear applied to LCP polymer melt forces to quasi-isotropic random coil to align and orient in the flow direction during processing (Figure 2-24).

During orientation chains stack together in fibril form which reduce intermolecular distances and increase interaction between chains. By this way cohesive energy of the system increases and brings improved mechanical properties [67]. If LCP chain is distorted so much by inserting flexible spacers at the expense of lowering the T_m, the structure of it lose the continuity and will start to resemble to PET (Figure 2-24).
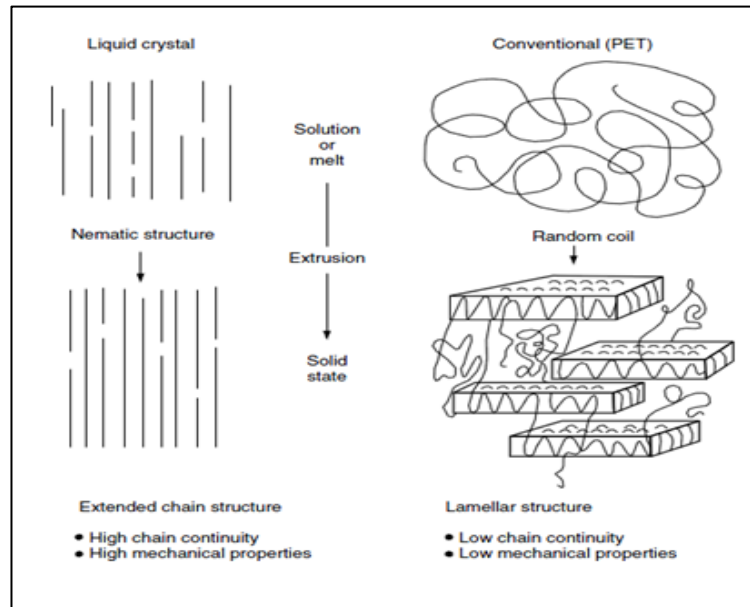
Figure 2-24 Structure development of LCP and PET under shear [67]

2.9.1 LCP Rheology and Blends

Since the main characteristic of TLCPs is the persistence of rigid rod order in the material even after the stresses causing shear deformation are removed, the rheological behavior of them is different from other conventional flexible coil polymers. Several factors are known to influence the fibrillation of LCP domains in the LCP/thermoplastic blends. These include melt viscosity ratio of LCP to polymer matrix (η_d/η_m), shear flow fields encountered during processing, aspect ratio of deformed droplets (L/d), capillary number (Ca), LCP concentration, processing temperature, miscibility and compatibility between the LCP and thermoplastics [68-99].

2.9.1.1 Viscosity and Shear

Among mentioned factors, melt viscosity ratio plays a decisive role in the development of oriented fibril morphology in the LCP/thermoplastic blends. Oriented LCP domains in the flow direction also lubricant effect on the blend and they ease

the flowing in the process [5-7]. The viscosity and shear rate relational behavior of LCPs is simulated by three distinct regions during flowing (Figure 2-25) [100, 101].

i) Shear thinning region at low shear rates

ii) Newtonian region in an intermediate shear rate region

iii) Power-law shear thinning region at high shear rates

That is, for a given fluid system, the droplet deformation is expected to increase as the droplet to matrix viscosity ratio (n_d/n_m) decreases and local stress (σ) increases.

However, these three flow regions may not fit to every LCP type [102]. In the Figure 2-25 shear rate increases continuously in flow direction on LCP droplets with different viscosity ($\eta 1 < \eta 2 < \eta 3$) and assumed to pass three distinct regions mentioned above [103].
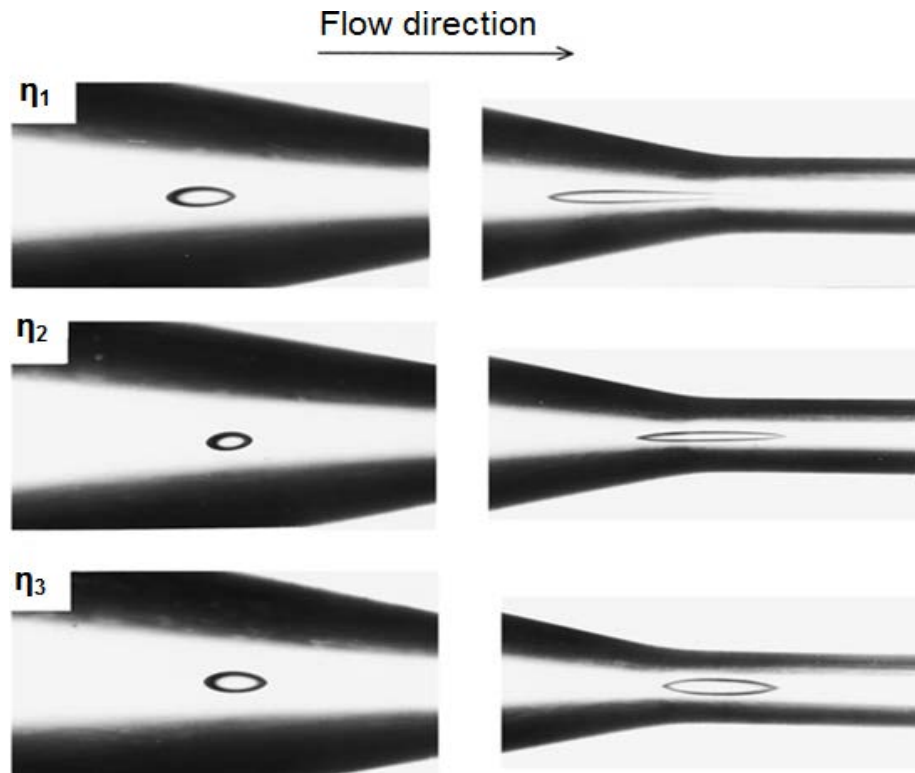
Figure 2-25 Deformation of droplets with different viscosity ($\eta 1 < \eta 2 < \eta 3$) at the entrance of a die [104]

The viscosity notation η in the Newtonian region is changed to μ in the non-Newtonian region. Where viscosity and shear rate conditions of two immiscible liquids is expressed by the following modified power-law equations [103]. Conditions can be listed as; constant viscosity for shear rate lower than critical shear rate of droplet or critical shear rate of matrix but exhibits power-law type dependence of viscosity on shear rate higher than that. Viscosity of surrounding liquid:

$$\mu(\dot{\gamma}) = \begin{cases} \mu_{m0} & \text{for} \quad \dot{\gamma} \leq \dot{\gamma}_{mc} \\ K_m \dot{\gamma}^{n_m - 1} & \text{for} \quad \dot{\gamma} \leq \dot{\gamma}_{mc} \end{cases}$$

Viscosity of drops:

$$\mu(\dot{\gamma}) = \begin{cases} \mu_{d0} & \text{for} \quad \dot{\gamma} \leq \dot{\gamma}_{dc} \\ K_d \dot{\gamma}^{n_d - 1} & \text{for} \quad \dot{\gamma} \leq \dot{\gamma}_{dc} \end{cases}$$

m and d denote matrix and droplet respectively. $\dot{\gamma}$ shear rate

μ_{m0} : viscosity of medium at zero shear rate

$\dot{\gamma}_{mc}$: critical shear rate for medium

$\dot{\gamma}_{dc}$: critical shear rate for droplet

Detailed description of the convergence of the morphological analysis of the two phases can be found in papers [55, 91, 103-106].

As a basic rule shear stress and viscosity should be adjusted together and viscosity ratio of the dispersed LCP phase to the thermoplastic matrix (η_d/η_m) to be lower than 1 at rest. If the viscosity ratio is 0.01 or smaller at the die region the fibrillation is favored. [10, 12].

2.9.1.2 Relaxation time

Contrary to traditional thermoplastic LCPs have two relaxation times;

   i)   Relaxation time of the stress
   ii)   Relaxation time of the nematic form to polymer coil

As 'relaxation time of the nematic form to polymer coil' is longer than 'relaxation time of the stress' extended chain achieved during processing will retained in the solid state [107].

2.9.1.3 Aspect ratio

During the phase transition under shear, quasi-isotropic phase and anisotropic phases coexist and have different dimensions. In the lattice model of the Flory, the aspect ratio is defined as L/d, in which L is the length and d is the diameter of the

coil. The predicted critical axial ratio (L/d) for the phase transition from coil to extended structure is 6.4 in many thermotropic LCPs [108].

2.9.1.4 Concentration

Phase transition from quasi-isotropic phase to anisotropic extended phases also depends on concentration. If concentration of the droplets present in a matrix is below critical value, dispersed phase cannot reach the critical droplet size with radius (r_0). As droplet size get smaller shear rate needed for the deformation of this droplet to extended chain increases. However excess LCP content brings another disadvantage, at which LCP domains tend to coalesce into a sheet like structure rather than dispersed phase.

2.9.1.5 Capillary number

The governing factors for droplet breakup in the equation are the viscosity ratio, the type of flow, and Capillary number. 'Fluid flow induced by surface tension' so called 'Capillary number (Ca)' equation below shows the relation between viscosity(η), shear rate($\acute{Y}$) and surface tension(τ) [103, 109]. In the equation, r is the drop radius of LCP melt prior to deformation.

$$Ca = \frac{Hydrodynamic\ Stress}{Interfacial\ Stress} = \frac{\eta\,\overset{*}{\gamma}}{\dfrac{\tau}{r}} \qquad (2\text{-}1)$$

There is a critical capillary number, beyond which the droplet can no longer sustain further deformation, and it breaks up into a number of smaller droplets. If Ca is small, the interfacial forces dominate, and a steady drop shape develops.

2.10 Compatibilization

In a polymer blend system, miscibility of the component polymers obeys the law of mixing and defined by equation below.

$$\Delta G_m = \Delta H_m - T\Delta S_m \qquad\qquad\qquad\qquad (2\text{-}2)$$

ΔG_m: Gibbs free energy, ΔH_m: Enthalpy, ΔS_m: Entropy change, T is temperature in Kelvin.

In the polymer blends, entropic change is significantly small. Interactions between the two components, such as hydrogen bonding and the formation of ionic bonds determine miscibility, therefore, they are required to produce sufficient heat of mixing to make the blend thermodynamically miscible. Most polymer blends are immiscible and a two-phase system exists with little or no interphase compatibility. In the incompatible blends, there are a few basic morphological structures envisaged for the minor component such as particles, fibrils and an interpenetrating network.

LCPs blends also suffer from poor adhesional strength between the LCP phase and the thermoplastic matrix. Forming cross-linkable LCP blends such as polymer brush connection to main backbone is one of the ways to overcome weak adhesion but no general way exists [110, 111].

Compatibilization is morphology improvement of the blends or composites by the specific additives which has interfacial adhesion activities on constituents. With the higher adhesion composite surfaces get more uniform well dispersed and fibrillar structures allows less fiber pullout from the matrix. Compatibilization has also been reported to improve the tensile strength of in situ composites because of improved adhesion between the two polymer phases. Not only have improvements in strength and modulus been reported, a reduction in anisotropy can also occur with the use of compatibilizers in LCP/thermoplastic systems.

LCP blends with ABS are immiscible due to the polar structure of LCP; therefore simple blends of LCP, ABS and PA6 do not exhibit desired properties. These systems have better heat and solvent resistance than the ones with reversed morphology. However, to preserve the ABS generated toughness in a wide range of conditions, the ABS phase should also be continuous. Thus, co-continuity of phases has been the preferred morphology of these blends and produced by

29

compatibilizers (Figure 2-26 and Figure 2-27) with reactive sides such as epoxy and maleic anhydride (MA) [112-120].
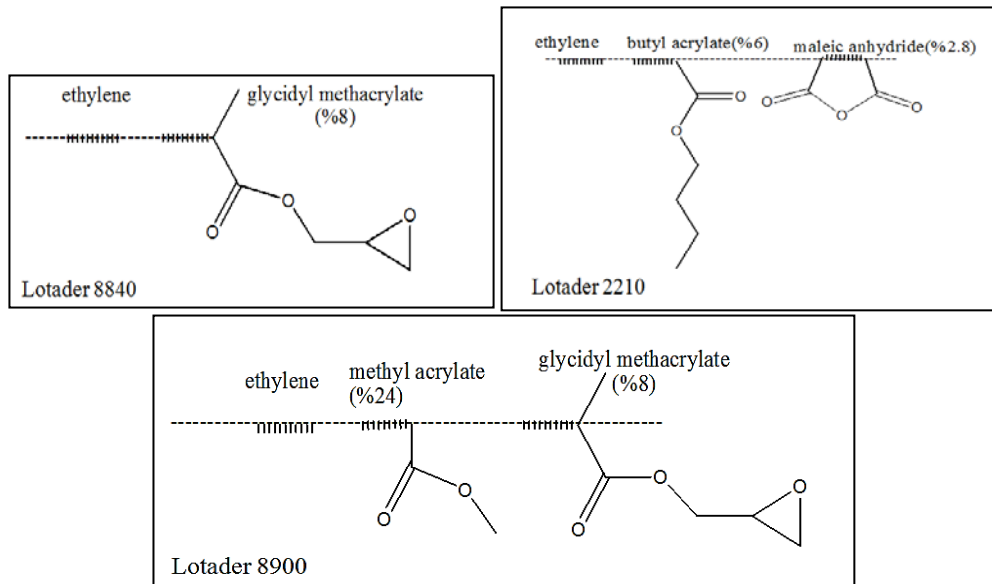
Figure 2-26 Compatibilizers have acrylate group together with epoxy and MA
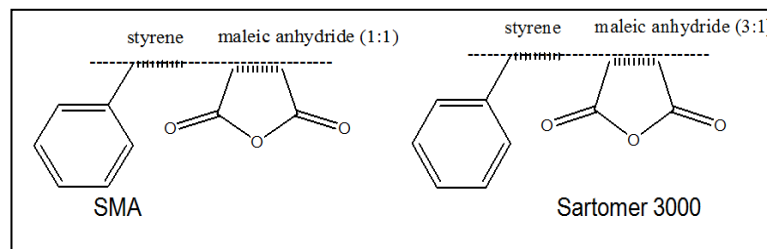
Figure 2-27 Compatibilizers with maleic anhydride group

The maleic anhydride (MA) and epoxy functional group can react either with the amide group of Nylon 6 , or with the hydroxyl group of LCP during processing, thereby forming graft polymers at the interfaces. Such graft forming polymers act as effective compatibilizers for the ternary blends of Nylon 6/ABS/LCP blends Figure 2-28 and Figure 2-29.
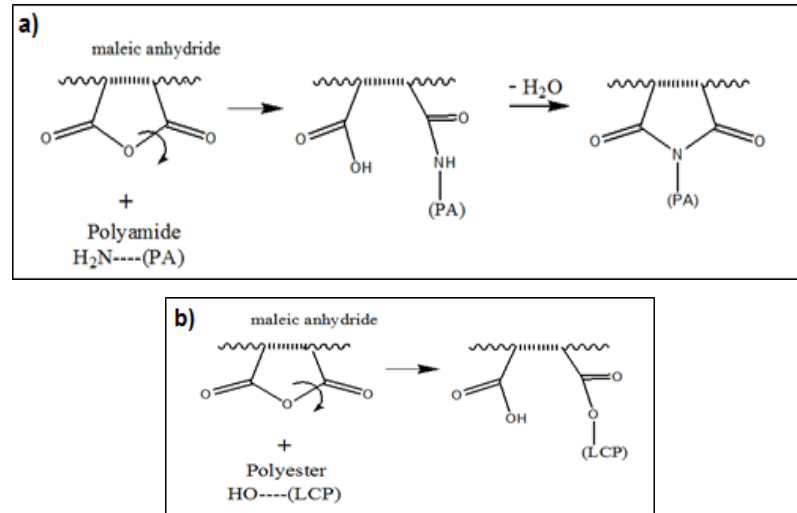
Figure 2-28 Possible reactions between PA (a) and LCP (b) with the MA group of compatibilizers
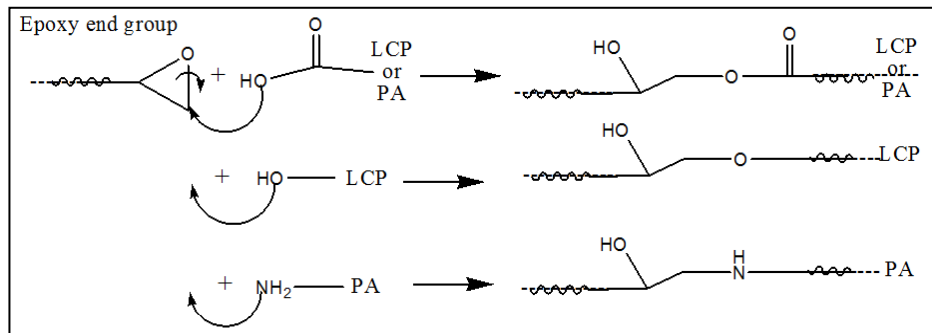
Figure 2-29 Possible reactions between LCP and PA with epoxy end groups

2.11 In situ Composite Processing

Composites materials are composed of at least two phases and called as matrix and reinforcing agent. The main reason of composite is to get weight reduction with improved mechanical properties of the materials [121-123]. One of the well-known examples is glass fiber filled PET in which embedded reinforcing fibrils toughens the brittle matrix and prevents crack propagation. However, high density of fillers brings disadvantages as weight in the composites. At this point LCP composites offer a different approach in composite formation [106, 124-165]. Fibril formation of reinforcing material in melt form is in the scope of material sciences so called in situ

composites and needs a detailed studies for optimum conditions in processing such as; dispersion (extrusion), interatomic forces and chain interactions (Compatibilization), molecular weight, temperature, pressure etc.

2.11.1 LCP Dispersion

Depends on the facilities of research laboratory double extruder or conventional twin screw extruders can be used in the LCP/thermoplastic blends. In the division of static mixer (in double extruder setup) or barrel and screw (in commercial extruder), the LCP melt is compressed and disintegrated. This involves drop forming and breakup, similar to the mixing of low molecular weight liquids. As the LCP phase deforms under the flow field, the surface tension force accelerates the breakup process.

At this point composition is important because at a high LCP content, the LCP domains tend to coalesce into a sheet like structure, whilst at a low content, they break up into small particles rather than fibril. It is preferable that in order to achieve a better dispersion of LCP in the matrix polymer, the LCP phase should have a lower viscosity than the matrix polymer. Many researchers have found that the formation of the morphology of the LCP phase takes place at the die entrance, where the converging force of the die generates a strong elongational flow field [104]. At a high extrusion rate, there is a high converging force at the die entrance, and a high degree of shearing is applied to the LCP phase. The coalescence and further deformation of the LCP domains in the die entrance lead to the increase in volume and aspect ratio of the fibrils [166].

2.11.1.1 Double Extruder

In the double extruder systems, LCP and thermoplastic melts are streamed from two separate extruders and combined with T-junction then pass through a static mixer and a die (Figure 2-30). In this process the difference of processing temperatures of the matrix and LCP is not a problem.
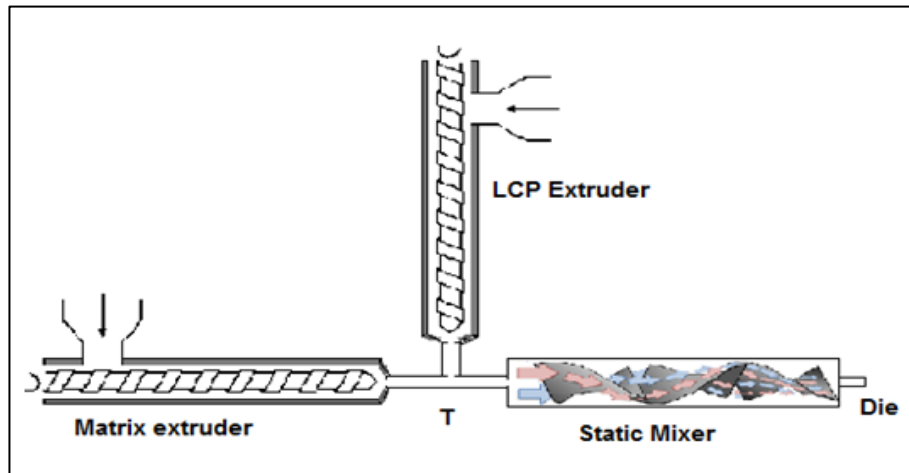
Figure 2-30 Double extruder designed for LCP/Thermoplastic blends [167]

Static mixers present 3-D chaotic blending with zigzag flowing and radial mixing together (Figure 2-31).
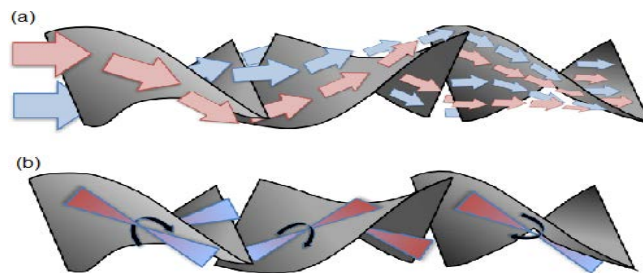
Figure 2-31 Zigzag flowing (a) and radial mixing (b) in static mixer

Depends on the viscosity of blends, speed of production and mixing quality aimed static mixers with different flow divisions (striations) are designed (Figure 2-32) [168]

Figure 2-32 Static mixers with different number of flow divisions (striations)

However when recycling of composites are considered, products from double extruder is problematic because they are composed of constituents that have

discrete processing temperature and have to be processed as one material in a standard extruder.

2.11.1.2 Conventional Extruder

Good dispersion of the LCP in the polymer blend can be serviced by twin screw extruder (Figure 2-33). During the mixing of the two polymers in an extruder by main feeder, the temperature of the screw barrel is set below the processing temperature of the LCP and above that of polymer matrix, so that a thorough distribution of the LCP powders in the polymer matrix is obtained. In the die zone, the temperature is raised above the melting point of the LCP powders, which are then deformed into an elongated structure in the final product. This process gets easy by using side feeder. But temperature difference of processing LCP and matrix is so high and mostly matrix starts to decompose. In addition side feeder in the twin screw extruder cannot take place of the 'LCP side extruder' mentioned in 'double extruder' section.

The rationale of this study addresses this issue by synthesizing low T_m LCP materials.
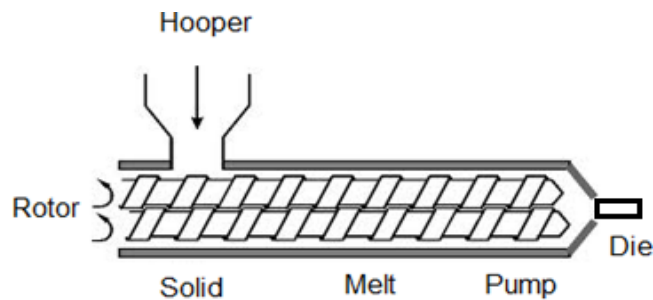
Figure 2-33 Twin screw extruder

2.11.2 Injection Molding

Injection molding is mold filling processes; in which material flows through the front advances to a mold, are typical examples of moving boundary problems. The moving contact line phenomenon is explained by employing no-slip or free-slip boundary condition at the mold walls. Generally two-dimensional flows are

simulated to simplify flow kinematics of complex filling process such as fountain flow and bifurcations. In order to incorporate the fountain effect in the flow front, special consideration is given to the boundary conditions (Figure 2-34). Experimental investigations and analytical solutions have shown that the fountain effect is limited to a distance that is approximately equal to thickness of the cavity [169]
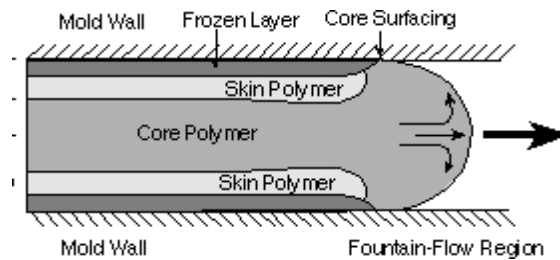
Figure 2-34 Fountain of the polymer melt in the mold

Kinematics of the polymer melt in the mold is related to:

a) Slip or no slip at the wall

b) Capillary number (Shear, viscosity, LCP concentration, interfacial tension)

These two definitions connected with other macroscopic parameters and needed to be optimized during injection molding such as:

i)   Temperature of the polymer melt
ii)   Temperature of the mold
iii)   Width of the mold
iv)   Injection speed
v)   LCP kinematic
vi)   Matrix kinematic
vii)   % amount of LCP in the matrix

Depending on the parameters mentioned above, shear field and viscosity shows alteration in the core-shell regions of the mold that brings the formation of ellipsoids and elongated fibrils in different extend. As illustrated, higher shear rate in shell region brings more fibril formation than core region (Figure 2-35).
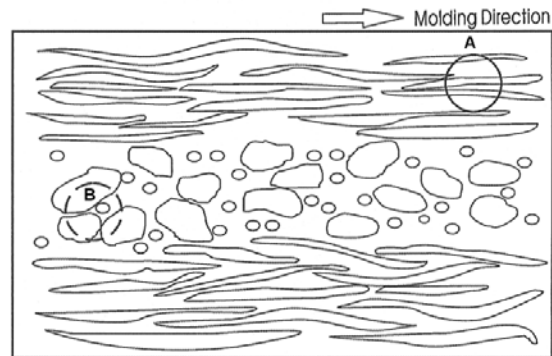
Figure 2-35 Illustrated Skin (A) and core (B) texture of LCP-Thermoplastic in situ composites in the mold [170]

2.12 Shortcomings of In Situ Composites

TLCPs used in the generation of in situ composites have been observed to fall short of fulfilling their reinforcing potential because of the following reasons:

i)   The transverse direction is usually not well reinforced, producing samples shows mechanical anisotropy.

ii)   Not all of the TLCP is deformed into long fibrils with high molecular orientation in the mold.

iii)   Most commercial TLCPs are processed at temperatures near or above the degradation temperature of many commodity resins which precludes their reinforcement.

iv)   Engineering thermoplastics can be used as matrix, but they are generally much more expensive.

v)   Processing and production conditions are not standard, changes for each LCP-thermoplastic combinations also changes the properties.

vi)   In recycling procedure, if matrix and reinforcing LCP have discrete processing temperatures processing it without decomposition is difficult.

2.13 Characterization Methods

The experimental techniques used to characterize the LCP and polymer blends with LCP reinforced in situ composites investigated in this dissertation are discussed here. Some specific experimental methods are visual observation, polarized light microscopy, nuclear magnetic resonance, carboxyl end group analysis, intrinsic viscosity, attenuated total reflectance infrared analysis, differential scanning calorimeter, thermogravimetric analysis, X-ray analysis (WAXS, fiber diffraction), surface energy, scanning electron microscopy, mechanical test (tensile, Impact), capillary rheometer, melt flow index.

In addition to the standard test methods listed above some LCP is tested for application such as fiber formation, electrospinning and electric properties.

2.13.1 Polarized Light Microscopy

Liquid crystalline (mesophase) formation can be checked by polarized light microscopy. Mesophases in the LCP chains behaves like a 'quarter wave plate' and de-polarize incoming polarized light (Figure 2-36). Due to the light scattering the de-polarized light intensity increases with crystallinity (mesophase formation). In melt form, under shear, mesophase transition from isotropic to mesophase is very fast and cause shear coloring of the material under polarized light microscopy.
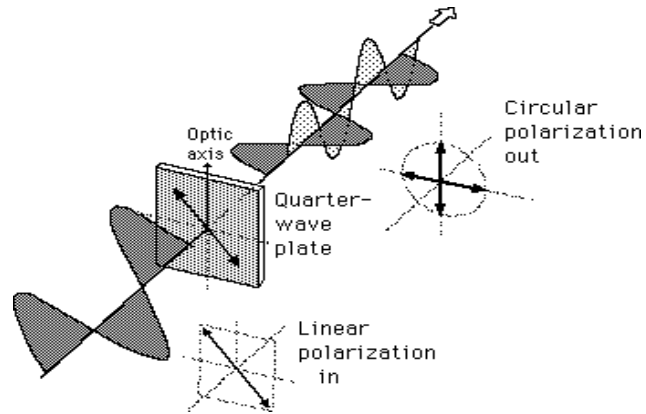
Figure 2-36 Depolarization of light due to the light scattering of polymer crystals

2.13.1.1 Texture

LCPs especially smectic types have specific textures under polarized light microscopy (Figure 2-37 a). However, in nematic LCP, also described as a monodomain, does not exhibit well-ordered textures and homogenously colored fields are observed (Figure 2-37 b.)
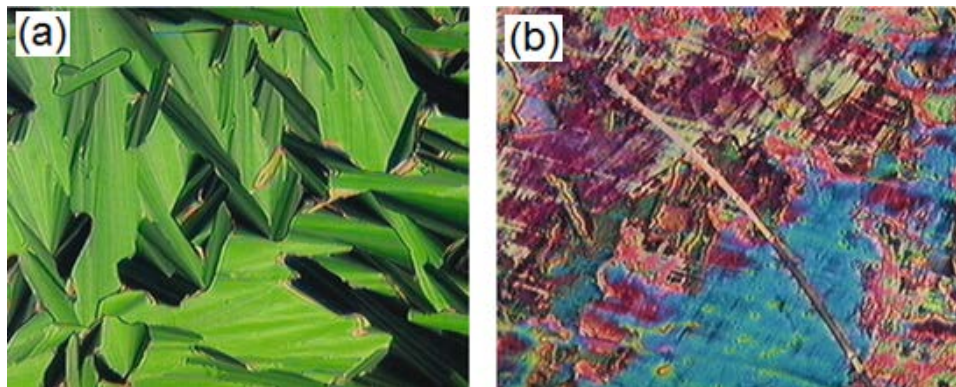
Figure 2-37 Textures of LCPs under polarized light microscope belongs to a type of (a) smectic, (b) nematic [171]

2.13.1.2 Transition Temperatures

As heat of fusion is almost negligible for most high molecular weight LCPs in differential scanning calorimeter, determination of solid to nematic transition temperature (T_m), nematic to isotropic transition temperature or called as clearing point (Ti) is measured by polarized light microscopy. The range between these two temperatures is called as nematic window.

2.13.2 Nuclear Magnetic Resonance (NMR)

Nuclear magnetic resonance (NMR) is a complicated spectroscopic technique for the characterization and identification of the materials by using magnetic moment of atomic nucleus under specified electromagnetic wave. Identification of covalent bond formation takes place between the reactant of mesogenic units in LCP can be studied by this method.

2.13.3 Carboxyl End Group Analysis (CEG)

The molecular weights of polymers can be determined by chemical or physical methods of functional group analysis. End-group analysis requires high solubility of the polymer and requires extrapolation to infinite dilution called as Θ state in ideal solution. In end-group analysis, number of molecules is counted in a fixed weight of sample.

Polyesters and polyester based LCPs have carboxyl (-COOH) end groups which are directly titrated with a base in a phenolic solvent. Molecular weight (Mwt) of these materials is inversely proportional with end groups. Analysis of carboxyl end group with acid-base titration method is simple and useful for the determination of Mwt. CEG analysis of PET by ASTM D7409-07 is standard reference methods for the polyester based LCPs.

2.13.4 Intrinsic Viscosity (IV)

For the determination of molecular weights of polymers by viscosity methods, dilute solutions (about 1%) are used. Viscosity is inversely proportional to elution time of a

free flowing solution in a capillary and related with concentration and size of the polymer chain (viscosity average molecular weight, M_v) of the dissolved polymer. This simple and widespread technique has some drawbacks such as Mv depends on the solvent used and bonds-groups in polymer chain. Solution viscosity of polymers by ASTM D2857-95 is standard reference methods for the polyester based LCPs.

2.13.5 Fourier Transfer Infrared Analysis (FTIR)

Fourier Transfer Infrared Analysis (FTIR) is spectroscopic technique for the characterization, identification and also quantification of the materials by using the mid-infrared wave length (600 - 4000 cm^{-1}). In attenuated total reflectance (ATR) mode, measurement is made by means of transmitting the infrared radiation directly through the sample without the matrix preparation.

2.13.6 Thermal Analysis Methods

2.13.6.1 Differential Scanning Calorimeter (DSC)

Differential scanning calorimetry (DSC) is a thermo analytical technique used for investigation of materials by monitoring temperature when subjected to controlled endothermic-exothermic heat flows. The difference in the amount of heat required to increase the temperature of the blank pan and sample filled pan is measured as a function of temperature. The glass transition temperature (Tg), melting temperature, crystallization temperature, enthalpy of melting and crystallization can be detected for unfilled plastic materials [172-175].
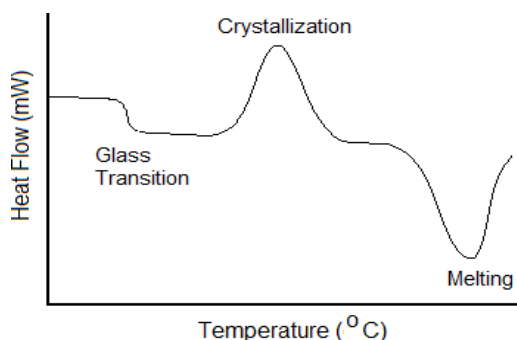
Figure 2-38 DSC curve of thermoplastics

In the case of amorphous materials, the primary relaxation process is associated with Tg and, for these systems, is termed as the α relaxation. However in the rigid mesogenic LCP, the change in the heat capacity associated with Tg can be relatively small and, therefore, DSC is not ideally suited to the study of the glass transition. Conversely, in DMTA, Tg is easily detected, since it is associated with a large change in the mechanical properties. At temperatures below Tg, molecular motion is related to molecular segments or side-groups, processes which can lead to a number of secondary relaxation peaks in tanδ, conventionally, these are sequentially indicated by other type relaxations with decreasing temperature.

2.13.6.2 Thermogravimetric Analysis (TGA)

TGA is a test method monitoring changes in the weight of a specimen in relation to change in temperature to control thermal stability and degradation of polymers. The principle is based on the loss of weight due to the evaporation and decomposition of additives and polymers at different temperatures. TGA analysis employed to determine polymer system properties, such as thermal stability, degradation temperatures, absorbed moisture and the level of organic-inorganic contents in materials.

Thermal stability, degradation behavior, and kinetics of commercially available main-chain LC polyesters have been tested by TGA analysis, by product mainly comes from dehydration, decarboxylation and scission product and can be listed as CO_2, CO water, ketones, phenols ,esters and aryl [176-179].

2.13.7 X-ray Diffraction

X-ray analysis is one of the most frequently used methods for the quantification of crystallinity and structural details of polymers. Basically X-ray methods use monochromatic radiation, X-ray detector and a goniometer situated on the circumference of circle centered on specimen. Rotation of the specimen through θ degrees corresponds to the rotation of the detector through 2θ degrees (Figure 2-39) [180].

Incident x-ray is partly absorbed and partly scattered, and the rest is transmitted. The scattered beam occurs as a result of collision with electrons in the material. At each angle electron density of the gate vary and lead to the different scattered beam intensities that figure out as X-ray pattern. The pattern provides information on the electron density distribution and hence the atomic positions within the material. Every crystalline solid have a unique X- ray pattern which is a "finger print" for that solid. Solids with the same chemical composition but different phases can be identified by their pattern [180].
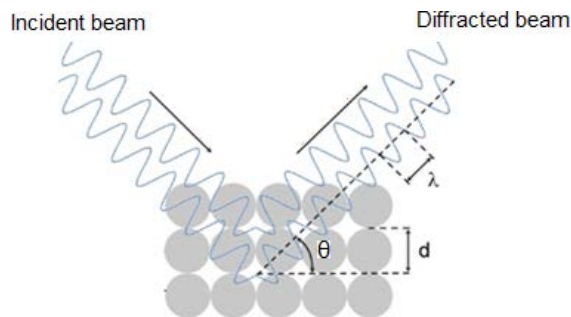
Figure 2-39 X-ray diffraction simulation by Bragg angle

In Bragg law, incident x-rays beam with λ wavelength at the incident angle θ collides with two consecutive layers with d-spacing and scatters. In Equation 2-3, n indicates the order of diffraction. Bragg's law describes the condition for constructive interference from successive crystallographic planes (h, k, l) of the crystalline lattice.

$$n\lambda = 2d\sin\theta \qquad \text{(2-3)}$$

Wide angle X-ray scattering (WAXS) is similar to Small-Angle X-ray Scattering (SAXS) however, the distance between sample and the detector is shorter and thus diffraction maxima at the larger angles are observed. Whilst WAXS uses angles between 5°-120° for the analysis of polymers with the interatomic distances from $1A^o$-$50A^o$, SAXS uses $1A^o$-$5A^o$.for the analysis of polymers with larger atomic distances from $5A^o$-$700A^o$ [181].

One difficulty is to determine when crystallinity is fully developed. The original cell parameters were established in 1954 and numerous groups have reexamined it [182, 183]. One researcher annealed PET at up to 290^oC for 2 years and find triclinic crystals with one polymer chain per unit cell with the parameters $a = 0.444$ nm; $b = 0.591$ nm; $c = 1.067$ nm; $\alpha = 100^o$; $\beta = 117^o$; $\gamma = 112^o$; density = 1.52 g/cm^3 [105].

2.13.7.1 Wide angle X-ray scattering (WAXS)

Practically purely crystalline and purely amorphous polymers is not possible to obtain, however semicrystalline forms are widely present and X- ray curves of them observed as in the Figure 2-40 .Relatively sharp peaks indicate scattering from crystalline regions while the broad underlying peak refers to amorphous scattering.
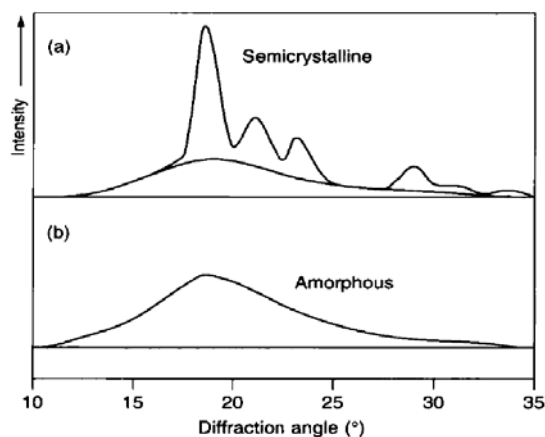
Figure 2-40 X-ray diffraction curves of (a) a semi crystalline and (b) an amorphous samples of polymers [181]

The mass fraction of crystals (Xc) can be calculated by the ratio (Eq. 2-4) of crystalline area to the total area; crystalline area (Ac) and amorphous area (Aa), (Figure 2.40)

$$Xc = \frac{Ac}{Ac + Aa}$$ (2-4)

Full width at half maximum (FWHM) is an expression of the intensity function, given by the difference between the two θ values at which the intensity is equal to half of its maximum value (Figure 2-41).
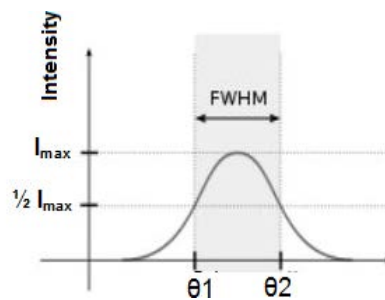
Figure 2-41 Full width at half maximum (FWHM) as a function of θ and intensity

Full width at half maximum (FWHM) is inversely proportional with d-spacing between the polymer chain in X-ray analysis (Figure 2-41). Spacing can be found from equation d = 2π/q where q = (4π/λ)sinθ, K_λ(Cu) = 1.54 ˚A for X-rays wavelength [184].

2.13.7.2 X-ray fiber diffraction

X-ray fiber diffraction technique shows similarities with Laue method in which monochromatic radiation is reflected from, or transmitted through, a fixed fiber instead of single crystal. Oriented fiber shows anisotropic character; it has well-defined periodicity parallel to the fiber axis, however it has random organization in the other directions. Aligned crystallites elongated along fiber direction scatter the incoming light intensely and observed as spots on the X-ray pattern screen (Figure

2-42) where the scheme does not change whilst the sample is rotated about a unique fiber axis.
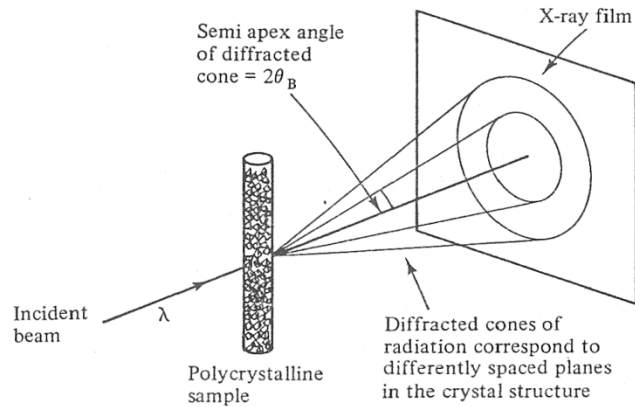
Figure 2-42 Illustration of fiber diffraction measurement [3]

In the pattern the fiber axis corresponds to the meridian and the perpendicular direction is named as equator. Reflections are tagged by the Miller index h,k,l such as reflection on the meridian are correspond to 00l and other indexes are shown in the Figure. Black region in the diffraction pattern indicates high intensities and black circle around the dots corresponds to amorphous halo line (Figure 2-43).
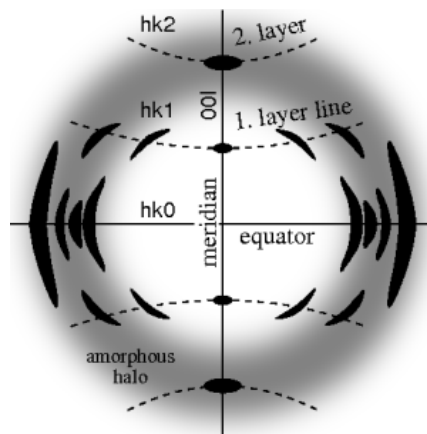
Figure 2-43 Ideal X-ray diffraction pattern of a semi crystalline polymer fiber [185]

Axial alignment of the nematic phase shows itself as intensity in the equatorial direction in pattern (Figure 2-43).

2.13.8 Surface Energy

There are several different ways of obtaining an estimate of the interaction between LCP macromolecules and the thermoplastic matrix [186]. One of them is surface energy measurement by static or mechanical way. In literature, commercially available main-chain LC polyesters have been tested by contact angle techniques at room temperature [187, 188]. Experimental data based on assumption that surface energy values match between the two-liquid geometric method and the three-liquid acid–base method [189-192]. However, three-liquid acid–base method is more suitable for the surface energy calculation of these kind of LCPs, and provides much more information, such as, acidity and basicity of LCP surfaces.

The average surface energies of Vectra LCPs are about 42 mN/. In addition, they are classed as monopolar Lewis bases because their Lewis acid components are negligible.

Surface free energy of polymers is an indication of interfacial attraction forces between reinforcing agent and matrix in polymeric composites. Interfacial attraction is directly proportional to work of adhesion and quantized as Van der Waals interaction (γ_S^{LW}), acid (γ_S^{+}), base (γ_S^{-}) and acid-base (γ_S^{AB}) values

Surface energy measurements can be made by static and dynamic way. Contact angle measurement of the probe solution on a film is a kind of static methods. Widely used probe solutions are DIM(diiodomethane), EG(ethylene glycol), FA(formamide), n-decane in Table 2-2.

Table 2-2 Surface energy of probe solution (mN/m)

	DIM	EG	FA	n-decane
γ_L^{TOT}	50.8	48	58	23.83
γ_L^{LW}	50.8	29	39	23.84
γ_L^{-}		30.1	39.6	
γ_L^{+}		3	2.28	
γ_L^{AB}		19	19	

Due to Diiodomethane (DIM), and n-decane molecular structure they have no dipole or induced dipole interactions, they only have .non polar Lw (Liftshitz-van der Waals) interactive forces. Both formamide (FA) and ethyleneglycol (EG) probe solutions have acid and base characters.

Depends on the need surface tension measurement can be made on film or fiber of the materials by static methods.

2.13.8.1 Surface Tension of Films

Dispersive non-polar and interactive polar forces define the shape of the droplet on testing surface (Eq. 2-5). In Figure 2-44, interfacial forces categorized as between liquid-vapor (γ_{Lv}), solid-liquid (γ_{SL}) and solid-vapor (γ_{sv}).

$$\cos(\theta) = \frac{\gamma_{sv} - \gamma_{SL}}{\gamma_{Lv}}$$

$$(2-5)$$
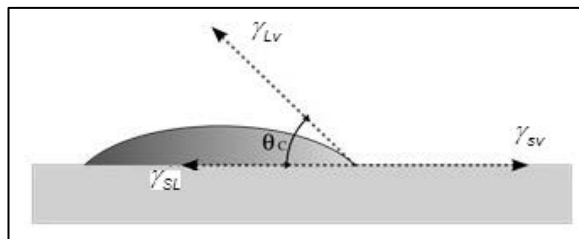
Figure 2-44 Contact angle of a solution on a solid matter

After some calculation work of adhesion between the contacting phases (W_a^{TOT}) is given below:

$$W_a^{TOT} = W_a^{LW} + W_a^{AB} = 2[(\gamma_f^{LW} \gamma_m^{LW})^{1/2} + (\gamma_f^+ \gamma_m^-)^{1/2} + (\gamma_f^- \gamma_m^+)^{1/2})]$$

$$(2-6)$$

2.13.8.2 Surface Tension of Fibers

Surface tension measurement of fiber is generally made by Wilhelmy method (Figure 2-45) where the few centimeter long specimen is placed to the hook of the microbalance and force (F) is measured while stage under the solvent cap decreases at a fixed velocity (1-3 µm/s).
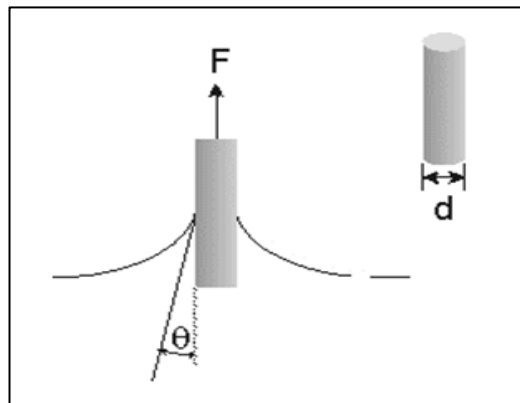
Figure 2-45 Contact angle of single-fiber in a solution

Nonpolar n-Decane is completely dispersive liquid and contact angle (θ) is zero on the most polymer surfaces, is used to find perimeter (P) of fiber by equation below.

The relation between surface tension of probe liquids (γ) and other parameters in the equation below is used to find θ angle, which is indirect method in contrary to direct θ measurement of droplet on polymer film.

$$F = (P)(\gamma)(\cos\theta) \tag{2-7}$$

After the finding θ value the way for the calculation of work of adhesion (W_a^{TOT}) is followed as in 'surface tension of films' section.

2.13.9 Scanning Electron Microscopy (SEM)

Scanning Electron Microscopy (SEM) is a common visualization technique giving 300-600 times better resolutions than optical microscopy in analysis of materials.

SEM observation up to 100 000 magnification can give detailed information in texture such as fractured surfaces, phase boundaries, adhesive failures etc [181].

2.13.10 Mechanical Test

2.13.10.1 Tensile Test

Tensile test of a polymeric material was standardized according to its shape. Tensile test of composite material in dog-bone shape and fiber samples was made according to ASTM D638-03 and ASTM-D3379, respectively. In tensile tests, a specimen is deformed at a constant rate until fracture, with a gradually increasing tensile load that is applied to longitudinal direction of the specimen. A 'strain gauge' connected to the 'load cell' convert force into electrical signals and give load versus elongation relation.

By using cross sectional area (A_o) and length (l) of the specimen, stress (σ) and strain (ε) calculated from load (F) and elongation (Δl) by the equations. By using stress strain curve, Tensile strength (maximum load carried during a tension test), Youngs' Modulus (the slope of the initial linear portion of a stress-strain curve), work of rupture can be obtained. Typical stress strain of a plastic material is shown in Figure 2-46. Some of the relations that are employed in tensile tests are given in the equations below.

$$\sigma = \frac{F}{A_o} \tag{2-8}$$

$$\varepsilon = = \frac{li - lo}{lo} = \frac{\Delta l}{lo} \tag{2-9}$$

where l_o is the initial gauge length, l_i is instantaneous length
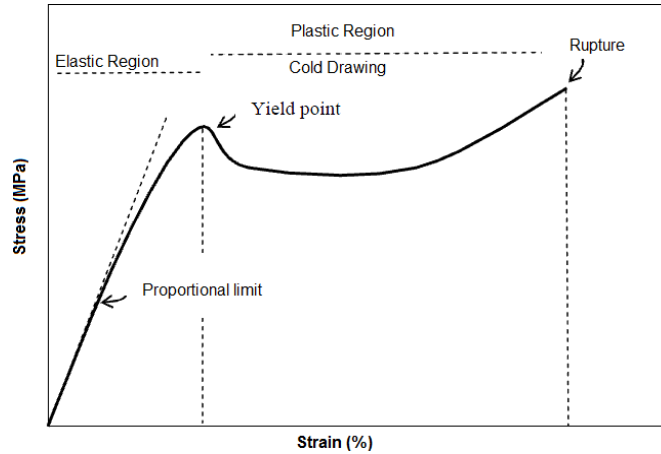
Figure 2-46 Stress-strain curve of a typical polymeric material [193].

In laboratory scale, tensile test specimens of polymer samples are generally prepared in dog-bone or fiber form by injection molding and fiber spinning device respectively (Figure 2-47).
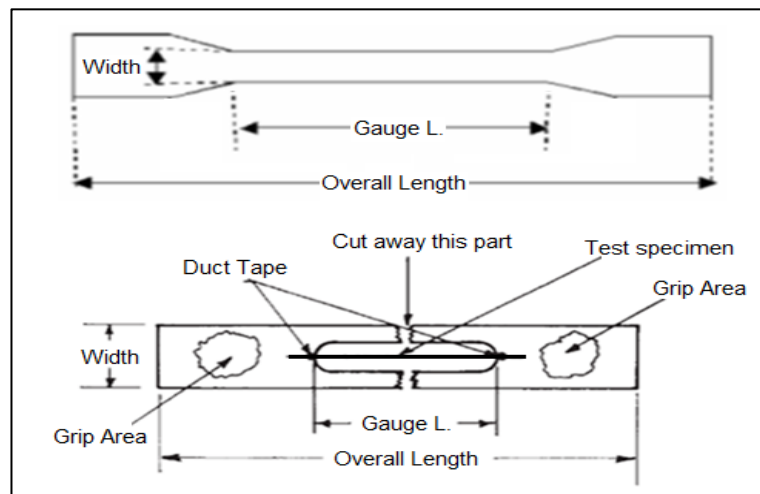
Figure 2-47 Dog-bone shaped (up) and mono filament (down) specimen mounted to load cell according to ASTM D638-03 and ASTM-D3379 [194, 195]

2.13.10.2   Impact Test

Impact test is a high strain rate test that determines the amount of energy absorbed by a material during fracture that gives information about toughness, ductile-brittle characters of the materials. Izod and Charpy are the most known impact test methods, in both of them a hammer-like weight strikes a specimen and energy-to-break is determined from the loss in the kinetic energy of the weight [196]. Charpy impact test was applied to polymeric material as specified in ASTM D256-92.

2.13.11   Rheological Characterization

Rheology is the science of the deformation and flow of matter. It is concerned with the response of materials to applied stress. That response may be irreversible viscous flow, reversible elastic deformation, or a combination of the two.

2.13.11.1   Capillary Rheometer

Capillary rheometer measurement is needed to understand shear viscosity (η) and flow dynamics as a function of temperature and shear rate. Optimal processing conditions can be found out by using capillary rheometer (Figure 2-48). In this method high pressure forces a polymer melt to flow through a capillary die with specified radius (R) and length (l). High l/R ratio (about 40) is preferred in measurement to minimize end effects and ensure fully developed velocity profile.
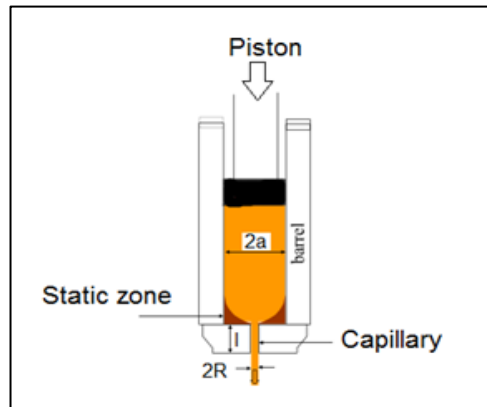
Figure 2-48 Schematic representation of capillary rheometer

Some of the relations that were employed in rheometer are given in the equations below. Where T is shear stress at the die wall, L is load on piston and 'a' is diameter of plunger.

$$T = LR/2l\pi a^2 \tag{2-10}$$

Shear rate (γ) at the die wall is given by the following equations, where Q is the rate of extrusion in mm^3/s.

$$\gamma = 4Q/\pi R^3 \tag{2-11}$$

By using the ratio shear stress to shear rate viscosity (η) is calculated

$$\eta = T/\gamma \tag{2-12}$$

By plotting the log γ vs. log η, viscosity at zero shear rates can be calculated.

2.13.11.2   Melt Flow Index (MFI)

The principle of the melt flow index (MFI) machine is similar to that of capillary rheometer; however, l/R ratio of the die is comparatively small. Aim in MFI is to measure the ease of flow (g/10min) of the polymer melt which is inversely

proportional to the melt viscosity. During the measurement load on piston is steady and produced by standard weights [172].

2.13.12 Electrical Properties

LCPs have different aromatic-aliphatic ratio that brings non-conjugated systems and having unique semiconducting properties. Semiconductors have conductivity 10^3 to 10^{-8} siemens (S) per centimeter have a wide place in electronic application such as transistors, diodes, solar cells and integrated circuits. A four point probe technique (Figure 2-49) is a simple apparatus for measuring the resistivity of semiconductor samples. By passing a current through two outer probes and measuring the voltage through the inner probes allows the measurement of the substrate resistivity.
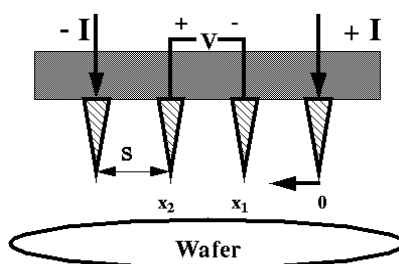
Figure 2-49 Four point probe for the measurement of resistivity of semiconductor film

2.13.13 Fiber from Solution

Fiber spinning from lyotropic LCP solutions generally needs pure acids and takes place under the extreme condition by complicated devices. For example polyaromatic amide (Kevlar^{TM}) needs %99 H_2SO_4 for spinning. However, semi crystalline LCPs may be put in fiber form with more common solvents and simple setup such as in electrospinning.

Although electrospinning (Figure 2-50) is a simple process, requiring just simple laboratory equipment to yield fibers down to the nanoscale, the science behind it is not simple at all. Electrospinning process involves the understanding of electrostatics, fluid rheology and polymer solution properties such as rate of solvent

evaporation, surface tension and solution conductivity. These fundamental properties are constantly interacting and influencing each other during the electrospinning process. Understanding the basics behind the materials and the fundamentals that affect electrospinning will open new avenues and applications for electrospun fibers.
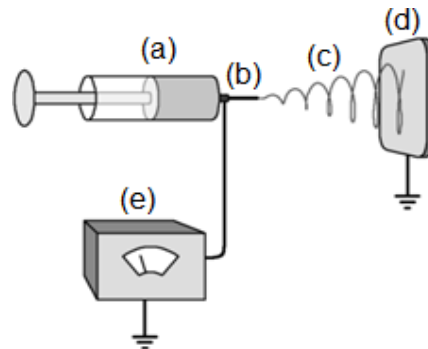
Figure 2-50 Schematic diagram of electrospinning system

In electrospinning setup (Figure 2-50) there are five main divisions; a syringe containing polymer solution (a), metal needle (b), jet of polymer solution (c), grounded metal plate (d), a high voltage DC supply (e).

Table 2-3 Physical properties of some electrospinning solvents

Solvents	Boiling Point (^{0}C)	Vapor Pressure at 25°C (Pa)
m-cresol	202	13
DMAc	165	330
DMF	153	492
NMP	202	66

In Table 2-3 abbreviations of solvents corresponds to Dimethylformamide (DMF), *N*-Methyl-2-pyrrolidone (NMP) and dimethylacetamide (DMAc)

CHAPTER III

EXPERIMENTAL WORK

3.1 Overview of the Experimental Work

Experimental procedure consists of following sequence;

- Synthesis of monomers involved in LCP synthesis by acetylation of phenolics and polyester oligomers (Figure 3-1).

- Synthesis, characterization and selection of LCPs for composite application (Figure 3-1).

- Composite and fiber production and characterization from selected LCPs (Figure 3-2).

- Testing these LCPs in other possible application areas such as; electrospinning and electronics (Figure 3-2).

Detailed content of materials in Figure 3-1 are given in the following 'LCP Synthesis' section.
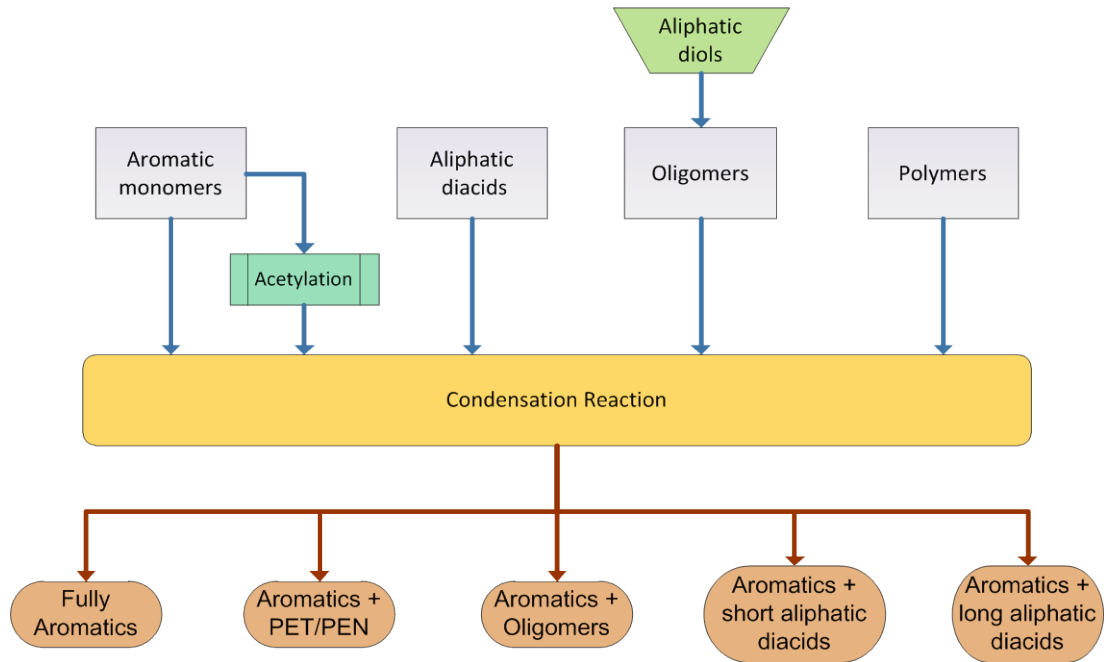
Figure 3-1 Selection of monomers for LCP synthesis and categorizations of LCPs
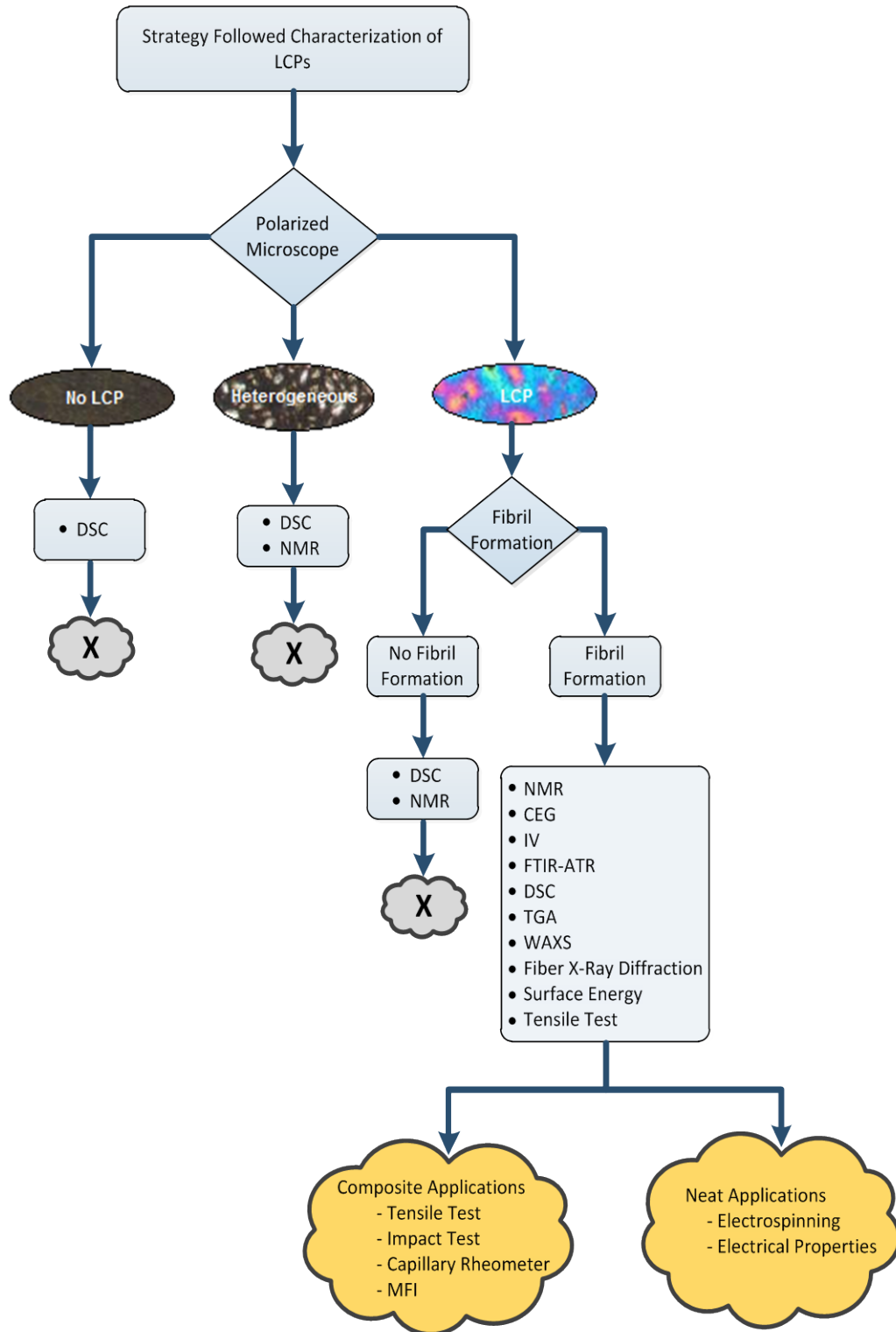
Figure 3-2 The scheme followed for the characterization of LCP's and their application areas

3.2   Materials

For synthesis of monomers, some of the commercially available starting materials were used directly; the rest of them were used after acetylation or after the synthesis of oligomer.

3.2.1   Monomers and Polymers Used as Received

The specifications (Table 3-1) and molecular structures of monomers (Figure 3-3) and polymers (Table 3-2) used as received in the LCP synthesis are given below.

Table 3-1 The specifications of as received starting materials

Chemicals	T_m (^{o}C)	T_b (^{o}C)	d (g/cm^3)	Purity (%)	Mw (g/mole)	Firm
Terephthalic acid	300	393	1.52	>99	166.1	Merck
Isophthalic acid	342	412	1.53	>99	166.1	Merck
Butanedioic acid	185	235	1.56	>99	118.1	Aldrich
Hexanedioic acid	152	265	1.36	>99	146.1	Aldrich
Octanedioic acid	142	230	1.27	>99	174.2	Acros
Decanedioic acid	134	295	1.1	>99	202.2	Acros
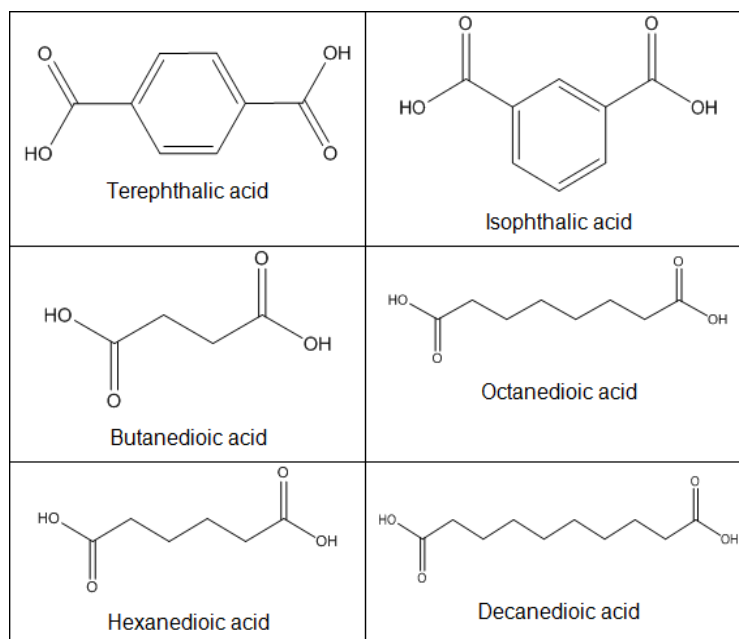
Figure 3-3 Structures of monomers used in LCP synthesis

Table 3-2 Polyesters used in LCP synthesis

Polymers	IV (dl/g)	IPA (%)	DEG (%)	CEG (meq/kg)	Grade	Firm
PET	0.63	0	1.5	20	Fiber	SASA
PEN	0.50	0	1	30	Fiber	SASA

In Table 3-2, abbreviations corresponds to the IV (intrinsic viscosity), IPA (isophthalic acid), DEG (Diethylene glycol), CEG (Carboxyl end group)

3.2.2   Synthesis of Oligomers for LCP

Although some of the polyesters (PET, PEN, and PBT) are commercially available, we synthesized Polybutylene naphthalene (PBN) and Polyhexylene naphthalene (PHN) in order to see the effect of different kinds of polyesters in LCPs [197].The properties of monomers and the catalysts used for the synthesis of polyester

oligomers are given in Table 3-3. They were synthesized in the condensation and transesterification systems as shown in Figure 3-4.

Table 3-3 Monomers and catalysts used in oligomer synthesis

Monomers and catalyst	T_m (°C)	T_b (°C)	d (g/cm^3)	Purity (%)	Mw (g/mole)	Firm
2,6-Naphthalene dicarboxylate	192	375	1.23	98	244.2	SASA
Dimethyl terephthalate	142	288	1.20	98	194.1	SASA
1,4 Butanediol	20	229	1.0	98	90.1	Acros
1,6 Hexanediol	42	255	0.96	99	118.2	Acros
MnAc(H$_2$O)$_4$	-	-	-	98	245	SASA
Sb$_2$O$_3$	-	-	5.2	99	291	Aldrich
Ti(OiPr)$_4$	19	232	0.94	99	284.2	Aldrich
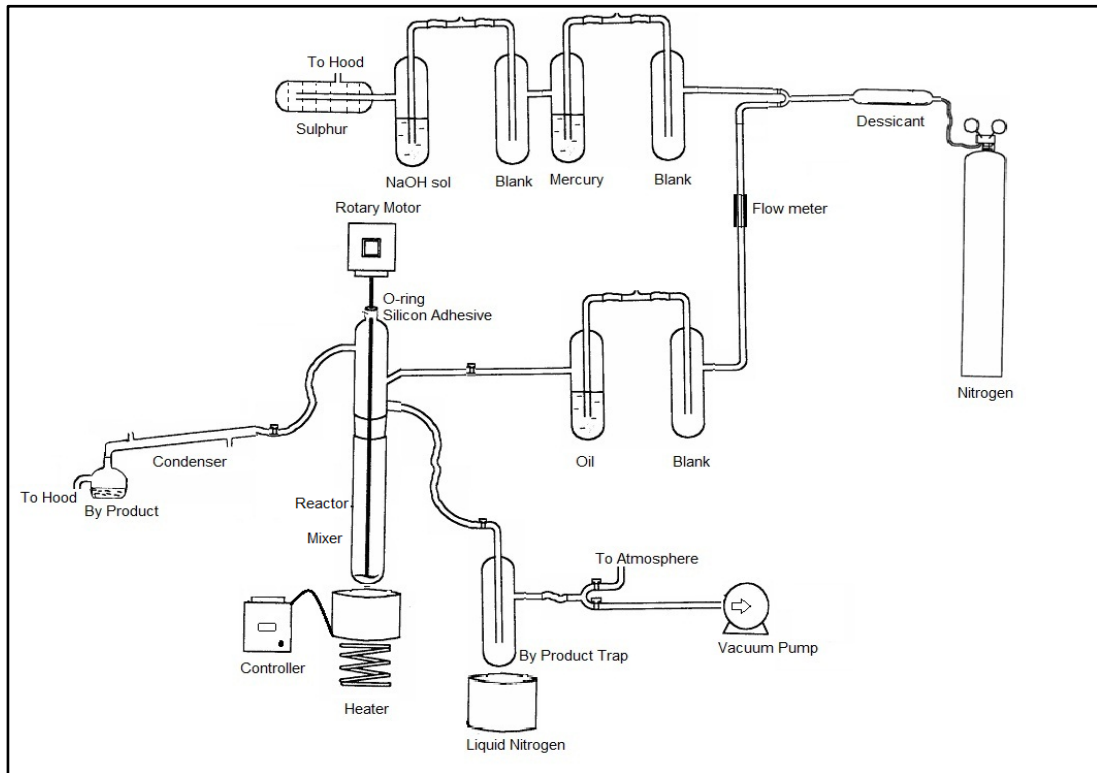
Figure 3-4 Schematic representation of condensation and transesterification setup
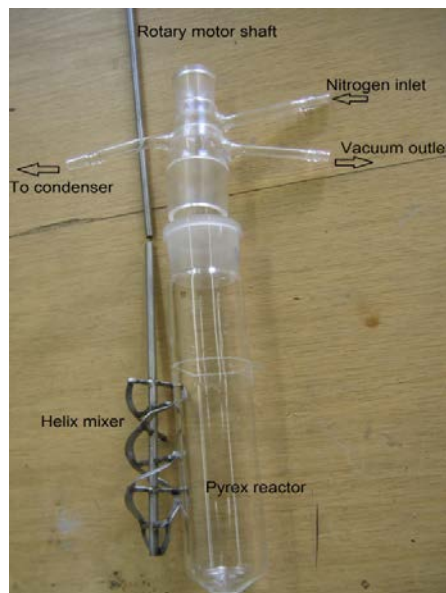
Figure 3-5 Reactor, connector and mixer in the setup in Figure 3-1

3.2.2.1 Polybutylene Naphthalene (PBN) Oligomer Synthesis

122g (0.5mol) 2,6-Naphthalene dicarboxylate was added to excess 50g (0.55mol) of 1,4 Butanediol under nitrogen atmosphere in the reactor (Figure 3-5). The bulk polyesterification was carried out between dimethyl ester and butanediol catalyzed by 200ppm manganese acetate (MnAc $5H_2O$) under nitrogen flow (0.1L/min) between 180-220°C for five hours yielding a low-molar-mass oligomer. After antimony trioxide (300ppm) addition the medium was then stepwise heated to 270–290°C under a progressively reduced pressure (0.1mbar) until excess butanediol was eliminated.

3.2.2.2 Polyhexylene Naphthalene (PHN) Oligomer Synthesis

Excess 59g (0.55mol) 1, 6 Hexanediol was added to 122g (0.5mol) of 2,6-Naphthalene dicarboxylate under nitrogen atmosphere in the reactor (Figure 3-5). The bulk polyesterification was carried out between dimethyl ester and hexanediol catalyzed by manganese acetate (200ppm) under nitrogen flow (0.1L/min) between 180-220°C for five hours yielding a low-molar-mass oligomer. After antimony trioxide (300ppm) addition the medium was then stepwise heated to 270–290°C under a progressively reduced pressure (0.1mbar) until excess hexanediol was eliminated.

3.2.2.3 Polybutylene Terephthalate (PBT) Oligomer Synthesis

97g (0.5mol) dimethyl terephthalate was added to excess 50g (0.55mol) of 1,4 Butanediol under nitrogen atmosphere in the reactor (Figure 3-5). The bulk polyesterification was carried out between dimethyl ester and butanediol catalyzed by manganese acetate (200ppm).under nitrogen flow (0.1L/min) between 180-220°C for five hours yielding a low-molar-mass oligomer. After antimony trioxide (300ppm) addition the medium was then stepwise heated to 270–290°C under a progressively reduced pressure (0.1mbar) until excess butanediol was eliminated.

3.2.3 Synthesis of Reactants for LCP synthesis

Preparation of monomers for LCP synthesis is made via acetylation of phenol containing monomers and polyester oligomers.

3.2.3.1 Preparation of Acetylated Monomers

Although some of the acetylated monomers are commercially available, we preferred to synthesize them by acetylation because of the cost, from the monomers listed in Table 3-4. These monomers were acetylated by acetic anhydride in acidic medium. The acidity of the medium was provided by weak phosphoric acid.

Table 3-4 Properties of monomers and reagents used in acetylation

Reagent-Monomers for acetylation	Tm (oC)	Tb (oC)	d (g/cm3)	Purity (%)	Mw (g/mole)	Firm
p-Hydroxybenzoic acid	215	336	1.46	>99	138.1	Acros
m-Hydroxybenzoic acid	201	347	1.37	>99	138.1	Acros
Hydroquinone	172	287	1.27	>99	110.1	Aldrich
Bisphenol-A	154	220	1.19	>98	228.3	Acros
1,7 Naphthalenediol	180	375	1.33	98	160.2	Acros
Acetic anhydride	-73	140	1.08	>98	102.1	Merck
Phosphoric acid (85%)	21	158	1.68	98	98	Riedel

3.2.3.2 Preparation of Hydroquinone diacetate

110 g. (1.0 mole) of hydroquinone was added to 236 ml. (2.5 moles) of acetic anhydride containing 2ml of H_3PO_4 in a 1L erlenmeyer flask connected to a distillation column at room temperature. The mixture warms up spontaneously, and the hydroquinone dissolves. For complete acetylation (Figure 3-6), clear solution was stirred for 30-45 minutes at $80^{o}C$ then poured onto 1L cold ($0-5^{o}C$) distilled water. The white precipitate collected on a Buchner filter was dissolved in 500ml hot

ethanol (80°C) and poured on 1L hot distilled water (90°C), re-crystallized product filtered-off and collected on filter paper. NMR result and melting point (Table 3-5) indicates that a pure product that weighed 180–185g with yield 93–95% was collected. The product was dried in two stages in an oven with an opening/orifice to remove excess moisture and with vacuum (0.5mmHg) to remove residual moisture. The melting point coincides with the literature values 122-124°C.
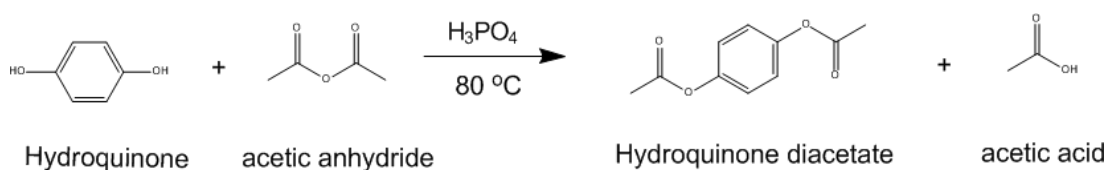
Figure 3-6 Acetylation of Hydroquinone to Hydroquinone diacetate with acetic anhydride

3.2.3.3   Preparation of para and meta Acetoxybenzoic Acids

138 g (1.0 mole) of para or meta hydroxybenzoic acid was added to hot (80°C) 236 ml, (2.5 moles) of acetic anhydride containing 2ml of H_3PO_4(85%) in a 1L erlenmeyer flask connected to a distillation column. For complete acetylation (Figure 3-7) clear solution was stirred 30-45 minutes at 80°C-100°C, then poured onto 1L cold (0-5°C) distilled water. The white precipitate collected on a Buchner filter was dissolved in 500ml of hot (80°C) ethanol and poured onto 1L of hot (90°C) distilled water, re-crystallized product was filtered-off and collected on filter paper. NMR result and melting point (Table 3-5) indicated that pure product weighed 168–171 g with yield 93–95% was collected. The product was dried in two stages; oven with an opening/orifice to remove excess moisture and oven with vacuum (0.5mmHg) to remove residual moisture. The melting points were found to be 132°C and 190°C for meta and para acetoxybenzoic acids respectively.
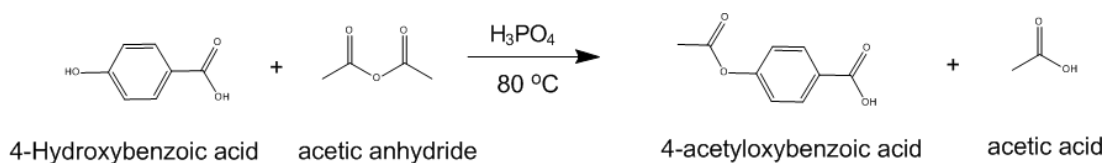
Figure 3-7 Acetylation of 4-hydroxybenzoic acid to 4-acetoxybenzoic acid with acetic anhydride

3.2.3.4 Preparation of Bisphenol-A Diacetate

228 g. (1.0 mole) of Bisphenol-A was added to hot (80°C) 357 ml, (3.5 moles) of acetic anhydride containing 3.5ml of H_3PO_4 (85%) in a 1L erlenmeyer flask connected to a distillation column. For complete acetylation (Figure 3-8) clear solution was stirred 30-45 minutes at 80°C-100°C, then poured onto 1.5L of cold (0-5°C) distilled water. The white precipitate collected on a Buchner filter was dissolved in 750ml hot (80°C) ethanol and poured on 1.5L of hot (90°C) distilled water, re-crystallized product was filtered-off and collected on filter paper. As NMR result and melting point (Table 3-5) indicated that pure product weighing 280–290g with yield 90–93% was collected. The product was dried in two stages; oven with an opening/orifice to remove excess moisture and oven with vacuum (0.5mmHg) to remove residual moisture. The melting point was found as 93°C.
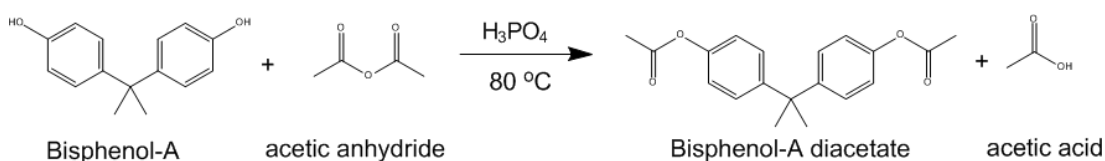
Figure 3-8 Acetylation of Bisphenol A with acetic anhydride to Bisphenol A diacetate

3.2.3.5 Preparation of 1,7 Naphthalene Diacetate

160g (1.0 mole) of 1,7 Naphthalenediol was added to hot (80°C) 306 ml, (3 moles) of acetic anhydride containing 3ml of H3PO4 (85%) in a 1L erlenmeyer flask connected to a distillation column. For complete acetylation (Figure 3-9), clear solution was stirred 30-45 minutes at 80°C-100 °C then poured onto 1.5L of cold (0-

5^oC) distilled water. The white precipitate collected on a Buchner filter was dissolved in 750ml hot(80^oC) ethanol and poured on 1.5 L hot (90^oC) distilled water, re-crystallized product was filtered-off and collected on filter paper. NMR result and melting point (Table 3-5) indicated that pure product weighing 219–225g. with yield 90–93% was collected. The product was dried in two stages; oven with an opening/orifice to remove excess moisture and oven with vacuum (0.5mmHg) to remove residual moisture. The melting point is found as 188^oC.
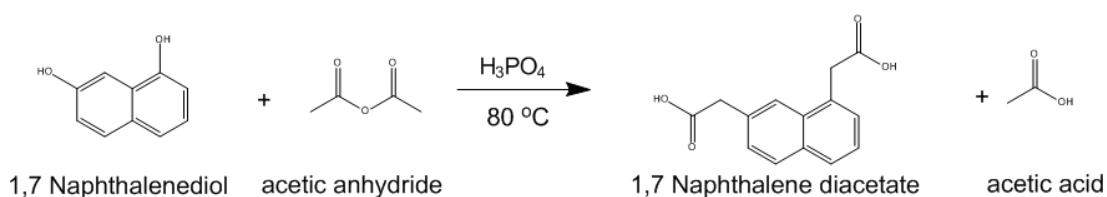
Figure 3-9 Acetylation of 1,7 Naphthalenediol with acetic anhydride to 1,7 Naphthalene diacetate

3.2.3.6 Characterization of Acetylated Monomers

Characterization of acetylated monomers (Figure 3-10) was done by melting point determination (Table 3-5) and NMR.

Table 3-5 Physical properties of acetylated monomers

	T_m (^oC)	T_b (^oC)	d (g/cm^3)	Mw (g/mole)
p-acetoxy benzoic acid	191	325	1.92	180.1
m-acetoxy benzoic acid	132	-	-	180.1
Hydroquinone diacetate	121	sublimation	-	194.2
Bisphenol A diacetate	93	421	1.12	312.3
1,7 Naphthalene diacetate	188	375	1.22	244.2
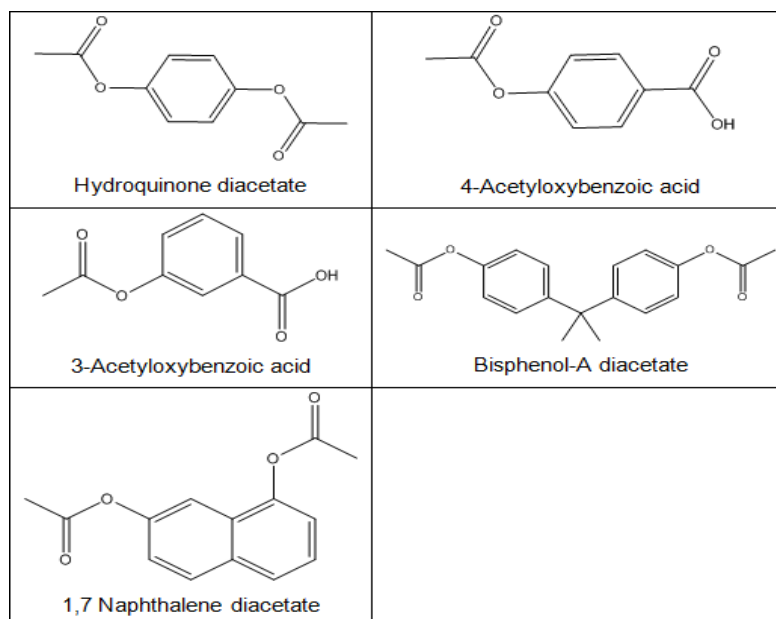
Figure 3-10 Structures of acetylated monomers

H[1] and C NMR results of acetylated monomers show that acetylation is completed and OH groups completely disappeared (Figure 3-11 to Figure 3-14). Chemical shifts are labeled on structures.
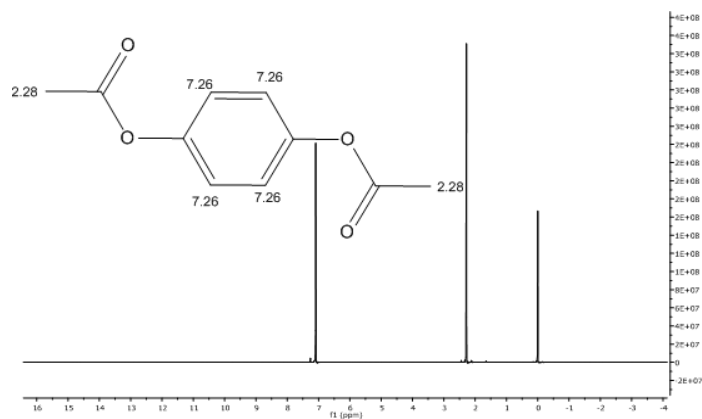
Figure 3-11 H-NMR of hydroquinone diacetate (HQDA)
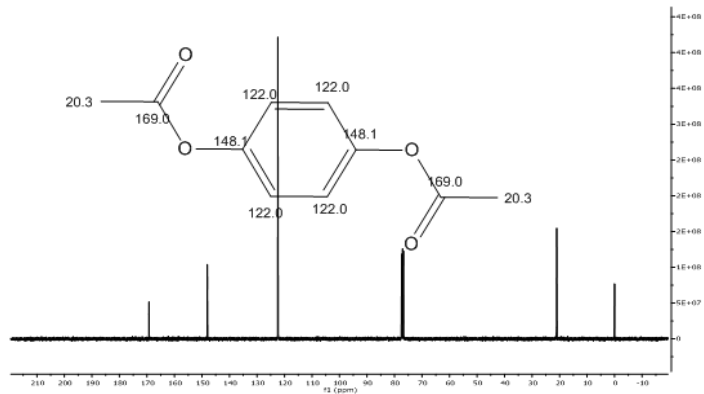
Figure 3-12 C-NMR of hydroquinone diacetate (HQDA)
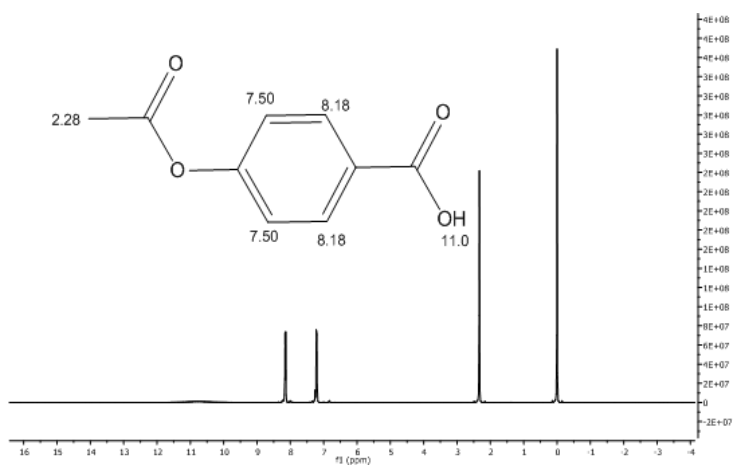
Figure 3-13 H-NMR of p-acetoxy benzoic acid (p-ABA)
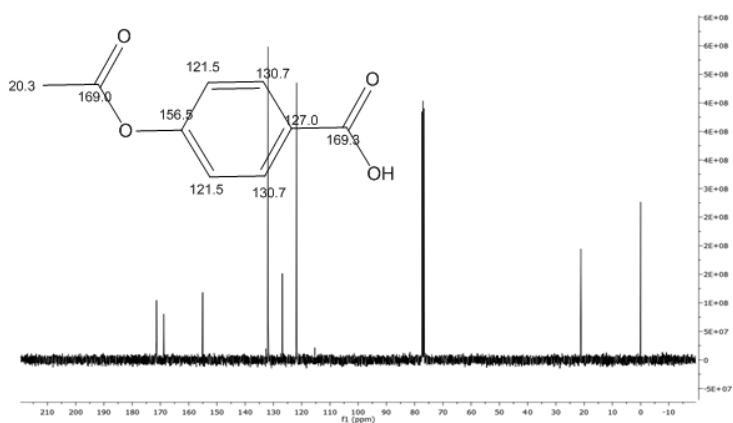
Figure 3-14 C-NMR of p-acetoxy benzoic acid (p-ABA)

3.2.4 Matrix Materials and Compatibilizers

In composite application, LCPs are blended with ABS, PA6, PET, PP and compatibilizers. Their trade names and grades are listed below (Table 3-6). Detailed specification of them can be found in data sheets at their web pages.

Table 3-6 Materials and their specifications for composite application

Polymers	Grade	Type
ABS	Standard	Lustran M202 AS00,Ineos
PA6	Standard	Teklamid 6, Polyone
PET	Fiber grade	SASA
PET	Engineering grade	Kordsa
PP	Fiber grade	Petoplen EH-251, PETKIM
en-baco	Compatibilizer	DuPont
MA and epoxy	Compatibilizer	Lotader(2210, 8840, 8900), Arkema
SMA	Compatibilizer	S 3000, Sartomer
MA g PP	Compatibilizer	Exxelor PO1015, Exxon

Main properties and structures of polymers and compatibilizers are mentioned in the theoretical section. However, ratios of en-baco constituents (ethylene, n-butyl acrylate, carbon monoxide, maleic anhydride) are under the DuPont patent.

3.3 LCP Synthesis

In this study, 30 different types of LCPs were synthesized by using aromatic monomers, aliphatic diacids, oligomers and polymers. Abbreviations of these reactants are tabulated in Table 3-7.

Table 3-7 Reactants used in LCP synthesis and the procedure followed to obtain them

	Reactant1	+ Reactant2	→ Reactant in LCP	Code
Aromatic monomers	p-Hydroxybenzoic acid	Acetic anhydride	p-acetoxy benzoic acid	Ar1
	m-Hydroxybenzoic acid	Acetic anhydride	m-acetoxy benzoic acid	Ar2
	-	-	Terephthalic acid	Ar3
	-	-	Isophthalic acid	Ar4
	Hydroquinone	Acetic anhydride	Hydroquinone diacetate	Hq
	Bisphenol-A	Acetic anhydride	Bisphenol-A diacetate	Bp
	1,7 Naphthalenediol	Acetic anhydride	1,7Naphthalene diacetate	Nd
Aliphatic diacids	-	-	Butanedioic acid	Al1
	-	-	Hexanedioic acid	Al2
	-	-	Octanedioic acid	Al3
	-	-	Decanedioic acid	Al4
Oligomers	2,6-Naphthalene dicarboxylate	1,4 Butanediol	Poly(butylene naphthalene)	PBN
	2,6-Naphthalene dicarboxylate	1,6 Hexanediol	Poly(hexylene naphthalene)	PHN
	Dimethyl terephthalate	1,4 Butanediol	Poly(butylene terephthalate	PBT
Polymers	-	-	Poly(ethylene terephthalate)	PET
	-	-	Poly(ethylene naphthalate)	PEN

Some of the aromatic monomers were acetylated (Ar1, Ar2, Hq, Bp, Nd) before use, and some of them were used as received (Ar3, Ar4). Whole aliphatic diacids were used as received (Al1, Al2, Al3, Al4). Flexible diols were included the LCP structures via oligomers (PBN, PHN, PBT). PET and PEN were directly used.

Synthesized LCPs were classified into five main categories according to their structural units. These categories are (I) fully aromatics, (II) fully aromatics + PET/PEN, (III) aromatic acids + diol, (IV) aromatics + short aliphatic chain, (V) aromatic acids + Long Aliphatic chain. The compositions of categories I, II, III, IV and V are given in Table 3-8 , Table 3-9, Table 3-10, Table 3-11 and, Table 3-12 respectively.

The schematic representation of reaction set-up is given in Figure 3-4. Monomers (0.1-0.2 mole in total) were charged into a cylindrical glass reactor (Figure 3-5) with diameter 50mm and length 26cm, fitted with a stainless helix stirrer, nitrogen inlet, vacuum outlet, and a tube connected via a condenser to a condensate collector. The reaction flask was evacuated and purged with nitrogen gas three times to remove all air. The temperature of silicone oil bath was increased to 280°C, and then the reactor was placed in oil bath while the reactants were stirred under a dry nitrogen flow of 30mL/min. The homogeneous reaction mixture was then maintained at 280°C under nitrogen flow for 45min, and at this point, most of the acetic acid as reaction byproduct had been collected. After a while, melt form of LCP reactants turns to turbid and acetic acid which is side product started to bubble. The next stage was carried out under vacuum for an additional 120 min. During this period, vacuum was gradually applied and reached 0.075mmHg at the end of the reaction period. The reaction was stopped by introducing nitrogen gas into the reaction medium and then the flask was immersed in a liquid nitrogen bath. The resulting copolyesters were recovered by breaking the glass container, and dried at 60 °C in vacuum oven overnight. LCPs composed of fully aromatic reactants and acetylated monomers are listed in Table 3-8.

Table 3-8 LCPs (group I) synthesized from fully aromatic acids and acetylated monomers

Sample	Form*	Ar1	Ar2	Ar3	Ar4	Hq	Hq-Cl**	BP
LCP1	100/85	56	16	14	-	14	-	-
LCP2	100/66	22	34	22	-	22	-	-
LCP3	100/66	22	34	22	-	-	22	-
LCP4	100/85	70	-	7.5	7.5	-	-	15
LCP5	100/70	40	-	30	-	-	-	30

In Table 3-8 abbreviations Form* and Hq-Cl** correspond to monomer aromaticity/linearity, and chlorinated hydroquinone respectively.

Form of LCPs indicates the percent aromaticity/ linearity of constituent monomers. The LCPs prepared (Table 3-9) with PET, PEN and other monomers of Group1 is listed in Table 3-9.

Table 3-9 Inclusion of PET and PEN to fully aromatic LCPs (II group)

Samples	Form	Ar1	Ar2	Ar3	Ar4	Hq	Nd	PET	PEN
LCP6	85/85	70	-	-	-	-	-	30	-
LCP7	80/80	60	-	-	-	-	-	40	-
LCP8	75/75	50	-	-	-	-	-	50	-
LCP9	80/80	60	-	-	-	-	-	-	40
LCP10	90/90	80	-	-	-	-	-	-	20
LCP11	80/80	60	-	-	-	-	-	20	20
LCP12	90/90	80	-	-	-	-	-	10	10
LCP13	85/85	50	-	10	-	10	-	30	-
LCP14	90/90	40	-	10	10	20	-	20	-
LCP15	85/75	40	10	10	-	-	10	30	-

The third group based on the inclusion of flexible segments by aliphatic diol into the aromatic structure, different combinations of them is given in Table 3-10.

Table 3-10 Inclusion of butanediol and hexanediol via PBT, PBN and PHN polyesters to aromatic LCPs (group III)

Samples	Form	Ar1	PEN	PBT	PBN	PHN
LCP16	80/80	60	20	20	-	-
LCP17	80/80	60	-	-	40	-
LCP18	80/80	60	-	-	-	40

Effect of flexible short diacid chain length is investigated in fourth group LCPs (Table 3-11). Here decarboxylation mechanism is important.

Table 3-11 Short aliphatic diacid inclusion to fully aromatic LCPs (IV group)

Samples	Form	Ar1	Al1	Al2	HQ	BP
LCP19	70/70	40	30	-	30	-
LCP20	65/65	30	35	-	35	-
LCP21	50/50	-	50	-	50	-
LCP22	65/65	30	-	35	35	-
LCP23	65/30	30	-	35	-	35

Decarboxylation problem in group IV is solved by using long aliphatic diacids in group V (Table 3-12).

Table 3-12 Long aliphatic diacid inclusion to fully aromatic LCPs (V group)

Samples	Form	Ar1	Al3	Al4	HQ	HQ-Cl	BP	PET	PEN
LCP24	70/70	40	20	-	20	-	-	20	-
LCP25	70/70	40	20	-	20	-	-	-	20
LCP26	62/37	25	25	-	-	-	25	-	25
LCP27	62/62	25	-	25	25	-	-	25	-
LCP28	62/62	25	-	25	-	25	-	25	-
LCP29	70/70	40	-	20	20	-	-	-	20
LCP30	70/70	40	-	20	20	-	-	20	-

3.3.1 Effect of Catalyst and Charged Amount on LCP Synthesis

In this study, most of the LCP syntheses have been done based on polycondensation kinetics without catalyst, LCP 24 which shows better mechanical performance with respect to others was synthesized with catalyst to see the effect of longer chain compared to uncatalyzed samples.

When different amount of reactants are used (reactant ratios are same) different visual textures and colors are observed. We investigated this peculiar phenomenon in LCP25 synthesis and characterization.

3.4 Characterization of LCPs

The strategy followed during the characterization of LCPs which is illustrated in Figure 3-2 depends on the experimentally observed characteristics of the LCPs synthesized.

3.4.1 Visual Observation

Visual observations; opacity, transparency, shear whitening, fibril formation, brittleness and toughness of species are primary characterization techniques of LCPs. If opaque specimens whiten under shear with fibrils, most probably it will show Schlieren pattern under polarized light microscope.

Specimens were placed between preheated Teflon sheets on hot stage. After spreading the LCP melt, Teflon films were replaced between the cold iron blocks. At the same time shear was applied in uniaxial direction. LCP films produced enforced uniaxially to check any anisotropic character. These samples are also investigated by X-ray measurements to observe their shear induced crystallization.

3.4.2 Polarized Light Microscope

The liquid–crystalline texture observed using a polarizing microscope shows a typical Schlieren pattern, which is evidence for the presence of nematic phases.

The optical textures of the LCP were studied with a plane polarized light microscope (Figure 3-15) equipped with a digitally controlled hot-stage that can be heated up to 400 °C. The sample was heated between two glass plates up to isotropic transition temperature which is understood via disappearance of birefringence.

Shear was applied during temperature increase to observe the mesomorphic transition temperatures, which are crystal to nematic (T_m) and nematic to isotropic transitions (T_i). Some samples showed fiber formation between T_m and T_i which was noted as T_f point.
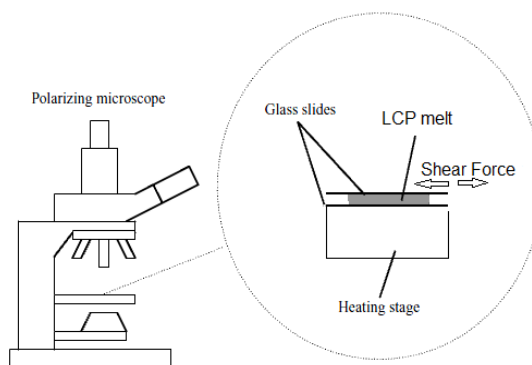
Figure 3-15 Polarized light microscopy system

3.4.3 Fiber Forming Capacity of LCPs

Fiber spinning by micro compounder machine needs at least 13g of material that is significantly high weight for LCPs. Prior to fiber spinning small amount of LCP was used to check fiber formation before working with micro compounder's fiber drawing unit. To prevent oxidation LCPs were heated in the closed quartz; one side is nitrogen gas input (0.1L/min) and another side is closed with holed cork. Piece of LCP was placed on a wire (Figure 3-16) via an orifice and heated up to melting temperature, then pull out suddenly to form fiber.
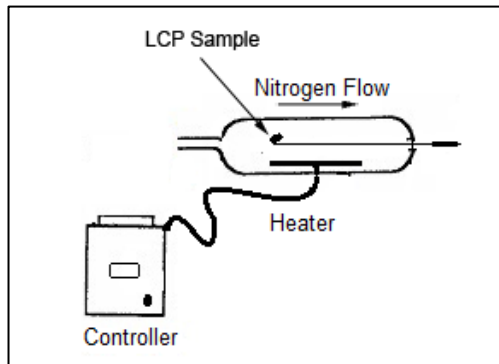
Figure 3-16 Setup to check fiber forming capacity of LCPs

3.4.4 Drying Procedure of Thermoplastics

Drying of thermoplastics, especially in PET and polyamide, is the most critical point before processing. Failure in meeting the correct drying criteria cannot be corrected in subsequent melt operation. Obtaining dry materials from manufacturers is mostly problematic. To solve this problem, by using Fick's law of diffusion phenomena we modified our reactor setup (Figure 3-17) and connected to vacuum oven (Figure 3-18). The oven was evacuated and purged with nitrogen gas three times to remove all air. The temperature then increased to 60°C for PA6 and 170°C for PET. One hour dry nitrogen flow (0.1L/min) was followed by 15 min vacuum (0.1mbar) in sequence. From the mechanical performance of these fibers, we concluded that 12h for PA6 and 24h for PET was enough. In addition, ABS was dried at 80°C for 12h under the same condition. Because of the non-polar character, PP was dried 24h in conventional oven at 50°C.
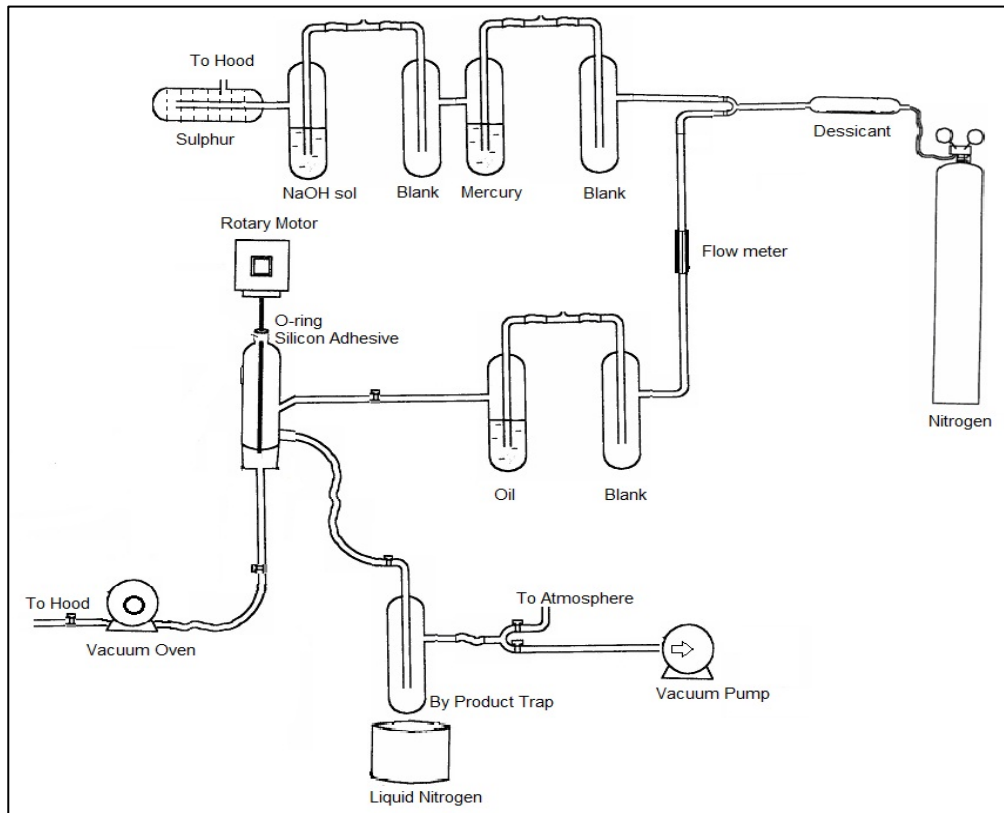
Figure 3-17 Setup for drying of thermoplastics modified from the setup used in LCP synthesis

Figure 3-18 Vacuum oven for sample drying

3.4.5 Micro-Compounder and Spin Line

Fiber studies of LCP and LCP-thermoplastic blends were performed by a twin screw micro compounder (Figure 3-19) coupled with winding unit between 2-100 rpm, at melting temperatures under nitrogen atmosphere. After spinning process, as-spun monofilaments were drawn (1:4) at room temperature and 130 ^{o}C with varying diameters of 40-50 µm by using drawing unit (Figure 3-20).
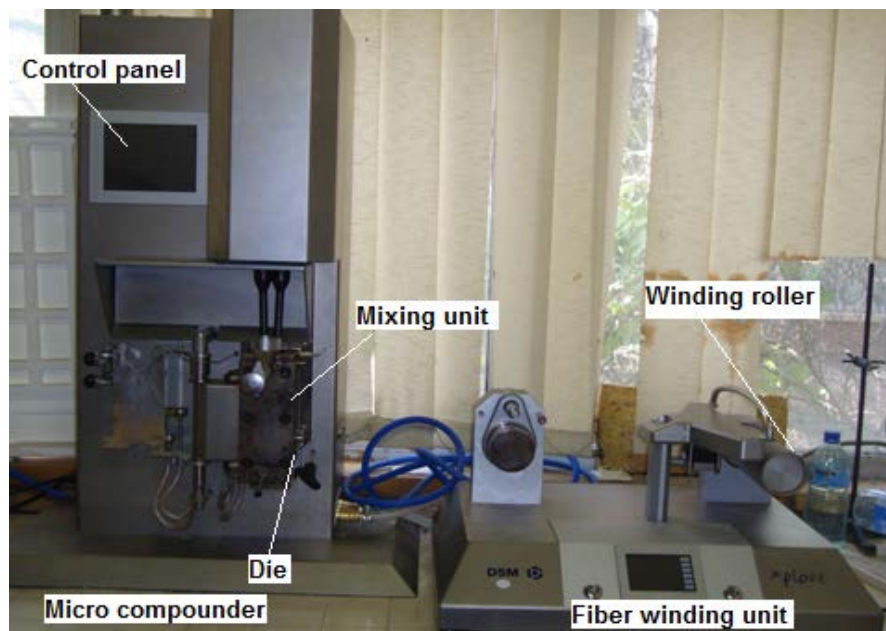
Figure 3-19 Micro-compounder (DSM Xplore, 15 ml capacity) and fiber winding unit
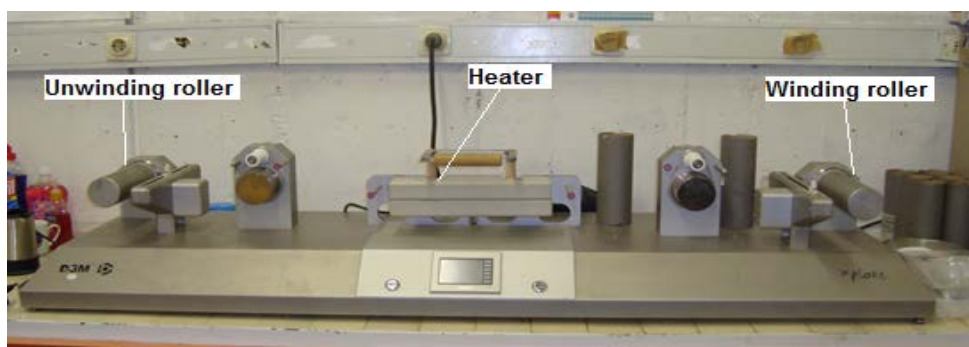
Figure 3-20 DSM Xplore Microfiber spin line

After completing mixing, the twin screw extruder is operated in force controlled mode, melt flow rate around 0.5 g/min with 0.25 mm die diameter and 200 m/min spinning speed.

Twin screw compounder with a capacity of just a few grams of material presents unique quality (Table 3-13) for the well-developed dispersion and mixing.

Table 3-13 Specification of Xplore Micro-Compounder

Mixing/Dispersion control type	RPM or Axial Force
Maximum axial Force:	8000 N
Screw speed range	1-250 RPM
Hopper volume:	15 ml
Maximum torque	10 N/m per screw

3.4.6 Extrusion

Thermo Prism TSE 16 TC twin screw extruder (Figure 3-21) was used for the preparation of the blends/composites.
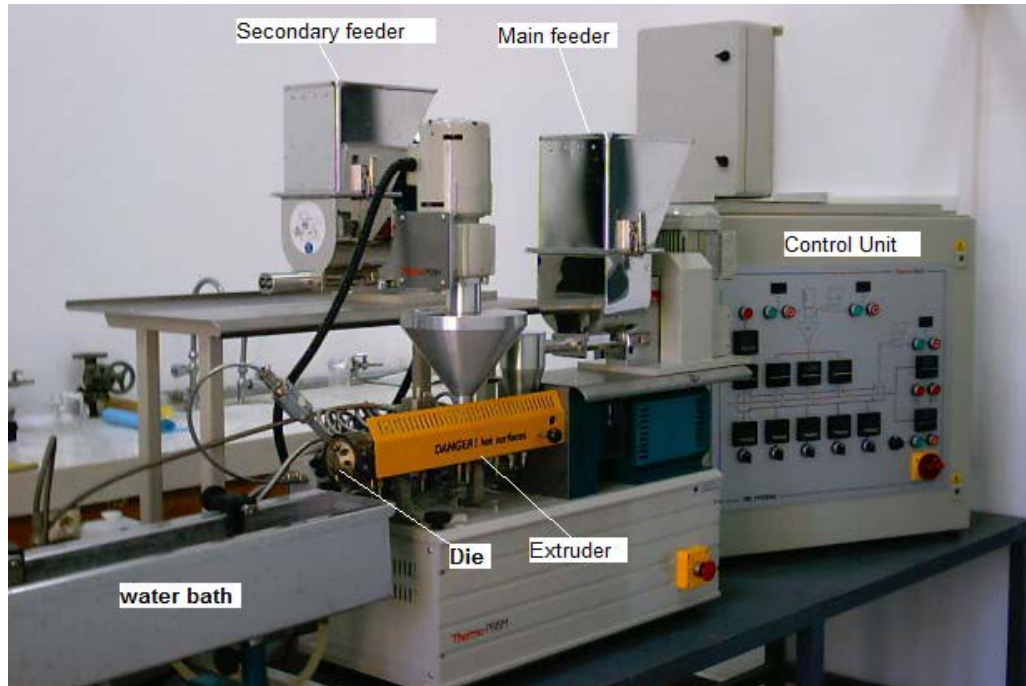
Figure 3-21 Thermo Prism TSE 16 TC twin screw extruder

Table 3-14 Specification of the twin screw extruder

Screw Type	Co-rotating
Twin Bore Diameter	16 mm
Screw Diameter	15.6 mm
Maximum Screw Speed	500 rpm
Barrel Length	384 mm
Die Length	16 mm
Torque per shaft	12 N/m

Temperature profile throughout the screw has five zones and the temperature was adjusted to processing temperatures of thermoplastics (Table 3-15). Prior to processing, the polymers and LCP were dried as mentioned in drying section. The ABS/PA/LCP batches containing compatibilizers were processed in a co-rotating twin-screw extruder at a screw speed of 190rpm and barrel temperature profile of 200-220-220-230-230°C. The extrudate was cooled in water bath and then chopped into pellets. The pellets produced were dried at 80°C for 12 h prior to the injection molding.

Table 3-15 Barrel temperature profiles for different thermoplastics containing LCP

	Temperature (°C) (feeder to die)	Screw speed
ABS	195-230-230-235-240	150
PP	190-220-220-220-220	100
PET	190-250-270-270-270	100

3.4.7   Fiber Tensile Test

Tensile test of LCP mono filaments were made on the specimens spun from fiber spinning device (Figure 3-19) and from second drawing unit (Figure 3-20) with 0.1-0.4 mm diameter and 20-30 mm gauge length. The measurement was made with 10N load cell on Lloyd tensile machine (Figure 3-22) according to ASTM-D3379.
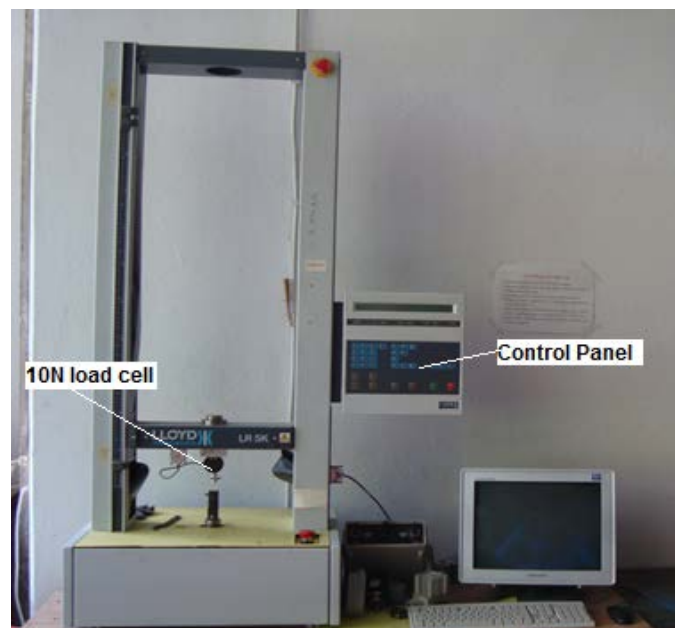
Figure 3-22 Lloyd Tensile Machine

Dimensional measurement of fibers was made by 400 X usb microscopes. Tensile measurements of fibers were repeated five times for each sample and the average value was calculated.

3.4.8 Microinjection

A laboratory scale injection molding machine (Microinjector, Daca Instruments) shown in Figure 3-23 was used to mold (Figure 3-24) thermoplastic-LCP blends. Tensile test for composite applications of LCP blends were made on injection molded dog-bone shape specimens with dimension (50x7.2x2) mm (Figure 3-25) for mechanical characterization. The measurement was repeated three times for each type of sample and the average value was calculated. Molding parameters given in Table 3-16 were kept constant throughout the molding process.

The tensile measurement of dog-bone was made with 5kN load cell on Lloyd tensile machine (Figure 3-22) according to ASTM D638-03.
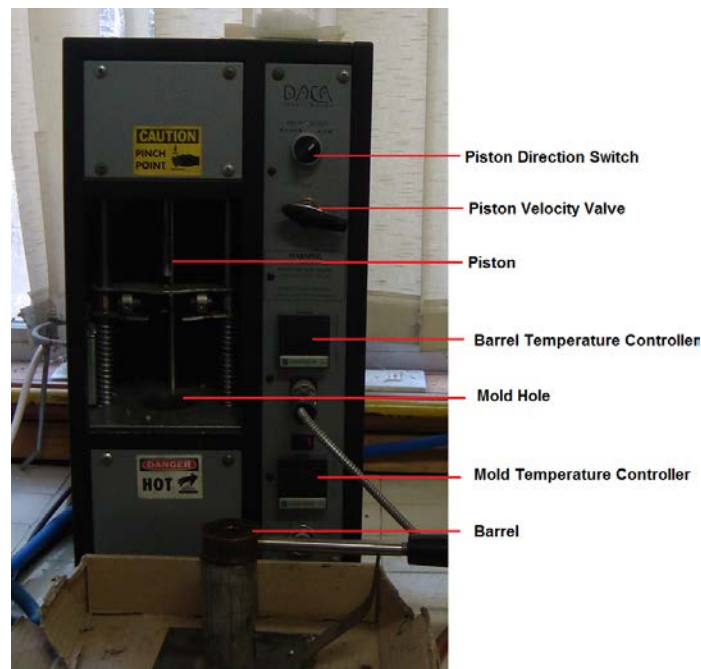
Figure 3-23 Micro injection Molding Machine

Figure 3-24 The mold in Daca micro injection machine
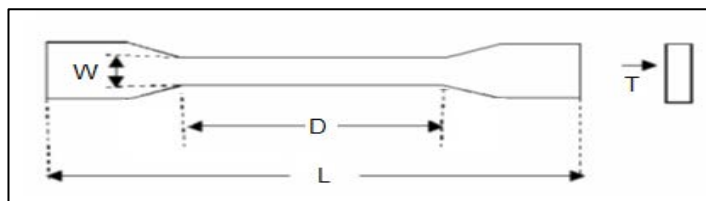
Figure 3-25 Daca injection molded sample with dimensions

In Figure 3-25 dimensions of the dog-bone are D= 50mm, Width (W)= 7.2mm, Thickness(T)= 2mm

Table 3-16 Molding parameters for Injection Molding

Thermoplastics	Nozzle T. (^{o}C)	Mold T. (^{o}C)	Fill Time (sec)	Hold Time (sec)	Pressure (bar)
ABS	230	80	30	60	8
PP	190	25	30	60	8
PET	275	25	30	60	8

3.4.9 Differential Scanning Calorimeter (DSC)

DSC analyses were carried out from 25 °C to 400 °C with a 10 °C/min heating rate under nitrogen atmosphere by using a differential scanning calorimeter Scinco N-

650. The transition temperatures and annealing phenomena of species checked by two sequential heating as 25°C-400°C, 400°C-25°C, 25°C-400°C.

3.4.10 Nuclear Magnetic Resonance (NMR)

Nuclear Magnetic Resonance (NMR) (1H, 13C) spectra was recorded as in parts per million (δ) by Bruker Avance DPX 400 at a frequency 400 MHz, reference downfield shift from tetramethylsilane (δH 0.00) Coupling constants (J values) are reported in hertz (Hz), and spin multiplicities are indicated by the following symbols; s: singlet, d: doublet, t: triplet, q: quartet, dd: doublet of doublet.
1:1 trifluoroacetic acid:chloroform mixture was used to dissolve LCP specimens.

3.4.11 Thermogravimetric Analysis (TGA)

Termogravimetric analyses (TGA) of species were made by Perkin Elmer Pyris-I under nitrogen atmosphere between 25°C-700°C with 10°C/min speed.

3.4.12 X-Ray Diffraction (XRD)

3.4.12.1 Wide Angle X-ray Scattering (WAXS)

X-ray diffraction patterns were recorded by a RIGAKU Ultima IV (settled in METU Central Lab) X-ray diffractometer at 40 kV and 30 mA, using a monochromatic Cu Kα radiation source (λ=1.54). Samples were scanned from 2$\emptyset$ =10 to 40° at a scan rate of 1° / min with step size 0.01°.

3.4.12.2 Fiber Diffraction

Rigaku R-Axis IIc, (settled in Kordsa Global) is a diffractometer system with an image plate (IP) and detector for crystalline structures of macromolecules. This system was used for fiber diffraction study of LCP samples by Laue method.

3.4.13 Fourier Transfer Infrared Analysis (FTIR)

For film formation LCP species are pressed at their melting point between teflon films before FT-IR Spectroscopy measurement in attenuated total reflectance (ATR) mode using IR-spectrometer (Varian). The measurement was done at a resolution of 2 cm^{-1} with 32 scans between 600-4000cm^{-1} wavenumbers.

3.4.14 Carboxyl End Group Analysis (CEG)

Ideally, number-average molecular weights (M_n), weight-average molecular weight (M_w) and the size average molecular weight (M_z) of polymers are determined by Gel Permeation Chromatography (GPC) which is a type of size exclusion chromatography (SEC) that separates analytes on the basis of size. However, theta state of our LCPs is reached by orthocresol solvent which is highly toxic and not used under standard laboratory conditions, thus number of –COOH terminal groups measured by CEG analysis was used for the determination of molecular weight and extent of the reaction.

Carboxyl End Groups (CEG) of LCP samples was determined by colorimetric acid-base titration, ASTM D 7409. This test method is for the determination of CEG of PET and applicable to polyester based LCPs. Approximately 0.25g of LCP was weighed and placed into a 125ml erlenmeyer flask, then 15ml of orthocresol solvent and a magnetic stir bar are added. The flask was connected with condenser to prevent evaporation and placed on a hot source (80°C) until dissolution is completed. The flask was removed from the hot source and quenched by adding 60ml of dichloromethane to the orthocresol solution. Stirred for an additional 5 min. PET solution was titrated with KOH/methanol solution in burette. 2 drops of 1% bromophenol blue indicator in methanol was added to the LCP solution and titrated to a violet end point. The test procedure was performed on three samples and a blank.

3.4.14.1 Molarity of KOH/Methanol Solution

Approximately 0.2g KOH (3 pellets) dissolved in 1L of methanol. After dissolution was completed, it is titrated with Potassium Hydrogen Phthalate (KHP) to determine the molarity of the KOH solution. 0.01 to 0.02g of KHP crystals were measured into a 150 ml beaker and dissolved in 50ml of DI water. KHP solution was titrated with the KOH/methanol solution until an endpoint of pH 7 is reached. Molarity of the KOH/methanol solution was calculated using the following formula:

[OH] = (w/204.23) x (1/v)   where:
w = weight of KHP (g),
v = volume to titrate to pH7 (L)

3.4.14.2 CEG Calculation

CEG values are calculated by using Equation 3-1.

$$CEG \ (mmol/kg) = [(Vs - Vb) \ x \ (M) x 1000] \ /w \tag{3-1}$$

Vs(ml): volume of KOH solution to titrate the sample,
Vb(ml): volume of KOH solution to titrate the blank,
M(mole/L): molarity of KOH/ methanol solution, and
w(g): weight of PET sample.

3.4.15 Intrinsic Viscosity (IV)

Intrinsic viscosity (IV) of LCP samples were determined by glass capillary Ubbelohde viscometer, ASTM D 4603 (Figure 3-26). This test method is for the determination of the inherent viscosity of PET and applicable to polyester based LCPs. LCP samples are prepared at $25^{o}C$ in 60/40 phenol/1,1,2,2-tetrachloroethane solution. If highly crystalline forms of LCP that are not soluble in this solvent it was dissolved in trifluoroacetic acid. The polymer solution (0.5g/dl) were prepared and waited about 24h at room temperature. Impurities are filtered before measurement.
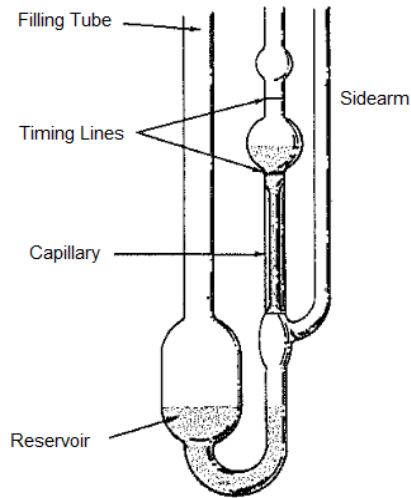
Figure 3-26 Ubbelohde viscometer [175]

Derivative of viscosity (η) of the solution is plotted (Figure 3-27) against its concentration C (g/dL). Two main parameters are utilized; relative viscosity (η_r) and reduced viscosity (η_{red}).

η_r= viscosity of solution/viscosity of the pure solvent=η/η_o

η_{red}=(n_r-1)/C
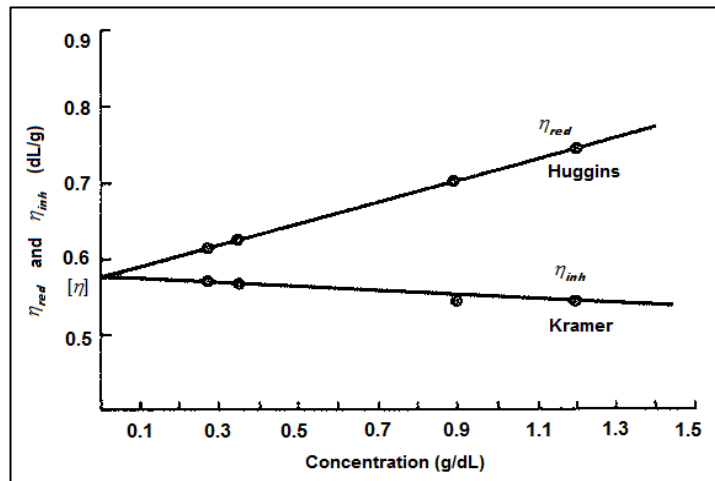
Figure 3-27 A typical graph for the determination of intrinsic viscosity

To check the compatibility of measured data, η_{red} (Huggins) and η_{inh}(Kramer) values plotted against the concentration, and they should have the same cross section point, so called intrinsic viscosity [η] (Figure 3-27).

The viscosity molecular weight (M_v) can be obtained if 'K' and 'a' constants are known by using the Mark-Houwink equation, given as:

$$[\eta] = KM_v^a$$

(3-2)

However 'K' and 'a' values are depends on polymer, solvent and temperature that cannot be generalized among polyesters.

3.4.16 Melt Flow Index (MFI)

Melt flow index (MFI) is defined as the mass flow rate of polymer through a specified orifice and expressed as grams per 10 minutes. Measurements were made by using Coesfeld Melt Flow Indexer (Figure 3-28) according to temperature and load of ASTM. LCP and PET blends measured according to ASTM D1238-79, at 250 °C under 2.16 kg load. ABS blends were measured according to ASTM D 1238 with 5 kg load at 230 °C.
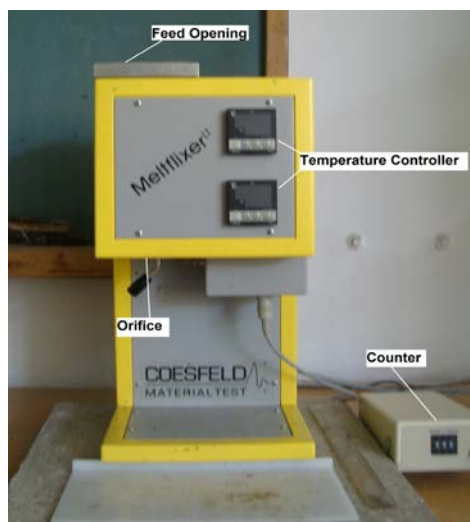
Figure 3-28 Device used for MFI measurement

3.4.17 Capillary Rheometry

The apparent shear viscosity of the ABS/PA6/LCP/Lotader2210 blends were measured by using LCR Series capillary rheometer. The experiments were performed at 230°C and at shear rate from 30 to 2700 s^{-1}. The dimensions of the die used in measurement were: 30.48 mm capillary length, 0.762 mm capillary diameter (L/D=40).

3.4.18 Surface Energy

Surface energy measurements of polymer films and fibers were made by two static techniques; direct and indirect contact angle measurement via camera and microbalance respectively.

3.4.18.1 Surface Energy of Polymer LCP Films

Interfacial adhesion forces between LCP and thermoplastic matrix are related with the surface free energies of species measured by modified Weissenberg camera system (Figure 3-29). Captured photos of probe solutions in the form of sessile drop at 60X in horizontal direction (Figure 3-30) on flat LCP film was used for direct contact angle measurement by using imageJ freeware software that was developed

89

by US National Institutes of Health [198]. Contact angle and surface energy relationship is explained in the theoretical part.
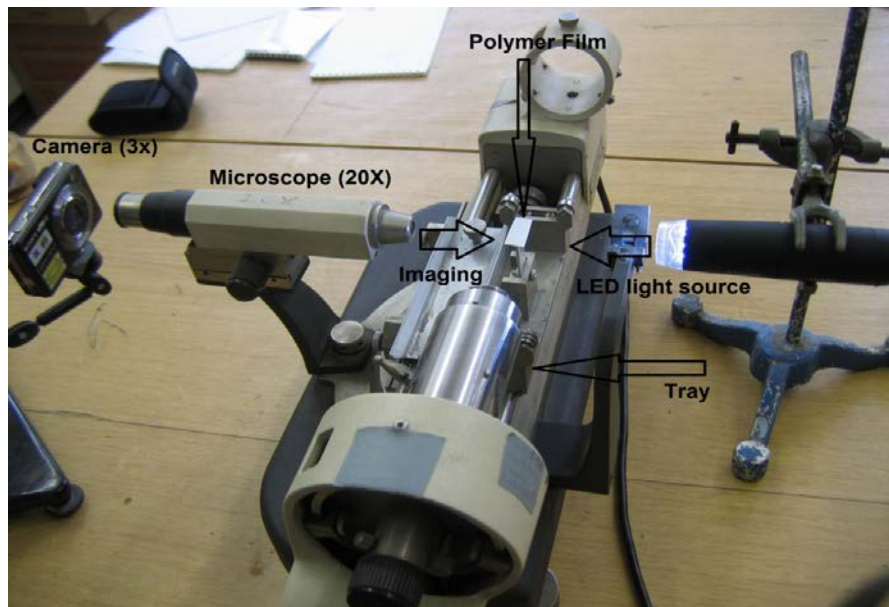
Figure 3-29 Polymer film contact angle measurement setup, modified from X-ray Weissenberg Camera
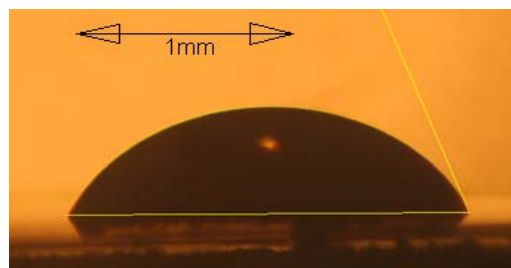
Figure 3-30 A probe solution on LCP film recorded by using setup in Fig 3-29

3.4.18.2 Surface Energy of LCP Fibers

Contact angles of fibers are indirectly measured by Wilhelmy plate methods [199]. Set up equipped with microbalance (Sartorious M25D) and a vertical motion stage with micrometer precision (Figure 3-31). Forces on 1-2 cm length fiber samples are

digitally read out. Force, contact angle and surface energy relationship is explained in theoretical part.
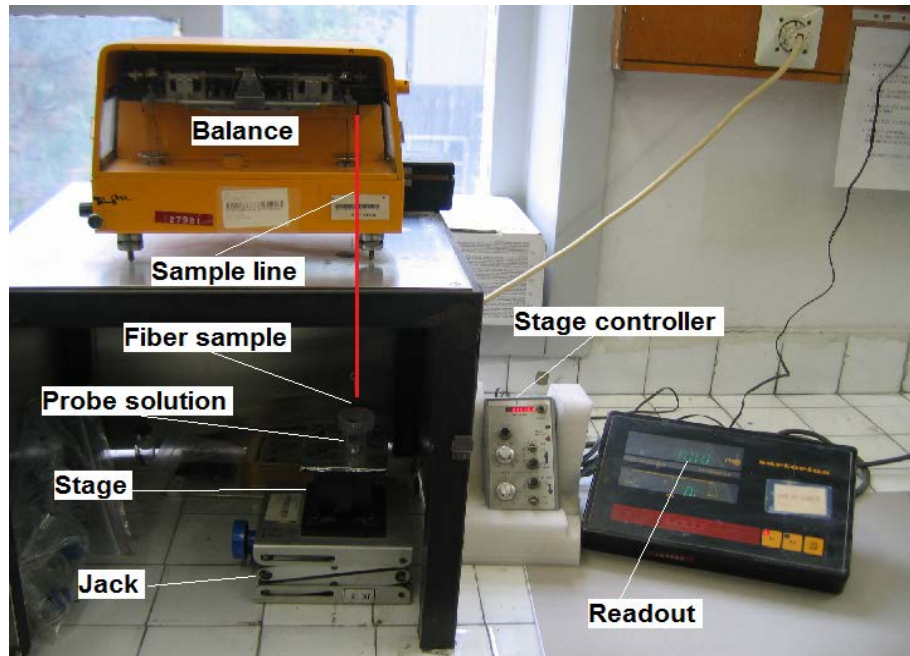
Figure 3-31 Setup used for surface energy of fibers

3.4.19 Electrospinning

In the electrospinning of the polymer solutions, when an appropriate dc voltage (10-30kV) with low current (milliampere) is applied to a liquid droplet, the body of the liquid becomes charged, and electrostatic repulsion counteracts the surface tension and droplet is stretched. A critical point a stream of liquid erupts from the surface and attracted towards the collector plate. Due to the whipping jet, sprayed jet dries during the flight between needle and collector thus polymer fibers are collected on collector plate. (Figure 3-32). Evaporation rate which is proportional with vapor pressure of the solvent is important for drying rate of the chains during jet (Table 3-17).

Table 3-17 Physical properties of solvents used in electro-spinning

Solvent	Density (g/cm^3)	Boiling Point (^{o}C)	Vapor Pressure (Pa)
Dimethylacetamide	0.94	165	330
Dimethylformamide	0.95	153	492
N-Methyl-2-pyrrolidone	1.03	202	66

Optimization of conditions such as solvent selection (Table 3-17), concentration of LCP, the needle-collector distance (NCD), solution injection rate, DC voltage, DC current are adjusted after tentative trial and error method (Table 3-18).

Table 3-18 Optimized conditions for LCP electrospinning

DC Voltage	DC current	NCD	Concentration	Injection rate
17kV	5mA	20 cm	60 wt.%	100 µl/min
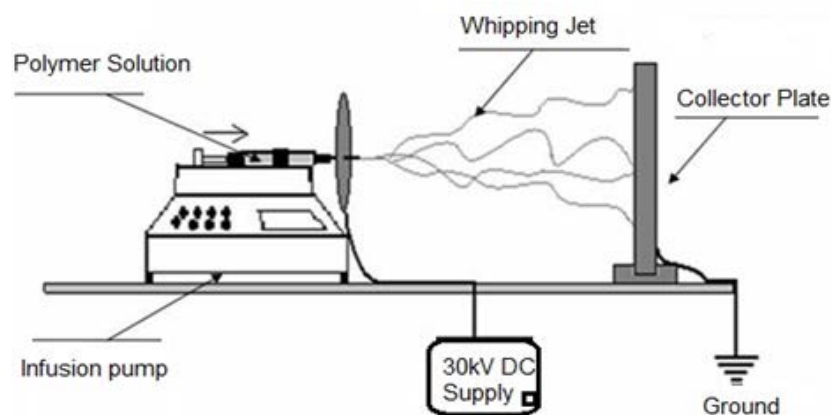
Figure 3-32 Scheme of the electro-spinning setup

3.4.20 Electrical measurement

For dielectric measurements, the surfaces of the samples were covered with silver paste to form electrodes. The dielectric measurements were performed between 20Hz and 1MHz frequency range at different temperatures (25°C-100°C) by using

Agilent 4284A LCR Meter. The real part of dielectric constant was calculated by using following equation:

$$\varepsilon' = \frac{C_P d}{\varepsilon_0 A}$$

(3-3)

where, C_p is the capacitance of the sample, ε_0 (dielectric permittivity in vacuum) which is equal to 8.85 x 10^{-4} F/cm, A is the effective surface area, and d is the thickness of the samples. AC-conductivities (σ_{ac}) of the samples were calculated with the following equation:

$$\sigma_{ac} = \frac{\omega C_p d \tan \delta}{A}$$

(3-4)

where ω is the angular frequency ($2\pi f$)

CHAPTER IV

RESULTS AND DISCUSSIONS

4.1 LCP Groups

Synthesized LCPs are categorized according to their constituents and their properties (Table 4-1). The LCP's synthesized are classified in 5 groups (Table 4-1); (I) fully aromatics, (II) fully aromatics+ PET/PEN, (III) Ar1+PEN+oligomer aromatic acids, (IV) aromatics + aliphatic di-acids, (V) aromatics + long aliphatic di-acids. Relaxation time of LCP increases with increasing the gap between T_m and T_{ni} which is defined as LCP temperature window. Polarized light microscopy is used for the observations given below.

Group I is composed of wholly aromatic polyesters. LCP1 is composed of all trans monomers hence has high T_m. LCP2 has relatively low melting point (260^OC) due to m-acetoxy benzoic acid that interferes with the all trans structure of LCP1 with a 60 ^{O}C nematic window. LCP3 has a lower melting point due to the presence of chlorinated hydroquinone diacetate. LCP3 has an extraordinary large (100^OC) nematic window. LCP3 can be used with polyamides with melting points above 250^OC and with other high melting polymers. LCP4 and 5 contain Bisphenol-A (BP) which prevents crystallizations due to bulky groups in this structure. LCP25 which also has 25% BP is also amorphous.

In Group II the novelty is the inclusion of PET and PEN polymers, 10% to 50%, with aromatic acid monomers and diol derivatives. Here, besides the polymerization of the monomers by condensation lots of trans-esterification reactions take place

between the oligomers and PET or PEN. Interesting structures arise in conjunction with these various reactions. We see that in LCP 6 the non-fusible para acetoxy benzoic acid (Ar1) is made fusible (310°C) by inclusion of PET 30%. LCP7 has a lower melting point (250°C) when PET content is increased to 40%. LCP8 has even lower T_m 220°C, a nice low value with about 40°C nematic processing window in these last three LCP's. It seems like that we can have required level of melting temperature and nematic window by adjusting the ratio of Ar1 to PET in the copolymer. This gives a simple and useful liquid crystalline polymer with low T_m.

LCP9 and LCP10 are not crystalline when we use PEN instead of PET. The asymmetry created due to naphthenic groups is responsible for the lack of crystallinity. As a result we can eliminate PEN in these types of binary copolyesters. LCP11 and LCP12 contain PET plus PEN in their structures. When used together the LCP phase is observed at surprisingly low temperature. When Ar1 content increase from 60% to 80% T_m increases from 190°C to 220°C. These three component LCP's are also good candidates as low T_m liquid crystalline systems. LCP13, LCP14 and LCP15 are all aromatic diacids and modified diol monomers with PET. One of them is kinked (LCP15) which contain m-acetoxy benzoic acid (Ar2) in its structure. Among these three only the kinked one has a low T_m of 210°C which can be considered as feasible LCP for low temperature applications.

Group III contains Ar1, our main monomer that is responsible from LCP behavior, with polymer PEN and PBT and oligomers PBN and PHN. These three samples (LCP16, LCP17, and LCP18) showed poor liquid crystalline behavior due to relatively long aliphatic chains. They have quiet small nematic windows and not suitable candidates as low T_m LCP compounds.

Group IV that has 5 different LCP compositions is interesting. Here we tried to investigate the effect of long aliphatic chain diacids on the melting temperature of copolyesters and their effect on the liquid crystalline behavior. As aliphatic diacids we used butanedioic acid (Al1) and hexanedioic acid (Al2). All the samples that have Al1 and Al2 underwent decarboxylation and decomposed [64]. We can say that these acids are not suitable for polyester formation.

Table 4-1 Melting temperature (T_m), fiber formation temperature (T_f) ,nematic to isotropic transition temperature (T_{ni}) and visual observation of LCP samples under polarized light microscopy.

	Samples	T_m	T_f	T_{ni}	Microscopy
	LCP1	-	-	-	Infusible
I	LCP2	260	280	310	Colorful
	LCP3	250	280	350	Colorful
	LCP4	300	-	-	Amorphous
	LCP5	230	260	-	Amorphous
II	LCP6	300	320	340	Colorful
	LCP7	250	270	300	Colorful
	LCP8	220	230	250	Colorful
	LCP9	240	260	290	Het.*
	LCP10	260	310	330	Het.*
	LCP11	190	210	240	Colorful
	LCP12	220	240	260	Colorful
	LCP13	280	300	320	Colorful
	LCP14	270	300	320	Colorful
	LCP15	210	250	300	Colorful
III	LCP16	250	-	-	Het.*
	LCP17	190	-	200	Het.*
	LCP18	190	-	200	Het.*
IV	LCP19	-	-	-	Decompose
	LCP20	-	-	-	Decompose
	LCP21	210	220	-	Het.*+ Decompose
	LCP22	190	210	-	Het.*+ Decompose
	LCP23	-	-	-	Decompose
V	LCP24	170	200	230	Colorful
	LCP25	195	210	300	Colorful
	LCP26	210	220	-	Amorphous
	LCP27	220	250	300	Colorful
	LCP28	160	180	220	Colorful
	LCP29	150	170	220	Colorful
	LCP30	200	220	300	Colorful

Abbreviations in Table 4-1 Het.* corresponds to heterogeneous LCP domains under polarized light microscope.

In group V besides our main component Ar1 long aliphatic chain, octanedioic and decanedioic diacids are used with a variety of diols and modified diols incorporating PET or PEN into the formulation. What was expected was to obtain even lower melting LCP's, lower than 200°C. Indeed excluding LCP26 which contains

Bisphenol-A (Bp) that is known to inhibit crystallinity, all the other compositions from LCP24 to LCP30 exhibited LCP behavior with very low T_m. In LCP29 a very low T_m of $150^O C$ is reached. Here we see again the effect of chlorinated hydroquinone diacetate.

In summary Group V is the culmination of the previous compositions where T_m is lowered without losing LCP behavior by inclusion of PET, using aliphatic diacids that contain at least 8 carbons, and using chlorinated hydroquinone diacetate. When we kept the p-acetoxybenzoic acid (Ar1) above %30, interesting low T_m LCP compounds are synthesized. These additives can be used as flow adjuster and viscosity reducers in fiber technology and in the production of molecularly reinforced thermoplastic matrices with superior qualities.

4.2 Notes on Visual Observation

As a primary method visual observations give clue about experimental success of LCP synthesis. If opaque species whitens under shear with fibrils (Figure 4-1 A) it will most probably show continuous birefringence pattern under polarized light microscope and shows LCP characters in following characterization methods. On the other hand transparent and brittle species (Figure 4-1 B) is most probably non LCP that may show partially birefringent pattern but no characteristics of LCP phase.
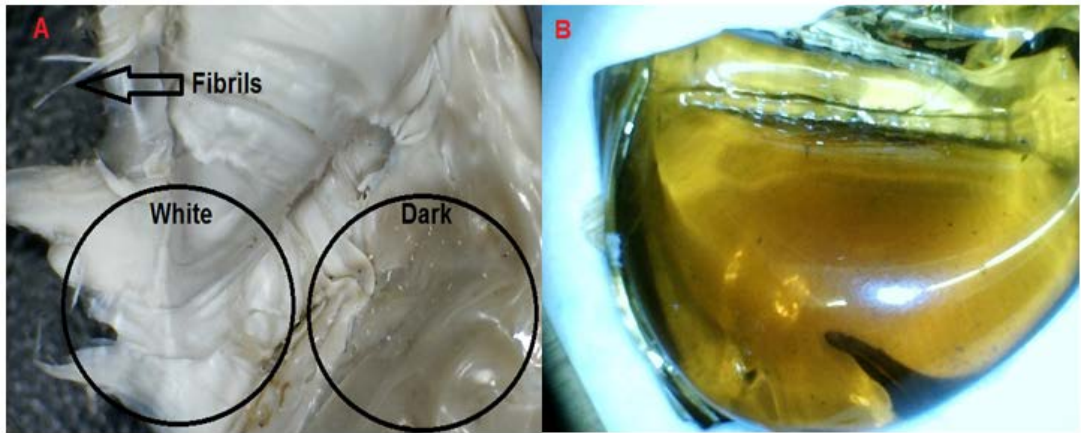
Figure 4-1 Photos shows shear whitening and fibril formation in opaque LCPs (A), brittle and transparent non LCPs (B).

LCP films produced between Teflon sheets are pulled manually in the flow direction and normal to the flow direction. In flow direction the films are stronger compared to normal direction. The films pulled in normal direction gave rise to delamination (Figure 4-2 a). This is again a simple test that shows uniaxial alignment of the polymer chains, i.e. nematic behavior. In Figure 4-2 b one can observe the delamination of a single fiber in knot formation which is an indication of uniaxially oriented LCP phase [200].
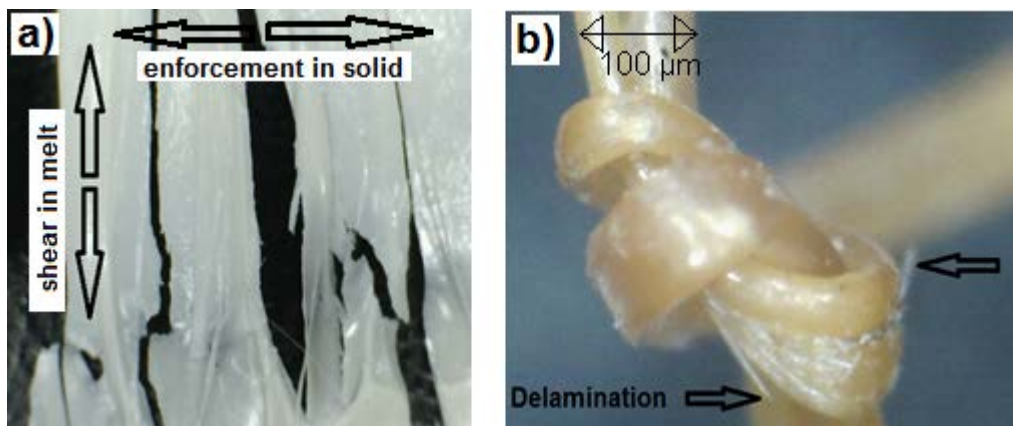
Figure 4-2 Delamination of LCP a) film and b) fiber

4.3 Notes on Polarized Light Microscopy

Microscopic Investigation on samples by polarized light microscopy is simple and fast method to observe the LCP behavior. On the other hand, melting temperature (T_m), fiber formation temperature (T_f) and nematic to isotropic transition temperatures (T_{ni}) were measured by microscopy and summarized (Table 4-1). The processing temperature of LCPs defined and labeled with T_f at which polymer chains are free enough to form fiber by applied shear in drawing line. Highly aromatic and para substituted constituent of LCPs such as LCP1 has infusible matter that cannot be investigated by microscopy.

In addition to observation of transition temperatures (T_m, T_f, T_{ni}), microscopic views (Table 4-1) are generalized as colorful, amorphous, heterogeneous and decomposed that give information about LCP characters. Each texture and color corresponds to the different morphology of LCPs and they are simplified by the above mentioned terms.

4.3.1 Specimens with no LCP Property

In polyester formation, condensation of monomers, transesterification of oligomers/polymer and side reactions proceed together. In this context there are two main reasons that give amorphous polyesters and decomposed products other than polyesters that are seen as dark matter at melting temperature under microscope (Figure 4-3).

i)   High kink monomer ratio,
ii)   Decarboxylation of diacids

i) As kink groups are not linear they should be kept less than 33% in LCP synthesis , that we obeyed this rule while using m-acetoxy benzoic acid (Ar2) and acetylated bisphenol-A (Bp), however, high bulky character of Bp prevents crystallization and gives amorphous specimens at 15% and 30% usage in LCP4 and LCP5 respectively.

ii) Decarboxylation of butanedioic and hexanedioic acids is a kind of decomposition that causes the loss of stoichiometric balance and brings side products in group IV; LCP19, LCP20, LCP23.
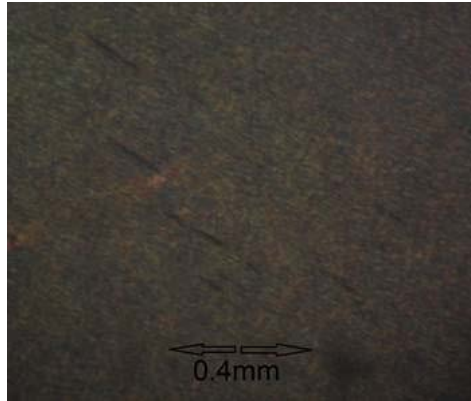
Figure 4-3 Microscopic view of specimens that have not LCP properties

4.3.2 Specimens that have Partial LCP Properties

Beside side reactions mentioned in section 4.3.1 there is another but less detrimental one that brings heterogeneous LCPs. Hydroxyl end groups of butanediol and hexanediol facilitate formation of cyclic oligomers via back-biting reaction that leads to unwanted products in group III members; LCP16, LCP17, LCP18 (Figure 4-4).
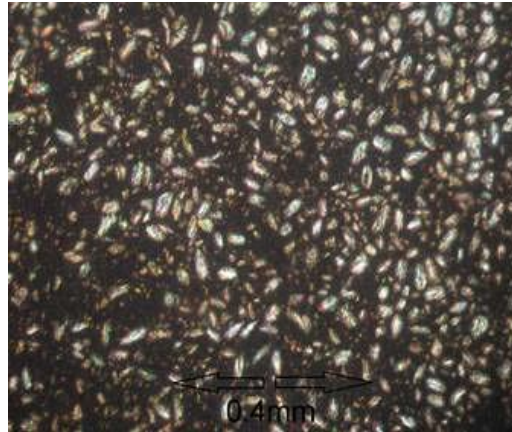
Figure 4-4 Microscopic view of heterogeneous LCPs

Heterogeneous and decomposed products may be present at the same time in LCP21 and LCP22 (Figure 4-5). In this case shiny heterogeneous domains found in part of picture and other decomposed part fills the rest.
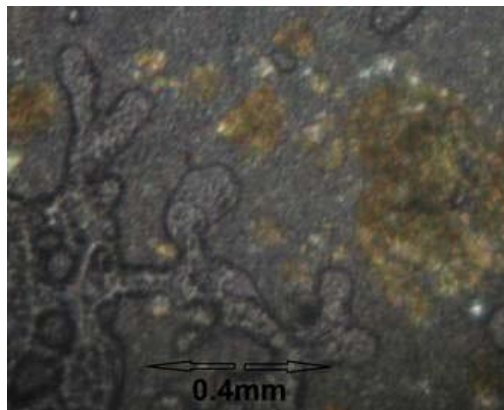
Figure 4-5 Microscopic view of heterogeneous LCP and decomposed specimens together

4.3.3 Specimens that have LCP Properties

Color development of LCP species under polarized microscope depends on the duration of the reaction in the reactor. If reaction time exceeds two hours LCP could not be spread completely between glasses and stays as shiny clusters between

glass plates (Figure 4-6). These high melt viscosity LCPs could not be drawn as a fiber and could not be used as reinforcing agent in a matrix.
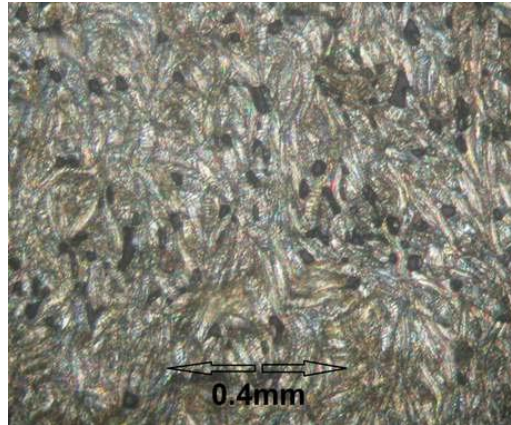
Figure 4-6 Microscopic view of high melt viscosity LCP

If reaction time is too short (less than an hour) low molecular weight LCP is produced with low melting point (180°C-250°C) that readily spreads between glasses and give a pale color. As short LCP chain has short relaxation time, the colors disappear in less than a second after removing pressure which is difficult to capture with standard photographic equipment. A blurry picture can be obtained (Figure 4-7).
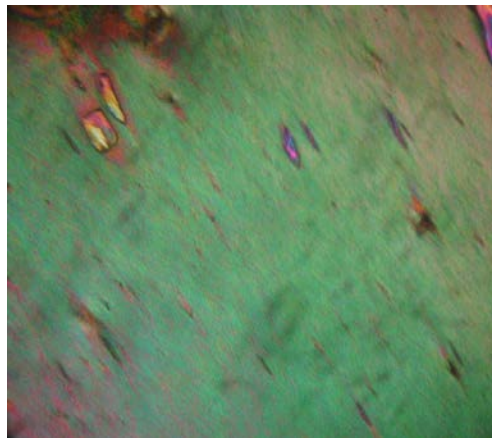
Figure 4-7 Microscopic view of low melt viscosity LCP

Members of group V LCPs are capable of fiber formation and have moderate relaxation time and maintain their sharp color (Figure 4-8) for a few second after

removing the force (Figure 4-9). If relaxation time is long enough color stays even more after removing the pressure from top cover (Figure 4-10).
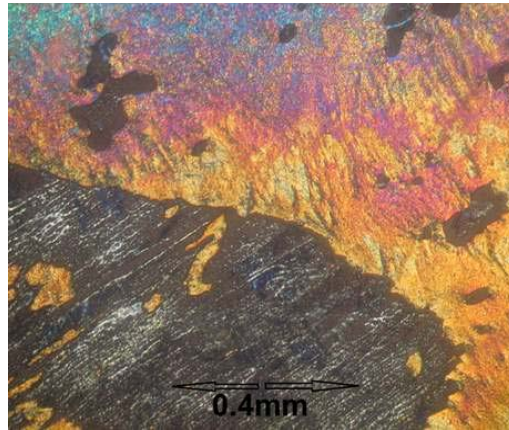
Figure 4-8 LCP under shear between nematic to isotropic transition temperature. Dark region comes from emptiness or insufficient matter for shear application
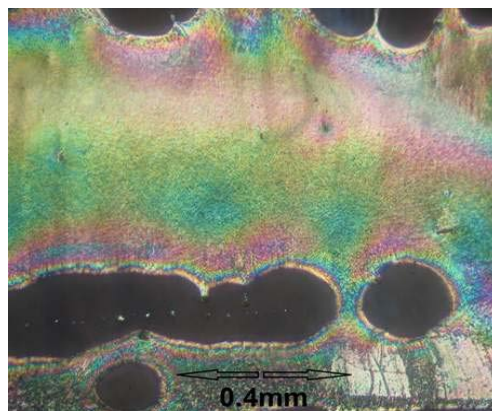
Figure 4-9 LCP sustain its color after removing shear, between nematic to isotropic transition temperature. Black holes represent empty regions
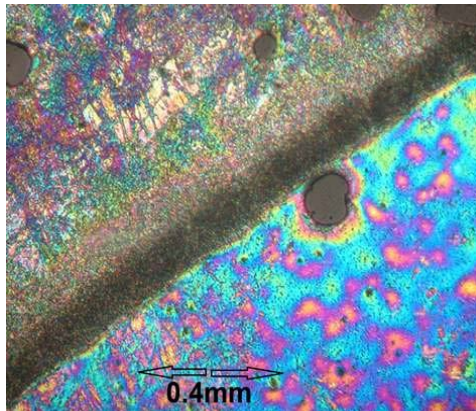
Figure 4-10 LCP sustain its color even after removing glass top cover, between nematic to isotropic transition temperature

If colorful LCPs heated up to isotropic transition temperature color vanishes and turns to shiny liquid under microscope (Figure 4-11).
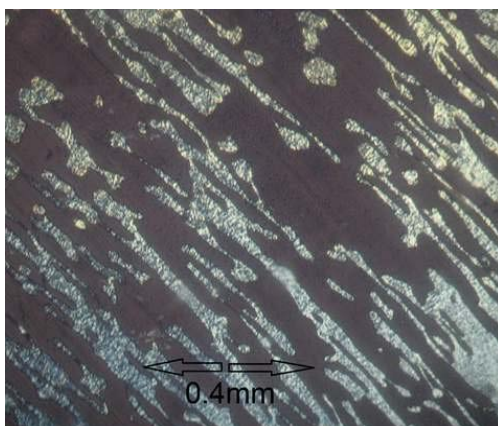
Figure 4-11 LCP above isotropic transition temperature

4.4   Probable Structures of LCPs from Stoichiometry of Monomers

As a function of the monomer types and amounts there are various structures possible for each sample. Figure 4-12 shows possible structures that may arise in polymerization of LCP1. For other LCP samples there are many different types of combinations that are possible. The figures that follow gives only one possible combination for each LCP sample taking into account the stoichiometry of the feed to the reactor. They by no means indicate the most probable structure,

nevertheless, they give an approximate feasible structure. Some of these structures will be compared to the experimental NMR data in the following sections. The figure from 4-13 to 4-17 are helpful in order to understand the molecular structures that may arise as a result of polyesterification reaction.

As reaction time increases there will be more random structures arising. In the end for long periods of reaction all the LCP character can be lost with diffusion of the p-acetoxybenzoic acid inside the developing structure. The molecular sequence and molecular weight of the polymer chains will depend on the composition of the feed as well as the duration of the synthesis in each case.
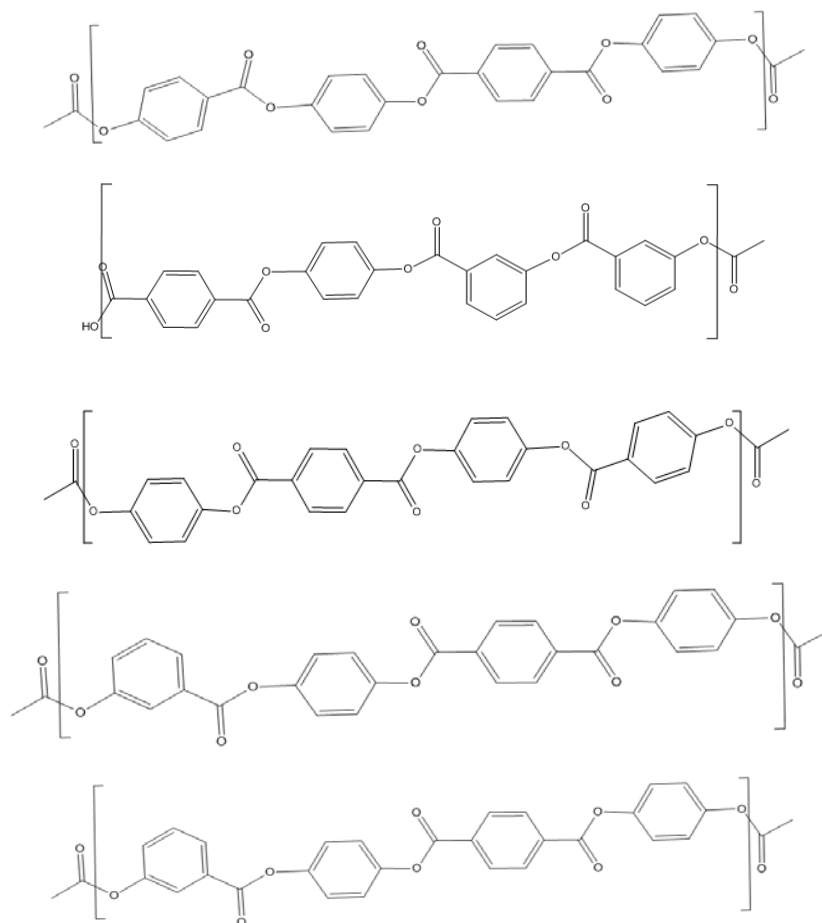
Figure 4-12 Some of the possible structures of LCP1
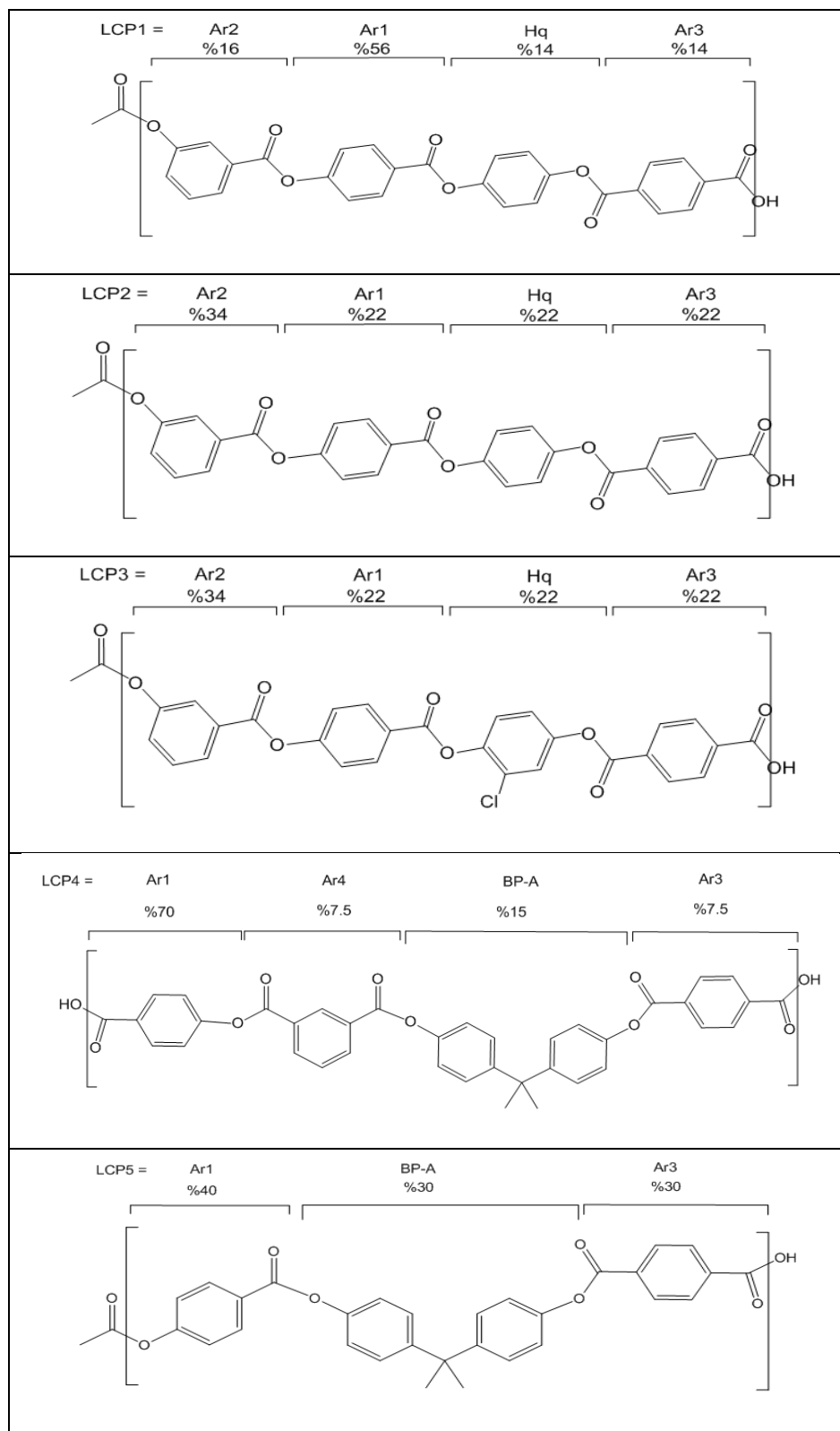
Figure 4-13 One of the possible structures for each composition in Group 1 with their ratios in the feed charged to the reactor
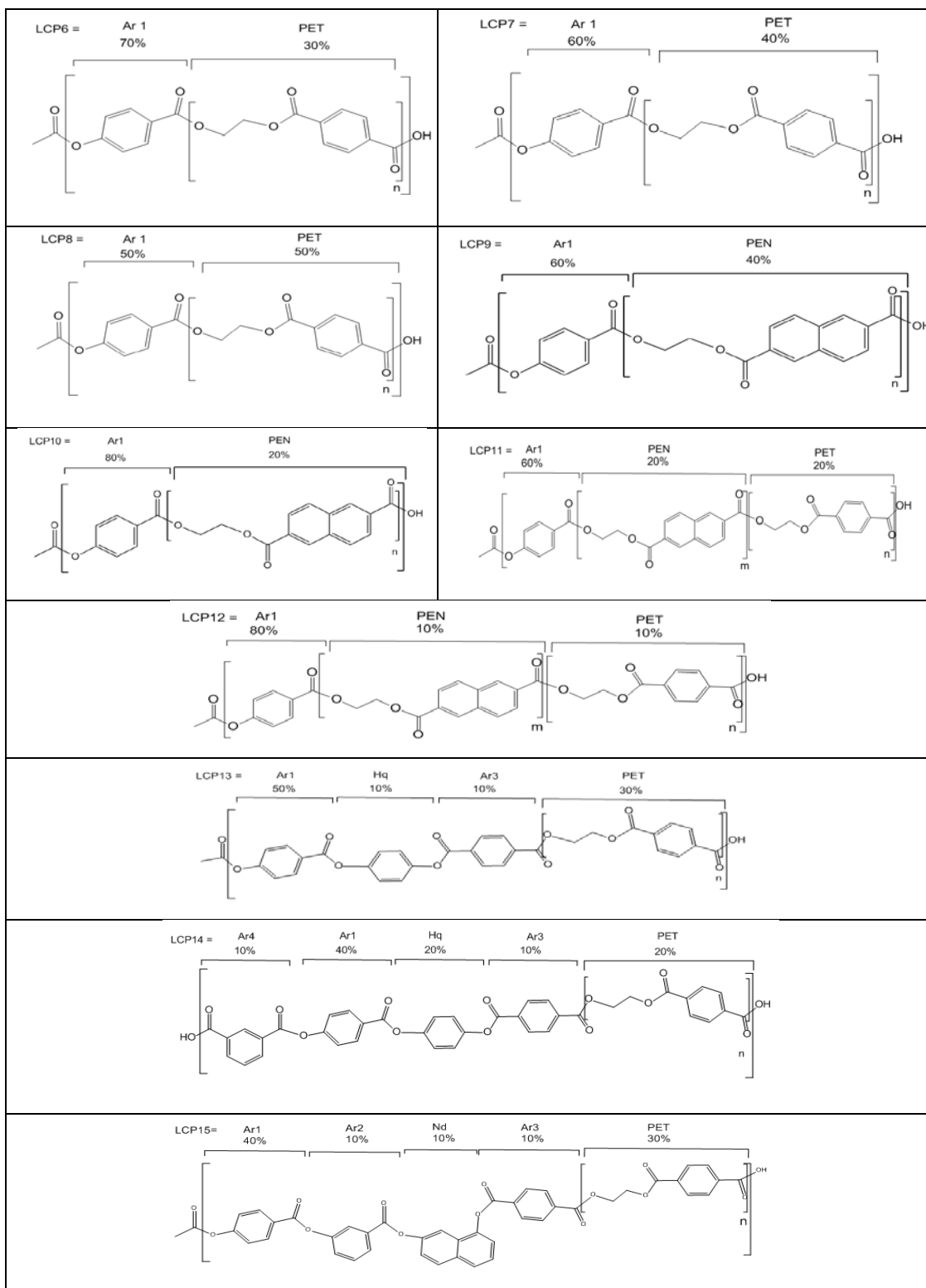
Figure 4-14 One of the possible structures for each composition in Group 2 with their ratios in the feed charged to the reactor
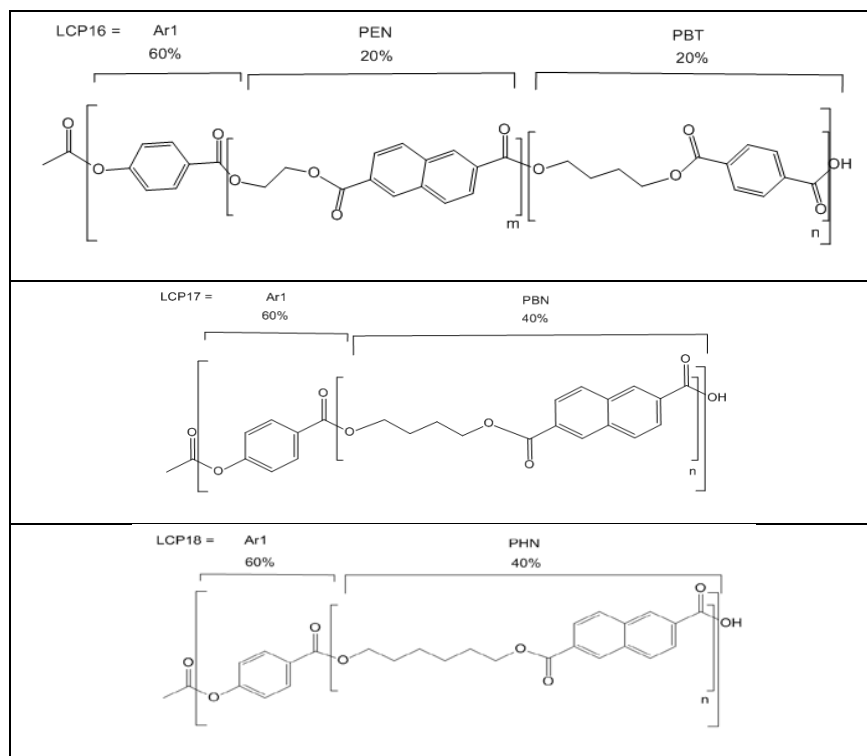
Figure 4-15 One of the possible structures for each composition in Group 3 with their ratios in the feed charged to the reactor
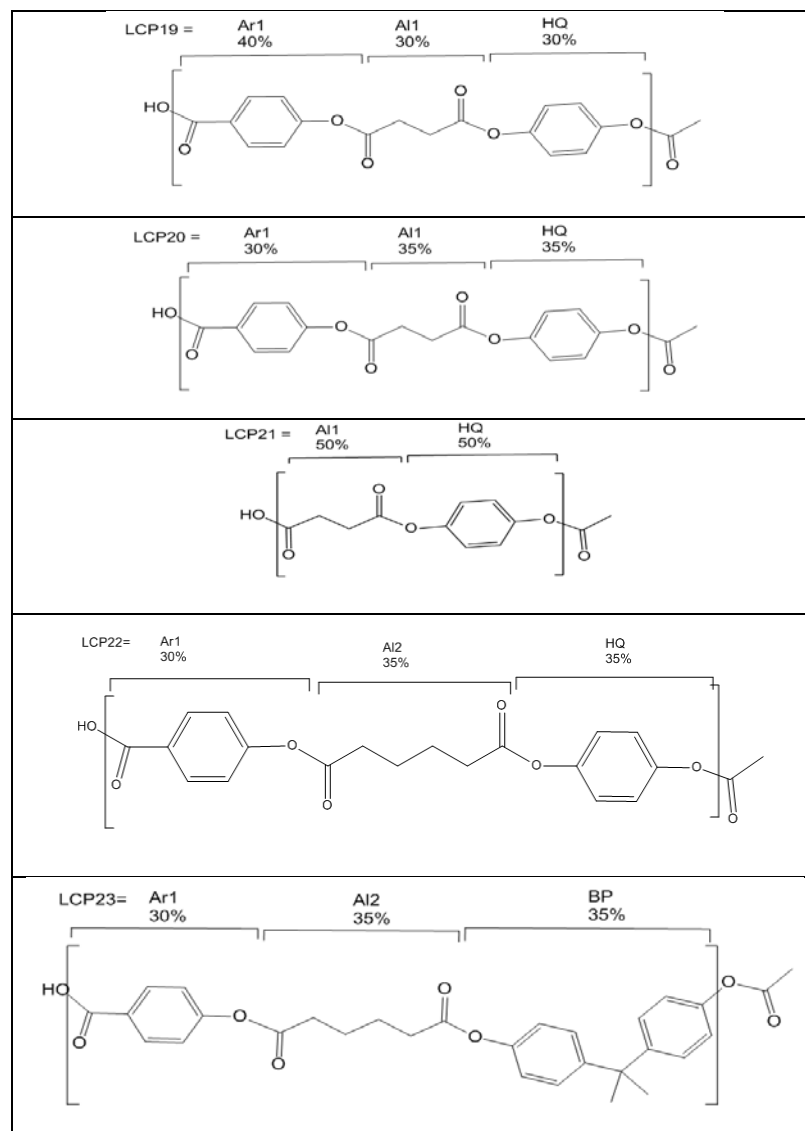
Figure 4-16 One of the possible structures for each composition in Group 4 with their ratios in the feed charged to the reactor
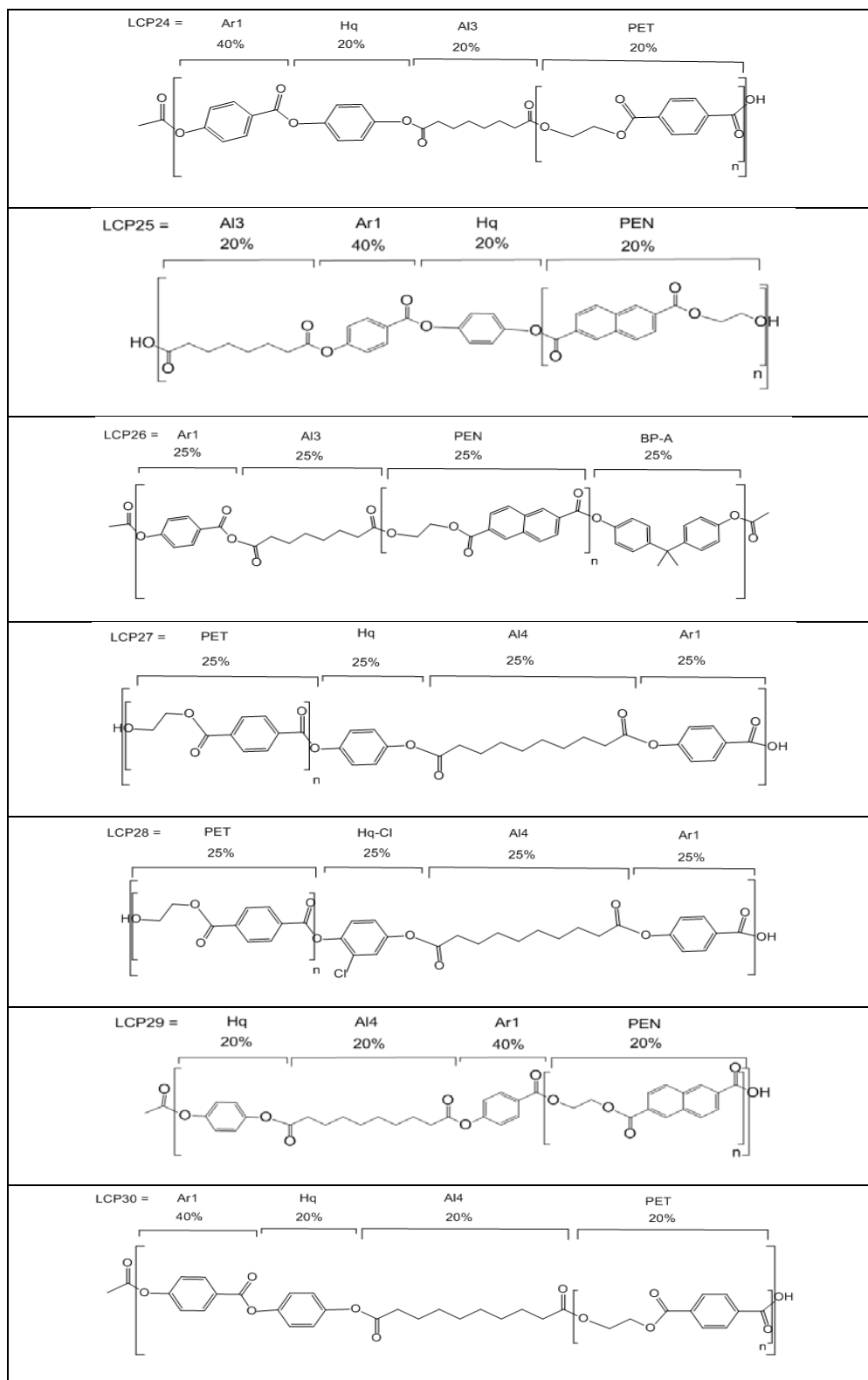
Figure 4-17 One of the possible structures for each composition in Group 5 with their ratios in the feed charged to the reactor

4.5 Nuclear Magnetic Resonance (NMR)

^{1}H-NMR spectra are compared with expected theoretical chemical shifts, % content of reactants their corresponding protons, integrated areas and their ratios are tabulated for group V LCP species. Predicted structures from reactant monomers, their chemical shifts coincide with the results in the following figures and tables.

Some of the members first and second group of LCPs species did not dissolve in the solvents that are used in the NMR analysis. Due to the side reactions, cyclization and decomposition of monomers in Group III and IV polymers, NMR results were not clear enough for interpretation. Sharp singlet with insignificant integration area at 11ppm in the following 1H NMR spectra comes from OH peak of d-trifluoroacetic acid which is used as solvent.

4.5.1 H[1] NMR of LCP7

Vanishing of acetyl end group and acid end group of Ar1 in LCP7 (Figure 4-18) spectrum (Figure 4-19) indicate the self-condensation reaction of Ar1 and various esterification reactions (transesterification, alcoholysis, acidolysis, etc) between Ar1 and PET.
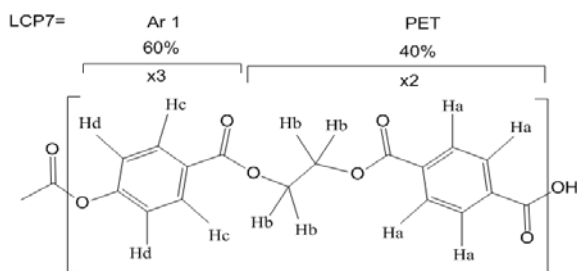
Figure 4-18 Predicted structures of LCP7 and ^{1}H labels
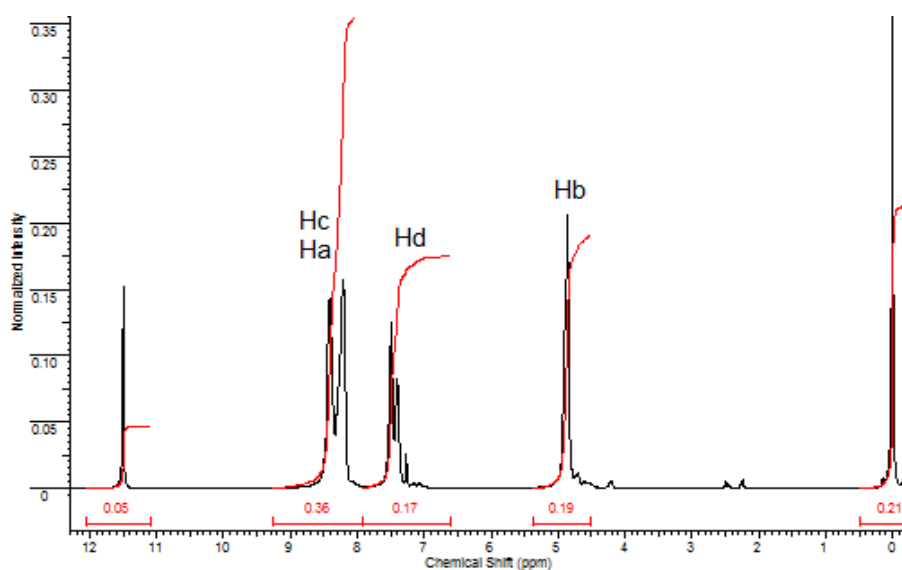
Figure 4-19 ^{1}H-NMR of LCP7

Table 4-2 Assignment of ^{1}H-NMR peaks of LCP7

LCP7	Chemical Shift (ppm)	Proton type	Theoretical H Ratio (%)	Area	Experimental H ratio(%)	Peak type
Hb	4.86	8Hb	29	0.19	26	Singlet
Hd	17.40-7.49	6Hd	21	0.17	23	Doublet
Hc	8.21-8.41	6Hc	50	0.36	50	Multiplet
Ha		8Ha =14				

Total number of H= 28, Total integral area=0.72

4.5.2 H[1] NMR of LCP24

Disappearance of acetyl end group of Ar1, Hq and disappearance of acid end group of Ar1, Al3 in LCP24 (Figure 4-20) spectrum (Figure 4-21) indicate the self-condensation reaction of Ar1 and various esterification reactions (transesterification, alcoholysis, acidolysis, etc) between Ar1, Hq, Al3 and PET. LCP24 is one of the samples that showed the highest LCP character which can be as a result of all trans phenyl groups plus the flexibility of octane chain.
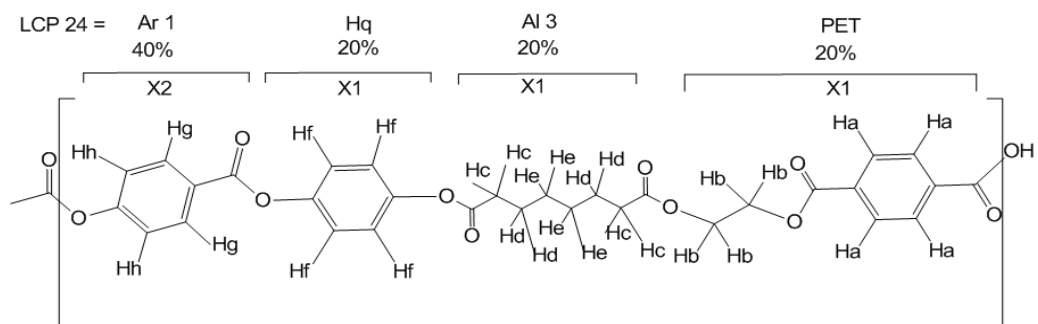
Figure 4-20 Predicted structures of LCP24 and ^{1}H labels
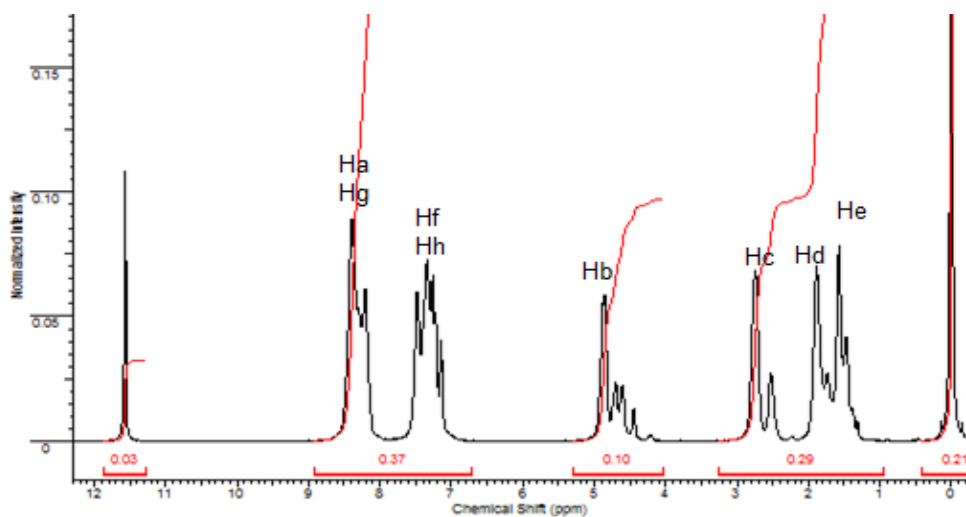
Figure 4-21 ^{1}H-NMR of LCP24

Table 4-3 Assignment of ^{1}H-NMR peaks of LCP24

LCP24	Chemical Shift (ppm)	Proton type	Theoretical H Ratio (%)	Area	Experimental H ratio(%)	Peak type
He	1.25-1.66	4He	12.5	0.1	12.9	Doublet
Hd	1.66-2.16	4Hd	12.5	0.1	12.9	Doublet
Hc	2.34-3.10	4Hc	12.5	0.1	12.9	Doublet
Hb	4.17-5.14	4Hb	12.5	0.1	12.9	Multiplet
Hf	6.71-7.80	4Hf+4Hh =8	25	0.19	24.6	Multiplet
Hh	6.71-7.80					
Ha	7.88-8.80	4Ha+4Hg =8	25	0.18	23.3	Multiplet
Hg	7.88-8.80					

In Table 4-3, total number of H= 32, total integral area=0.77

4.5.3   H[1] NMR of LCP25

Vanishing of acetyl end group of Ar1, Hq and vanishing of acid end group of Ar1, Al3 in LCP25 (Figure 4-22) spectrum (Figure 4-23) indicate the self-condensation reaction of Ar1 and various esterification reactions (transesterification, alcoholysis, acidolysis, etc) between Ar1, Hq, Al3 and PEN.

Figure 4-22 Predicted structures of LCP25 and ^{1}H labels

Figure 4-23 ^{1}H NMR of LCP25

Table 4-4 Assignment of ^{1}H-NMR peaks of LCP25

LCP25	Chemical Shift (ppm)	Proton type	Theoretical H Ratio(%)	Area	Experimental H ratio(%)	Peak type
Hn	1.16-1.65	4Hn	11.8	0.1	12.5	Doublet
Hm	1.65-2.14	4Hm	11.8	0.09	11.2	Doublet
Hl	2.32-3.10	4Hl	11.8	0.09	11.2	Doublet
Ha	4.16-5.15	4Ha+4Hb	11.8	0.1	12.5	Multiplet
Hb	4.16-5.15	=4				
Hi	6.83-7.76	4Hi+4Hk	23.5	0.19	23.7	Multiplet
Hk	6.83-7.76	=8				
Hd	7.92-8.61	1Hd+1Hc				
Hc	7.92-8.61	1Hg+1Hf				
Hg	7.92-8.61	4Hj	23.5	0.19	23.7	Multiplet
Hj	7.92-8.61	=8				
Hf	7.92-8.61					
Hh	8.59-9.10	1Hh+1He	5.9	0.04	5	Doublet
He	8.59-9.10	=2				

Total number of H=34, Total integral area = 0.8 in the Table 4-4.

4.5.4 H[1] NMR of LCP27

Disappearance of acetyl end group of Ar1, Hq and disappearance of acid end group of Ar1, Al4 in LCP27 (Figure 4-24) spectrum (Figure 4-25) indicate the self-condensation reaction of Ar1 and various esterification reactions (transesterification, alcoholysis, acidolysis, etc) between Ar1, Hq, Al4 and PET.
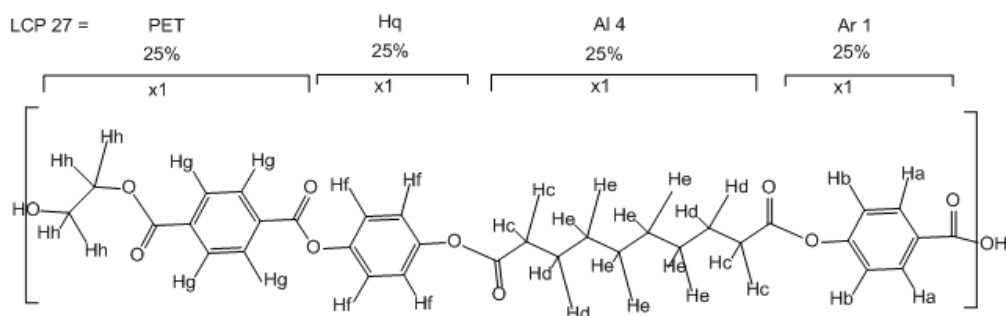
Figure 4-24 Predicted structures of LCP27 and ^{1}H labels
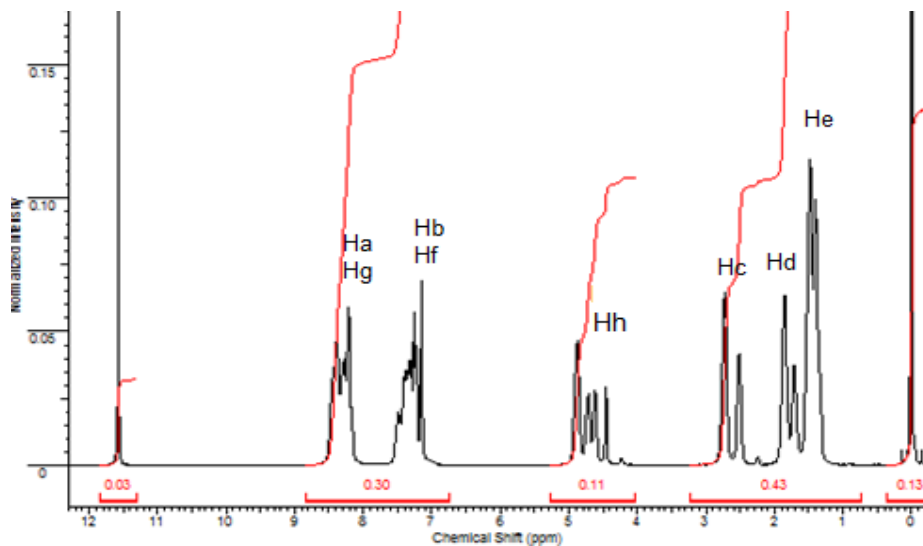
Figure 4-25 ^{1}H NMR of LCP27

116

Table 4-5 Assignment of ^{1}H-NMR peaks of LCP27

LCP27	Chemical Shift (ppm)	Proton type	Theoretical H Ratio(%)	Area	Experimental H ratio(%)	Peak type
He	1.28-1.62	8He	25	0.21	25	Doublet
Hd	1.64-1.96	4Hd	12.5	0.11	13	Doublet
Hc	2.43-2.83	4Hc	12.5	0.11	13	Doublet
Hh	4.41-4.98	4Hh	12.5	0.11	13	Multiplet
Hf	6.92-7.60	4Hf+2Hb		0.15	18	Multiplet
Hb	6.92-7.60	=6	18.7			
Hg	8-8.66	4Hg+2Ha	18.7	0.15	18	Multiplet
Ha	8-8.66	=6				

Total number of H =32, Total integral area=0.84

4.5.5   H[1] NMR of LCP29

Disappearance of acetyl end group of Ar1, Hq and disappearance of acid end group of Ar1, Al3 in LCP29 (Figure 4-25) spectrum (Figure 4-26) indicate the self-condensation reaction of Ar1 and various esterification reactions (transesterification, alcoholysis, acidolysis, etc) between Ar1, Hq, Al3 and PEN.

Figure 4-26 Predicted structures of LCP29 and ^{1}H labels

Figure 4-27 ^{1}H NMR of LCP29

Table 4-6 Assignment of ^{1}H-NMR peaks of LCP29

LCP29	Chemical Shift (ppm)	Proton type	Theoretical H Ratio(%)	Area	Experimental H ratio(%)	Peak type
Hl	1.2-1.62	8Hl	21	0.18	21	Doublet
Hk	1.62-2.03	4Hk	10	0.09	10	Doublet
Hj	2.37-2.85	4Hj	10	0.09	10	Doublet
Hg	4.37-5.09	4Hg	10	0.1	11	Multiplet
Hm	6.97-7.71	4Hm+4Hi				
Hi	6.97-7.71	=8	21	0.18	21	Multiplet
Hb	7.94-8.59	4Hh+1Hb				
Hh	7.94-8.59	1Hc+1He				
Hc	7.94-8.59	1Hf				
He	7.94-8.59	=8	21	0.19	22	Multiplet
Hf	7.94-8.59					
Hd	8.60-9.09	1Hd+1Ha				
Ha	8.60-9.09	=2	5	0.02	23	Doublet

Total number of H=38 Total integral area=0.85

4.6 Carboxyl End Group (CEG) Analysis and Intrinsic Viscosity (IV)

Number of repeating unit (X_n) and molecular weight (M_n) are determined via reduction of the number of carboxyl end groups (CEG).

Carboxyl end group (CEG) analysis is an indication of the progress of the reaction, since the initial value of the end groups are known. The final experimental CEG values can be used to calculate the approximate value of the repeating unit (X_n). CEG values of the two promising liquid crystalline compositions, LCP24 and LCP25 are studied in some detail. In these samples we have commercially produced PET and PEN polymers with 20% weight fraction. Carboxyl end groups of these polymers calculated from the reported molecular weights are small for PET (20meq/kg) and for PEN (30meq/kg).

On the other side the initial CEG values of monomers in LCP24 and LCP25 are 4300 mmol/kg and 4110 mmol/kg respectively. The reported CEG values of the copolyesters given in Table 4-7 and Table 4-8 are therefore to a large extent from the condensation reactions of the monomers the reactivity of the PET and PEN is further reduced due to the very low diffusivities compared to the monomers. Another factor that reduces the molecular weights of PET and PEN are transesterification reactions in the duration of the particular polymerization which does not change CEG value of the copolymer. As a result of the above considerations the following two assumptions are made in the calculation of average molecular weight of the LCP specimens.

1) The M_n of the PET and PEN groups stays almost constant during polymerization.
2) The increase in the M_n value is due to the polymerization of the monomeric units, hence, reduction of the CEG value is solely from the reactions of

     i)   *p*-acetoxy- benzoic acid
     ii)   octanedioic acid monomer

In Table 4-7 and Table 4-8 the reported values of X_n and M_n are for the monomer's polymerization only, including PET or PEN molecular weight. Formation of a visually homogenous polymer melt as the reaction progresses shows the inclusion of PET and PEN into the chain structure through trans-esterification reactions. In Table 4-7 the effect of various catalysts on the M_n is given.

Molecular weight of LCP (M_n) calculated via the equations below.
N_o=CEG initial, N=CEG final, M_o=488g/mole (repeating unit molecular weight excluding PET or PEN), p=extend of reaction.

The highest IV reached (0.58 dL/g) poses problems in processing. The extent of reaction should be adjusted for IV less than this value for processable LCPs.

In LCP24 synthesis similar to PET synthesis, 200ppm manganese acetate(MnAc) and 300ppm antimony oxide(Sb_2O_3) added in two step that give the highest molecular weight of LCP (Figure 4-28). 100ppm titanium isopropoxide ($Ti(iOPr)_4$) is the second catalyst that gives higher molecular weight than that of uncatalyzed LCP. An antimony oxide usage solely is not useful and gives the lowest M_n that is lower than uncatalyzed LCP. The overall M_n value of LCP24 is the sum of M_n+M_n(PET). M_n(PET) is calculated from the IV value given by the manufacturer. Mn (PET)=18974 g/mol.
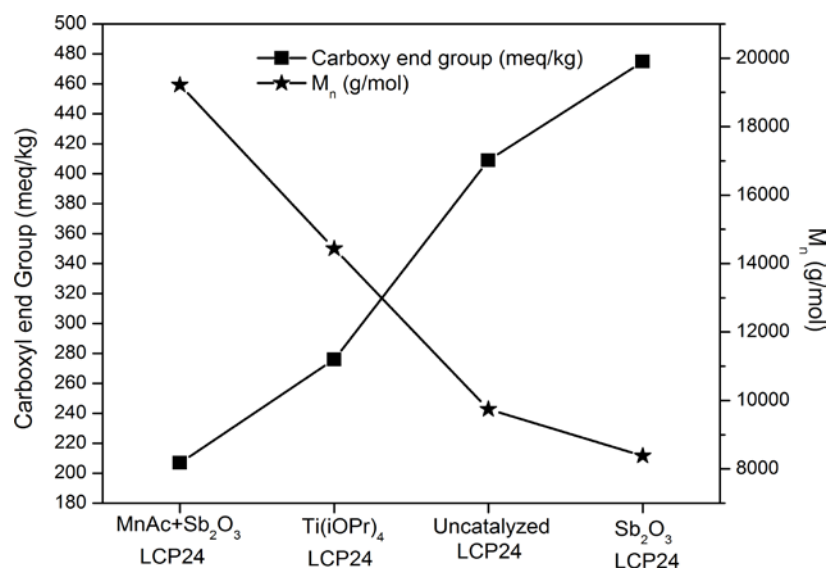
Figure 4-28 The catalyst effect on carboxyl end group (CEG) and molecular weight (M_n) of LCP24

Table 4-7 Carboxyl end Group (CEG), Intrinsic Viscosity (IV), Molecular weight (M_n) of LCP24

LCP24 (0.1mol)	IV (dL/g)	CEG (meq/kg)	p	X_n	M_n	M_n+ M_n(PET)
MnAc+Sb$_2$O$_3$	0.586	207.2	0.974608	39.4	19219	38193
Ti(iOPr)$_4$	0.488	275.8	0.966201	29.6	14438	33412
Uncatalyzed	0.383	408.5	0.949939	20.0	9748	28722
Sb$_2$O$_3$	0.343	474.9	0.941801	17.2	8385	27359

The compositional stoichiometry of LCP25 is same in all specimens, only the amount charged into the reactor changes (Table 4-8). The CEG number is different from each other and depends on initial amount of reactants (Figure 4-29). The difference of mechanical properties and polarized microscopy observations support this phenomenon. This peculiar result is also observed in other synthesis. The M_n value is dependent on the amount of charge to the reactor. As the amount of the charge to the reactor increases the I.V. and X_n of the product decreases and CEG values becomes larger. (Private communication with B. Erdemir)

Similar to interesting observation on butanedioic and hexanedioic acids decarboxylation reactions, this result is also a peculiar finding on the dependence of reaction rate on the amount of feed charged to the reactor. One needs to investigate this behavior separately in perhaps another study.
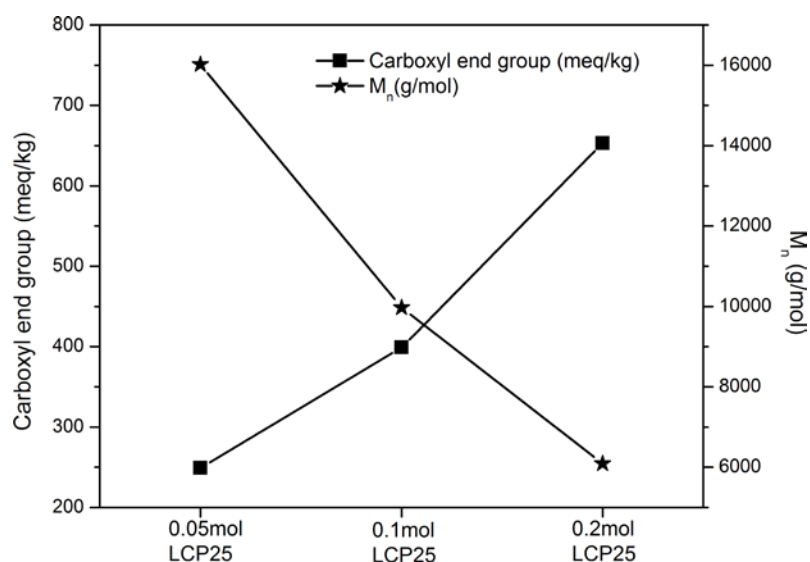
Figure 4-29 The reactant amount and relation with carboxyl end group (CEG) and molecular weight (Mn) of LCP25.

The overall M_n value of LCP25 is the sum of Mn+M_n(PEN). M_n(PEN) is calculated from the IV value given by the manufacturer.

Table 4-8 The reactant amount and Carboxyl end Group (CEG), Intrinsic Viscosity (IV), Molecular weight (M_n) of LCP25.

LCP25	IV (dL/g)	CEG (meq/kg)	p	X_n	M_n	M_n+ M_n(PEN)
0.05mol	0.578	248.6	0.969534	32.8	16018	35018
0.1 mole	0.427	399.3	0.951066	20.4	9973	28973
0.2 mole	0.256	653.4	0.919926	12.5	6094	25094

As a result of CEG analysis the chain length of LCP24 and LCP25 is found to be quiet large. Parts of this chain gives rise to liquid crystalline morphology due to the

presence of 40% *p*-acetoxy benzoic acid (Ar1), the main component responsible from LCP behavior.

One possible explanation of the above phenomenon can be as follows: As given in Table 4-9 high amount of feed means an increase in the byproduct acetic acid formed.

Table 4-9 LCP25 reactant amount and theoretical side product acetic acid

LCP25 reactant	Reactant (g)	CH$_3$COOH (g)
0.05mol	9.71	1.76
0.1mol	19.42	3.52
0.2mol	38.84	7.04

As the amount of reactants increases the amount of formed acetic acid (CH$_3$COOH) increase (Table 4-9). To remove acetic acid from reaction mixture which is essential in order to obtain high molecular weight LCPs, more reaction time is needed due to the fixed capacity of reactor, pump and nitrogen inlet outlet. At this point reaction time needs to be longer which brings another risk. High number of carboxyl end group above 270°C facilitate formation of cyclic oligomers via back-biting reaction that leads to unwanted products far from linearity. The rate of the polyesterification reaction, therefore, decreases as the amount of charge, increases.

4.7 Attenuated Total Reflectance (ATR) of the Products

Due to the similarities of synthesized LCP and PET constituents, PET is taken as reference material whilst FTIR evaluation (Table 4-10). Many of the peaks constitute gauche-trans pairs arising from vibrations of the glycol moiety: CH$_2$ bending at 1456 cm^{-1}; CH$_2$ wagging at 1373 and 1340 cm^{-1}. Others correspond to vibrations of the benzene ring: in-plane vibrations at 1576, 1506, 1408, and 1015 cm-1 and out of-plane vibrations at 875 and 727 cm^{-1}. The complex bands around 1237 and 1090 cm^{-1} are mainly due to C-O stretching vibrations of the ester group. There is also the carbonyl stretching band between 1715-1730 cm^{-1} [201-203]. Typical FTIR spectra of PET and some LCP composites are given in Figure 4-30 to Figure 4-34.

Table 4-10 FTIR spectral features of PET

Wavenumber(cm^{-1})	Group	Moment
872,722	benzene group	Out of plane vibration
1576,1506,1408,1015	benzene group	In plane vibration
1373,1340	CH$_2$(ethyl)	wagging
1456	CH$_2$(ethyl)	bending
1237,1090	C-O(ester)	stretching
1715	C=O(carboxyl)	stretching
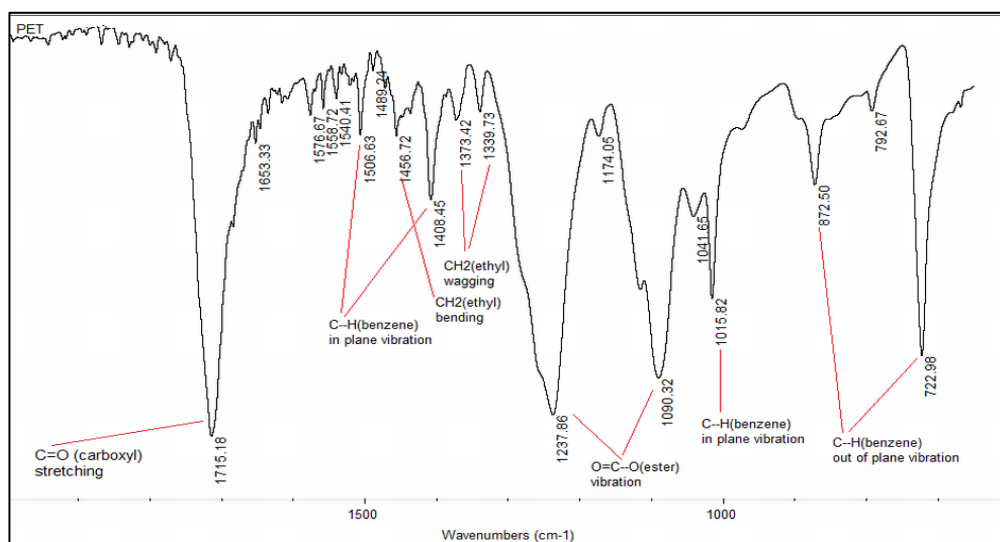
Figure 4-30 FTIR of PET

The differences between the FTIR spectra are indicated on the spectra. For example in Figure 4-31 (LCP2) and Figure 4-32 (LCP3), formation of new peak at 1050 cm^{-1} belong to C-O vibration of hydroquinone (HQ) and the loss of CH$_2$ groups are seen at 1340-1370 cm^{-1}

LCP24 (Figure 4-33) and LCP25 (Figure 4-34) have peaks at about 1050 cm^{-1} that belongs to HQ , in addition, CH$_2$ groups are seen at 1339-1379 cm^{-1} which comes from ethylene spacers of aliphatic diacids.

Due to the inclusion of new moieties, several peaks appear in the range of ester groups that corresponds between 1230-1012 cm^{-1}.
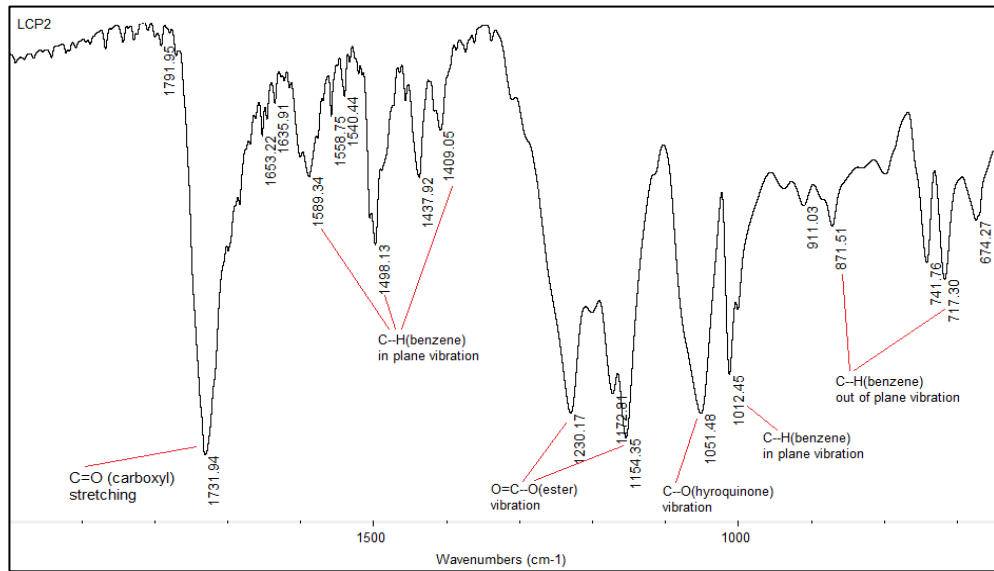
Figure 4-31 FTIR of LCP2
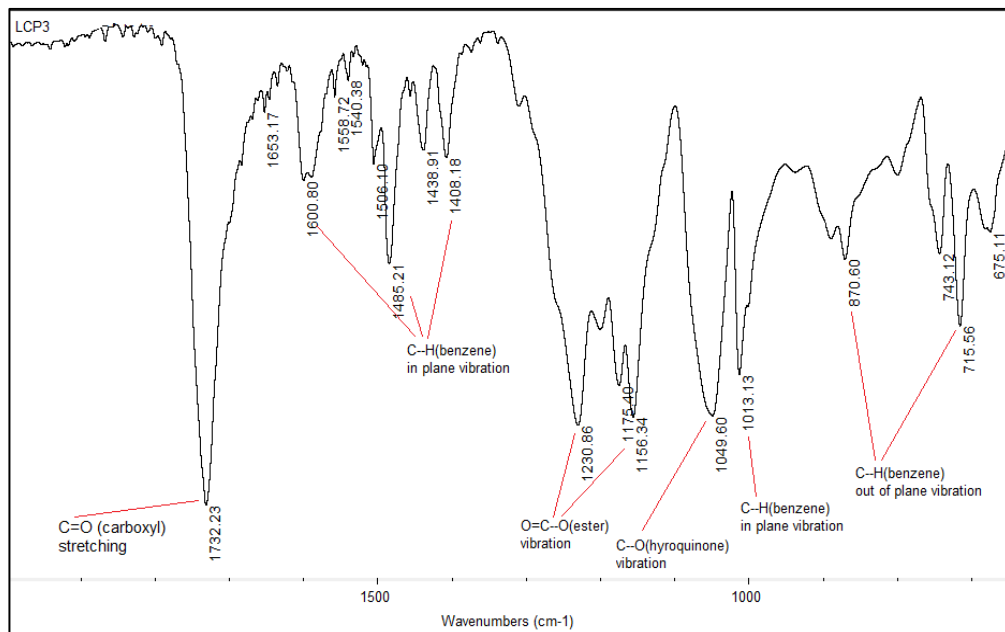
Figure 4-32 FTIR of LCP3

125
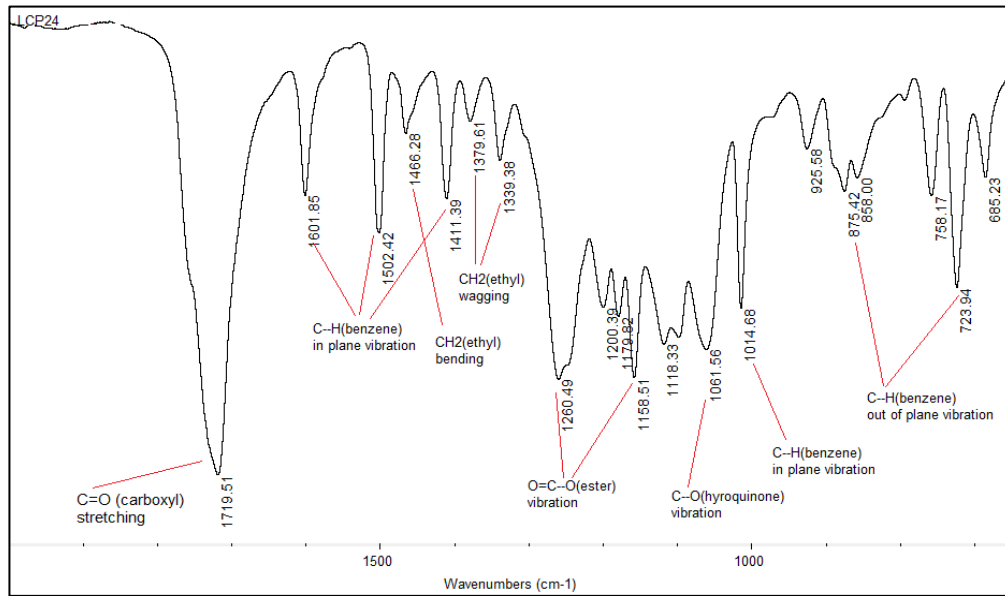
Figure 4-33 FTIR of LCP24
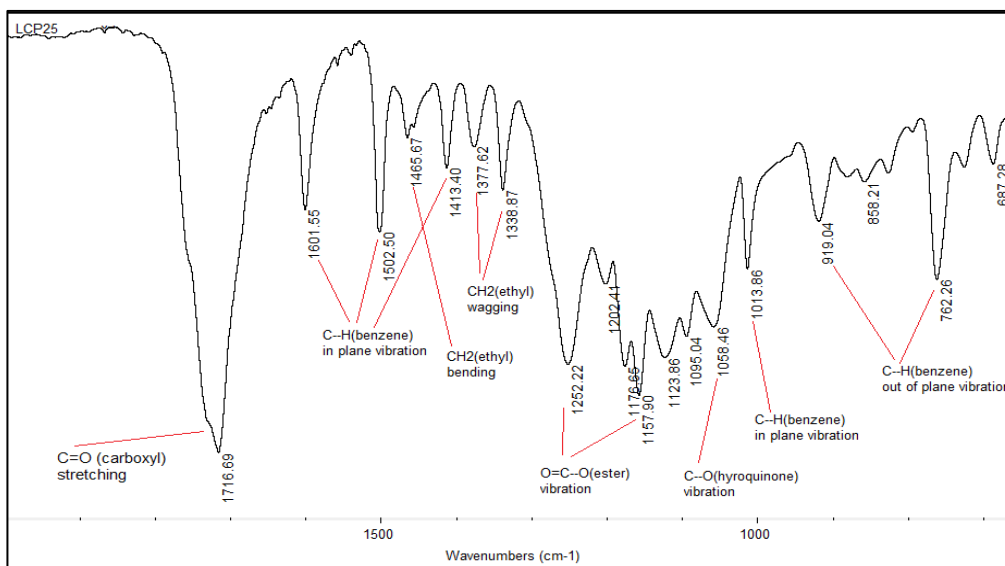
Figure 4-34 FTIR of LCP25

4.8 Differential Scanning Calorimeter (DSC)

In liquid crystalline material, heat of fusion (ΔH_f) is almost negligible for solid to nematic transition, no melting peak (T_m) is observed for LCP species, therefore, T_m measured by polarized light microscopy are noted on DSC thermograms. These temperatures sometimes coincide with small endothermic peaks. Some of the DSC measurements are not given in the manuscript due to lack of information to be gained. In Table 4-11 the accomplished DSC measurement are indicated by (+) sign and no DSC measurement performed for (-) sign, for example fully aromatic LCP1 is infusible, and some specimens (LCP16-18) started to overflow hermetic DSC pan, also, decomposed specimens such as LCP20 start to fume while measuring and measurements were halted.

Table 4-11 DSC measurements made on LCP samples. Melting temperature (T_m) and nematic to isotropic transition temperature (T_{ni}) measured by microscopy

	Samples	T_m	T_{ni}	DSC
	LCP1	-	-	- (Infusible)
	LCP2	260	310	+
I	LCP3	250	350	+
	LCP4	300	-	+
	LCP5	230	-	- (Amorphous)
	LCP6	300	340	-
	LCP7	250	300	+
	LCP8	220	250	-
	LCP9	240	290	+
	LCP10	260	330	-
II	LCP11	190	240	+
	LCP12	220	260	+
	LCP13	280	320	+
	LCP14	270	320	+
	LCP15	210	300	-
	LCP16	250	-	- (Overflow pan)
III	LCP17	190	200	- (Overflow pan)
	LCP18	190	200	- (Overflow pan)
	LCP19	-	-	+
	LCP20	-	-	-
IV	LCP21	210	-	-
	LCP22	190	-	+
	LCP23	-	-	-
	LCP24	170	230	+
	LCP25	195	300	+
	LCP26	210	-	+
V	LCP27	220	300	+
	LCP28	160	220	+
	LCP29	210	310	+
	LCP30	200	300	+

4.8.1   DSC Results of Group 1

Fully aromatic and melt processable LCP2 was a desirable product regarding the aims of this study and synthesized without and with a catalyst. Whilst uncatalyzed one (Figure 4-35) has T_m: 260°C and T_{ni}: 310°C which is measured by microscopy,

catalyzed specimens (Figure 4-36) do not melt probably due to high molecular weight. Microscopic investigation shows that the catalyzed product is infusible and solid-like. Melting temperature and isotropic transition temperature are measured by microscope and noted on thermogram.
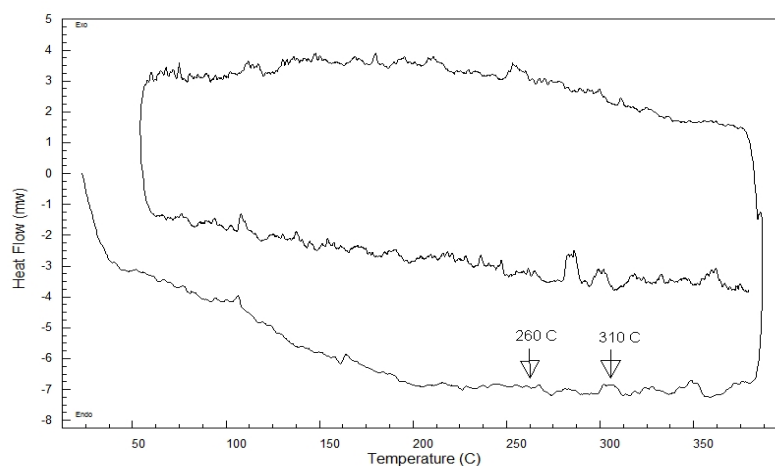
Figure 4-35 DSC of LCP2

The catalyst used is titanium isopropoxide $(Ti(iOPr)_4)$. The noise in DSC thermogram disappeared. No melt formation is observed and did not dissolve in any type of solvent for NMR, electrospinning and intrinsic viscosity measurements.
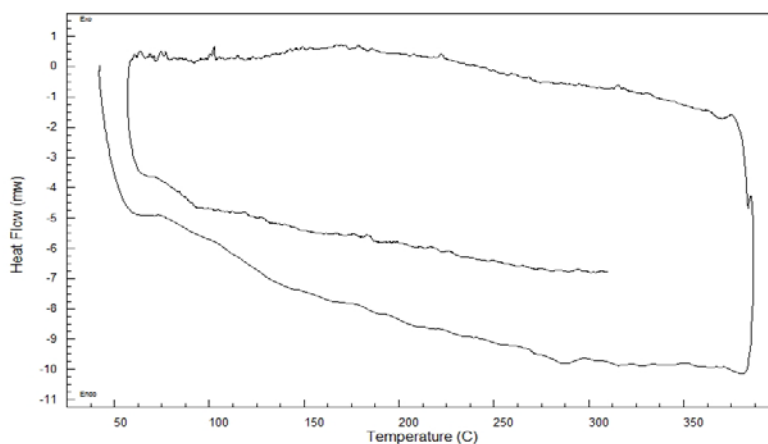
Figure 4-36 DSC of catalyzed LCP2

LCP3 (Figure 4-37) differs from LCP2 only by chlorinated form of hydroquinone content which corresponds to small fraction of total amount. Despite the small fraction, it has big effect on LCP properties, chain packing decrease and freedom of chains increase, melting point decreases from 260°C to 250°C and processing window increases to 250-350°C from 260-310°C.
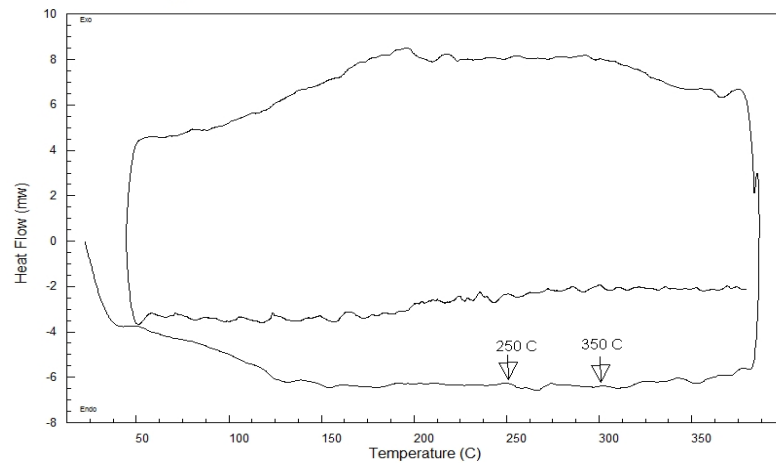
Figure 4-37 DSC of LCP3

Acetylated Bisphenol A is bulky molecule and crank shaft motion causes the dislocation of chains and distorts LCP packing in amorphous LCP4 (Figure 4-38) and LCP5. Whilst %15 Bisphenol A in LCP4 has melting point of 300°C, increasing the percent composition to %30 causes an abrupt decrease of T_m to 230°C. In polarized light microscopy no liquid crystalline behavior is observed. It should be noticed that LCP4 shows a melting point due to the lack of LCP behavior.
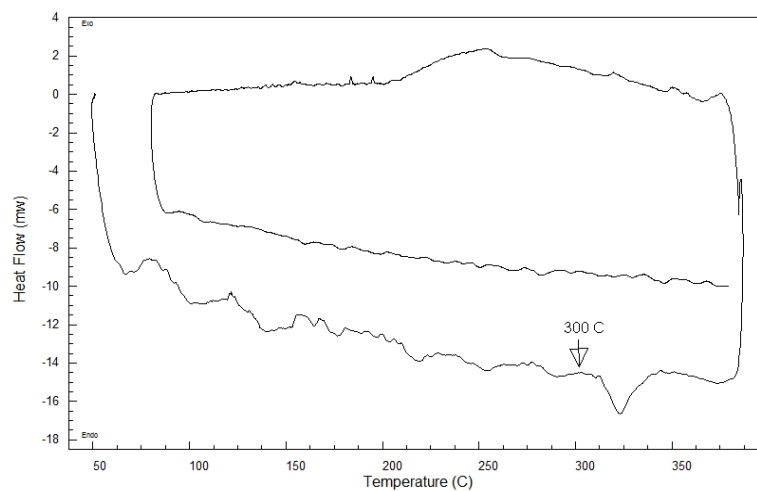
Figure 4-38 DSC of LCP4

4.8.2 DSC Results of Group 2

DSC thermograms of group 2 are different from fully aromatic group 1 by the appearance of endothermic peaks. LCP6 and LCP7 have the same content of commercial products known as XG7 which has T_m: 270 ^{o}C in literature that coincides with endothermic peak at 275 ^{o}C in thermogram (Figure 4-39). The difference between endothermic peak (275°C) of DSC and melting temperature (300^{0}C) from microscopy is due to hot plate-thermocouple distance on microscope that causes a lag in temperature reading.
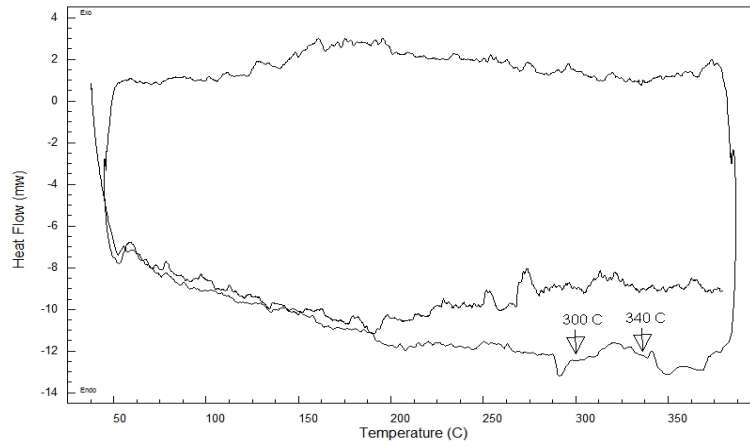
Figure 4-39 DSC of LCP7

High melting points of LCP6 and LCP7 bring disadvantages in polymer composite applications. To overcome this difficulty PET is displaced by PEN in LCP9 that causes melting point lowering to 240°C (Figure 4-40) but heterogonous domains show discontinuity. Naphthalene in PEN has crank shaft mobility and distorts chain packing that causes disruptions in chain order. When PEN is compared to other crank shaft molecule Bisphenol-A in amorphous LCP4 and LCP5 volume is not as huge, so, LCP domains are observed in LCP6 and LCP7.
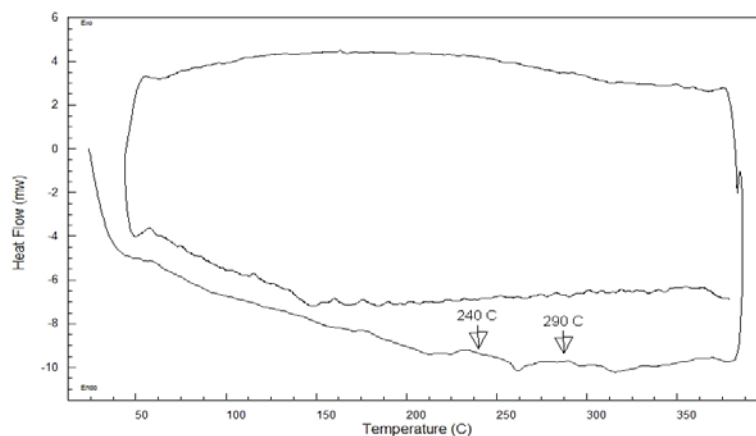
Figure 4-40 DSC of LCP9

LCP 11 has both %20 PET and %20 PEN and can be conceived as mixture of LCP 6 and LCP9, rule of mixture plays role in the decrease of melting point to 190°C

(Figure 4-41). Whilst LCP 9 is heterogeneous under microscope, LCP11 is colorful and uniform with low nematic to isotropic transition temperature 240°C. This composition can be promising in composite applications.
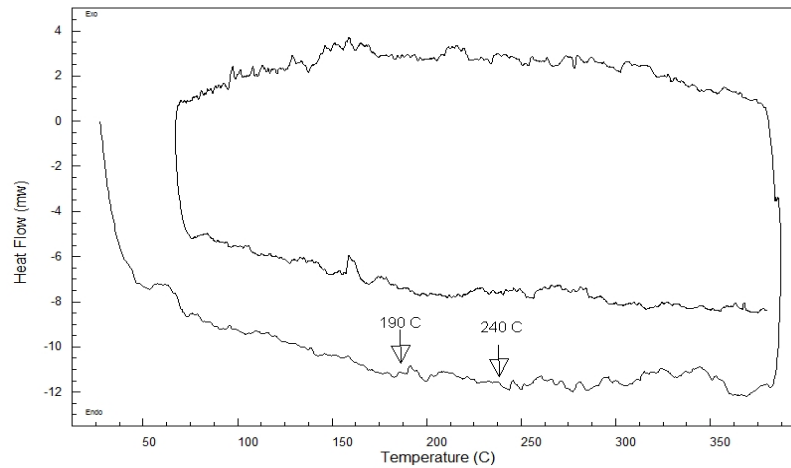
Figure 4-41 DSC of LCP11

Inclusion of %30 PET to fully *p*-aromatic reactants changes LCP behavior from infusible to thermoplastic with melting temperature at 280°C and isotropic transition temperature 320°C in LCP13 (Figure 4-42). Nevertheless, these are high T_m values not very promising in composite applications.
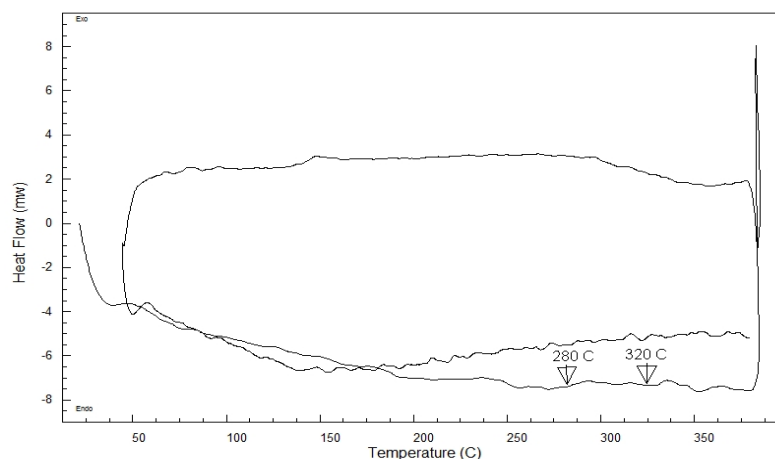
Figure 4-42 DSC of LCP13

LCP14 composed of %10 isophthalic acid, and *p*-aromatic monomers. Inclusion of kinked monomer decreases melting temperature somewhat to 270°C (Figure 4-43).
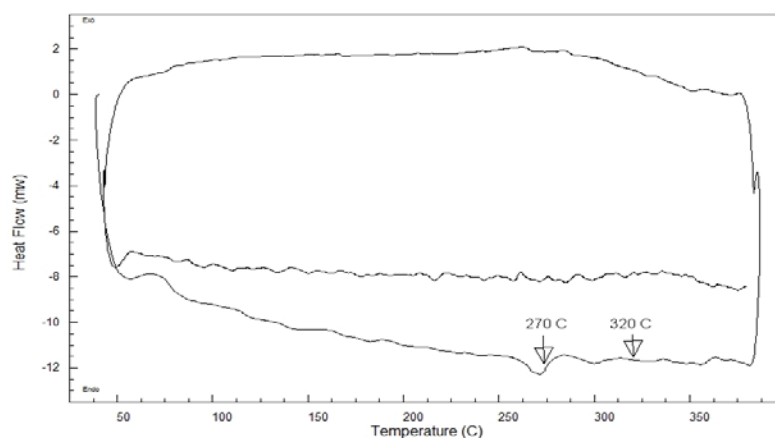
Figure 4-43 DSC of LCP14

4.8.3 DSC Results of Group 3

Butanediol and hexanediol inclusion to LCP structure give low molecular weight copolyesters due to probably back-biting and cyclization reactions. DSC hermitic pan overflowed by vaporization of small cyclic molecules with heterogeneous domains.

4.8.4 DSC Results of Group 4

Decarboxylation of butanedioic (LCP19-LCP21) acid and hexanedioic (LCP22, LCP23) acid in Group 4 LCP specimens resulted in the loss of stoichiometric balance that create side products and oxides whilst synthesis. Black colored oxides cover the shiny LCP domains under microscope prevent determination of transition temperatures. Exothermic peak at 90°C and endothermic peak at 210°C (Figure 4-44) may be due to various reactions in the half-complete char formation reaction. Exothermic increment between 220°C-250°C at second run may come from decomposition products at elevated temperatures.
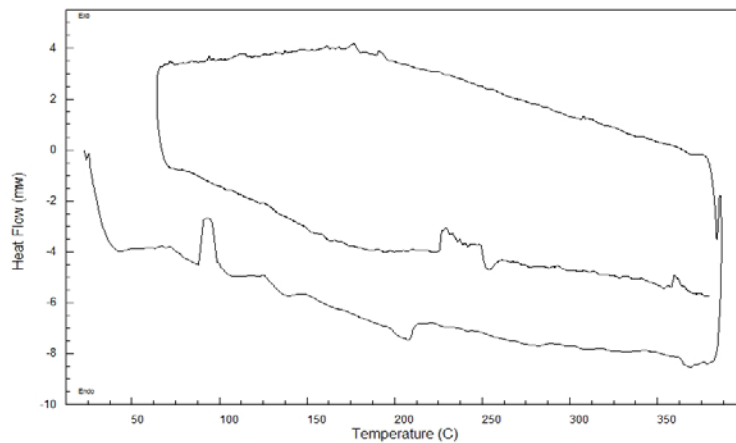
Figure 4-44 DSC of LCP19

LCP22 decarboxylate partially and it shows LCP behavior under polarized light microscopy. Due to decarboxylation of hexanadioic acid melting temperature, 190°C (Figure 4-45), endothermic peak (200°C), and isotropic transition temperature (210°C) is recorded in a narrow range.

135
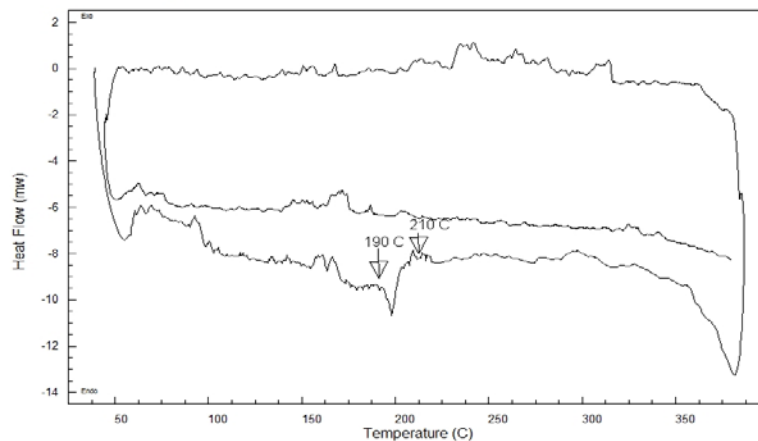
Figure 4-45 DSC of LCP22

4.8.5 DSC Results of Group 5

Octanedioic acid and decanedioic acid withstand decomposition by decarboxylation at reaction temperatures that make possible synthesis of low melting temperature LCP. Melt processability and fiber formation of group 5 members are good and can be used as reinforcing agents in thermoplastic processing. LCP24 has narrow LCP window (Figure 4-46) between low melting temperature 170°C and low isotropic transition temperature of 230°C.
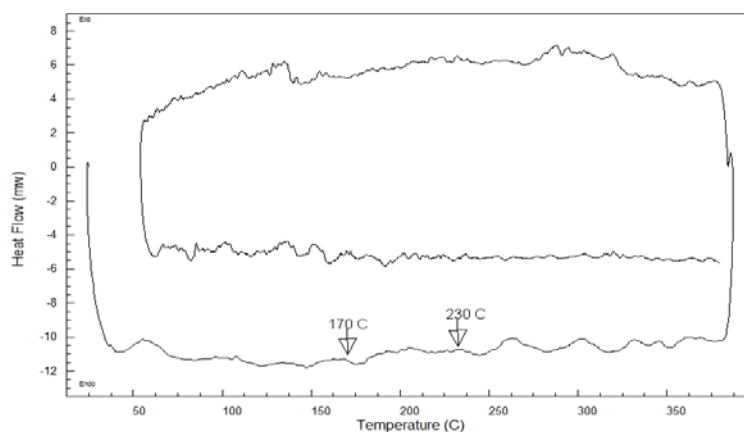
Figure 4-46 DSC of LCP24

LCP25 has tensile strength that is comparable with industrial reinforcing agents and used in blends of PET and PP for fiber and composite application. LCP transition

window (Figure 4-47) between low melting temperature 195°C and high isotropic transition temperature 300°C makes it ideal for processing with thermoplastics.
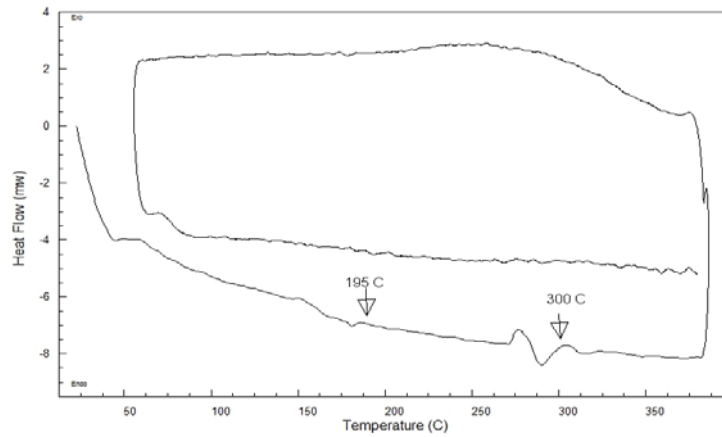
Figure 4-47 DSC of LCP25

Due to fuming during DSC measurement of LCP26 (Figure 4-48) containing Bisphenol-A, test was halted at 380°C. This phenomenon was interpreted as inclusion of Bisphenol-A to main chain was not satisfactory and decomposed at high temperatures.
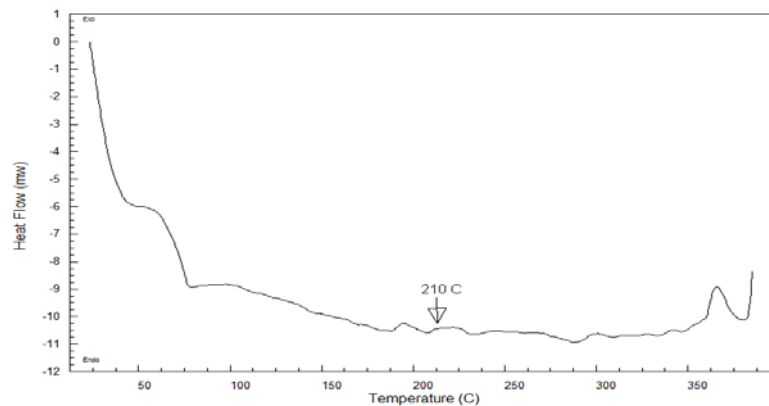
Figure 4-48 DSC of LCP26

LCP27 (Figure 4-49) is different from other synthesized LCPs by its electrospinable characteristics due to chains that do not pack tightly to resist solvent and heat. The

liquid crystalline behavior may be the result of using four different monomers in equal ratio, %25 each.
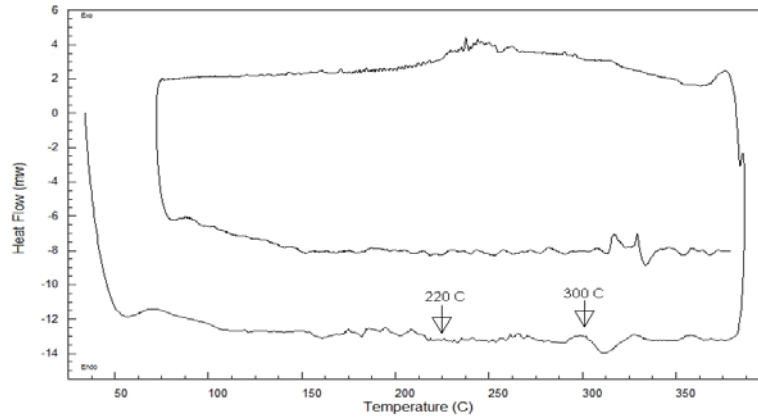
Figure 4-49 DSC of LCP27

When chlorine atom is included to LCP27 waxy compound that has a melting temperature at 160°C is synthesized and marked as LCP28 (Figure 4-50). Chlorine distorts the chain order so much that it results is waxy liquid crystalline polymer.
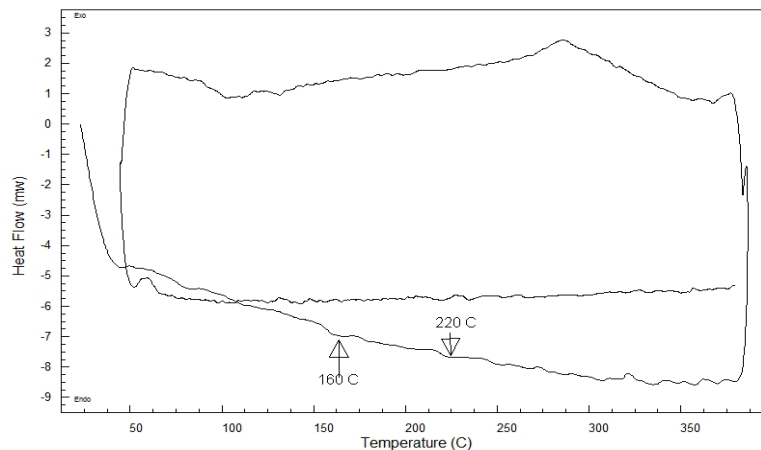
Figure 4-50 DSC of LCP28

Low melting point LCP29 (Figure 4-51) start to decompose above 300°C and measurement was halted at second run. Melting temperature (150°C) is low enough to be processable with polypropylene.

138
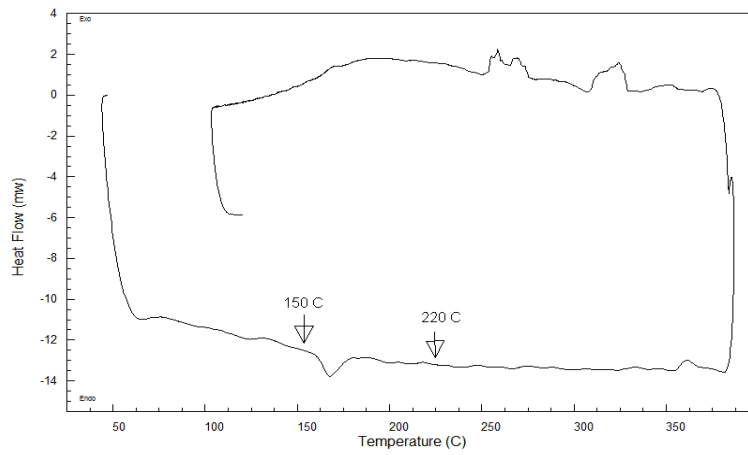
Figure 4-51 DSC of LCP29

Film and fiber formation capacity of LCP30 (Figure 4-52) is good and has low melting temperature (200°C) and high LCP transition temperature (T$_{ni}$) between 200 and 300°C which corresponds to a large processing window. At around 120°C, melting of low molecular weight crystallites are observed.
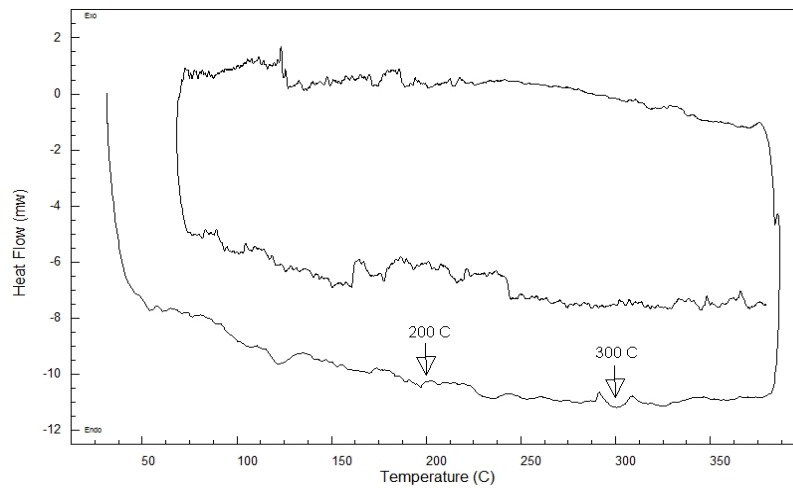
Figure 4-52 DSC of LCP30

4.9 Thermogravimetric Analysis (TGA)

Thermal stability of LCPs with different aromatic-aliphatic ratio content were measured by thermogravimetric analysis on LCP 2, 7,15, 24, 25 samples. Samples were selected among LCP species that are capable of film formation and they are used for composite production. T_{onset} of weight loss of LCPs weight is observed at around 400 ^{o}C and thereafter, char yield is determined at 700°C. LCPs either show one weight loss step or two weight loss step according to their structures. Whilst decomposition of aliphatic group (CH$_2$) is responsible for weight loss of species at lower temperature region, aromatic groups (benzoyl and naphthalene) decomposes at higher temperature and responsible for second stage decomposition. The general trend observed in TGA studies is that the higher aromatic ratio causes higher char yield and higher thermal stability. Accordingly, the aliphatic and aromatic content of LCPs are calculated and exemplified for LCP25 (Figure 4-53) as given below. Aromaticity wt.% and aliphaticity wt.% of LCPs are given in Table 4-12. The stoichiometric amounts of aliphatic groups, aromatic groups, carboxyl groups (C=O) and the remaining oxygen make the total weight of the sample. The ratios of aliphatic contents and aromatic contents are calculated and given in Table 4-12.
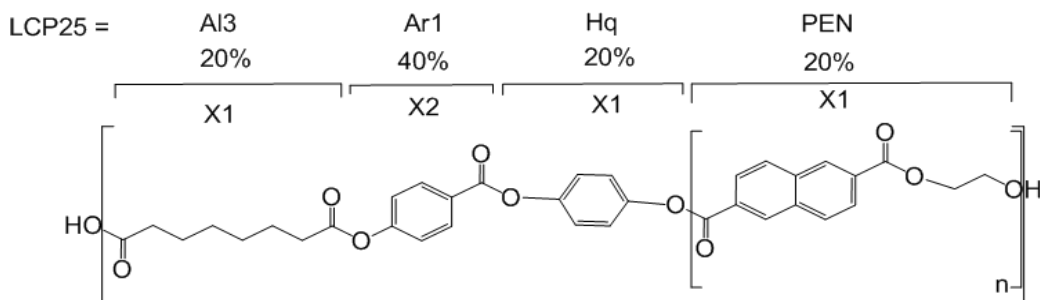
Figure 4-53 Possible molecular structure used for calculation of the mole % of the LCP25 constituents.

Table 4-12 Weight % of constituents of LCP25

LCP25 constituents	Weight	Weight %
Benzoyl	228	31
Naphthalene	126	17
Carboxyl	168	23
Oxygen	96	13
CH$_2$	112	15

As an example detailed calculation for LCP25 is given below

$$LCP25 \; aromaticy \; wt.\% \; = \; \frac{\text{Benozyl wt.\% +Naphthalene wt.\%}}{\text{total weight}} \times 100$$

$$aromaticy \; wt.\% = \frac{[(3\times76)+(1\times126)]\text{g/mol}}{[(3\times76)+(1\times126)+(6\times28)+(6\times16)+(8\times14)]\text{g/mol}} \times 100 = 48$$

$$LCP25 \; aliphacity \; \%wt \; = \; \frac{\text{CH2 wt. \%}}{\text{total weight}} \times 100$$

$$LCP25 \; aliphacity \; wt.\% \; = \; \frac{(8\times14)}{(3\times76)+(1\times126)+(6\times28)+(6\times16)+(8\times14)} \times 100 = 15$$

TGA curves of chosen LCPs are given in Figure 4-54 and data are summarized in Table 4-13. LCP2 with non-aliphatic content and LCP15 with low aliphatic content (5 wt.%) decompose at a single step. High thermal stability and high char yield of LCP2 and LCP15 result from high aromatic content, 63 wt.% and 55 wt.%, respectively. Compositions with significant aliphaticity and Aromaticity in LCP7, LCP24, LCP25 cause decomposition at two steps.
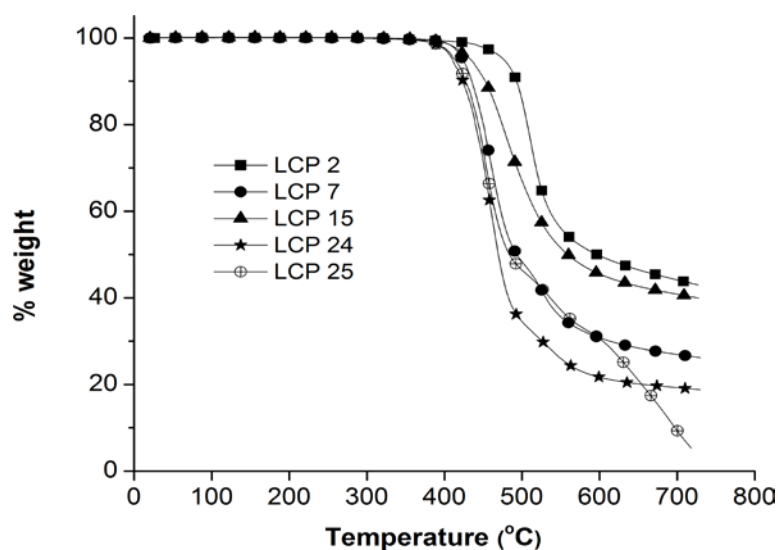
Figure 4-54 TGA curves of selected LCPs

Table 4-13 TGA data of selected LCPs

SAMPLE	$T_{5\%}$ (°C)	$T_{50\%}$ (°C)	T_{max} (°C) 1st step	2nd. Step	Char Yield (%)	Aromacity (wt.%)	Aliphacity (wt.%)
LCP2	476	596	515	----	43	63.3	-----
LCP7	423	493	465	530	26	51.1	7.5
LCP15	433	559	488	----	40	55.3	5.7
LCP24	410	469	460	540	19	44.7	16.5
LCP25	413	483	450	540	5	48.5	15.3

$T_{5\%}$: Temperature at 5% weight loss, $T_{50\%}$: Temperature at 50% weight loss,

T_{max}: The maximum rate degradation temperature, char yield: % remained matter at 700°.

$T_{5\%}$ gives information about initial weight loss temperature of compounds. As seen from Figure 4-55 when the aromaticity increases $T_{5\%}$, $T_{50\%}$, T_{max} values increases. As seen from Figure 4-56 the char yield increases with aromaticity.
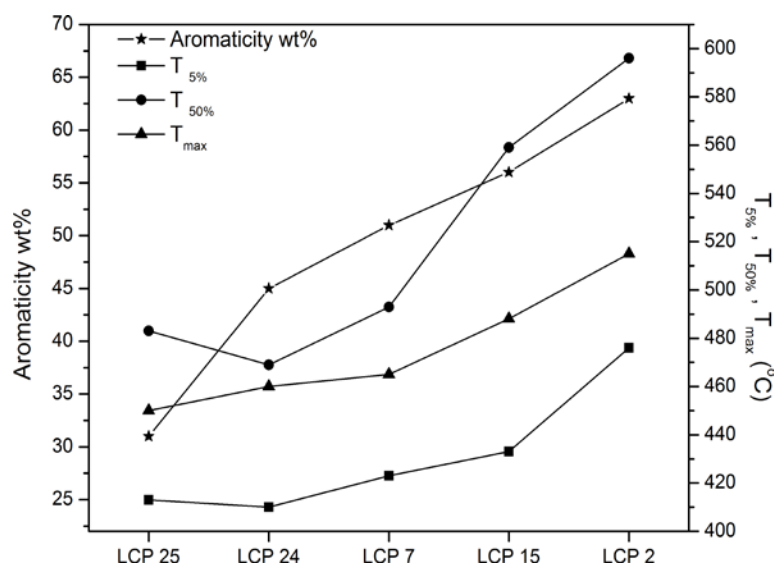
Figure 4-55 Aromaticity and $T_{5\%}$, $T_{50\%}$, T_{max} relation
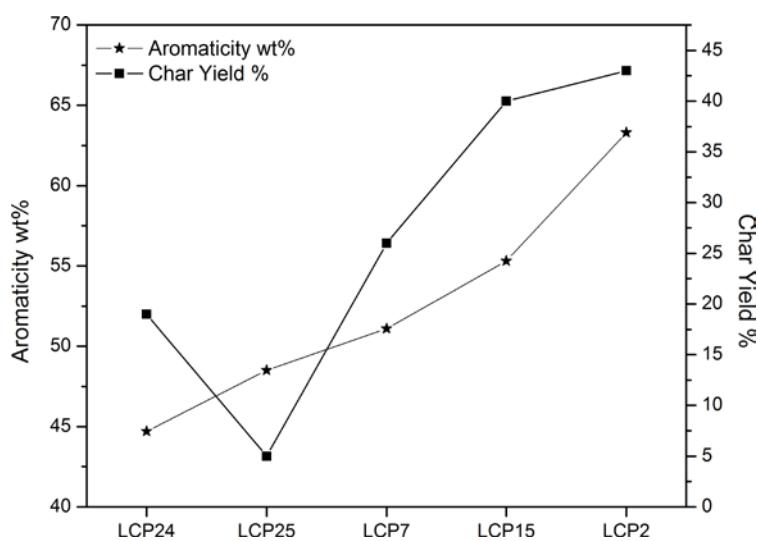
Figure 4-56 Aromaticity and char yield of LCPs

An opposite trend is observed for LCP25 (Figure 4-56) that gives very low char yield (5%) on contrary to higher aromaticity (%48.5). Here most probably the aromaticity which is due to naphthalene dicarboxylate has a different char forming mechanism.

4.10 Wide-Angle X-ray Diffraction (WAXS)

Wide angle X-ray diffraction (WAXS) measurements (Figure 4-57) of LCP films as a function of 2θ give crystalline peaks at a fixed angle, 20°. The films are produced on hot plate between Teflon sheets. The shear force applied on LCP films make chain orientation that cause the increase of % crystallinity and summarized in Table 4-14.
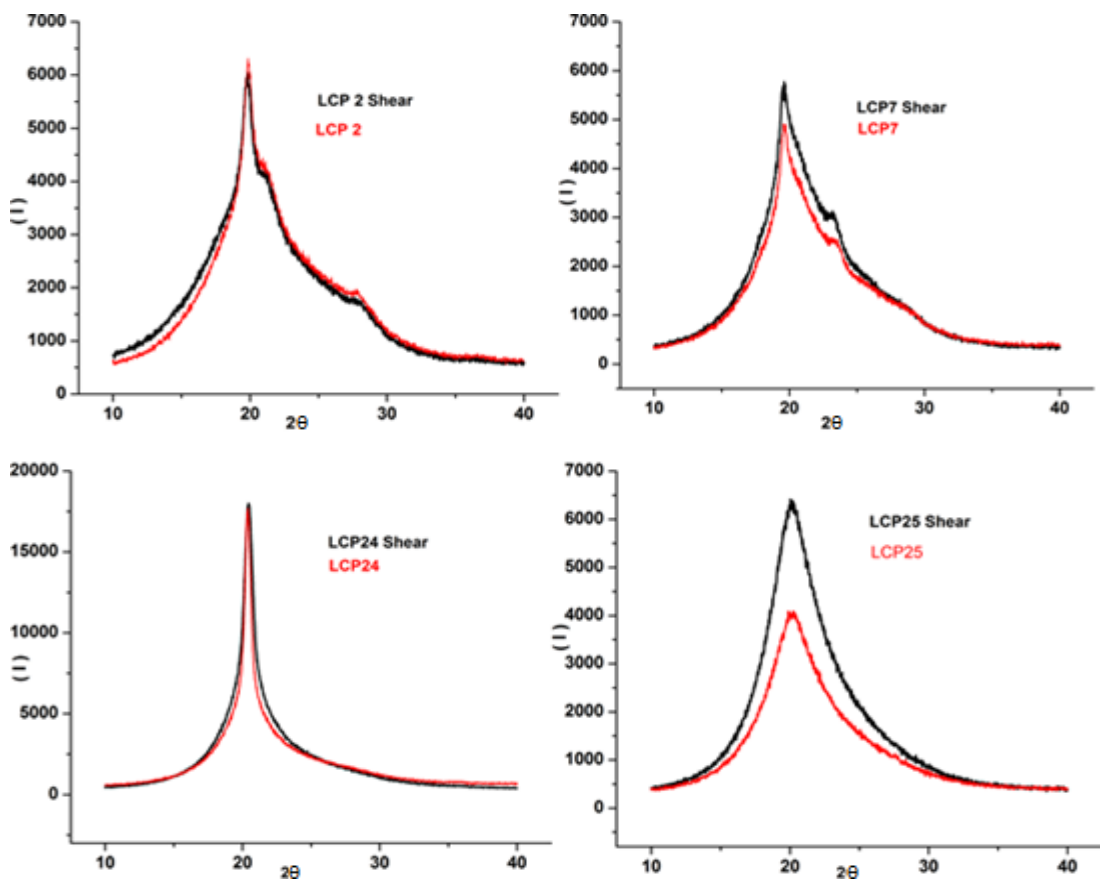
Figure 4-57 WAXS intensities (I) as a function of 2θ for the LCP films

Full width at half maximum (FWHM) in WAXS is inversely proportional with d-spacing between the polymer chains. Thus, when 1/FWHM value are compared (Table 4-14) d spacing between the chains of LCPs are ranked from small to high (LCP24<LCP2<LCP7<LCP25). Sequence shows that LCP containing PET (LCP24) are more crystalline than LCP25 that containing PEN, probably due to the symmetric morphology of terephthalic acid compared to 2,6 naphthalene

144

dicarboxylate. Kink groups in LCP2 and ethylene spacer in LCP7 make almost same effect on behalf of distorted chain packing and have the same FWHM values.

In LCP systems d spacing of the lamellar structures is affected by shear forces and d spacing changed to LCP24<LCP2=LCP7<LCP25 with small alteration [204-206].
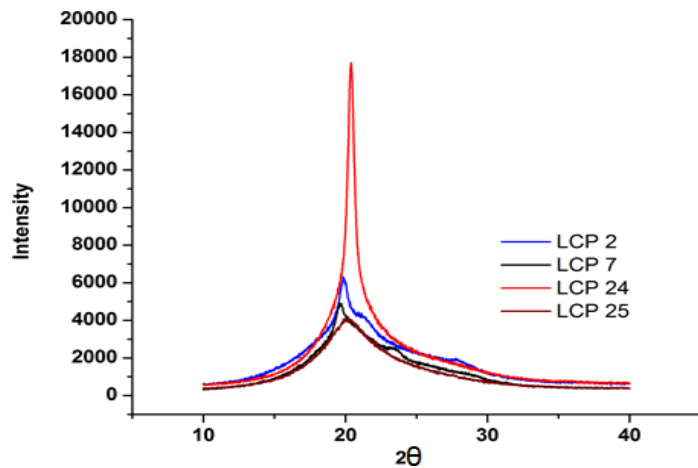
Figure 4-58 Comparison of baseline corrected WAXS intensities between LCP films

Numerical results of WAXS such as crystallinity, shear induced crystallinity, FWHM of polymer films are summarized in Table 4-14.

Table 4-14 Crystalline area and amorphous area of the WAXS, % crystallinity, 2θ max, FWHM

LCPs	Shear	Cryst. area	Amorph. area	crystallinity (%)	$2\theta^o$ max	FWHM^o	1/FWHM
2		540	5319	10	19.86	3.7	0.27
2	Shear	775	2953	26	19.82	4.0	0.25
7		836	7151	11	19.58	4.2	0.24
7	Shear	989	6183	15	19.62	4.0	0.25
24		780	4288	18	20.40	0.8	1.25
24	Shear	1149	4124	27	20.44	1.1	0.91
25		1200	5211	23	20.02	5.0	0.20
25	Shear	1817	6144	29	20.22	4.6	0.22

The area under red line indicates amorphous region and the area between red and blue lines indicates crystalline region (Figure 4-59). Percent crystallinity derived from the ratio of crystalline area to amorphous area by using Peak Processing Software (PDXL) of Rigaku Company.
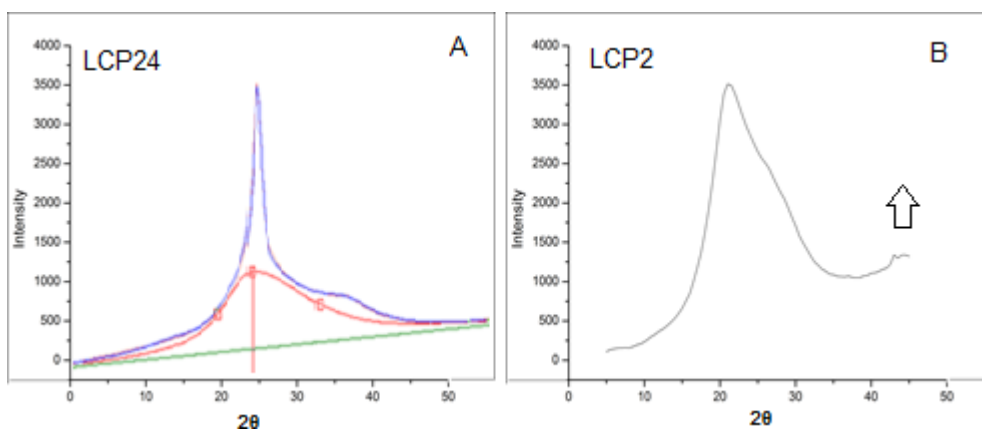
Figure 4-59 Peak Processing Software (PDXL) evaluation of LCP24 on WAXS, amorphous and crystalline region bordered by red and blue color (A), Intensity of LCP2 as a function of 2θ before baseline correction (B).

Asymmetry between shoulders, right side up (Figure 4-59) indicates block polymers rather than alternating monomers in LCP chains. Thus, LCP2 (Figure 4-59, B) which is composed of fully aromatic monomers has more blocks when compared with LCP24 (Figure 4-59, A) which has flexible spacers. From this finding, we can conclude that flexible spacers support the alternation of monomer in the backbone of the LCP chain.

4.11 X ray Fiber Diffraction

Fiber diffraction geometry of selected LCP fibers by X ray scattering represents alignment of chains. While uncatalyzed LCP24 (Figure 4-60,a) has only equatorial intensity diffraction representing axial alignment of the nematic phase, catalyzed one (Figure 4-60,b) has also weak meridian intensity that indicates the higher order in the crystal lattice. The pattern given below indicates an orientation of polymer chains along the fiber axis in LCP24.
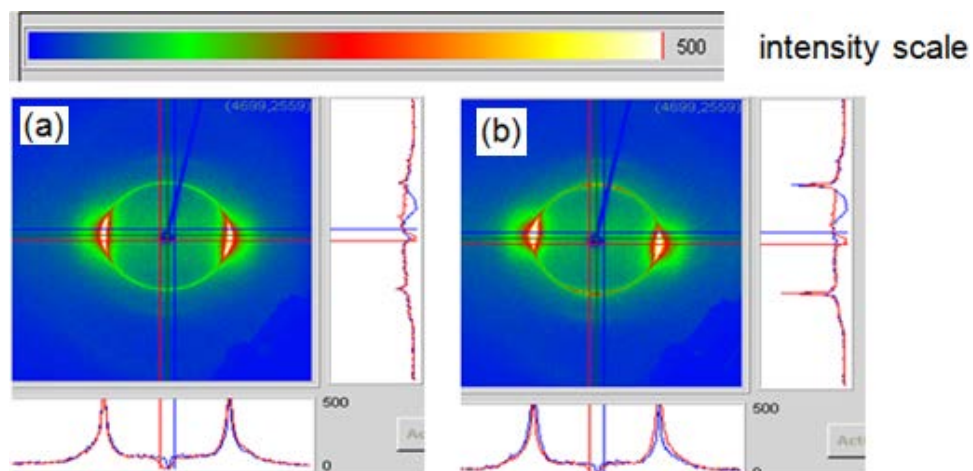
Figure 4-60 Fiber diffraction geometry of LCP24 synthesized in uncatalyzed (a) and catalyzed (b) medium
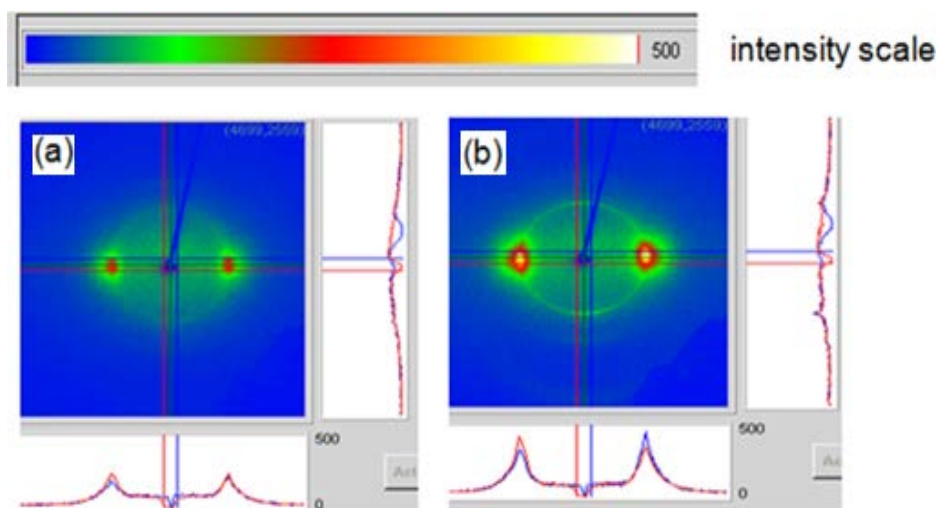
Figure 4-61 Fiber diffraction geometry of LCP25 synthesized from 0.1 mole of reactant (a) and 0.05 mole of reactant (b)

As discussed earlier in the CEG analysis the average molecular weight of the LCP's depend on a curious way on the amount of monomers charged into the reactor. A similar situation exists in Figure 4-61 for LCP25 composition. When a small amount of reactants are used (reactant ratios are same) a sharper pattern with halo lines is observed (Figure 4-61, b). This may indicate a well-developed crystal structure compared to higher charge amount of LCP25 (Figure 4-61, a). One other

observation is that the pattern for PET (LCP24) are sharper that PEN (LCP25) which is most probably is due to the symmetric morphology of terephthalic acid compared to 2,6 naphthalene dicarboxylate.

Blurred (Figure 4-61, a) and sharp (Figure 4-61, b) borders in halo intensities referred to the LCP25 that has 0.1 mole and 0.05 mole of reactants respectively. The diffraction geometry in Figure 4-61 belongs to the same compositional stoichiometry however the amount charged into the reactor changes.

Intensity on diffraction pattern is proportional with nematic order and crystallinity thus, we can say less amount charged into reactor give more crystalline product. This finding is supported by the finding in CEG analysis where we concluded that, less amount charged into reactor give higher molecular weight. A possible explanation is discussed in CEG analysis section.

4.12 Surface Free Energy

Surface energy is an indication of adhesive forces between reinforcing agent and matrix in polymeric composites. Interfacial attraction present in in situ composites can be explained by acid base theory of surface energies where Van der Waals interaction (Lw), acid (γ_s^+) and base (γ_s^-) characters of LCP surface energy signify the compatibility between the different constituents of the material [207-209].

Relatively high (larger than 35 mN/m) surface free energy of LCPs indicates the matrix-LCP adhesive forces will be enough to facilitate wetting of in situ composites (Table 4-15).

Table 4-15 Surface free energies of selected LCP films

	Surface Energy (mN/m)			
	γ_s^{LW}	γ_s^{+}	γ_s^{-}	γ_s^{total}
LCP 3	28.6	0.1	2.6	31.3
LCP 6	28.0	1.9	0.4	30.3
LCP 11	28.6	1.9	1.5	32.0
LCP 13	29.2	2.5	0.0	31.7
LCP 14	32.6	0.0	0.4	33.0
LCP 22	33.2	5.5	0.0	38.6
LCP 24	38.6	7.8	0.0	46.4
LCP 25	28.0	0.1	5.9	34.0
LCP 27	35.4	4.7	0.0	40.1
LCP 28	38.6	7.0	0.0	45.6
LCP 30	28.6	0.3	4.5	33.4

Comparison of adhesive forces between LCPs synthesized in this work and reinforcing agents commercially available can give information about the compatibility of LCPs in the matrix. Surface energy of carbon fiber and PA66 measured via Wilhelmy method in our laboratory are given in Table 4-16. Due to inert surface of carbon fiber, the surface energy is low. On the other hand LCPs are produced in some cases have large surface energy.

Table 4-16 Surface free energy of PA66 and carbon fibers (mN/m) measured by balance

sample no	γ_s^{LW}	γ_s^{+}	γ_s^{-}	γ_s^{total}
PA66	31.7	2.7	0.1	34.5
Carbon fiber	33.6	0.0	0.0	33.6

4.13 LCPs as Processing Aids

The main objective of this work is to develop liquid crystalline reinforcing agents that can be processed with structural or fiber forming polymers. It is expected that the shear alignment and thinning of the molten LCP phase will give micro or nano scale

reinforcement that will be advantageous compared to glass fiber or carbon fiber reinforced matrices.

Fully aromatic LCPs, group I (Table 4-17) have high melting temperature ($T_m >$ 260°C) than the temperature of processing of most thermoplastics. Fiber formation of them is hard to obtain by drawing machine. Even substituted aromatic groups in the main backbone exemplified as chlorine in LCP3 do not change general characteristics of group I. Vectran trademark is the only fully aromatic polyester LCP that can be melt processed produced as a result of more than 15 years of dedicated development and research by Cleanase scientists. But, even Vectran and other LCPs the LC5000 (Rodrun) or XG7 can be considered as high temperature melting materials.

Inclusion of PET and PEN to fully aromatic monomers gave melt processable LCPs and grouped as II (Table 4-17) for reinforcement application.

Table 4-17 LCP types and corresponding properties

LCP Type	T_m (°C)	Melt Process	Fiber Formation	Microscopy
(I) Fully aromatics	$T_m > 260$	Not Suitable	No	LCP
(II) Fully aromatics+ PET,PEN	280-190	Moderate	Moderate	LCP
(III) Aromatics + Diol	190-250	Easy	Weak	Heterogeneous
(IV) Aromatics + Short Aliphatic chain	190-220	Easy	Weak	Heterogeneous
(V) Aromatics + Long Aliphatic chain	190-250	Moderate	Moderate	LCP

Flexible spacer inclusions as aliphatic diols in group III (Table 4-17) give easily processable but heterogonous, unreacted LCP domains that give rise to brittle products. Four and six membered dicarboxylic acids, butanedioic and hexanedioic

acids decarboxylated at reaction temperatures that causes a loss of stoichiometric balance in the synthesis of group IV LCPs (Table 4-17).

The most appropriate LCP specimens among the synthesized groups that have melting temperature range which coincides with commodity thermoplastics. LCP24, LCP25, LCP30 were strong enough for tensile measurement (Figure 4-62) and were used as reinforcing agent in the thermoplastic blends.
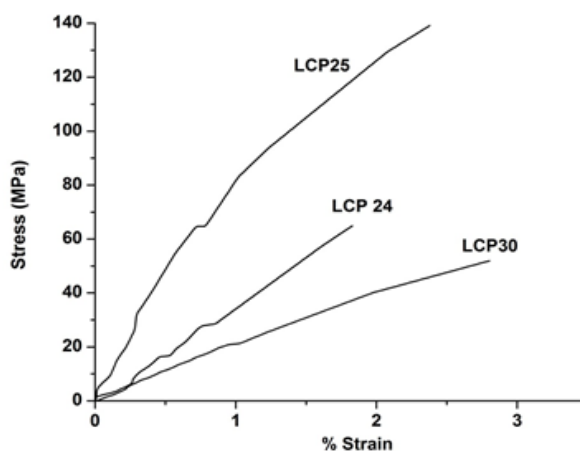
Figure 4-62 Tensile strength vs. % strain behavior of group V fibers of LCPs

4.14 Mechanical Behavior of the LCP Blends

In the tensile studies, mechanical properties of some of the LCP + matrix thermoplastic polymer compositions were tested to have an overall view of the possible application of the LCP's synthesized in this study.

In the LCP/PET and LCP/PP fibers, compared to neat PET and neat PP fibers respectively, no improvement in the mechanical properties was observed. However, in composite application, significant increase of tensile strength was observed in LCP/PP blends together with maleic anhydride grafted PP compatibilizer.

In terms of structural applications with ABS, promising compositions are tested which did not deteriorate the mechanical properties of ABS and improved in certain occasions. In future work shear alignment and thinning of the LCP phase should be

studied in injection molding using higher shear rates compared to shear rates that could be achieved in this study.

Selected LCP specimens are employed as reinforcing agents by mixing with the thermoplastics; acrylonitrile-butadiene-styrene (ABS), nylon6 (PA6), polyethylene terephthalate (PET) and polypropylene (PP) in micro compounder and twin screw extruder.

Some of the samples are tested as dog-bones and some are tested in fiber form as-spun or after cold-drawing with1:4 ratio.

4.14.1 PET/ LCP Fibers

DSM micro compounder is used in order to obtain undrawn fibers where PET and LCP24 are mixed (2% LCP content) gave similar tensile properties. The initial flat part is due to neck formation and extension of the sample by almost 300% (Figure 4-63). After cold-drawing with 1:4 ratio the tensile strength of the blends increased up to 200 MPa which is an indication of chain alignment of the samples along the fiber axis (Figure 4-64).
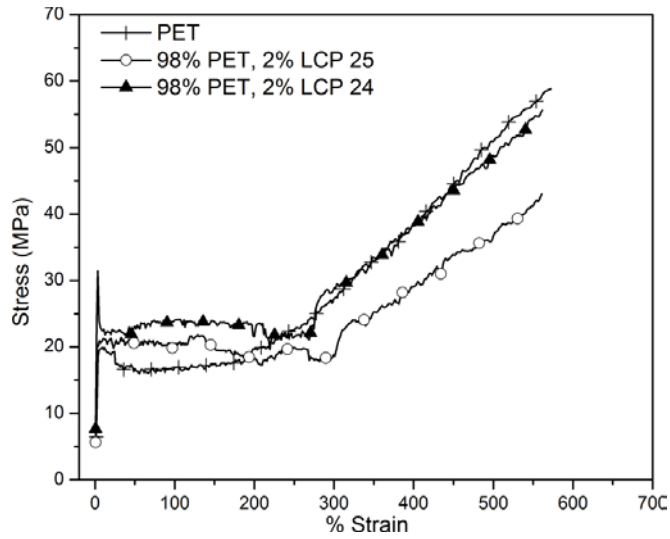
Figure 4-63 Tensile strength vs. %strain of PET-LCP24 and 25 fibers as spun at 200m/min
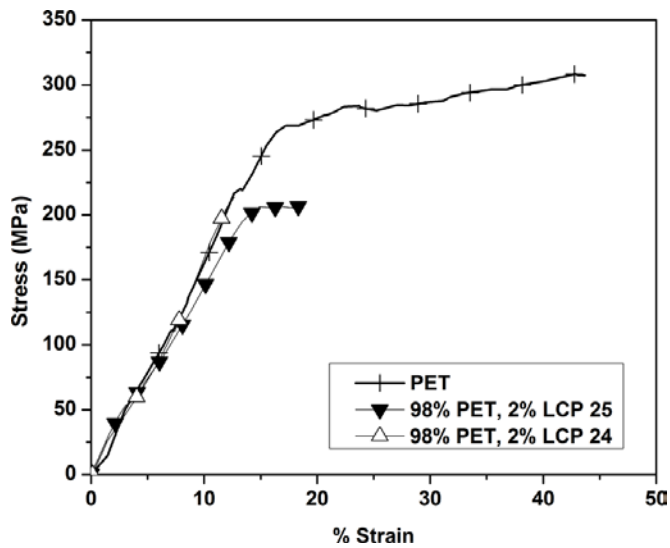
Figure 4-64 Tensile strength vs. %strain of PET/LCP24 and 25 fibers at ultimate draw down ratio 1:4 after spinning at 200m/min

LCP12, 15 and 28 cold drawn fibers increased their tensile strength up to 500 MPa which may be due to reactive mixing of PET with the LCP components (Figure 4-65). PET used in the Figure 4-65 is monofilament grade with IV:0.95 which is kindly supplied by Kordsa firm.
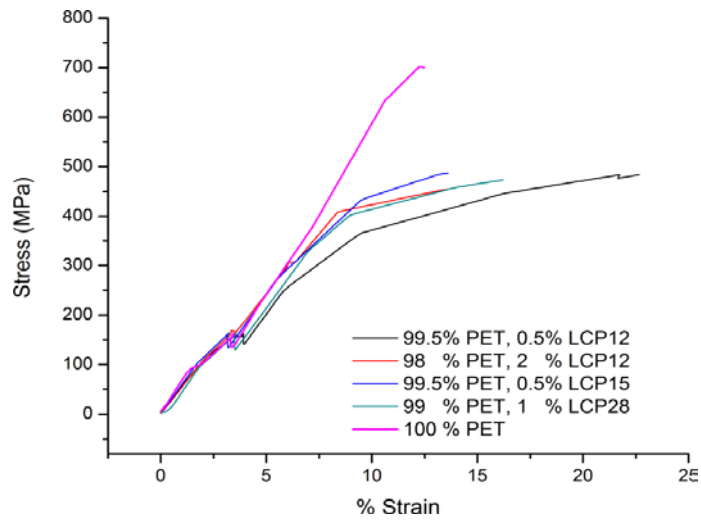
Figure 4-65 Tensile strength vs. %strain of PET/LCP12,15 and 28 fibers at ultimate draw down ratio 1:4 after spinning at 200m/min

4.14.2 PET, PEN/LCP Dog-bones

The lack of chain alignment in dog-bone sample can be observed in Figure 4-66 where the maximum stresses are in the vicinity of 55 MPa. A direct comparison with fiber form PET is not possible because of the difference in composition.
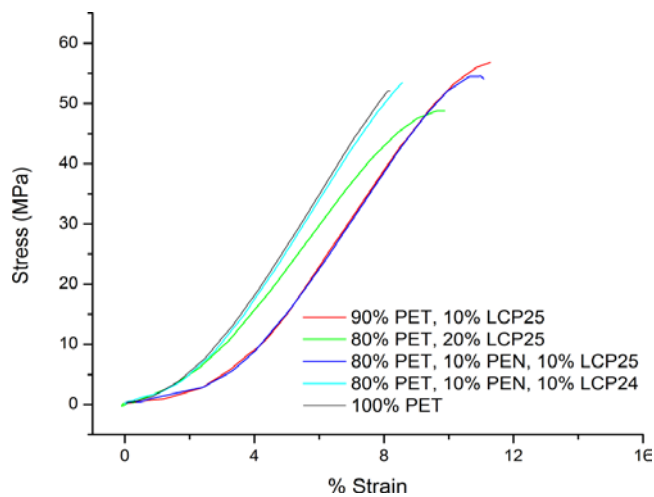
Figure 4-66 Tensile strength vs. %strain of PET/ LCP24 and LCP25 dog-bone

LCP inclusion to PET is not feasible because of possible esterification reactions when only mechanical property improvement is aimed. Another important problem is the oxygen and water vapor diffusivity of polyester films. LCP inclusion to PET can reduce the diffusion of gases which can be subject of future studies.

4.14.3 PP/LCP Fibers

Polypropylene used in these tests are functionalized by the inclusion of 10% maleic anhydride grafted PP to act as a compatibilizers between the inert PP and the LCP additives. The fibers obtained in this trial were of poor quality, so, we can conclude that LCPs synthesized are not feasible additives for PP fibers (Figure 4-67).
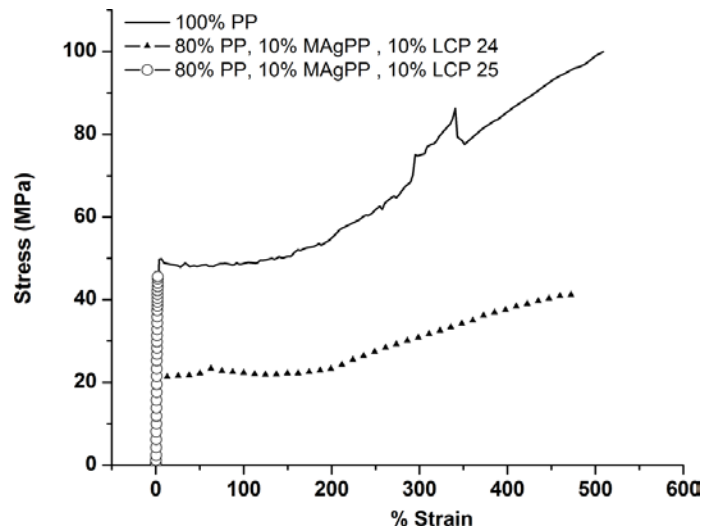
Figure 4-67 Tensile strength vs. %strain of PP/LCP24, 25 fiber as spun at 200m/min

4.14.4 PP/LCP Dog-bones

In dog-bone experiments of PP blend there is an improvement of the tensile strength values with LCP24 and LCP25. The maximum strain values decreased compare to PP, but for LCP24 a 25% increase in maximum stress value obtained (Figure 4-68).
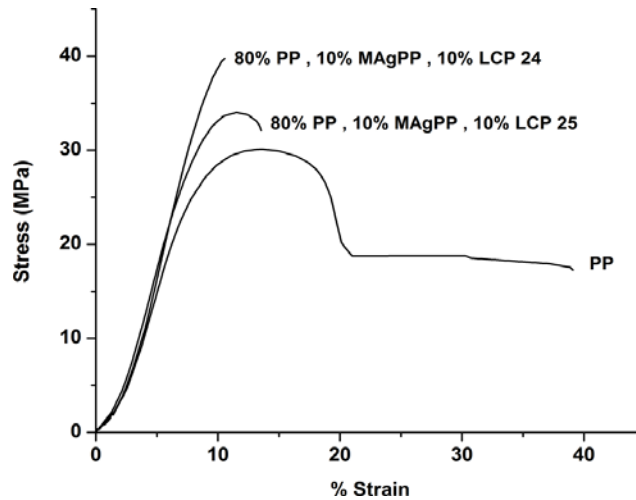
Figure 4-68 Tensile strength vs. %strain of PP/LCP24 and LCP25 dog-bone

4.14.5 ABS/LCP Blends

ABS is one of the commodity thermoplastics where glass fibers are utilized to obtain high strength structural composite materials. The use of LCP to replace the glass fiber will bring a weight advantage plus an ease in processing of ABS composites. A large number of various combinations of ABS, Nylon6, LCP together with compatibilizers are extruded and tested in the following trials (Figure 4-69 to Figure 4-78). In general no specific change is observed with and without the LCP addition.

It is possible that the shear rates employed in this study are not capable of elongating the LCP phase to a sufficiently narrow diameter. The results are promising, but, further trials at high shear rates are required for definitive answers.

4.14.6 ABS/LCP2 Dog-bone Blends

ABS and LCP2 is used and no specific change is observed even when 10% LCP is used (Figure 4-69 and Figure 4-70). In the trials with PA6 and n-baco as a compatibilizers between ABS and LCP2, with or without LCP there is no dramatic change in tensile properties (Figure 4-71 and Figure 4-72).
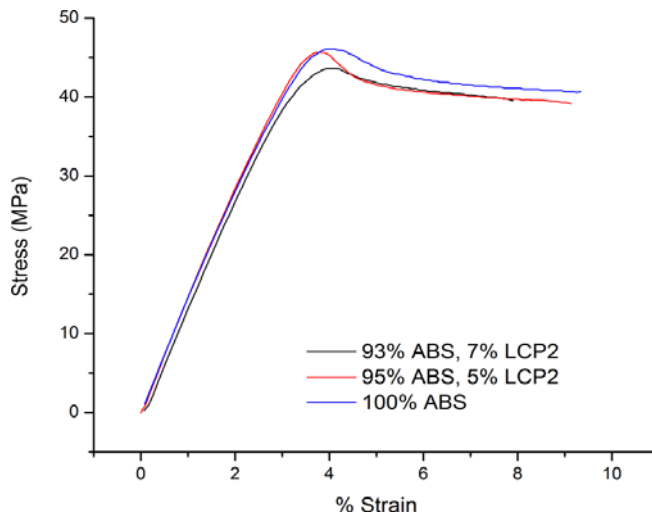
Figure 4-69 Tensile strength vs. % strain of ABS/LCP2 dog-bone
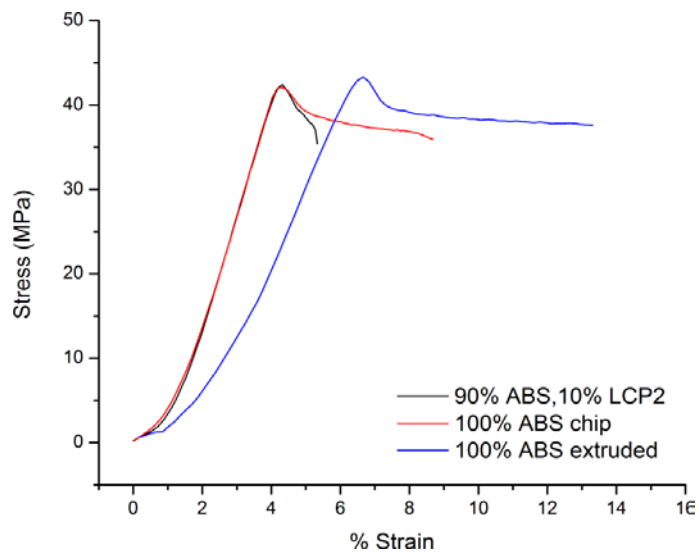
Figure 4-70 Tensile strength vs. %strain of ABS/LCP2 dog-bone

The use of compatibilizers n-baco and Nylon6 with LCP2 and ABS did not change the overall tensile properties of the blends. The maximum tensile strength and % strain values are more or less in the same vicinity (Figure 4-71).
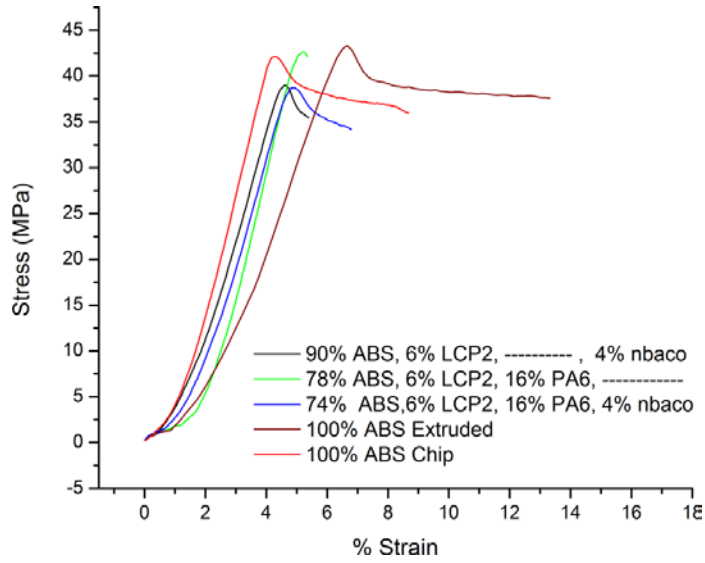
Figure 4-71 Tensile strength vs. %strain of ABS/LCP2 dog-bone
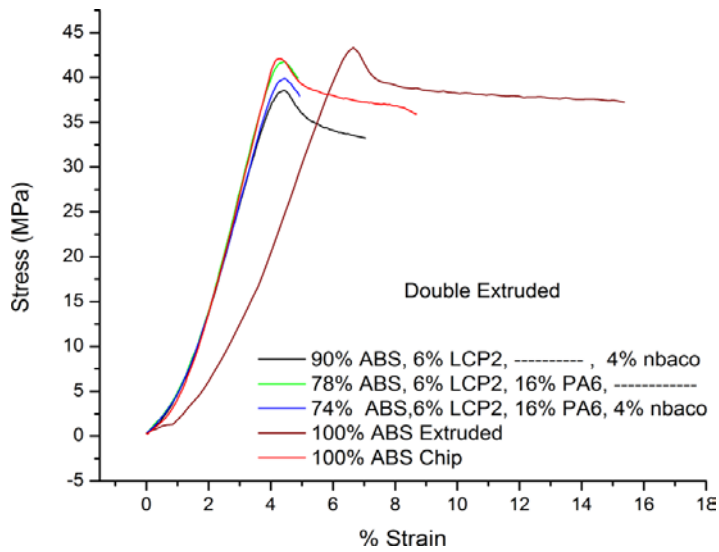
Figure 4-72 Tensile strength vs. %strain of double extruded ABS/LCP2 dog-bone

In Figure 4-73 instead of nbaco, lotader 8900 is used as the compatibilizers. Again no major change is observed in the tensile behavior of the blend containing PA6 and LCP2.
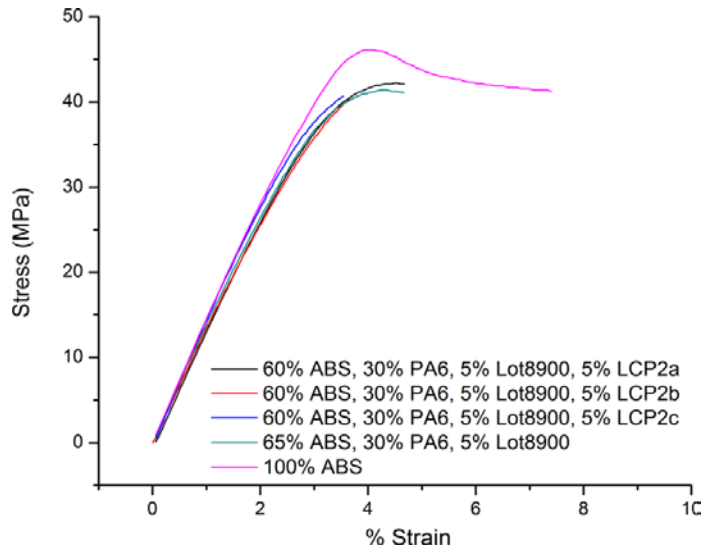
Figure 4-73 Tensile strength vs. %strain of ABS/LCP2 dog-bone

In the following trial Lot 8900 is employed with the addition of LCP5 and LCP8. Almost no change is observed in the tensile properties compared to 100% ABS sample (Figure 4-74).
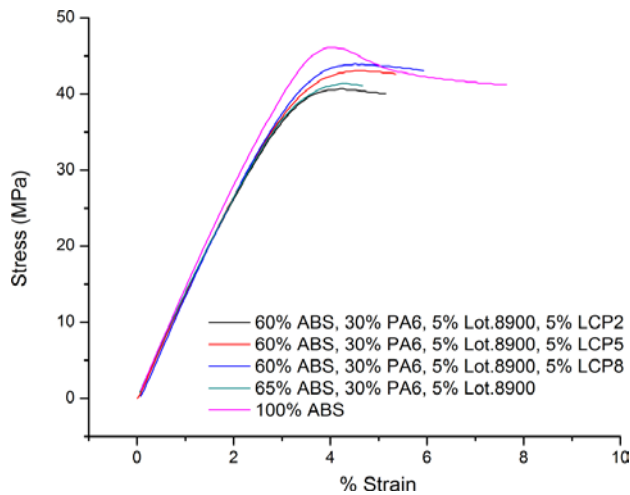
Figure 4-74 Tensile strength vs. %strain of ABS/LCP2, 5 and 8 dog-bone

When Lotader 2210 is used instead of Lotader 8900 with twice the amount (10%) of LCP4 and LCP5 the maximum tensile strength value and %strain values decreased

considerable which is an indication of a poor mechanical performance exhibited with Lotader 2210 (Figure 4-75).
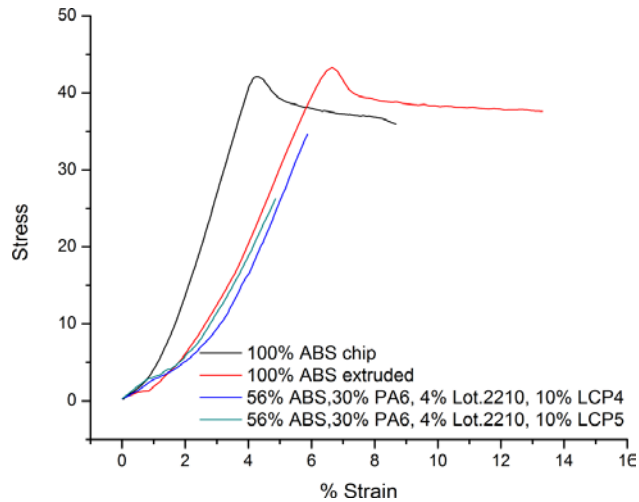
Figure 4-75 Tensile strength vs. %strain of ABS/LCP4 and 5 dog-bone

When styrene-maleic-anhydride (SMA) compatibilizer is employed, on the other hand, considerable increase to above 50MPa is obtained in Figure 4-76. This performance is achieved at low LCP7 % and 1% SMA, 80% ABS with about 18% PA6 in the blend composition.
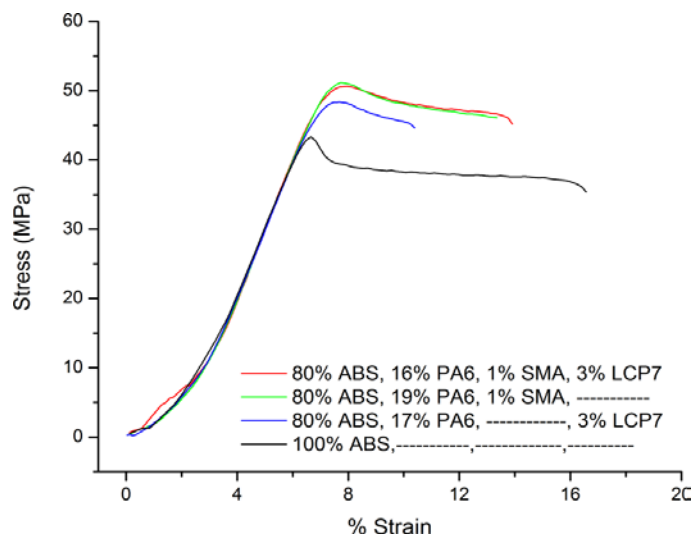
Figure 4-76 Tensile strength vs. %strain of ABS/LCP7 dog-bone
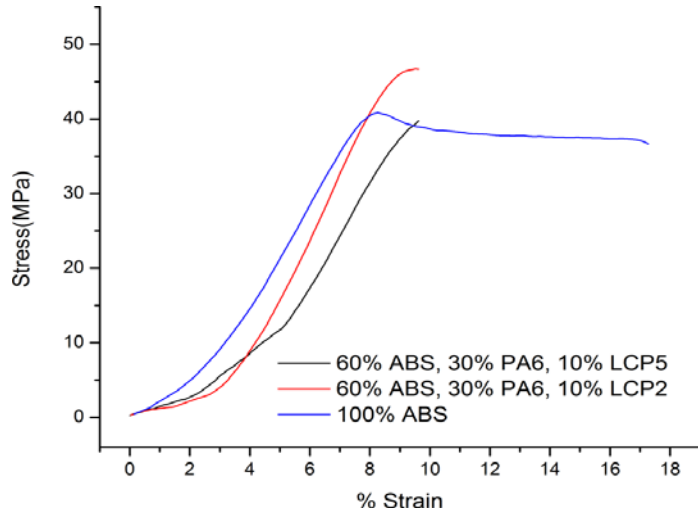
Figure 4-77 Tensile strength vs. %strain of ABS/LCP2 and 5 dog-bone

Without the compatibilizers with about 20% reductions in tensile strength value was obtained (Figure 4-78). LCP24 and 25 with aliphatic constituent caused a reduction in tensile strength.
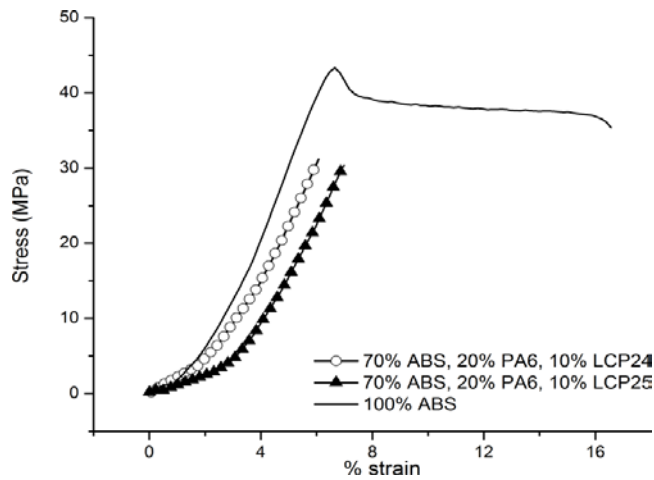
Figure 4-78 Tensile strength vs. %strain of ABS/LCP24 and 25 dog-bone

4.15 Charpy Impact Test of ABS/PA6/LCP7/SMA Blends

The ability of a composite to withstand a sudden impact is an important issue and can be improved by addition of suitable ingredients. Due to the presence of butadiene group, ABS is inherently tough material, however, when LCP7 is added

161

with PA6 and SMA to see whether it will create synergy. The result is tabulated (Table 4-18) and given in Figure 4-79.

Table 4-18 Charpy impact results of ABS/PA6/LCP7/SMA blends

no	ABS(%)	PA6(%)	LCP7(%)	SMA(%)	Impact(kJ/m^2)
1	80	13	6	1	30
2	80	20	0	0	32
3	78	16	6	0	39
4	80	16	3	1	42
5	80	19	0	1	45
6	93	0	7	0	45
7	96	0	3	1	51
8	100	0	0	0	58

Due to the disruption of the continuity of ABS, fracture energy of ABS/LCP7 blends decreases significantly as the LCP7 content increases. (Figure 4-79). LCP is anisotropic material and has weak resistance in perpendicular compared to longitudinal direction of specimens that cause weakness in fracture test. Thus LCP is not a suitable agent for toughness in composites especially perpendicular to flow direction.
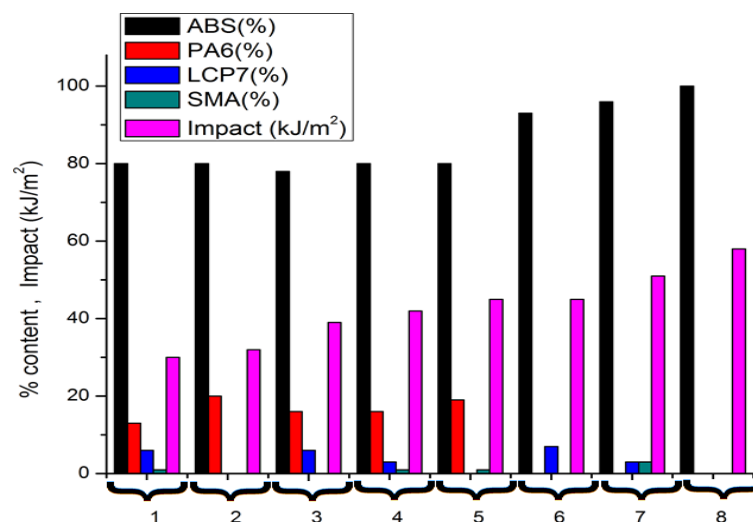
Figure 4-79 Fracture energy (kj/m^2) of ABS/PA6/LCP7/SMA blends

4.16 Rheological Analyses

Fibril formation of LCPs in the matrix which is the basic condition for improved mechanical performance of materials depends directly on shear and temperature together with compatibility of phases. Both capillary viscosity and Melt Flow Index (MFI) measurements have been done to check whether axially oriented LCP domains present, and if under which conditions. Axially oriented domains show itself as high MFI value and low viscosity under low shear rate, because they behaves as slip agents and cause the composite flow easily.

Contrary to oriented domains, unoriented LCP domains retard the flow and show itself as low MFI value and high viscosity material under high shear rate.

4.16.1 Capillary Rheometer

In capillary rheometer, viscosity (η) is measured as a function of shear rates which create a fibrous structure from droplet of LCP and other dispersed liquid phases that may be present in the blend of polymers. Apparent viscosity vs. shear rate (γ) relation of the ABS/PA6/LCP and lotader 2210 compatibilizers is given in Figure 4-80 at 230°C.
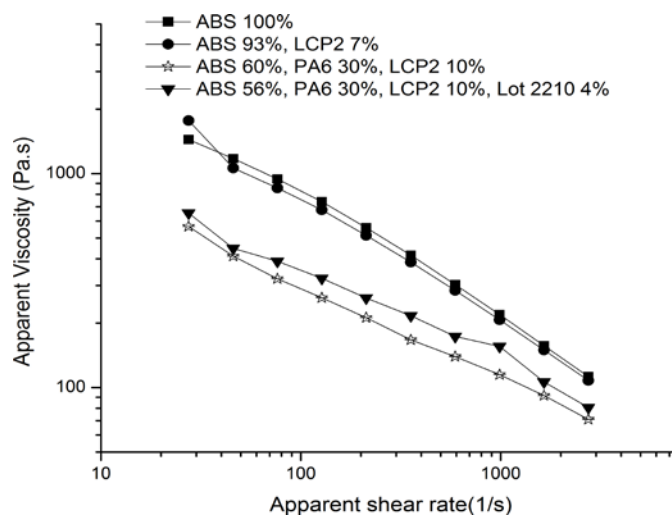
Figure 4-80 Apparent shear viscosity of the ABS-PA6 blends at 230°C at different shear rates

It is also possible to investigate the capillary rheometer samples by scanning electron microscopy to check out the fiber formation of LCP in the matrix at different shear rates

Due to the inherent end effect, correction was made by Rabinowitsch approach for calculation of true shear viscosity and true shear rate in viscosity and shear rate relation (Figure 4-82).

The flow of copolyester blend is non-Newtonian with viscosity decreasing with increasing rate for all samples. The LCP containing specimens have even lower viscosity with increasing shear rate. This may be the result of chain orientation in the blends.
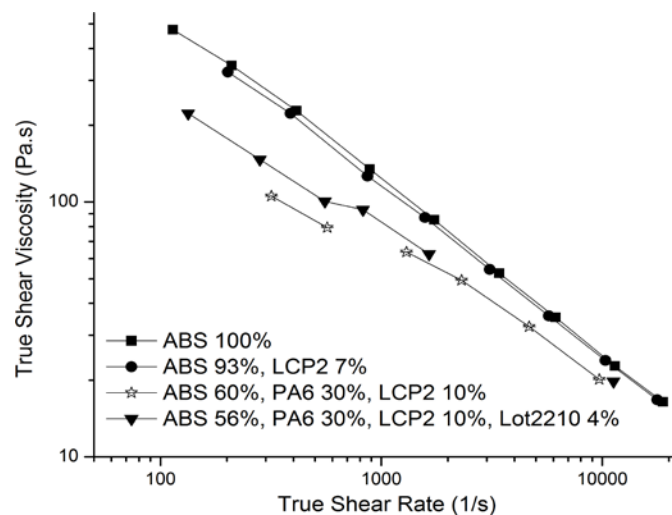
Figure 4-81 True shear viscosity of the ABS/LCP as a function of true shear rate after Rabinowitsch correction

4.16.2 Melt Flow Index (MFI) measurement

MFI values are inversely related to the melt viscosity. Flow behaviors of the blends are investigated by MFI measurement. MFI is related to molecular weight, degree of branching, thermal effects and in situ bonds between matrix and added components.

Melt flow index (MFI) and capillary rheometer measures ease of flow, thus orienting and unorienting types of mesogenic units of LCPs have importance. It

164

is obvious that low shear rates produced in MFI measurements cannot serve as orienting force on LCP mesogens.

4.16.2.1 MFI of PET blend

The MFI value of pure PET increases from 27g/10min to 31g/10min when it is extruded. During the processing, the Mwt of PET decreases due to thermal degradation arising from heat and shear. The low MFI value (21g/10min) of LCP25 stems from its unoriented rigid rod like mesogens. The MFI value of PET/LCP25 blend is between pure PET and LCP25. (Figure 4-82).
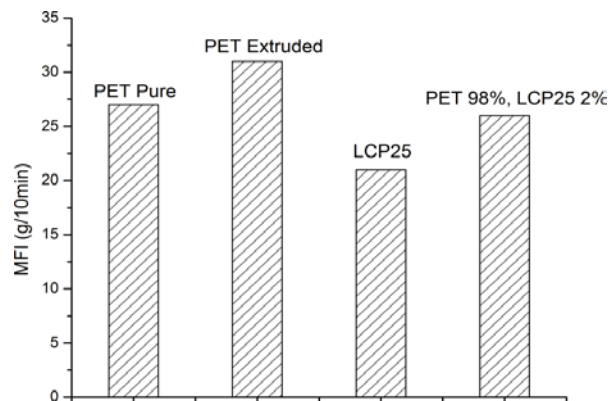
Figure 4-82 MFI values of PET/LCP25 blends

4.16.2.2 MFI of ABS Blends

The samples used in capillary rheometer are also investigated by MFI measurement to check the consistency between the results. ABS and LCP blend with low LCP ratio (ABS 93%, LCP2 7%) do not disrupt continuity of the matrix so much that MFI result of the blend is found between extruded and pure ABS (Figure 4-83 and Figure 4-84). Doubling of MFI value from 26 to 50 g/10min with the inclusion of PA6 which has cooperatively high MFI (35 g/10 min) parallels the rule of mixture in ABS 60%, PA6 30%, LCP2 10% blend. However, lotader2210 compatibilizers improve new bond formation between constituents and unoriented rigid rod like mesogens of LCP25 that cause to decrease MFI value to 45 g/10min.
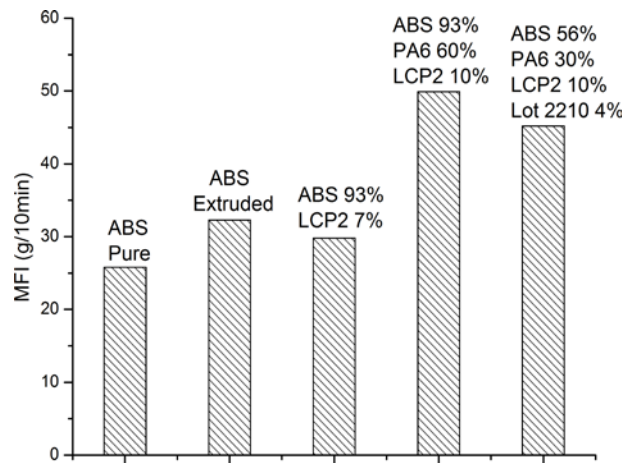
Figure 4-83 MFI values of ABS blends that measured in capillary rheometer

The effect of thermal degradation of ABS (230°C) during processing is also observed in the MFI results (Figure 4-84). Whilst pure ABS has MFI value as 26g/10min, extruded ABS has 32 g/10min.
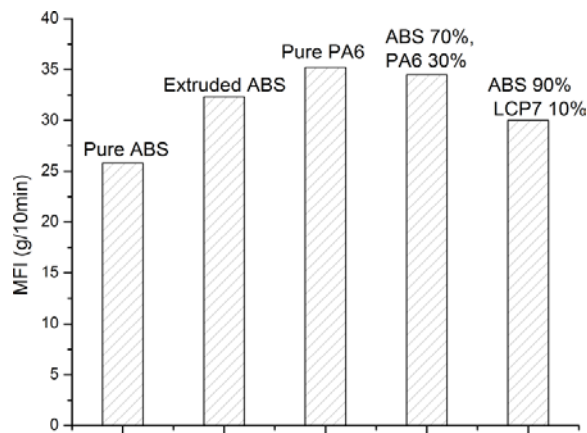
Figure 4-84 MFI values of ABS/PA6/LCP7 blends

Effect of the compatibilizers (Lotader 8900) and comparison of fully aromatic LCP2 with LCP8 that have flexible units are compared in the Figure 4-85. More rigid and unoriented LCP2 backbone has more detrimental effect on MFI, than that of LCP8.

For detailed rheological analysis each specimens needs to be examined by capillary rheometry however a detailed study with capillary rheometer is outside the scope of this work.
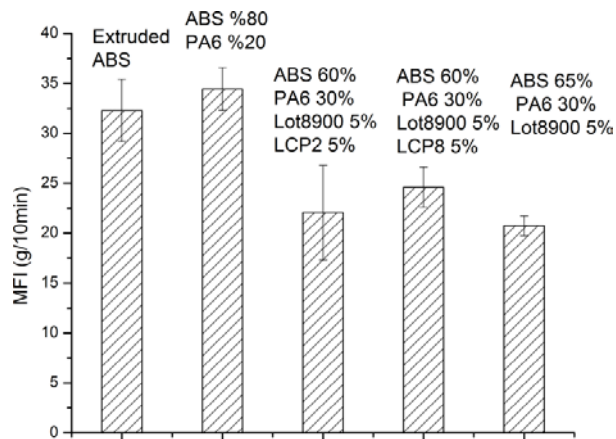
Figure 4-85 MFI values of ABS/PA6/LCP2 and LCP8

Due to the unoriented rigid rod like mesogens in the LCP7, as it increases in ABS matrix MFI values decrease (Figure 4-86).
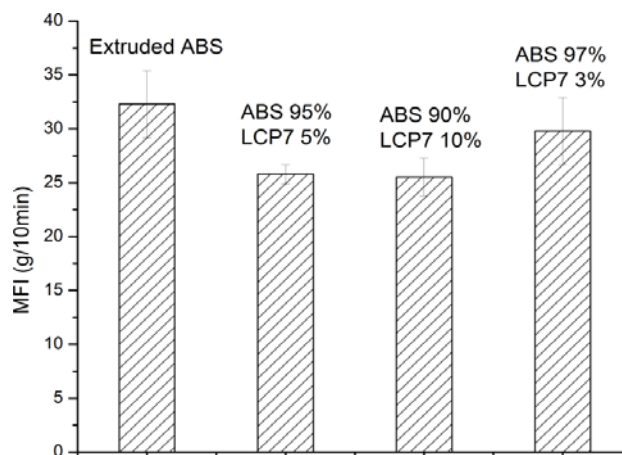
Figure 4-86 MFI values of ABS blends with LCP7 at different ratios

4.17 Scanning Electron Microscopy (SEM)

The SEM micrographs of crycroscopic fracture surfaces of ABS/LCP2 blends in different forms; dogbone (core-shell), capillary rheometer end product and fiber are examined to understand the effect of shear rate increases (Figure 4-87) on fiber formation of LCP droplets in matrix. The fracture surfaces of ABS/PA-6/LCP2 blend is also examined whether LCP2 has compatibilizing effect between ABS and PA-6.
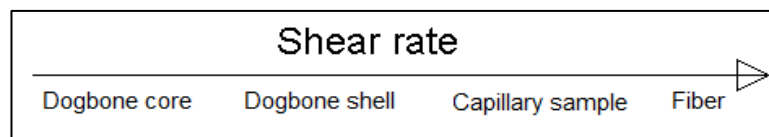
Figure 4-87 Shear rate increase in the preparation of SEM samples

Due to the geometry and boundary conditions of mold, applied shear rate on the blend decreased from shell to core of blend in dog-bone. (Figure 4-88-a and Figure 4-88-b respectively). If LCP droplets were aligned as expected, anisotropic mechanical behavior will rise with high shear rates that occur in shell of the dog-bone specimens.

We tried to collect samples at maximum shear rate (2700 s^{-1}) however, device need to be modified to prevent the building up of massive extrudate. The capillary rheometer samples (Figure 4-88-c) was collected at 100 s^{-1} shear rate with 1 mm diameter, represents the intermediate shear values between dog-bone and fiber.

To observe the effect of higher shear rates on LCP fibril formation, ABS matrix were extra dried (4 days 60°C) and spinned (100m/min) with average diameter 50µm.

As the shear rate increases the appearance of fracture surface does not change and there is no fiber formation of LCP seen on these surfaces (Figure 4-88-a,b,c,d). It is observed that LCP2 is completely dispersed and as LCP domains stays as droplet and cannot form fiber within the matrix (Figure 4-89).
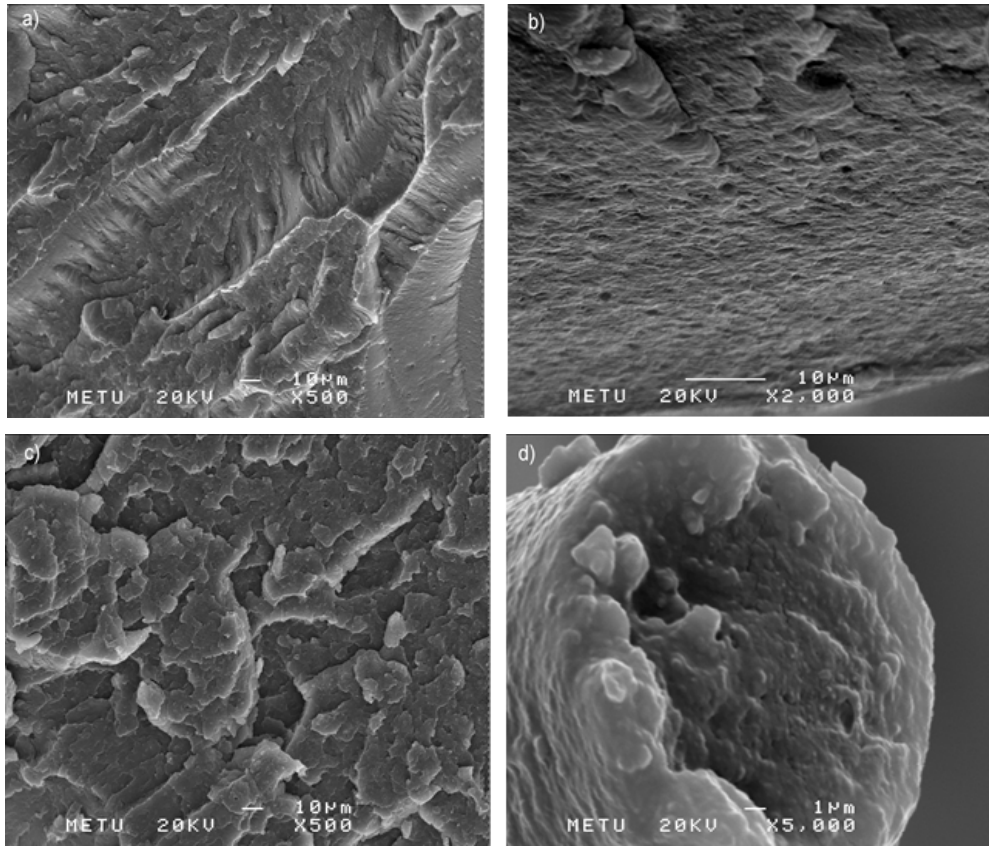
Figure 4-88 SEM micrographs of fracture surfaces of ABS, LCP2 (93%- 7%) blends in a) core of dog-bone b) shell of dog-bone c) capillary rheometer sample d) fiber
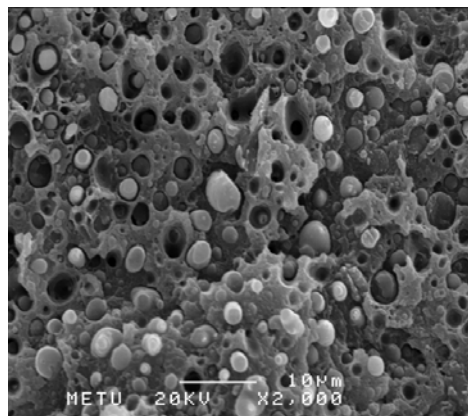
Figure 4-89 SEM micrographs of fracture surfaces of ABS, LCP2, PA6 (60%, 10%, 30%)

4.18 Possible Technological Applications and Processing Techniques

LCP usage in such processes as extrusion, lamination and composite applications are currently being explored. Film, sheet made from unfilled LCPs have high barrier properties which is a major interest today in medical, chemical, and industrial packaging applications. Moreover, new LCP grades and alternate processing technologies may lead to the development of novel products for the markets. A few of the promising area of research is the use of LCPs as nanofiber in composites and electrical semiconductors in the capacitors.

4.18.1 Electrospinning Results

Micro or nano sized fiber formation of LCP in a matrix cannot be achieved in most cases due to the inherent LCP-matrix problems. Addition of LCP in fiber form to master batch can be useful approach to surmount this difficulty. Electrospinning of solution is one of the LCP fiber production methods that involve the interaction of electrostatics, fluid rheology and polymer solution properties such as solution conductivity, surface tension, and the rate of solvent evaporation. Understanding these interactions for an LCP specimen needs a wide and detailed study and can be a separate thesis topic.

In this study, the dissolution of LCPs was checked by trial and error method in different solvents [(dimethylformamide (DMF), *N*-Methyl-2-pyrrolidone (NMP) and dimethylacetamide (DMAc), formic acid] to understand LCP/solvent combination that is eligible for electrospinning. The detailed information about LCP/solvent type is given in Table 4-19. The soluble ones are tested in spinning but only LCP 27/DMAc combination gives nanofiber structure with a diameter of 200 nm (see Figure 4-90). These fibers can be used as reinforcing agents in polymer blends and composites.

Table 4-19 The results of electrospinning of LCPs by different solvents

	NMP	**DMF**	**DMAc**	**Formic acid**
LCP15	Not Dissolved	Not Dissolved	Dissolved, Not Fiber	Not Dissolved
LCP25	Not Dissolved	Not Dissolved	Not Dissolved	Not Dissolved
LCP27	Dissolved, Not Fiber	Not Dissolved	**Dissolved Nano Fiber (d:200nm)**	Dissolved Not fiber
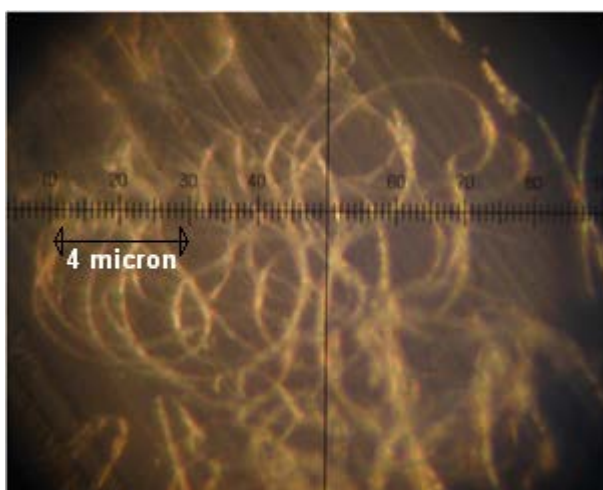
Figure 4-90 Microscopic view of electrospinning product of LCP27

4.18.2 Electrical Application

Each synthesized LCP in this study has different aromatic-aliphatic ratio that brings non-conjugated systems having unique semiconducting properties. Semiconductors have conductivity 10^3 to 10^{-8} siemens (S) per centimeter have fundamental place in electronic application such as transistors, diodes, solar cells and integrated circuits. Electrical properties such as dielectric constant (ε'), dissipation factor (tanδ) and conductivity (S/m) of a candidate semiconductor needs to be measured to understand whether it has any application area or not.

Due to high dipole moment density of LCP29 high dielectric constant is observed when compared with the other samples (Figure 4-91). At the lower temperatures than 340K for the samples LCP24, 25 and 27 and 360K for the LCP29 dielectric constant (ε') varies slowly with increasing temperature. Whilst approaching to the phase transition temperature determined by DSC at 150°C dipole moment thus dielectric constant increases together. As temperature increases higher numbers of dipoles are rotated by external electric field that induces internal dipole moment thus ε' increases.
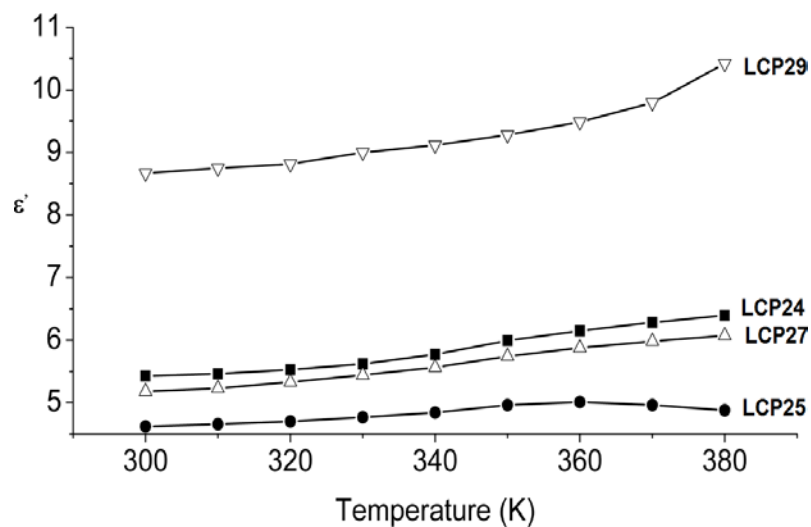
Figure 4-91 Dielectric constants (ε') of LCPs as a function of temperature

It is known that, conductivity is characterized by the activity of charge carriers. This activity is easier at higher temperatures that lead increased conductivity and dielectric loss. At the lower temperatures (340K) LCP24 has higher conductivity than other samples (Figure 4-92). When temperature increases, conductivity of the LCP29 starts to increase while the conductivity of the LCP27 decreases however others (LCP24 and LCP25) stay almost stable (Figure 4-92).
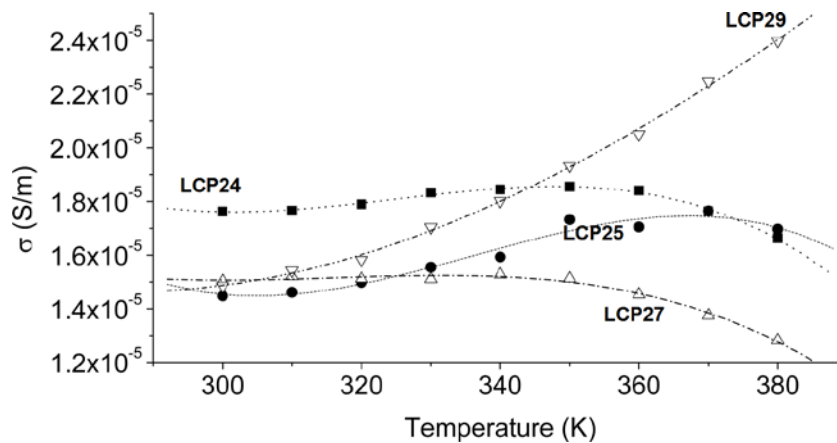
Figure 4-92 Conductivity (σ) of LCPs as a function of temperature

Dissipation factor (tanδ) is the reciprocal of quality factor and measure of loss-rate of power in an electrical system. Dissipation factor of LCP29 increases with temperature however always stays at low values at measurement temperatures (Figure 4-93) and has the least amount of dissipation compared to other samples.
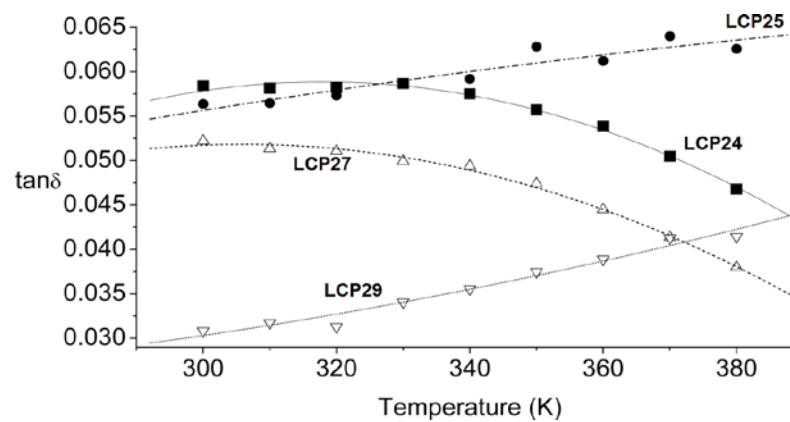
Figure 4-93 Dissipation factors (tanδ) of LCPs as a function of temperature

The LCP copolyesters synthesized in this study seems to be high quality capacitance material. Further work is needed to characterize their electrical properties.

CHAPTER V

CONCLUSIONS

In light of the LCP characterizations certain inferences can be made. For composite applications, first aim was to synthesize wholly aromatic melt processable form of LCP which was achieved by LCP2 via kinked monomer (*m*-acetoxy benzoic acid) and torsionally mobile monomer (hydroquinone diacetate). Moderately high process temperature of LCP2 is lowered by adjustments in reaction time. Weak fiber formation capacity of fully aromatics in melt and their potentially weak capacity as reinforcing agent persuade us to synthesize and use PET based TLCP. Ethylene inclusion to fully aromatic backbone via PET gave the best formulation in LCP7. In the framework of the synthesis of LCPs that have lower melting temperatures, linear aliphatic diols and dicarboxylic acids are used. A few of them achieved the intended quality and were labeled as LCP12, LCP15, LCP24 and LCP25; LCP29, LCP30. The others gave side reactions such as back-biting, decarboxylation, thermal decomposition. As a result of this study, the following highlights are emphasized;

Flexible spacer inclusions as aliphatic diacid can be used as eight membered octanedioic acid and ten membered decanedioic acid. In four and six membered dicarboxylic acids, butanedioic and hexanedioic acids decarboxylated at reaction temperatures that causes a loss of stoichiometric balance whilst the synthesis.

Flexible spacer inclusions as aliphatic diols give easily processable but heterogeneous, unreacted LCP domains that give rise to brittle products due to the side reactions, thus only diols with two membered CH_2 (ethylene glycol) are suitable in melt condensation polymerization.

Similar to PET synthesis, the highest molecular weight of LCP24 is obtained by using manganese acetate and antimony oxide as catalysts.

X- ray fiber diffraction pattern shows that LCP containing PET are more crystalline than LCP containing PEN which is most probably is due to the symmetric morphology of terephthalic acid compared to 2,6 naphthalene dicarboxylate.

In WAXS graph, asymmetry between shoulders indicates block polymers are found in fully aromatic LCP2. However LCP24 is less blocky in the backbone due to the flexible spacers involved.

As the amount of the charge to the reactor increases the IV and X_n of the product decrease and CEG values become larger, in addition low crystallinity is observed as determined from X-ray fiber diffraction pattern.

Capillary rheometer studies show that the true viscosity decreases with increasing shear rate. The effect is more pronounced in sample with LCP and the compatibilizer. This is an indication of chain orientation.

Melt flow index (MFI) results coincide with that of capillary rheometer. Low shear rates in MFI measurement cannot orient the LCP mesogens.

Scanning Electron Microscopy (SEM) photos support the results obtained from MFI and capillary rheometer measurements. Fiber formation is not observed.

The LCP copolyesters did not usually improve the mechanical properties except in composite application with polypropylene. A significant increase in tensile properties is observed by LCP24 and LCP25 usage.

LCP27 gives nanofiber structure with a diameter of 200 nm by electrospinning. These fibers can be used as reinforcing agents in polymer blends and composites and also hopefully in nonwoven fabric application.

Work of adhesion between some of the LCPs and matrix is higher than that of carbon fiber and PA66 which have significantly lower surface energies.

Dielectric constant (ε') of LCP29 varies slowly with increasing temperature and have much better properties when compared to PET which finds applications as insulator and capacitance material in electrical devices.

Another important property of LCP copolyesters is their use as low diffusivity material in medical vacuum test tube and food packing applications. Further work is needed to characterize their gas and liquid diffusivities.

REFERENCES

[1]   W. Jackson Jr and H. Kuhfuss, "Liquid crystal polymers. I. Preparation and properties of p hydroxybenzoic acid copolyesters," *Journal of Polymer Science: Polymer Chemistry Edition,* vol. 14, pp. 2043-2058, 1976.

[2]   G. Gray and P. Winsor, "Liquid crystals & plastic crystals," *New York,* 1974.

[3]   A. M. Donald*, et al.*, *Liquid crystalline polymers*: Cambridge Univ Pr, 2006.

[4]   P. Flory, "Phase equilibria in solutions of rod-like particles," *Proceedings of the Royal Society of London. Series A. Mathematical and Physical Sciences,* vol. 234, p. 73, 1956.

[5]   A. Siegmann*, et al.*, "Polyblends containing a liquid crystalline polymer," *Polymer,* vol. 26, pp. 1325-1330, 1985.

[6]   Q. Lin*, et al.*, "Effect of drawing on structure and properties of a liquid crystalline polymer and polycarbonate in situ composite," *Polymer Engineering & Science,* vol. 33, pp. 789-798, 1993.

[7]   G. Kiss, "In situ composites: blends of isotropic polymers and thermotropic liquid crystalline polymers," *Polymer Engineering & Science,* vol. 27, pp. 410-423, 1987.

[8]   Y. Meng*, et al.*, "Morphology, rheological and thermal properties of the melt blends of poly (phthalazinone ether ketone sulfone) with liquid crystalline copolyester," *Polymer,* vol. 39, pp. 1845-1850, 1998.

[9]   D. Dutta*, et al.*, "Polymer blends containing liquid crystals: a review," *Polymer Engineering & Science,* vol. 30, pp. 1005-1018, 1990.

[10]   M. Y. Ju*, et al.*, "Morphologies and mechanical properties of polyarylate/liquid crystalline polymer blends compatibilized by a multifunctional epoxy resin," *Macromolecular Chemistry and Physics,* vol. 201, pp. 2298-2308, 2000.

[11]   D. Beery*, et al.*, "Structure development during flow of polyblends containing liquid crystalline polymers," *Polymer Engineering & Science,* vol. 31, pp. 451-458, 1991.

[12]   S. Pisharath and S. C. Wong, "Processability of LCP-nylon-glass hybrid composites," *Polymer Composites,* vol. 24, pp. 109-118, 2003.

[13]   K. Jin-ling, "Liquid Crystal Polymers and Their Applications," *Plastics,* 2004.

[14]   T. S. Chung*, et al.*, "Liquid Crystal Polymers and Their Applications," *Marcel Dekker, Inc., Handbook of Polymer Science and Technology.,* vol. 2, pp. 625-675, 1989.

[15]   C. B. McArdle, *Side chain liquid crystal polymers*: Springer, 1989.

[16]   G. H. Brown and P. P. Crooker, "Liquid crystals a colorful state of matter," *Chemical and Engineering News,* vol. 31, 1983.

[17]   W. Krigbaum*, et al.*, "Thermotropic polyesters. 2. Investigation of the mesophase properties of polymers based on 4, 4'-dihydroxybiphenyl," *Macromolecules,* vol. 16, pp. 1271-1279, 1983.

[18]   W. Krigbaum and J. Watanabe, "Thermotropic homopolyesters: 5. Investigation of the smectic phase of polyesters based on p, p'-bibenzoic acid," *Polymer,* vol. 24, pp. 1299-1307, 1983.

[19]   D. K. Yang and S. T. Wu, *Fundamentals of liquid crystal devices*: Wiley, 2006.

[20]   T. S. Chung, "The recent developments of thermotropic liquid crystalline polymers," *Polymer Engineering & Science,* vol. 26, pp. 901-919, 1986.

[21]   S. X. Cheng*, et al.*, "Novel thin-film polymerization and time evolution of liquid crystal texture during polymerization," *Chemical Engineering Science,* vol. 54, pp. 663-674, 1999.

[22]   S. X. Cheng and T. S. Chung, "Configuration effects of ortho, meta, and para linkages on liquid crystallinity during thin film polymerization of poly (ester amide) s," *Journal of Polymer Science Part B: Polymer Physics,* vol. 38, pp. 2221-2231, 2000.

[23]   F. Rybniká *, et al.*, "Thin film melt polymerized single crystals of poly (p oxybenzoate)," *Macromolecular Chemistry and Physics,* vol. 195, pp. 81-104, 1994.

[24]   J. Liu*, et al.*, "Morphology of solution-and melt-polymerized poly (p-oxybenzoate/2, 6-naphthoate) copolymers: Single crystals, disclination domains, and superlattices," *Journal of Macromolecular Science, Part B,* vol. 35, pp. 375-410, 1996.

[25]   F. Rybnikar*, et al.*, "Lamellar crystallization during bulk polymerization of poly (p-oxybenzoate)* 1," *Polymer,* vol. 35, pp. 1863-1868, 1994.

[26]   F. La Mantia*, et al.*, "Relationships between mechanical properties and structure for blends of nylon-6 with a liquid crystal polymer," *European Polymer Journal,* vol. 26, pp. 323-327, 1990.

[27]   T. T. Hsieh*, et al.*, "Miscibility of a nematic liquid crystalline polymer pair," *Polymer,* vol. 42, pp. 8007-8011, 2001.

[28]   P. K. Bhowmik*, et al.*, "Thermotropic liquid crystalline polyesters of 4, 4 biphenol and phenyl substituted 4, 4 biphenols with 4, 4 oxybisbenzoic acid," *Journal of Polymer Science Part A: Polymer Chemistry,* vol. 40, pp. 141-155, 2002.

[29]   S. Ponomarenko*, et al.*, "Liquid crystalline carbosilane dendrimers: First generation," *Liquid Crystals,* vol. 21, pp. 1-12, 1996.

[30]   A. Ciferri, *Supramolecular polymers*: Taylor & Francis New York, 2005.

[31]   G. Mao*, et al.*, "Molecular design, synthesis, and characterization of liquid crystal-coil diblock copolymers with azobenzene side groups," *Macromolecules,* vol. 30, pp. 2556-2567, 1997.

[32]   S. X. Cheng*, et al.*, "Effects of monomer structures on the evolution of liquid-crystal texture and crystallization during thin film polymerization," *Journal of Polymer Science Part B: Polymer Physics,* vol. 37, pp. 3084-3096, 1999.

[33]   C. He*, et al.*, "Synthesis and structure of wholly aromatic liquid-crystalline polyesters containing meta and ortholinkages," *Journal of Polymer Science Part A: Polymer Chemistry,* vol. 39, pp. 1242-1248, 2001.

[34]   B. K. Chen*, et al.*, "Synthesis and properties of liquid crystalline polymers with low Tm and broad mesophase temperature ranges," *Polymer,* vol. 46, pp. 8624-8633, 2005.

[35]   A. Collyer, "Thermotropic liquid crystal polymers for engineering applications," *Materials Science and Technology,* vol. 5, pp. 309-322, 1989.

[36]   M. M. Teoh*, et al.*, "Thin-film polymerization and RIS Metropolis Monte Carlo simulation of fluorinated aromatic copoly (ester-amide) s," *Polymer,* vol. 46, pp. 3914-3926, 2005.

[37]   F. P. La Mantia*, et al.*, "Compatibilization of blends of polyethylene with a semirigid liquid crystalline polymer by PE-g-LCP copolymers," *Polymer Engineering and Science,* vol. 37, pp. 1164-1170, 1997.

[38]   F. P. La Mantia*, et al.*, "Effect of the Components' Molar Mass and of the Mixing Conditions on the Compatibilization of PE-LCP Blends by PE-g-LCP Copolymers," *Journal of Applied Polymer Science,* vol. 71, pp. 603-613, 1999.

[39]   P. Magagnini*, et al.*, "Phase behavior of blends of polyethylene terephthalate with liquid-crystalline polymers," *Polymer Engineering and Science,* vol. 38, pp. 1572-1586, 1998.

[40]   P. L. Magagnini*, et al.*, "Synthesis of PP-LCP graft copolymers and their compatibilizing activity for PP/LCP blends," *Journal of Applied Polymer Science,* vol. 69, pp. 391-403, 1998.

[41]   R. Miliè*, et al.*, "Segregation of liquid crystalline mesophases during the transesterification of PET with sebacic acid, hydroquinone and 4-hydroxybenzoic acid," *Molecular Crystals and Liquid Crystals Science and Technology Section A: Molecular Crystals and Liquid Crystals,* vol. 372, pp. 37-50, 2001.

[42]   L. Minkova*, et al.*, "Ester exchange reactions in equimolar poly(ethylene terephthalate)/poly(phenylene sebacate) blends," *Macromolecular Chemistry and Physics,* vol. 202, pp. 681-688, 2001.

[43]   L. Minkova and P. Magagnini, "Characterization of a PE-g-LCP compatibilizer, prepared by reactive blending of acrylic acid grafted polyethylene (PE) and a semiflexible liquid crystalline polymer (LCP)," *Macromolecular Chemistry and Physics,* vol. 200, pp. 2551-2558, 1999.

[44]   L. Minkova*, et al.*, "Crystallization behavior and morphology of PE-g-LCP copolymers," *Colloid and Polymer Science,* vol. 275, pp. 520-529, 1997.

[45]   L. Minkova and Y. Peneva, "Microhardness of PET-based liquid crystalline copolyesters: Influence of the microstructure," *Polymer,* vol. 44, pp. 6483-6488, 2003.

[46]   L. Minkova*, et al.*, "Crystallization and morphology of fibers prepared from compatibilized blends of polyethylene with a liquid crystalline polymer," *Macromolecular Materials and Engineering,* vol. 280-281, pp. 7-13, 2000.

[47]   L. Minkova*, et al.*, "Microhardness of compatibilized blends of polypropylene with a semiflexible liquid-crystalline polymer," *Colloid and Polymer Science,* vol. 280, pp. 358-364, 2002.

[48]   L. I. Minkova*, et al.*, "Morphology and Rheology of HDPE/LCP Blends Compatibilized by a Novel PE-g-LCP Copolymer," *Journal of Applied Polymer Science,* vol. 73, pp. 2069-2077, 1999.

[49]   T. Miteva and L. Minkova, "Effect of PP-g-LCP compatibilizer on the structure and crystallization of blends of isotactic polypropylene (PP) with a semiflexible liquid crystalline polymer (LCP)," *Macromolecular Chemistry and Physics,* vol. 199, pp. 597-606, 1998.

[50]   T. Miteva*, et al.*, "Isothermal crystallization kinetics of compatibilized blends of polyolefines with a semiflexible liquid crystalline polymer," *Macromolecular Chemistry and Physics,* vol. 199, pp. 1519-1527, 1998.

[51]   Z. Yerlikaya*, et al.*, "Structure and Properties of Fully Aromatic Thermotropic Liquid-Crystalline Copolyesters Containing m-Hydroxybenzoic Acid Units," *Journal of applied polymer science,* vol. 90, pp. 3260-3269, 2003.

[52]   Z. Yerlikaya*, et al.*, "Synthesis and properties of thermotropic liquid crystalline copolyesters containing p-Hydroxyphenylacetic acid and m-hydroxybenzoic acid units," *Journal of Macromolecular Science - Pure and Applied Chemistry,* vol. 43, pp. 433-447, 2006.

[53]   M. Yikici*, et al.*, "Effect of polycondensation reaction conditions on the properties of thermotropic liquid-crystalline copolyester," *Journal of Macromolecular Science, Part A: Pure and Applied Chemistry,* vol. 45, pp. 620-627, 2008.

[54]   R. W. Gray IV*, et al.*, "Effects of processing conditions on short TLCP fiber reinforced FDM parts," *Rapid Prototyping Journal,* vol. 4, pp. 14-25, 1998.

[55]   S. Y. Kim*, et al.*, "Internal structure and physical properties of thermotropic liquid crystal polymer/poly (ethylene 2, 6-naphthalate) composite fibers," *Composites Part A: Applied Science and Manufacturing,* vol. 40, pp. 607-612, 2009.

[56]   Q. Xu*, et al.*, "Melt flow behavior of liquid crystalline polymer in-situ composites," *Journal of Materials Processing Technology,* vol. 63, pp. 519-523, 1997.

[57]   M. Jaffe, "Encyclopedia of Polymer Science and Engineering," *New York,* p. 699, 1987.

[58]   G. Calundann and M. Jaffe, "Anisotropic polymers, their synthesis and properties," 1982.

[59]   J. Karger Kocsis, "Recycling Options for Post Consumer PET and PET Containing Wastes by Melt Blending: Sections 3-5."

[60]   S. Fakirov, *Handbook of condensation thermoplastic elastomers*: Wiley-VCH Verlag GmbH, 2005.

[61]   E. Marechal, "Polyesters: Synthesis and chemical aspects."

[62]   J. Scheirs and T. E. Long, *Modern polyesters: Chemistry and Technology of Polyesters and Copolyesters*: Wiley, 2003.

[63]   A. S. Coolidge and M. S. Coolidge, "The Sublimation Pressures of Substituted Quinones and Hydroquinones," *Journal of the American Chemical Society,* vol. 49, pp. 100-104, 1927.

[64]   V. Korshak and S. Rogozhin, "Macromolecular compounds communication 61. Decarboxylation of dicarboxylic acids during polycondensation," *Russian Chemical Bulletin,* vol. 3, pp. 461-466, 1954.

[65]   Ö. Özarslan*, et al.*, "Novel poly (arylene ether ketone ketone) s synthesized by Friedel Crafts acylation," *Macromolecular Chemistry and Physics,* vol. 199, pp. 1887-1893, 1998.

[66]   S. Hovenkamp and J. Munting, "Formation of diethylene glycol as a side reaction during production of polyethylene terephthalate," *Journal of Polymer Science Part A 1: Polymer Chemistry,* vol. 8, pp. 679-682, 1970.

[67]   M. Lewin and E. M. Pearce, *Handbook of fiber chemistry* vol. 15: Marcel Dekker Inc, 1998.

[68]   X. Zheng*, et al.*, "Compatibilization of nylon 6/liquid crystalline polymer blends with three types of compatibilizers," *Journal of Applied Polymer Science,* vol. 87, pp. 1452-1461, 2003.

[69]   X. Zheng*, et al.*, "Flow properties and morphology of PC/LCP blends affected by the addition of glass fiber and resulted mutual influences," *International Polymer Processing,* vol. 18, pp. 3-11, 2003.

[70]   J. Zhao*, et al.*, "A new liquid crystalline polymer based processing aid and its effects on micro-molding process," *Journal of Materials Processing Technology,* vol. 168, pp. 308-315, 2005.

[71]   W. Yu*, et al.*, "Dynamic rheology of the immiscible blends of liquid crystalline polymers and flexible chain polymers," *Rheologica Acta,* vol. 45, pp. 105-115, 2005.

[72]   Y. Xue*, et al.*, "Mechanical performance of blends of thermotropic liquid crystalline polymer spheres-dispersed polycarbonate," *Journal of Applied Polymer Science,* vol. 89, pp. 1493-1499, 2003.

[73]   W. B. Xie*, et al.*, "Mechanical properties and morphology of LCP/ABS blends compatibilized with a styrene-maleic anhydride copolymer," *Polymer International,* vol. 52, pp. 733-739, 2003.

[74]   S. Viswanathan and M. D. Dadmun, "Optimizing hydrogen-bonding in creating miscible liquid crystalline polymer blends by structural modification of the blend components," *Macromolecules,* vol. 36, pp. 3196-3205, 2003.

[75]   L. P. Tan*, et al.*, "Relaxation of liquid-crystalline polymer fibers in polycarbonate-liquid-crystalline polymer blend system," *Journal of Polymer Science, Part B: Polymer Physics,* vol. 41, pp. 2307-2312, 2003.

[76]   L. P. Tan*, et al.*, " Effects of shear rate, viscosity ratio and liquid crystalline polymer content on morphological and mechanical properties of polycarbonate and LCP blends," Polymer International,vol. 51, pp. 398-405, 2002.

[77]   L. P. Tan*, et al.*, "Phase diagram for predicting in situ fibrillation of LCP during molding," *Materials and Manufacturing Processes,* vol. 21, pp. 127-134, 2006.

[78]   L. P. Tan*, et al.*, "Effect of shear heating during injection molding on the morphology of PC/LCP blends," *Acta Materialia,* vol. 51, pp. 6269-6276, 2003.

[79]   P. Sukananta and S. Bualek-Limcharoen, "In situ modulus enhancement of polypropylene monofilament through blending with a liquid-crystalline copolyester," *Journal of Applied Polymer Science,* vol. 90, pp. 1337-1346, 2003.

[80]   S.   Saikrasun,   *et   al.*,   "Thermotropic   liquid-crystalline copolyester/thermoplastic elastomer in situ composites. I. Rheology, morphology, and mechanical properties of extruded strands," *Journal of Applied Polymer Science,* vol. 89, pp. 2676-2685, 2003.

[81]   N. G. Sahoo*, et al.*, "Structure -Properties Relations of Polypropylene/Liquid Crystalline Polymer Blends," *Macromolecular Research,* vol. 11, pp. 224-230, 2003.

[82]   A. Retolaza*, et al.*, "Structure and mechanical properties of polyamide-6,6/poly(ethylene terephthalate) blends," *Polymer Engineering and Science,* vol. 44, pp. 1405-1413, 2004.

[83]   H. Orihara*, et al.*, "Observations of immiscible polymer blend electrorheological fluids with a confocal scanning laser microscope," *Journal of Rheology,* vol. 47, pp. 1299-1310, 2003.

[84]   W. Mormann and T. Pokropski, "Blends of a main chain liquid-crystalline polyester with a diepoxide and with a diepoxide/amine mixture prepared in a twin-screw extruder," *Macromolecular Materials and Engineering,* vol. 289, pp. 975-983, 2004.

[85]   P. K. Mandal*, et al.*, "Studies on morphology, mechanical, thermal, and rheological behavior of extrusion-blended polypropylene and thermotropic liquid crystalline polymer," *Journal of Applied Polymer Science,* vol. 88, pp. 767-774, 2003.

[86]   M. W. Lee*, et al.*, "Effect of fillers on the structure and mechanical properties of LCP/PP/SiO2 in-situ hybrid nanocomposites," *Composites Science and Technology,* vol. 63, pp. 339-346, 2003.

[87]   M. W. Lee*, et al.*, "PP/LCP composites: Effects of shear flow, extensional flow and nanofillers," *Composites Science and Technology,* vol. 63, pp. 1921-1929, 2003.

[88]   H. S. Lee*, et al.*, "Formation of nanoparticles during melt mixing a thermotropic liquid crystalline polyester and sulfonated polystyrene ionomers: Morphology and origin of formation," *Polymer,* vol. 46, pp. 10841-10853, 2005.

[89]   J. Y. Kim and S. H. Kim, "Influence of viscosity ratio on processing and morphology of thermotropic liquid crystal polymer-reinforced poly(ethylene 2,6-naphthalate) blends," *Polymer International,* vol. 55, pp. 449-455, 2006.

[90]   J. Y. Kim and S. H. Kim, "Fibril formation of thermotropic liquid crystal polymer and polyester blends by controlling viscosity ratio," Journal of Polymer Science Part B: Polymer Physics, vol 43, pp. 118-122, 2005.

[91]   J. Y. Kim and S. H. Kim, "In situ fibril formation of thermotropic liquid crystal polymer in polyesters blends," *Journal of Polymer Science, Part B: Polymer Physics,* vol. 43, pp. 3600-3610, 2005.

[92]   M. García*, et al.*, "Miscibility level and mechanical characterization of blends of two liquid-crystalline polymers based on p-hydroxybenzoic acid," *Journal of Polymer Science, Part B: Polymer Physics,* vol. 41, pp. 1022-1032, 2003.

[93]   M. García*, et al.*, "Processability, Morphology and Mechanical Properties of Glass Fiber Reinforced Poly(Ether Sulfone) Modified by a Liquid Crystalline Copolyester," *Polymer Composites,* vol. 24, pp. 686-696, 2003.

[94]   S. Filipe*, et al.*, "Influence of type of compatibilizer on the rheological and mechanical behavior of LCP/TP blends under different stationary and nonstationary shear conditions," *Journal of Applied Polymer Science,* vol. 98, pp. 694-703, 2005.

[95]   S. Filipe*, et al.*, "A study of rodrun LC3000/PP blends under different stationary and non-stationary shear conditions: The influence of LCP content and processing temperature," *Journal of Polymer Engineering,* vol. 25, pp. 527-552, 2005.

[96]   S. Filipe*, et al.*, "Evolution of the morphological and rheological properties along the extruder length for compatibilized blends of a commercial liquid-crystalline polymer and polypropylene," *Journal of Applied Polymer Science,* vol. 99, pp. 347-359, 2006.

[97]   B. J. Edwards and K. L. Williams, "A Rheological and Morphological Model for Blends of Flexible and Rigid Macromolecules," *Polymer Engineering and Science,* vol. 43, pp. 1778-1787, 2003.

[98]   L. B. da Silva*, et al.*, "Transient shear and elongational behavior of blends of PET with a LCP," *Rheologica Acta,* vol. 45, pp. 268-280, 2006.

[99]   P. Chen*, et al.*, "Morphology evolution of a liquid crystalline polymer confined by highly packed glass beads in polycarbonate," *Polymer,* vol. 46, pp. 7652-7657, 2005.

[100]   V. A. Davis*, et al.*, "Phase behavior and rheology of SWNTs in superacids," *Macromolecules,* vol. 37, pp. 154-160, 2004.

[101]   D. Acierno and A. Collyer, "Rheology and processing of liquid crystal polymers," *Chapman & Hall, London,* 1995.

[102]   K. F. Wissbrun, "Rheology of rod-like polymers in the liquid crystalline state," *Journal of Rheology,* vol. 25, p. 619, 1981.

[103]   S. J. Kim*, et al.*, "Deformation of multiple non-Newtonian drops in the entrance region," *Korea-Australia Rheology Journal,* vol. 15, pp. 75-82, 2003.

[104]   S. J. Kim and C. D. Han, "Finite element analysis of axisymmetric creeping motion of a deformable non-Newtonian drop in the entrance region of a cylindrical tube," *Journal of Rheology,* vol. 45, p. 1279, 2001.

[105] Y. Kitano*, et al.*, "Morphology and crystal structure of an a axis oriented, highly crystalline poly (ethylene terephthalate)," *Polymer,* vol. 36, pp. 1947-1955, 1995.

[106] M. W. Lee*, et al.*, "Deformation study of the dispersed phase in filled polymer blends using LCP/PP/SiO2 as model systems," *Acta Materialia,* vol. 54, pp. 3359-3367, 2006.

[107] C. Noel*, et al.*, "Polymers with mesogenic elements in the main chain: a nematic aromatic copolyester," *Polymer,* vol. 25, pp. 263-273, 1984.

[108] V. Arrighi*, et al.*, "Characterization of a main-chain semiflexible liquid crystalline polymer: degree of orientational order," *Polymer,* vol. 37, pp. 141-148, 1996.

[109] M. Favelukis*, et al.*, "Deformation and breakup of a non-Newtonian slender drop in an extensional flow," *Journal of Non-Newtonian Fluid Mechanics,* vol. 125, pp. 49-59, 2005.

[110] H. R. Kricheldorf and A. Gerken, "New polymer syntheses 87. Thermosetting nematic or cholesteric diesters having propargyl endgroups," *High Performance Polymers,* vol. 9, p. 75, 1997.

[111] B. Zhao and W. J. Brittain, "Polymer brushes: surface-immobilized macromolecules," *Progress in Polymer Science,* vol. 25, pp. 677-710, 2000.

[112] G. Ozkoc*, et al.*, "Compatibilization of ABS/PA6 blends using olefiv based polymers," 2006, pp. 650-654.

[113] A. D. De Oliveira*, et al.*, "Effect from the blending sequence on the properties of PA6/ABS blends compatibilized with SMA copolymer," *Efeito da sequência de mistura nas propriedades de blendas PA6/ABS compatibilizadas com o copolímero SMA,* vol. 21, pp. 27-33, 2011.

[114]   G. Ozkoc*, et al.*, "Effects of olefin-based compatibilizers on the morphology, thermal and mechanical properties of ABS/polyamide-6 blends," *Journal of Applied Polymer Science,* vol. 104, pp. 926-935, 2007.

[115]   G. Ozkoc*, et al.*, "Impact essential work of fracture toughness of ABS/polyamide-6 blends compatibilized with olefin based copolymers," *Journal of Materials Science,* vol. 43, pp. 2642-2652, 2008.

[116]   S. Sun*, et al.*, "Influence of epoxy resin on the properties of maleic anhydride functionalized acrylonitrile-butadiene-styrene copolymer toughened polyamide 6 blends," *Journal of Applied Polymer Science,* vol. 121, pp. 909-915, 2011.

[117]   A. Mojarrad*, et al.*, "Investigation on the correlation between rheology and morphology of PA6/ABS blends using ethylene acrylate terpolymer as compatibilizer," *Journal of Applied Polymer Science,* vol. 120, pp. 2173-2182, 2011.

[118]   A. Arsad*, et al.*, "Mechanical and rheological properties of PA6/ABS blends - With and without short glass fiber," *Journal of Reinforced Plastics and Composites,* vol. 29, pp. 2808-2820, 2010.

[119]   J. B. Guo*, et al.*, "Morphology and mechanical properties of polymer blends of ABS/PA6 compatibilized by styrene-maleic anhydride," *Zhongbei Daxue Xuebao (Ziran Kexue Ban)/Journal of North University of China (Natural Science Edition),* vol. 31, pp. 318-322, 2010.

[120]   X. F. Cai*, et al.*, "Study on the structure and properties of ABS/PA6/SMA blends," *Sichuan Daxue Xuebao (Gongcheng Kexue Ban)/Journal of Sichuan University (Engineering Science Edition),* vol. 37, pp. 81-86, 2005.

[121]   R. A. Vaia*, et al.*, "Kinetics of polymer melt intercalation," *Macromolecules,* vol. 28, pp. 8080-8085, 1995.

[122]   P. C. LeBaron*, et al.*, "Polymer-layered silicate nanocomposites: an overview," *Applied Clay Science,* vol. 15, pp. 11-29, 1999.

[123]   M. Alexandre and P. Dubois, "Polymer-layered silicate nanocomposites: preparation, properties and uses of a new class of materials," *Materials Science and Engineering: R: Reports,* vol. 28, pp. 1-63, 2000.

[124]   K. Gunes and A. I. Isayev, "In-situ ultrasonic compatibilization of PEN/LCP blends," Journal of Apllied Polymer Science, pp. 1141-1145, 2010.

[125]   X. Y. Xu, "Compatibilization and strengthen of PBT/PP blends by adding liquid crystalline polymer with carboxylic group," *Shiyou Huagong Gaodeng Xuexiao Xuebao/Journal of Petrochemical Universities,* vol. 23, pp. 1-4, 2010.

[126]   Y. Tang*, et al.*, "A comparative study of thermotropic LCP and organoclay as fillers in high molecular mass polyethylene with different blending sequences," *Polymer Engineering and Science,* vol. 50, pp. 1679-1688, 2010.

[127]   P. K. Mandal*, et al.*, "Studies on the engineering properties of LCP-Vectra B 950/PP blends with the variations of EAA content," *Journal of Applied Polymer Science,* vol. 119, pp. 1034-1041, 2011.

[128]   K. W. D. Lee*, et al.*, "Thermally induced phase separation in liquid crystalline polymer/polycarbonate blends," *Journal of Applied Polymer Science,* vol. 117, pp. 2651-2668, 2010.

[129]   T. Ivanova*, et al.*, "Mechanical properties of injection moulded binary blends of polyethylene with small additions of a liquid crystalline polymer," AIP Conf. Proc. June 2, Volume 1255, pp. 310-312, 2010.

[130]   K. Gunes and A. I. Isayev, "In situ compatibilization of PEN/LCP blends by ultrasonic extrusion," *Journal of Applied Polymer Science,* 2011.

[131] R. Foudazi and H. Nazockdast, "Rheology of polypropylene/liquid crystalline polymer blends: Effect of compatibilizer and silica," *Applied Rheology,* vol. 20, pp. 122-128, 2010.

[132] H. K. F. Cheng*, et al.*, "Molecular interactions in PA6, LCP and their blend incorporated with functionalized carbon nanotubes," Key Engineering Materials vol. 447, pp. 634-638, 2010.

[133] J. Bandyopadhyay*, et al.*, "Effect of nanoclay incorporation on the thermal properties of poly(ethylene terephthalate)/liquid crystal polymer blends," *Macromolecular Materials and Engineering,* vol. 295, pp. 822-837, 2010.

[134] X. Zheng and J. He, "Mechanical performance of LCP/PA6 blends with LCP microspheres," *Fuhe Cailiao Xuebao/Acta Materiae Compositae Sinica,* vol. 26, pp. 47-53, 2009.

[135] B. Yin*, et al.*, "Polycarbonate/liquid crystalline polymer blend: Crystallization of polycarbonate," *Polymer,* vol. 47, pp. 8237-8240, 2006.

[136] C. Wei and J. Lu, "Effects of the kinds of liquid crystalline polymers on the structure and properties of the liquid crystalline polymers/epoxy resin blends," *Cailiao Kexue yu Gongyi/Material Science and Technology,* vol. 15, pp. 286-289, 2007.

[137] C. Wei, "Effects of the kinds of liquid crystalline polymers on the structure and properties of the liquid crystalline polymers/epoxy resin blends," *Gaofenzi Cailiao Kexue Yu Gongcheng/Polymeric Materials Science and Engineering,* vol. 22, pp. 137-140, 2006.

[138] Y. H. Tang*, et al.*, "Effects of thermotropic LCP on rheologica behavior of high molecular mass polyethylene/organoclay composites," *Journal of Central South University of Technology (English Edition),* vol. 14, pp. 192-195, 2007.

[139] E. Shiva Kumar, *et al.*, "Ternary blends of acrylic rubber, poly(butylene terephthalate), and liquid crystalline polymer: Influence of interactions on thermal and dynamic mechanical properties," *Journal of Applied Polymer Science,* vol. 100, pp. 3904-3912, 2006.

[140] J. Qiu, *et al.*, "Effects of injection-molded conditions on the microstructure and mechanical properties of PC/LCP blends," *Kobunshi Ronbunshu,* vol. 63, pp. 360-367, 2006.

[141] Y. H. Na, *et al.*, " Stripe formation in an immiscible polymer blend under electric and shear-flow fields," Phys. Rev. E 77, 4 pages, 2008

[142] M. Mukherjee, *et al.*, "Simulation of fibrillation of PC/LCP/kevlar blends and its characterizations," *Macromolecular Symposia,* vol. 277, pp. 24-35, 2009.

[143] K. W. D. Lee, *et al.,* "Rheology, morphology and properties of LCP/Nylon 66 composite fibers," Polymer Composites, vol. 21, pp. 114-123, 2000

[144] K. W. D. Lee, *et al.*, "Determination of the phase diagram of HBA-HNA liquid crystalline polymer/polycarbonate blends," *Journal of Applied Polymer Science,* vol. 111, pp. 394-407, 2009.

[145] K. W. Lee, *et al.*, "Phase separation under shear in liquid crystalline polymer/polycarbonate blends," *International Polymer Processing,* vol. 24, pp. 83-89, 2009.

[146] D. Kim, *et al.*, "Phase equilibria and phase separation dynamics in a polymer composite containing a main-chain liquid crystalline polymer," *Journal of Polymer Science, Part B: Polymer Physics,* vol. 44, pp. 3621-3630, 2006.

[147] A. K. Kalkar, *et al.*, "In situ composites from blends of polycarbonate and a thermotropic liquid-crystalline polymer: The influence of the processing temperature on the rheology, morphology, and mechanical properties of

injection-molded microcomposites," *Journal of Applied Polymer Science,* vol. 106, pp. 34-45, 2007.

[148]   S. A. R. Hashmi and T. Kitano, "Shear rate dependence of viscosity and first normal stress difference of LCP/PET blends at solid and molten states of LCP," *Journal of Applied Polymer Science,* vol. 104, pp. 2212-2218, 2007.

[149]   S. A. R. Hashmi and T. Kitano, "Effects of state change of liquid crystalline polymer on dynamic visco-elasticity of its blends wtih polyethylene-terephthalate," *Applied Rheology,* vol. 17, pp. 64510-1-64510-7, 2007.

[150]   S. A. R. Hashmi and T. Kitano, "Rheology of LCP/PET blends at solid and molten states of LCP," *Applied Rheology,* vol. 16, pp. 152-160, 2006.

[151]   S. Filipe*, et al.*, "Optimisation of rodrun LC3000/PP compatibilised blends: Influence of the compatibiliser and LCP contents on the rheological, morphological and mechanical properties," *Journal of Polymer Engineering,* vol. 26, pp. 511-545, 2006.

[152]   E. Fekete*, et al.*, "Effect of viscosity ratio of the components of thermoplastic and liquid-crystalline polymer blends on the properties," *Composite Interfaces,* vol. 13, pp. 737-755, 2006.

[153]   Y. Ding*, et al.*, "Rheological hybrid effect in nylon 6/liquid crystalline polymer blends caused by added glass beads," *Journal of Non-Newtonian Fluid Mechanics,* vol. 135, pp. 166-176, 2006.

[154]   T. Das*, et al.*, "The effect of glass fiber and coupling agents in the blends of silicone rubber and liquid crystalline polymers," *Macromolecular Research,* vol. 14, pp. 261-266, 2006.

[155]   T. Das*, et al.*, "Binary blends of polytetrafluoroethylene and liquid crystalline polymer," *Polymer - Plastics Technology and Engineering,* vol. 45, pp. 1047-1052, 2006.

[156] M. T. Cidade*, et al.*, "Synthesis of compatibilizers and characterization of the compatibilized and noncompatibilized blends of PP/rodrun LC3000," *Journal of Applied Polymer Science,* vol. 104, pp. 3001-3009, 2007.

[157] H. K. F. Cheng*, et al.*, "The role of functionalized carbon nanotubes in a PA6/LCP blend," *Journal of Nanoscience and Nanotechnology,* vol. 10, pp. 5242-5251, 2010.

[158] L. Chen*, et al.*, "Transesterification-controlled compatibility and microfibrillation in PC-ABS composites reinforced by phosphorus-containing thermotropic liquid crystalline polyester," *Polymer,* vol. 50, pp. 3037-3046, 2009.

[159] W. Ahn and K. Ha, "Field-induced liquid crystal texture development of a side-chain LCP/7CB blend," *Molecular Crystals and Liquid Crystals,* vol. 498, pp. 95-102, 2009.

[160] Y. Meng and S. Tjong, "Rheology and morphology of compatibilized polyamide 6 blends containing liquid crystalline copolyesters," *Polymer,* vol. 39, pp. 99-107, 1998.

[161] M. Kyotani*, et al.*, "Mechanical and structural properties of extruded strands of blends containing a liquid-crystalline polyester with poly (ethylene terephthalate)," *Polymer,* vol. 33, pp. 4756-4762, 1992.

[162] Q. Lin and A. F. Yee, "Mechanical properties of in situ composites based on polycarbonate and a liquid crystalline polymer," *Polymer,* vol. 35, pp. 3463-3469, 1994.

[163] K. Wei and G. Kiss, "Liquid crystalline polymer blends with stabilized viscosity," *Polymer Engineering & Science,* vol. 36, pp. 713-720, 1996.

[164] S. Lee*, et al.*, "Characterization and processing of blends of poly (ether imide) with thermotropic liquid crystalline polymer," *Polymer,* vol. 35, pp. 519-531, 1994.

[165] D. Acierno and F. P. La Mantia, *Processing and properties of liquid crystalline polymers and LCP based blends*: ChemTec Publishing, 1993.

[166] R. W. Ludignea, "*Thermotropic liquid crystal polymers: thin-film polymerization, characterization, blends, and applications"* CRC Press Chapter 11, LCP Extrusion and Applications p. 303, 2001.

[167] D. Baird and A. Sukhadia, "Mixing Process for Generating In Situ Reinforced Thermoplastics," *Patent Number US 5225488,* 1993.

[168] D. Hobbs and F. Muzzio, "Optimization of a static mixer using dynamical systems techniques," *Chemical Engineering Science,* vol. 53, pp. 3199-3213, 1998.

[169] M. Kamal*, et al.*, "Simulation of injection mold filling of viscoelastic polymer with fountain flow," *AIChE journal,* vol. 34, pp. 94-106, 1988.

[170] S. Tjong and W. Jiang, "Performance characteristics of compatibilized ternary Nylon 6/ABS/LCP in-situ composites," *Journal of Materials Science,* vol. 39, pp. 2737-2746, 2004.

[171] A. Ramamoorthy, *Thermotropic liquid crystals: recent advances*: Springer Verlag, 2007.

[172] F. W. Billmeyer, "Textbook of polymer science," *F. W. Billmeyer, Jr., John Wiley & Sons Inc., New York 1984, 3 rd Edition, xviii+ 578,* 1984.

[173] E. Watson*, et al.*, "A Differential Scanning Calorimeter for Quantitative Differential Thermal Analysis," *Analytical Chemistry,* vol. 36, pp. 1233-1238, 1964.

[174] H. Lobo and J. V. Bonilla, "General Introduction to Plastics Analysis," *Handbook of Plastics Analysis,* vol. 68, p. 1, 2003.

[175] S. L. Rosen, *Fundamental Principles of Polymeric Materials*: Wiley, 1982.

[176] S. Saikrasun and O. Wongkalasin, "Thermal decomposition kinetics of thermotropic liquid crystalline p-hydroxy benzoic acid/poly (ethylene terephthalate) copolyester," *Polymer Degradation and Stability,* vol. 88, pp. 300-308, 2005.

[177] X. Jin and T. S. Chung, "Thermal decomposition behavior of main chain thermotropic liquid crystalline polymers, Vectra A 950, B 950, and Xydar SRT 900," *Journal of Applied Polymer Science,* vol. 73, pp. 2195-2207, 1999.

[178] T. S. Oh*, et al.*, "Transesterification reaction of polyarylate and copolyester (PETG) blends," *Polymer Engineering & Science,* vol. 37, pp. 838-844, 1997.

[179] K. Pramoda*, et al.*, "Characterization and thermal degradation of polyimide and polyamide liquid crystalline polymers* 1," *Polymer Degradation and Stability,* vol. 67, pp. 365-374, 2000.

[180] B. D. Cullity and S. Stock, *Elements of X-ray Diffraction*: Prentice Hall, 2002.

[181] B. H. Stuart, *Polymer analysis*: Wiley, 2002.

[182] M. Imai*, et al.*, "Structural formation of poly (ethylene terephthalate) during the induction period of crystallization: 1. Ordered structure appearing before crystal nucleation," *Polymer,* vol. 33, pp. 4451-4456, 1992.

[183] S. Fakirov*, et al.*, "Unit cell dimensions of poly (ethylene terephthalate)," *Die Makromolekulare Chemie,* vol. 176, pp. 2459-2465, 1975.

[184] S. H. J. Idziak*, et al.*, "Undulating membrane structure under mixed extensional-shear flow," *The European Physical Journal E: Soft Matter and Biological Physics,* vol. 6, pp. 139-145, 2001.

[185] N. Stribeck and SpringerLink, *X-ray scattering of soft matter*: Springer Heidelberg, 2007.

[186] X. Xie*, et al.*, "Flory-huggins interaction parameters of LCP/thermoplastic blends measured by DSC analysis," *Journal of Thermal Analysis and Calorimetry,* vol. 70, pp. 541-548, 2002.

[187] W. Y. Chen*, et al.*, "Surface study of ladderlike polyepoxysiloxanes," *Journal of Polymer Science Part B: Polymer Physics,* vol. 38, pp. 138-147, 2000.

[188] T. S. Chung*, et al.*, "Liquid Crystalline Polymers, Main Chain." Polymer Engineering & Science, vol.26, pp 901-919, 1986.

[189] A. Gent and J. Schultz, "Effect of wetting liquids on the strength of adhesion of viscoelastic material," *The Journal of Adhesion,* vol. 3, pp. 281-294, 1972.

[190] D. Kaelble and J. Moacanin, "A surface energy analysis of bioadhesion," *Polymer,* vol. 18, pp. 475-482, 1977.

[191] C. J. Van Oss*, et al.*, "Interfacial Lifshitz-van der Waals and polar interactions in macroscopic systems," *Chemical Reviews,* vol. 88, pp. 927-941, 1988.

[192] R. J. Good, "Contact angle, wetting, and adhesion: a critical review," *Journal of Adhesion Science and Technology,* vol. 6, pp. 1269-1302, 1992.

[193] A. B. Strong "Plastics, Materials & Processing", Prentice Hall, New York, 2000

[194]   A. Standard, "D638-03," *Standard test method for tensile properties of plastics*.

[195]   C. L. Tsai and I. Daniel, "Method for thermo-mechanical characterization of single fibers," *Composites Science and Technology,* vol. 50, pp. 7-12, 1994.

[196]   D. I. Bower, *An introduction to polymer physics*: Cambridge Univ Pr, 2002.

[197]   D. Chen and H. Zachmann, "Glass transition temperature of copolyesters of PET, PEN and PHB as determined by dynamic mechanical analysis," *Polymer,* vol. 32, pp. 1612-1621, 1991.

[198]   T. J. Collins, "ImageJ for microscopy," *Biotechniques,* vol. 43, pp. 25-30, 2007.

[199]   K. Holmberg and B. Jönsson, *Surfactants and polymers in aqueous solution*: Wiley, 2003.

[200]   M. Dobb*, et al.*, "Compressional behaviour of Kevlar fibres," *Polymer,* vol. 22, pp. 960-965, 1981.

[201]   A. Cunningham*, et al.*, "An infra-red spectroscopic study of molecular orientation and conformational changes in poly (ethylene terephthalate)," *Polymer,* vol. 15, pp. 749-756, 1974.

[202]   J. Stokr*, et al.*, "Conformational structure of poly (ethylene terephthalate). Infra-red, Raman and nmr spectra," *Polymer,* vol. 23, pp. 714-721, 1982.

[203]   F. Boerio*, et al.*, "Vibrational analysis of polyethylene terephthalate and its deuterated derivatives," *Journal of Polymer Science: Polymer Physics Edition,* vol. 14, pp. 1029-1046, 1976.

[204] S. E. Welch*, et al.*, "Intermembrane spacing and velocity profiling of a lamellar lyotropic complex fluid under flow using x-ray diffraction," *Physical Review E,* vol. 65, pp. 61511, 2002.

[205] M. Kisilak*, et al.*, "An x-ray extensional flow cell," *Review of Scientific Instruments,* vol. 72, 3 pages, 2001.

[206] S. Manneville, "Recent experimental probes of shear banding," *Rheologica Acta,* vol. 47, pp. 301-318, 2008.

[207] C. Van Oss*, et al.*, "Monopolar surfaces," *Advances in colloid and interface science,* vol. 28, pp. 35-64, 1987.

[208] C. Van Oss*, et al.*, "Additive and nonadditive surface tension components and the interpretation of contact angles," *Langmuir,* vol. 4, pp. 884-891, 1988.

[209] C. Van Oss*, et al.*, "The Mechanism of Phase Separation of Polymers in Organic Media-Apolar and Polar Systems," *Separation Science and Technology,* vol. 24, pp. 15-30, 1989.

CURRICULUM VITAE

Personal Information

Name & Surname: Selahattin ERDOĞAN

Nationality: Turkish

Date and Place of Birth: 01.05.1975 – Urla/İzmir

e-mail: serdogan@metu.edu.tr

Education

Degree	Institution	Year
M.Sc.	METU, Chemical Oceanography	2002
B.Sc.	METU, Chemistry Dept.	1999
High School	Urla Lisesi	1993

Work Experience

Place	Position	Year
METU, Chemistry Dept.	Teaching Assistant	2003-2008
METU, Chemical Oceanography	Teaching Assistant	1999-2003

Foreign Language

English, Advanced

Projects

1. E. Bayramlı, M. Doğan, S Erdoğan., "Polipropilene güç tutuşurluk özelliği kazandırma", Arçelik A.Ş., ODAGEM Ostim Ortak Arş. Gel. Merkezi A.Ş., Temmuz 2010- Ocak 2011.

2. Doğan M., Erdoğan S., Bayramlı E. "Bor içeren güç tutuşur poliamid-6 ve polipropilen liflerin üretilmesi", BOREN Ç0209-2009, Şubat 2009-Şubat 2011

3. S. Erdoğan, Bayramlı E., "Alevsiz Polipropilen Boyama Teknolojisi ", TOFAŞ Türk Otomobil A.Ş., ODTÜ Biltir Merkezi, Haziran 2008- Aralık 2009.

4. Yılmazer Ü, Yeniova C.E., Erdoğan S. 'Beyaz Eşya Endüstrisinde Kullanım İçin Nanokompozit Malzeme Geliştirilmesi' TUBİTAK Research Project 106T425. Ocak 2007-Eylül 2008

5. Participant in the Black Sea Expedition R/V Knorr Voyage 162, Leg 17 - Leg 2, NATO Science for Peace-971818, ODBMS (June 2001)

Books:

1. M. Dogan, S. Erdogan, S. Kiralp, P. Camurlu, G. Ozkoc, T. Baydemir, "Plastikler", ODTU Yayıncılık (2006).

Publications

1. Yemenicioglu S.; Erdogan S.,; Tugrul S., , 'Distribution of dissolved forms of iron and manganese in the Black Sea' , Deep-Sea Research, Part II: Topical Studies in Oceanography (2006), 53(17-19), 1842-1855

Presentations:

1. Synthesis of low T_m liquid crystalline copolyesters (LCP) for self-reinforced composite application. 3. National Polymer Science and Technology Conference. 12-14 May 2010. Kocaeli University/Turkey

2. Erdogan S., Yemenicioglu S., Tugrul S., 'Distribution of dissolved and particulate forms of iron and manganese in the Black Sea' (447-451),. II. International Marine Science Conference. 14-18 October 2002. METU. Ankara/TURKEY

Attended Courses:

1. Mass Spectroscopy, Institute of Health Sciences, Gazi University (1999-2000)

2. Analysis of trace metals in marine samples, International Atomic Energy Agency (IAEA), Monaco (22 Nov – 3 Dec, 1999)

Research Interest:

Liquid crystalline polymers, synthesis, composites, trace metal analysis, marine samples

Awards:

1. Köseoğlu D,; Erdoğan S.; 'Detection of War and Narcotic Agents by Terahertz Spectroscopy' Undersecretariat for Defense Industries (Savunma Sanayii Müsteşarlığı) , New Ideas and New Business, second rank, METU (2008)